

**ENERGY BUDGET AND WHEAT YIELD PREDICTION  
OVER SEMI-ARID AGRO-ECOSYSTEM USING  
SATELLITE DATA**

**A**

**THESIS**

**SUBMITTED TO THE  
ANAND AGRICULTURAL UNIVERSITY  
IN PARTIAL FULFILMENT OF THE REQUIREMENTS  
FOR THE AWARD OF THE DEGREE**

**OF**

***Doctor of Philosophy***

**IN**

**AGRICULTURAL METEOROLOGY**

**BY**

**DAKHORE KAILAS KAMAJI**

**M.Sc. (Agri.)**

**DEPARTMENT OF AGRICULTURAL METEOROLOGY  
B. A. COLLEGE OF AGRICULTURE  
ANAND AGRICULTURAL UNIVERSITY  
ANAND-388 110**

**2007**

**Reg. No.: 04-0010-2004**




**Dr. A. M. SHEKH**  
PRINCIPAL AND DEAN  
B. A. College of Agriculture  
Anand Agricultural University  
ANAND - 388 110

## **C E R T I F I C A T E**

---

This is to certify that the thesis entitled "ENERGY BUDGET AND WHEAT YIELD PREDICTION OVER SEMI-ARID AGRO-ECOSYSTEM USING SATELLITE DATA" submitted by DAKHORE KAILAS KAMAJI in partial fulfillment of the requirements for the award of the degree of DOCTOR OF PHILOSOPHY in AGRICULTURAL METEOROLOGY of the Anand Agricultural University is a record of bonafide research work carried out by him under my guidance and supervision and the thesis has not previously formed for the award of any degree, diploma or any other similar title.

**PLACE : ANAND**  
**DATE : 24<sup>th</sup> DEC., 2007**

  
**(A. M. SHEKH)**  
**MAJOR ADVISOR**



**Dedicated**  
**To**  
**My beloved**  
**Parents & Guruji**





# ABSTRACT





# **ENERGY BUDGET AND WHEAT YIELD PREDICTION OVER SEMI-ARID AGRO-ECOSYSTEM USING SATELLITE DATA**

Name of the student  
**K. K. Dakhore**

Major Advisor  
**Dr. A. M. Shekh**

**B.A. College of Agriculture  
Anand Agricultural University  
Anand-388 110**

## **ABSTRACT**

---

The wheat is important staple food. Timely information of production estimates help planner and government machinery to arrange uninterrupted supply to the consumers. The advance information of estimate needs the values weather parameters over a region, in which net radiation is driving the all physical process. Net radiation ( $R_n$ ) is defined as the difference between the incoming and outgoing radiation fluxes including both long- and shortwave radiation at the surface of Earth. It is a key quantity for the estimation of surface energy budget and is used for various applications including climate monitoring, weather prediction and law of conservation of energy. Remote sensing provides an unparalleled spatial and temporal coverage of land surface attributes, thus several studies have attempted to estimate net radiation (or its components) by combining remote sensing observations with surface and atmospheric data serves as a key driving force for the evapotranspiration (ET). The daily evapotranspiration over regional scales is essential in agricultural and hydrological practice. Unfortunately, estimates of daily evapotranspiration at these regional scales are seldom available because conventional techniques give only point measurements and represent only the limited surrounding area within which the

meteorological variables and surface characteristics are nearly constant. Remote sensing techniques offer a reasonably viable means of evaluating evapotranspiration over large areas, hence overcoming the spatial problems involved in conventional methods.

Evaporation is the largest single component of the terrestrial hydrological cycle and its accurate estimation is important in water resource management, crop yield forecasting and understanding the links between land use changes and climate.

An approach for estimating regional scale clear sky evapotranspiration from single source surface energy balance using Moderate Resolution Imaging Spectroradiometer (MODIS) TERRA (morning overpass) and AQUA (noon overpass) reflectances and the land surface temperature (LST) was implemented over a semi-arid agroecosystem in Gujarat. Validation of two major energy balance components, net radiation ( $R_n$ ) and latent heat flux ( $\lambda E$ ) over Chalindra ( $22^{\circ} 46' 41.165$  N  $72^{\circ} 34' 28.412$  E), Muktipur ( $22^{\circ} 49' 32.754$  N  $72^{\circ} 34' 41.770$  E) and Nawagam ( $22^{\circ} 46' 45.639$  N  $72^{\circ} 34' 31.118$  E) showed that AQUA based estimates produced better accuracy than TERRA estimates on daily scale when compared to portable Bowen ratio energy balance measurements. The daytime estimates of  $R_n$  and  $\lambda E$  from AQUA produced RMSE of  $40 \text{ Wm}^{-2}$  (12 % of measured mean) and  $28 \text{ Wm}^{-2}$  (13 % of measured mean). The errors are comparable with the errors obtained through other global experiments.

It was also found that the accuracy of MODIS based  $\lambda E$  estimates was improved (9 % of measured mean) when compared with in situ measurements with limited area averaged sensible heat fluxes from Large Aperture Scintillometer (LAS). The correlation coefficient between estimates and measurements was also improved ( $r = 0.97$ ).

The spatial outputs of the different energy balance components ( $R_n$ ,  $G$ ,  $\lambda E$  and evaporative fraction ( $\Lambda$ )) over agricultural land use in Gujarat

were generated. There were substantial differences in mean, standard deviation (SD), histogram peak and range of  $R_n$ . These have consistently increased from November to March. Histogram peak and ranges were 390  $Wm^{-2}$ , 345 - 450  $Wm^{-2}$  in November, 440  $Wm^{-2}$ , 354 - 481  $Wm^{-2}$  in January and 550  $Wm^{-2}$  and 450-650  $Wm^{-2}$  in March.

The means and SD of (Ground heat flux)  $G$  did not show substantial differences between November and January. These varied between 70-75  $Wm^{-2}$  and 9-6  $Wm^{-2}$  respectively. But the ranges were different. It was high in January (40-90  $Wm^{-2}$ ) as compared to November (50-84  $Wm^{-2}$ ). A substantial increase in mean (123  $Wm^{-2}$ ) and SD (35  $Wm^{-2}$ ) was prominent in March. This could be due to increase in  $R_n$  input to  $G$  computation.

There are certain pockets such as area adjacent to Sabarmati river basin in Kheda district where  $\Lambda$  was consistently high ( $> 0.5$ ) due to cultivation of *rabi* crops with assured irrigation facility. The distribution clearly indicated that  $\Lambda$  had hardly crossed 0.5 in majority of the agricultural grids ( $0.01^\circ$ ) throughout *rabi* season in this semi-arid climate.

The mean  $\lambda E$  was found to be the highest (140  $Wm^{-2}$ ) in March corresponding to peak growth as compared to other two stages in November (111  $Wm^{-2}$ ) and January (129  $Wm^{-2}$ ). The higher variability in vegetation fraction due to differentially maturing crops in March could have produced highest SD (59  $Wm^{-2}$ ) in March as compared to 48  $Wm^{-2}$  in January and 52  $Wm^{-2}$  in November.

The spatial outputs of net radiation partitioning ratios (expressed as percent of  $R_n$ ),  $H/R_n$ ,  $G/R_n$  and  $\lambda E/R_n$ , averaged across *rabi* 2002-03, 2003-04 and 2004-05 over agricultural land uses were generated. The analysis indicated that though there was overall decrease in mean  $H/R_n$ , but regional  $H/R_n$  distribution was towards higher side in November and included more proportion of pixels in the relatively lower  $H/R_n$  range during peak growth.

A November like peak  $H/R_n$  was found in March that corresponds physiological maturity of *rabi* crops.

The distribution is restricted to lower  $\lambda E/R_n$  range (8 – 50 %) in November as compared to higher range (15 – 60%) in January. The coincidence of peak growth of most *rabi* crops in January could lead to more vegetation fraction. In March, majority of the pixels showed 10-35%  $\lambda E/R_n$  ratio corresponding to physiological maturity.

The majority of the grids showed higher  $G/R_n$  ratio in the range of 15-20% in November and 19-25% in March that corresponds to relatively low fractional vegetation cover.

An unsupervised classification scheme through hierarchical decision rules was applied to MODIS AQUA 250m NDVI data. Stacks of eight-day NDVI composite for the period 1 November to 16 March were prepared to generate wheat mask of Gujarat for *rabi* 2002-03, 2003-04 and 2004-05. District level wheat mask was generated first and regional mask was subsequently generated from district mask.

District wise consumptive water use (CWU) was computed by summing up eight-day ET for the wheat grid over entire growth period followed by averaging CWU over wheat grids for three major critical growth stages, vegetative, flowering and grain filling. These were carried out for all individual *rabi* seasons 2002-03, 2003-04 and 2004-05. There was gradual increase in mean CWU from vegetative (60 mm) to grain filling (100 mm) stages.

The impact of deviation in CWU on yield deviation, percent deviation of district mean wheat CWU from three seasons (2002-03, 2003-04 and 2004-05) were plotted against deviation in reported district wheat yield from three seasons district mean. The deviation from simple averaging produced better correlation ( $r = 0.74$ ) than with area weighting ( $r = 0.66$ ).

Two different efficiency based approaches were attempted to predict wheat yield of major wheat growing districts. These are (i) Water use efficiency (WUE) and (ii) Radiation use efficiency (RUE) based approaches. RUE approach through CASA model was found to produce better yield prediction accuracy (RMSE 17.7 % of reported mean) as compared to the RMSE (18 % of reported mean) from WUE approach. Moreover, the correlation coefficient between predicted and reported district yield was also found to be higher ( $r = 0.90$ ) in RUE based approach than the other one ( $r = 0.80$ ).

CASA (Carinege Ames Stanford Approach) model NPP was put to sensitivity test to error associated using satellite based inputs such as LAI, albedo, daily mean air temperature and LST. The estimated error in wheat NPP could be between 10-12% that could have propagated same level of error to predict yield. Rest 4-5% error in yield prediction through CASA model could be attributed to uncertainty associated with misclassification of wheat using 250m MODIS data.

A satellite based single source surface energy balance and evapotranspiration scheme has been successfully implemented and validated for the first time over semi-arid wheat growing conditions in India and Gujarat in particular. This is the first time in India, that area integrated heat flux measuring equipment (LAS) was operational. It was proved that accuracy of satellite based estimates improve with the use of area averaged data from such measurements. Efficiency based models can provide wheat yield prediction accuracies comparable with RS forced process models but the former is more robust, easy to handle for operational implementation.

## CONTENTS

Chapter No.	Title		Page No.
I	INTRODUCTION		1-4
II	BASIC CONCEPT OF REMOTE SENSING AND ITS APPLICATION IN AGRICULTURE		5-26
	2.1	Sensors and the Electromagnetic Spectrum	5
	2.2	Spectral Vegetation Response	7
	2.3	Types of Orbit of a satellite	8
	2.4	Sensors	11
	2.5	Remote Sensing for vegetation classification	14
	2.6	Resolution	16
	2.7	Image analysis and interpretation	17
	2.8	Potential Agricultural Applications of Remote Sensing	21
	2.8.1	Crop inventory and yield prediction	21
	2.8.2	Useful agromet parameters retrievable with satellite based RS data	22
III	REVIEW OF LITERATURE		27-66
	3.1	Evapotranspiration versus crop growth and yield	27
	3.2	Evapotranspiration using surface energy balance	30
	3.2.1	Using <i>in situ</i> measurements	30
	3.2.1.1	Field scale	30
	3.1.1.2	Landscape scale	32
	3.1.1.3	Regional scale	34
	3.2.2	Model simulation	38
	3.2.3	Using RS-based observations	42
	3.2.3.1	From ground platform	42
	3.2.3.2	Satellite platform	45
	3.2.3.2.1	Polar orbiting	45
	3.2.3.2.2	Geostationary	54
	3.3	RS-based yield prediction	56
	3.3.1	Spectral yield model	56
	3.3.2	Agromet model	60
	3.3.2.1	Multiple regression	60

	3.3.2.2	Efficiency model	63
	3.3.2.3	Relative evapotranspiration (RET)	64
	3.3.3	RS forcing to crop simulation model	64
<b>IV</b>	<b>MATERIALS AND METHODS</b>		
	4.1	Approach for estimating surface energy balance components	68
	4.1.1	Estimation of $\Lambda_m$	69
	4.1.2	Estimation of $Q_m$	70
	4.1.3	Estimation of daytime net available energy ( $Q_d$ ) and latent heat flux ( $\lambda E_d$ )	72
	4.2	Regional yield prediction approaches	73
	4.3	Satellite data used and their processing	76
	4.4	Validation methodology	79
	4.4.1.1	Characteristics of validation region	79
	4.4.1.2	Climate	81
	4.4.1.3	Description of the Soil	84
	4.4.1.4	Cropping pattern	84
	4.4.1.5	Management practices	85
	4.4.1.6	<i>In situ</i> measurements and preparation of validation datasets	85
	4.4.1.6.1	Attended	85
	4.4.1.6.2	Unattended	95
	4.5	Statistical analysis	98
<b>V.</b>	<b>RESULTS AND DISCUSSION</b>		99-167
	5.1	Characterization of energy budget over semi-arid wheat	99
	5.1.1	Temporal evolution of different radiation parameters	100
	5.1.1.1	Using <i>in situ</i> measurements	100
	5.1.1.2	Using satellite based observations	106
	5.1.2	Energy partitioning behavior	110
	5.2	Validation of satellite based estimates net radiation and latent heat fluxes	112
	5.2.1	Net radiation	112
	5.2.2	Latent heat fluxes	115
	5.2.2.1	Using Bowen ratio energy balance (BREB)	115
	5.2.2.2	Using area integrated sensible heat fluxes	118

		from LAS	
	5.3	Spatio-temporal variability	121
	5.3.1	Energy budget components	122
	5.3.2	Partitioning ratios	128
	5.4	Wheat mask generation	133
	5.5	Multi-temporal analysis of energy budget estimates in wheat	136
	5.5.1	Energy budget components	136
	5.5.2	Partitioning ratios	138
	5.6	Evapotranspiration (ET) and consumptive water use (CWU) of wheat	140
	5.6.1	Regional pattern of wheat evapotranspiration	140
	5.6.2	Regional pattern of wheat consumptive water use	141
	5.6.3	Relation between deviation in CWU and district yield deviation	144
	5.7	District level wheat yield prediction	147
	5.7.1	Calibration of seasonal consumptive water use	147
	5.7.2	Validation of WUE based yield prediction	148
	5.7.3	Generation of basic inputs for estimating net primary productivity (NPP)	151
	5.7.3.1	LAI / fAPAR estimation	151
	5.7.3.2	Radiation use efficiency (RUE)	154
	5.7.3.2.1	Determining temperature scalars	154
	5.7.3.2.2	Evaporative fraction	156
	5.7.4	Validation of RUE based yield prediction	158
	5.7.4.1	Sensitivity analysis of CASA model	159
	5.7.4.2	District wise Yield prediction	160
	5.8	Comparison of regional wheat yield distribution from two approaches	161
VI	SUMMARY AND CONCLUSION		167-175
	REFERENCES		i - xxi



## LIST OF TABLES

Table No.	Title	Page No.
2.1	Regions of Electromagnetic Spectrum	6
2.2	Major atmospheric windows available for remote sensing	14
2.3	Current and Future Indian Satellite Missions	18
4.1	Clear sky dates of daily MODIS reflectance and LST products used for estimating energy balance components	77
4.2	Climatic variability of weather parameters during wheat growing period at Nawagam for the period 1997-2006	83
4.3	Soil physical and physicochemical properties	84
4.4	Observational details	85
5.1	Variation of Ratio of measured hourly to daytime average net radiation at different wheat growth stages	103
5.2	Variation of ratio of measured hourly evaporative fraction ( $\lambda E / R_n - G$ ) at different wheat growth stages	105
5.3	Stage wise net radiation partitioning over semi-arid wheat using Bowen ratio energy balance (BREB) measurements	111
5.4	Validation of MODIS based net radiation estimates	113
5.5	Error statistics of MODIS based latent heat flux estimates ( $\lambda E$ )	116
5.6	District mean seasonal water use, average thermal condition and reported mean yield	144
5.7	Stage wise WUE over different districts	148
5.8	Error statistics of WUE based district yield prediction using different accumulation period for seasonal water use	150
5.9	Error statistics of district wheat yield prediction from WUE based approach using stage wise water use	150
5.10	Observed and estimated air temperature over different locations in Gujarat	155
5.11	Sensitivity analysis CASA model NPP to different satellite derivable input parameters	160
5.12	District wise yield prediction using two approaches	161

## LIST OF FIGURES

Figure No.	Title	Page No.
2.1	The visible region of the spectrum ranges from about 0.4 $\mu\text{m}$ to 0.7 $\mu\text{m}$	6
2.2	Spectral signatures of crops and soil	8
2.3	Polar orbit	9
2.4	Sun Synchronous	10
2.5	Geosynchronous Orbits	11
2.6	Example of a Passive Sensor	11
2.7	Example of a Active Sensor	12
2.8	Atmospheric windows in the electromagnetic spectrum	13
2.9	Typical Spectral response characteristics of green vegetation	15
4.1	Conceptual diagram of two-dimensional scatter of land surface temperature (LST) and surface albedo	69
4.2	Data processing flow using MODIS TERRA and AQUA product for Energy Balance	78
4.3	Location of Study Region	80
4.4	Average weather parameters at Nawagam from 1997-2006	81
4.5	Large Aperture Scintillometer and its components	98
5.1	Temporal variation of measured instantaneous insolation at MODIS TERRA ( 11.00 hrs) and MODIS AQUA (13.30 hrs) overpass timings for <i>rabi</i> (a) 2005-06 and (b) 2006-07 over study site	102
5.2	Temporal variation of wheat albedo over study region derived from MODIS TERRA and AQUA surface reflectances during <i>rabi</i> (a) 2005-06 and (b) 2006-07	107
5.3	Temporal variation of wheat NDVI over study region derived from MODIS TERRA and AQUA red and NIR surface reflectance during <i>rabi</i> (a) 2005-06 and (b) 2006-07	108
5.4	Temporal variation of wheat LST over study region derived from MODIS TERRA and AQUA during <i>rabi</i> (a) 2005-06 and (b) 2006-07	109
5.5	Validation plot of estimated and measured (a) instantaneous (TERRA+AQUA) and (b) daytime net radiation (AQUA only)	114

Figure No	Title	After page
5.6	Validation plot of estimated and measured instantaneous latent heat fluxes for (a) TERRA and (b)AQUA	117
5.7	Validation plot of estimated and measured daytime latent heat fluxes for AQUA	118
5.8	Validation of TERRA and AQUA ' $\lambda E$ ' estimation with <i>in situ</i> measurements when area averaged LAS 'H' was used	119
5.9	Temporal comparison of instantaneous $\lambda E$ estimates from TERRA and AQUA and through LAS measurements	120
5.10	Validation plot of estimated and measured daytime latent heat flux with AQUA and LAS	121
5.11	Histogram analysis of spatial distribution of net radiation (Rn) over agricultural land use in <i>rabi</i> at (a) end of November (b) middle of January (c) in 1 <sup>st</sup> week of March	124
5.12	Histogram analysis of spatial distribution of ground heat flux (G) over agricultural land use in <i>rabi</i> at the (a) end of November (b) end of January (c) in 1 <sup>st</sup> week of March	125
5.13	Histogram analysis of spatial distribution of evaporative fraction $\Lambda$ over agricultural land use in <i>rabi</i> at the (a) end of November (b) end of January (c) in 1 <sup>st</sup> week of March	126
5.14	Histogram analysis of spatial distribution of latent heat flux ( $\lambda E$ ) over agricultural land use in <i>rabi</i> at the (a) end of November (b) middle of January (c) in 1 <sup>st</sup> week of March	127
5.15	Histogram analysis of spatial distribution of H/Rn ratio over agricultural land use in <i>rabi</i> at the (a) end of November (b) end of January (c) in 1 <sup>st</sup> week of March	130
5.16	Histogram analysis of spatial distribution of G/Rn ratio over agricultural land use in <i>rabi</i> at the (a) end of November (b) end of January (c) in 1 <sup>st</sup> week of March	131
5.17	Histogram analysis of spatial distribution of $\lambda E$ /Rn ratio over agricultural land use in <i>rabi</i> at the (a) end of November (b) end of January (c) in 1 <sup>st</sup> week of March	132
5.18	Criteria used in hierarchical decision tree to generate district wheat mask in Gujarat	134

5.19	Characteristic NDVI profiles from MODIS AQUA 250 m for (a) wheat (b) mustard (c) tobacco (d) forest and (e) cumin	135
5.20	Temporal evolution of noon time estimates of energy budget components in wheat over validation site during 2002-03, 2003-04 and 2004-05 from eight-day MODIS AQUA products	137
5.21	Multi-temporal analysis of energy partitioning ratios in wheat over validation site from eight-day MODIS AQUA products during 2002-03, 2003-04 and 2004-05	139
5.22	Temporal variation of average eight-day district wheat ET over (a) Ahmedabad, (b) Junagadh, (c) Kheda and (d) Vadodara	140
5.23	Mean regional wheat consumptive water use (CWU) at different phenophases in Gujarat	141
5.24	Percent change from mean in regional wheat consumptive water use (CWU) at critical phenophases in Gujarat	143
5.25	(a) Plot of district percent deviation in consumptive water use (CWU) from simple average and percent yield deviation	146
	(b) Plot of district percent deviation in consumptive water use (CWU) from area weighted mean and percent yield deviation	146
5.26	Validation of WUE based predicted district yield and reported yield	149
5.27	Validation plot of estimated LAI from MODIS AQUA 250m NDVI	152
5.28	Temporal variation of measured and estimated LAI at Chalindra and Muktipur	153
5.29	Pooled validation of mean air temperature	154
5.30	Two-dimensional scatter of TERRA-AQUA evaporative fraction and NDVI at vegetative, flowering, grain filling and maturity	157
5.31	Validation of RUE based district yield estimates and reported yield	158
5.32	Comparison of regional distribution of wheat yield for 2004-05 from (a) WUE based (b) RUE based approach	166

## LIST OF PLATES

<b>Plate No.</b>	<b>Title</b>	<b>Page No.</b>
1	(a) Pyranometer (b) Net Radiometer (c) Thermal Property Analyzer	90
2	(a) Pocket Weather Meter (b) Automatic Weather Station at Nawagam in Wheat Field	91
3	Multi-level automatic weather station at Chalindra in Wheat Field	92
4	Sun Scan Canopy Analysis System	94

## List of Abbreviations and Acronyms

LST	Land Surface temperature
ET	Evapotranspiration
MODIS	Moderate Resolution Imaging Spectroradiometer
AQUA	Noon time over pass satellite
TERRA	Morning time over pass satellite
AET	Actual evapotranspiration
( $\lambda E$ )	Latent heat flux
(M)	Metabolic activities
$R_n$	Net radiation,
$H$	Sensible heat flux,
$G$	Ground heat flux,
$Q$	Net available energy
$\Lambda_{ins}$	Instantaneous evaporative fraction
LMT	Local Mean Time
$Ts_H$	LST on dry edge computed as linear function of surface albedo
$Ts_{\lambda E}$	LST on wet edge computed as linear function of surface albedo
$Ts$	Pixel LST
$Q_{ins}$	Instantaneous net available energy
$G_{ins}$	Instantaneous ground heat flux
$Rns_{ins}$	Instantaneous net shortwave radiation ( $Wm^{-2}$ )
$\alpha$	surface albedo
$Rs_{ins}$	Instantaneous insolation ( $Wm^{-2}$ )
$I_0$	Solar constant = $1367 Wm^{-2}$
$\varepsilon$	Sun-earth distance correction factor
$Rnl_{ins}$	Instantaneous net longwave radiation ( $Wm^{-2}$ )
$T_i$	Land surface temperature (K). Here MODIS land surface temperature (LST)
$\sigma$	Stephan-Boltzmann constant ( $5.67 \times 10^{-8} Wm^{-2}s^{-1}K^{-4}$ )

$\varepsilon_s$	Surface emissivity
$(T_a)$	Air temperature
NDVI	Normalized difference vegetation index
$\lambda E_d =$	Daytime average latent heat fluxes ( $\text{Wm}^{-2}$ )
$Q_d =$	Daytime average net available energy ( $\text{Wm}^{-2}$ )
$\Lambda_d =$	Daytime average evaporative fraction
$t_{sat}$	Time of satellite overpass
$t_{rise}$	LMT (hrs) at sunrise
$t_{set}$	LMT (hrs) at sunset
$\text{mmd}^{-1}$	Millimeter per day
WUE	Water use efficiency
RUE	Radiation use efficiency
NPP	Net primary production
HI	Harvest index
LAI	Leaf area index
fAPAR	Fraction of Absorbed Photosynthetically Active Radiation
$S(x,t)$	Solar isolation,
$fAPAR(x,t)$	Fraction of photosynthetically active radiation absorbed by crop,
$RUE_{max}$	Maximum radiation use efficiency,
$T_1(x,t)$ and $T_2(x,t)$	Temperature scalars
$W(x,t)$	Water scalar.
APAR	Absorbed Photosynthetically Active Radiation
(MVC)	Maximum value composite
$\mu\text{m}$	Micrometer
SWIR	Short-wave infrared
ISIN	Integerised sinusoidal
(DN)	Digital numbers
(HDF)	Hierarchical data format

$(R_i)$	Insolation
(NIR)	Near-infrared
$(T_a)$	Air temperature
$(\Lambda_{ins})$	Instantaneous evaporative fraction
km	Kilometer
mm	millimeter
$^{\circ}\text{C}$	Degrees Celsius
$T_{\text{MAX}}$	Maximum temperature
$T_{\text{MIN}}$	Minimum temperature
PE	Pan Evaporation
(BSS)	Bright Sunshine Hours
(RF)	Rainfall
RH	Humidity
(SD)	Standard deviation
(CV)	Coefficient of variation
RH1	Morning relative humidity
RH2	After noon relative humidity
$\text{g cm}^{-3}$	Gram per cube centimeter
$\text{kgha}^{-1}$	Kilogram per hectare
%	Percentage
Cm	Centimeter
@	At the rate
CRI	Crown root initiation
PAR	Photosynthetically active radiation
$(\beta)$	Bowen ratio
(LAS)	Large Aperture Scintilometer
$\mu\text{V/W/m}^2$	Micro volt per watts per square meter
$\text{W/m}^2$	Watts per square meter
s	Second
m	Meter
$\text{ms}^{-1}$	Meter per second
(MAWS)	Multi-level automatic weather station
$\theta_g$	Gravimetric water content (g of water $\text{g}^{-1}$ of soil)
$\theta_v$	Volumetric water content ( $\text{m}^3\text{m}^{-3}$ )
$W_w$	Weight of moist soil and container (g)
$W_d$	Weight of oven dry soil and container (g)
$W_c$	Weight of container (g)



(EM)	Electromagnetic spectrum
(n)	Refractive index of air
(T)	Temperature
(Q)	Humidity
( $C_n^2$ )	Refractive index of air
$Z_{LAS}$	Height of the LAS above the surface
d	Zero plane-displacement height
T·	Temperature scale
$L_{MO}$	obukhov length.
'g'	Gravitational acceleration
MAE	Mean absolute error
RMSE	Root mean square error
$P_i$	i-th estimate,
$O_i$	i-th observations or measurements,
n	Number of datasets
TM	Thematic Mapper
$O_2$	Oxygen
$O_3$	Ozone
FASAL	Forecasting Agriculture output using Space Agrometeorology and Land based observations
AWiFS	Advanced Wide Field Sensor
CAPE	Crop Acreage and Production Estimation
SAR	Synthetic Aperture Radar
SR	Simple ratio
SAVI	Soil-Adjusted Vegetation Index
PVI	Perpendicular Vegetation Index
EVI	Enhanced Vegetation Index
NDWI	Normalized Difference Water Index
SSMI	Special Sensor Microwave Imager
AMSR	Advanced Microwave Scanning Radiometer

## Acknowledgement

---

*Emotions can't be adequately expressed in words hence my acknowledgement is much more and deep beyond the words used here.*

*I feel extremely blessed and fortunate to have Dr. A. M. Shekhi, Principal and Dean, B. A. College of Agriculture, Anand Agricultural University, Anand as Major Advisor. I take this precious opportunity to express my gratitude, indebtedness and sincere regards to him for his valuable guidance, fruitful and candid suggestions and his support, inspiration, encouragement, freedom and providing all facility throughout the degree. For his amicableness, amenity, incentive censure and invaluable advice with congenial atmosphere during tenure of my study I would remain indebted forever.*

*I am very grateful to Dr. B. K. Bhattacharya, (Co-guide), Scientist, CMD/AFEG/RESA SAC, ISRO, Ahmedabad, for his timely suggestions and for extending the facilities available at ISRO without which my study would have been an unmanageable venture. His intellectual foresight, zeal for hard work, greed for excellence and super eminent thoughts always had been a source of constant inspiration to me.*

*I am highly grateful to Dr. N. K. Patel, Head, CMD/AFEG/RESA SAC, ISRO, Ahmedabad, for his encouragement as well as providing the facilities in the SAC, ISRO. I also express my special thanks to Kanishka Mallick and Prof. Chetali Sarkar. For there unforgettable help, moral support and homely atmosphere. I also grateful to Dr. Rahul Nigam for always giving suggestions, help and support.*

*My sincere gratitude and regards are due to the members of my advisory committee, Dr. S. K. Dixit Professor and Head, Department of Agricultural Statistics and Dean PGDAIT; Dr. Vyas Pandey, Professor and Head, Department of Agricultural Meteorology; Dr. J. J. Patel, Professor, Department of Agronomy and Dr. Manjusha Kulshrestha, Asst. Professor of Mathematics, Department of Agricultural Meteorology, for their cooperation and concrete suggestions, for their encouragement and propulsive guidance during the course of my study.*

*I am fortunate to be blessed by the doyen of Agrometeorology Dr. P. D. Mistry, Ex Professor and Head, Department of Agricultural Meteorology, B.A. College of Agriculture, Anand, for his painstaking preview and suggestions during this write up.*

*I am thankful to our departmental staff members for their always help during my study period Dr. H. R. Patel, Associate Professor, Dr. V. K. Sood, Assit. Professor, Prof. B. I. Karande, Prof. V. B. Vaidya, Prof. M. Lunagaria. I can't express my feeling for the time and blessings provided by Dr. Manjusha Kulshirsha at every moment where I needed a moral support to stand hard to fight back to achieve my goals.*

*I owe thanks to Shri. C.T. Patel, by Shri. S. K. Sharma (IMD), D. K. Vasava, Adarbhahi, Jalamsingh, Sureshbhai, Ronak, of the Department is also greatly acknowledged.*

*The delimited words hampers to express the feeling of my indebtedness to my friends and seniors whose love and affection always make me feel homely. They are and will ever be in my heart with all the sweet and naughty moments spent together. I discovered the ever untouched corners of my heart because of them only. Unfortunately, I am not at freedom to name all, but I would like to pen down some of my seniors Dr. Ajith Pillai, Ajit Mokate Dr. Ganesh Kulakarni, D. K. Kakde, Gyan singh, Vikram, Dr. Harshal Patil, Dr. Choudhary, Kulakarni Anant and friends Ghanshyam and juniors Ananta, Girish, Govind, Ripoonjay, Sachin, Parag, Rahul, Sandy, Sidharth, Susheel, Udipt, Vinayak,*

*The Blessings of my Parents and affection of my sister, brother in law and vedika who are always with me. The words and actions will always fall short to thank them for their belief and patience. With all my love and respect, I dedicate this work to them.*

*Above all, I bow before The Almighty, who provided me the strength to make this venture, a successful one.*

Place : Anand

Date : 24<sup>th</sup> DEC., 2007

*Kailas*  
(Dakhore Kailas. K.)



# INTRODUCTION



## I. INTRODUCTION

---

Plant growth and development are primarily governed by genetic potential, the environmental conditions of the soil and climate. The success or failure of farming is intimately related to the prevailing weather conditions, if weather is suitable to that particular crop production, yield would be high and vice-versa. The modification of the weather, except on a very limited scale, is yet in realm of experimentation. It is nevertheless possible to optimize farm production by adjusting, cropping patterns and agronomic practices to suit the climate of a locality.

Country like India, where major portions of population hardly manage to fulfill their food requirement, weather's role becomes very significant in forming agricultural policy. Indian economy is said to be agriculture dependent, as more than 30% of GDP (gross domestic production) is coming from agricultural sector, and more than 34.5% of the budget is allocated to agriculture sector. Food grain production in India has increased about four fold since independence (200 mt marks in year 1999-2000, in comparison to 50.82 mt in 1950-51). In spite of technological advancement in agriculture, large year-to-year variation in production continues, which is related to fluctuations in monsoon at gross level (Gadgil *et al.*, 1999). Wheat, the second most important food-grain crop contributes about 37% to the total food grain production in India. In recent past, wheat production has fluctuated between high of 75.6 mt in 1999-2000 to 62 mt in 1995-1996 in India (Anonymous, 2000). Wheat is widely distributed in India, being grown from 15 °N to 32 °N, from 72 °N to 92 °N and from mean sea level to fairly high altitudes. Wheat is a dominant *rabi* crop in northern and central states of India, which include Punjab, Haryana, Uttar Pradesh, Rajasthan, Madhya Pradesh and Bihar.

In India, Gujarat state having an area of 0.47 million hectares under irrigated wheat and producing 1.14 million tones of grains with average productivity of 2435 kg ha<sup>-1</sup> during 2001-02 stands eighth in area and seventh in production. The wheat productivity in Gujarat (2435 kg ha<sup>-1</sup>) is low as compared to the average productivity at national level (2745 kg ha<sup>-1</sup>) and also the average productivity at Punjab and Haryana (>4000 kg ha<sup>-1</sup>). Within the state as well, there is wide variation in productivity, which ranges from as low as 1597 kg ha<sup>-1</sup> in Surat district to as high as 3639 kg ha<sup>-1</sup> in Junagadh district of the state (Agril. Statistics at a glance 2003, 2004 and Anonymous, 1997).

Wheat is an important *rabi* cereal of middle Gujarat zone and is commonly grown after *kharif* crops. The productivity of the crop was 2128 kg ha<sup>-1</sup> (Anonymous, 2001-02), which was considerably lower than that of the state average of 2435 kg ha<sup>-1</sup> during the year 2001-02. The average grain yield of wheat in India, in general and Gujarat in particular is considerably low.

In view of the above scenario, timely and accurate forecast of crop production is of immense value to growers and different agencies in government as well as trade and industry for planning distribution, processing, and export/import of crop products. Food security of the country has an important bearing on the ecological, biological, socio-economic, political, and cultural dimension. As the pressure on the natural resources increases, the forecasting of crop production becomes important to make judicious use of limited resources.

The crop production system in semi-arid climatic conditions is frequently encountered by water scarcity due to maldistribution of rainfall or lack of irrigation water or its timely availability. It gives low productivity to overall growth in agriculture. The characterization of water stress over large agriculture using thermal and radiation regime

over crop surface in periodic manner throughout crop growth cycle is extremely important. Though, conventional measurements with lysimeter keep record of field and soil specific water balances in root zone but cannot be extrapolated to larger area.

The ground based micrometeorological or Bowen ratio towers having net radiometer at one height and temperature, humidity, wind speed sensors at multiple heights are also used to compute energy budget components to derive stress behavior over relatively larger area depending on the fetch (Shekh *et al.*, 2001). Most of the times, the ground based equipments lose the proper calibration and become non-functional in the long run. These are rather more useful to derive crop and soil specific parameters and coefficients required to calibrate soil-atmosphere-vegetation-transfer (SVAT) models to simulate energy balance components. The concomitant use of satellite optical and thermal data directly or their assimilation through SVATs is useful to represent water stress on pixel-by-pixel basis using energy balance approach for regular monitoring on a regional scale (state level).

Land surface temperature is a good indicator of the evaporation from the Earth's surface and the so-called greenhouse effect because it is one of the key parameters in the physics of land-surface processes on a regional as well as global scale. It acts as a link for surface-atmosphere interactions and energy fluxes between the atmosphere and the ground [Mannstein, 1987; Sellers *et al.*, 1988]. Therefore, it is required for a wide variety of climatic, hydrological, ecological and biogeochemical studies [Camillo, 1991; Schmugge and Becker, 1991; Running, 1991; Running *et al.*, 1994; Zhang *et al.*, 1995]. Another important surface parameter is expressed in terms of the Normalized Difference Vegetation Index (NDVI), derived from the red and near infrared (NIR) channels in electromagnetic spectrum (Tucker *et al.*, 1984). The NDVI represents amount of greenness and fractional vegetation cover (Tucker *et al.*, 1984;

Townshend and Justice 1986; Tucker *et al.*, 1986) and is an indicator of leaf area index and energy partitioning between canopy and soil below. Thus, the combination of optical bands data in terms of albedo, NDVI threshold based emissivity and thermal bands data in terms of Land Surface Temperature from satellite platform can generate evapotranspiration on spatial scale through energy balance approach.

No study was conducted yet to derive energy budget estimates over wheat crop at landscape and regional scales in Gujarat using optical and thermal based remote sensing data from satellite platform. Regional wheat yield prediction using the advantage of surface energy balance approach and optical and thermal land data over this semi-arid climate is also, therefore, a untapped research area. The present research study was formulated with the following objectives.

**Objectives:**

1. To evaluate key energy balance components, estimated using polar orbiting satellite optical and thermal data.
2. Ground validation of satellite based energy budget estimates.
3. Intercomparision of two remote sensing based wheat yield prediction approaches for dominant wheat districts of Gujarat and their validation.





# **BASIC CONCEPT OF REMOTE SENSING**



## **II. BASIC CONCEPT OF REMOTE SENSING AND ITS APPLICATION IN AGRICULTURE**

---

Remote sensing is a technique used to collect data about the earth without taking a physical sample of the earth's surface. A sensor is used to measure the energy reflected from the earth. This information can be displayed as a digital image or as a photograph. Sensors can be mounted on a satellite orbiting the earth, or on a plane or other airborne structure.

### **2.1 Sensors and the Electromagnetic Spectrum**

The majority of sensors used in airborne and space borne platforms measure reflected solar energy. Specific regions of the electromagnetic spectrum (EM) are characterized by their wavelength (the distance between 2 successive peaks or troughs of a waveform). Wavelengths are commonly expressed in terms of micrometers where a micrometer is equivalent to  $1 \times 10^{-6}$  m. Although names are assigned to different regions of the EM spectrum there are no distinct boundaries separating one region from the next. The portion of the spectrum which can be sensed by the human eye is the visible range and is only fairly narrow as shown in Figure 2.1 and Table 2.1. The visible spectrum extends from approximately  $0.4 \mu\text{m}$  to  $0.7 \mu\text{m}$  and includes the 3 primary colors blue, green and red. When the primary colors are present at equal intensities, such as in sunlight, the result is white light. Different amounts of absorption and reflection of the primary colors will result in different colors and shades of colors.

Remote sensing data may consist of a single band of information (as found in panchromatic-black and white- images) or several bands (produced by a multi spectral system). Each band represents a specific portion of the reflected light or heat from the electromagnetic spectrum. Multi spectral images are often acquired by a series of cameras each having a different filter allowing light penetration in a specific portion of

the spectrum. These bands could be combined to produce a color composite image. Cameras with filters selecting green, red and near infra red light can be combined to create a composite image that appears infra red. A camera system which selects the red, green and blue can be combined to generate an image which looks like a color photo. High resolution hyper spectral imaging devices can sense in excess of several hundred bands. These sensors generally require a fairly stable platform such as a satellite or jet plane and produce considerably larger data sets than single band systems.

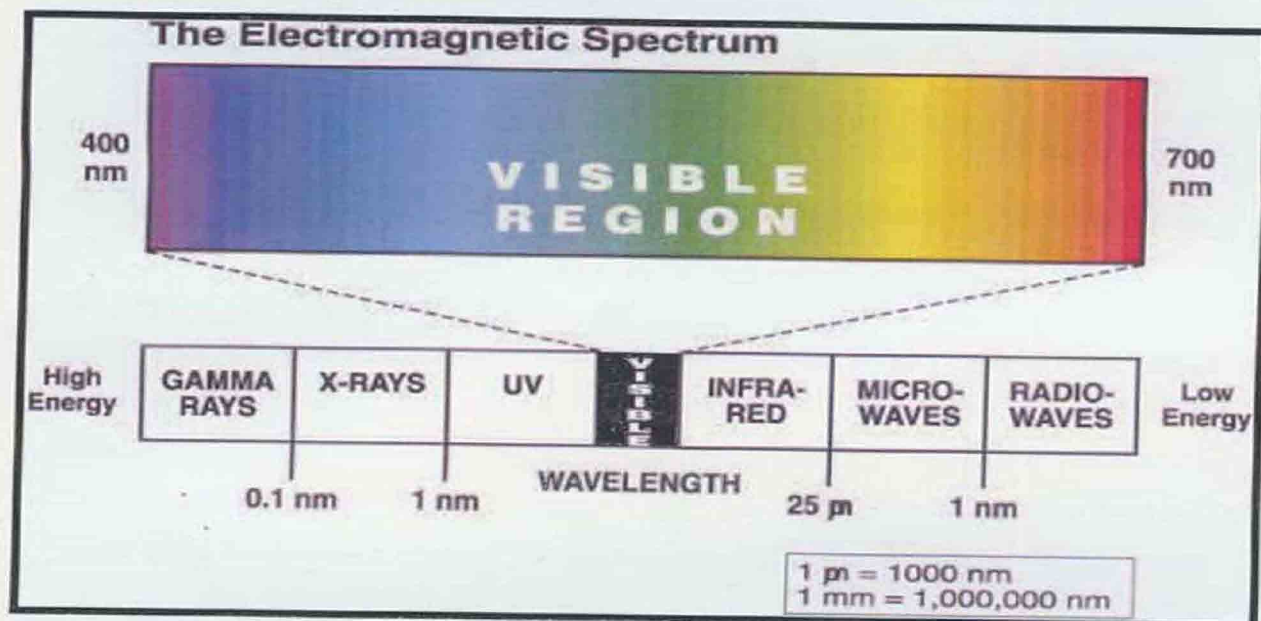


Figure 2.1 The visible region of the spectrum ranges from about 0.4  $\mu$ m to 0.7 $\mu$ m (Kyllo, 2004).

Table 2.1 Regions of Electromagnetic Spectrum

Region Name	Wavelength	Comments
Gamma Ray	< 0.03 nanometers	Entirely absorbed by the Earth's atmosphere and not available for remote sensing.
X-ray	0.03 to 30 nanometres	Entirely absorbed by the Earth's atmosphere and not available for remote sensing.
Ultraviolet	0.03 to 0.4 micrometres	Wavelengths from 0.03 to 0.3 micrometres absorbed by ozone in the

		Earth's atmosphere.
Photographic Ultraviolet	0.3 to 0.4 micrometres	Available for remote sensing the Earth. Can be imaged with photographic film.
Visible	0.4 to 0.7 micrometres	Available for remote sensing the Earth. Can be imaged with photographic film.
Infrared	0.7 to 100 micrometres	Available for remote sensing the Earth. Can be imaged with photographic film.
Reflected Infrared	0.7 to 3.0 micrometres	Available for remote sensing the Earth. Near Infrared 0.7 to 0.9 micrometres. Can be imaged with photographic film.
Thermal Infrared	3.0 to 14 micrometres	Available for remote sensing the Earth. This wavelength cannot be captured with photographic film. Instead, mechanical sensors are used to image this wavelength band.
Microwave or Radar	0.1 to 100 centimetres	Longer wavelengths of this band can pass through clouds, fog, and rain. Images using this band can be made with sensors that actively emit microwaves.
Radio	> 100 centimetres	Not normally used for remote sensing the Earth.

## **2.2 Spectral Vegetation Response**

When electromagnetic energy from the sun strikes plants, three things can happen. Depending upon the energy in the wavelength and characteristics of individual plants, the energy will be reflected, absorbed, or transmitted. Reflected energy bounces off leaves and is readily identified by human eyes as the green color of plants. A plant looks green because the chlorophyll in the leaves absorbs much of the energy in the visible wavelengths and the green color is reflected. Sunlight that is not reflected or absorbed is transmitted through the leaves to the ground.

Interactions between reflected, absorbed, and transmitted energy can be detected by remote sensing. The differences in leaf colors, size, composition and there arrangement determine how much energy will be reflected, absorbed or transmitted. The relationship between reflected, absorbed and transmitted energy is used to determine spectral signatures of individual plants. Spectral signatures are unique to plant species.

Remote sensing is used to identify stressed areas in fields by first establishing the spectral signatures of healthy plants. The spectral signatures of stressed plants appear altered from those of the healthy plants. Figure 2.2 compares the spectral signatures of healthy and stressed sugarbeets.

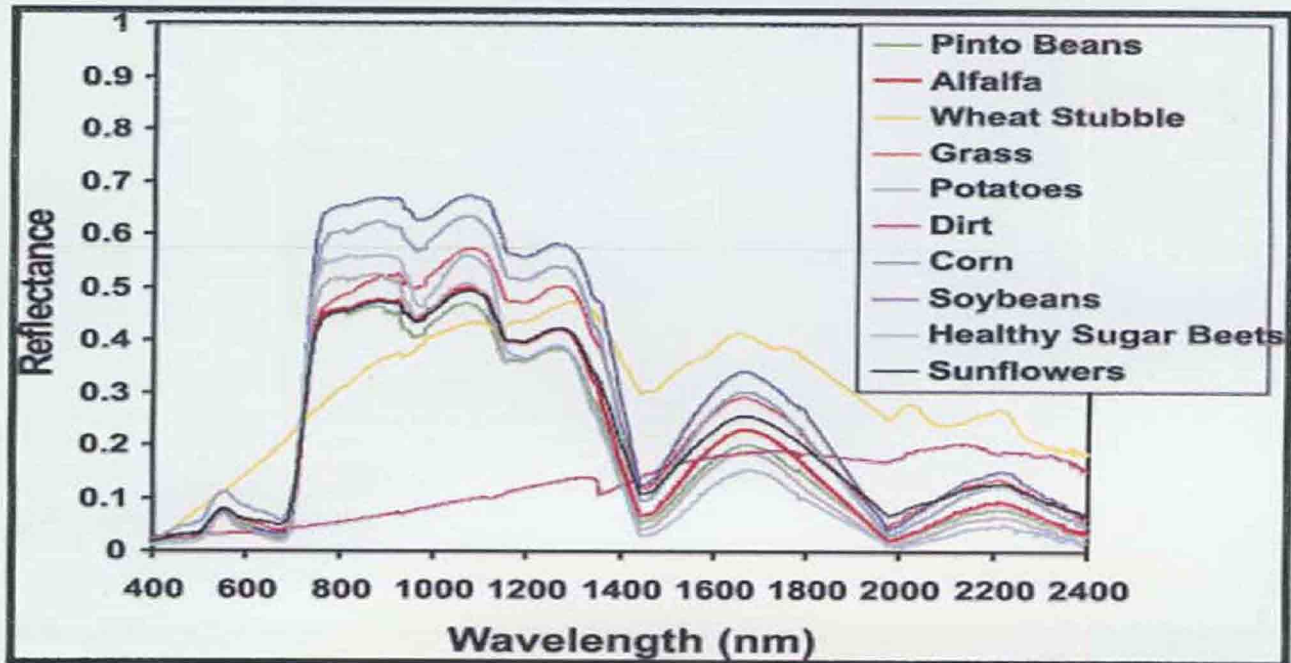


Fig. 2.2 Spectral signatures of crops and soil (Kyllo, 2003).

### 2.3 Types of Orbit of a satellite

There are several types of orbits:

1. Polar
2. Sun Synchronous
3. Geosynchronous

#### 1. Polar

The more correct term would be near polar orbits. These orbits have an inclination near 90 degrees (Figure 2.3). This allows the satellite to see virtually every part of the Earth as the Earth rotates underneath it. It takes approximately 90 minutes for the satellite to complete one orbit. These satellites have many uses such as measuring ozone concentrations in the stratosphere as well as measuring temperatures in the atmosphere.



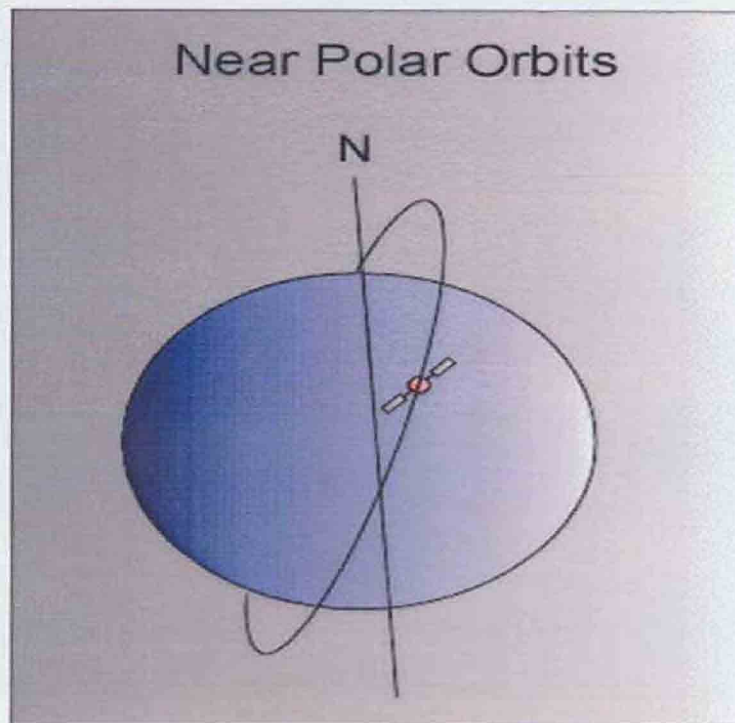


**Fig. 2.3** Polar orbit

## **2. Sun Synchronous**

This orbit allows a satellite to pass over a section of the Earth at the same time of the day. Since there are 365 days in a year and 360 degrees in a circle, it means that the satellite has to shift its orbit by approximately one degree per day. These satellites orbit at an altitude between 700 to 800 km. These satellites use the fact since the Earth is not perfectly round (the Earth bulges in the center, the bulge near the equator) will cause additional gravitational forces to act on the satellite. This causes the satellite's orbit to either proceed or recede. These orbits are used for satellites that need a constant amount of sunlight. Satellites that take pictures of the Earth would work best with bright sunlight, while satellites that measure longwave radiation would work best in complete darkness.

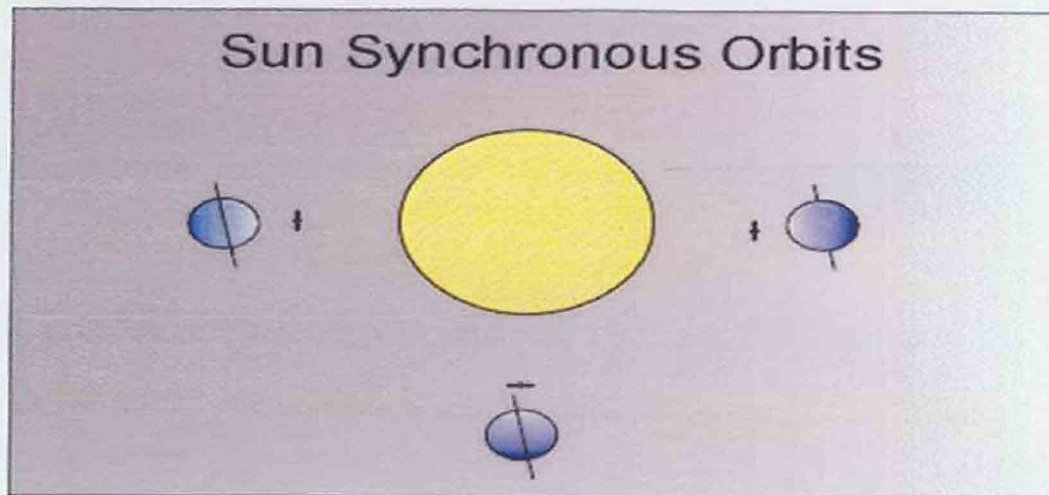


**Fig. 2.4** Sun Synchronous

### **3. Geosynchronous Orbits**

These orbits are also known as geostationary orbits. Satellites in these orbits circle the Earth at the same rate as the Earth spins. The Earth actually takes 23 hours, 56 minutes, and 4.09 seconds to make one full rotation. So based on Kepler's Laws of Planetary Motion, this would put the satellite at approximately 35,790 km above the Earth. The satellites are located near the equator since at this latitude; there is a constant force of gravity from all directions. At other latitudes, the bulge at the center of the Earth would exert a pull on the satellite.

Geosynchronous orbits allow the satellite to observe almost a full hemisphere of the Earth. These satellites are used to study large scale phenomena such as hurricanes, or cyclones. These orbits are also used for communication satellites. The disadvantage of this type of orbit is that satellites orbiting in these orbits are very far away, and hence they have poor resolution. The other disadvantage is that these satellites have trouble monitoring activities near the poles.



**Fig: 2.5** Geosynchronous Orbits

## 2.4 Sensors

There are two basic types of sensors: passive and active sensors. **Passive sensors** record radiation reflected from the earth's surface as shown in Fig. 2.6. The source of this radiation must come from outside the sensor; in most cases, this is solar energy. Because of this energy requirement, passive solar sensors can only capture data during daylight hours. The Thematic Mapper (TM) sensor system on the Landsat satellite is a passive sensor. The land cover and change analysis data provided on this CD-ROM are classified using Landsat TM imagery.

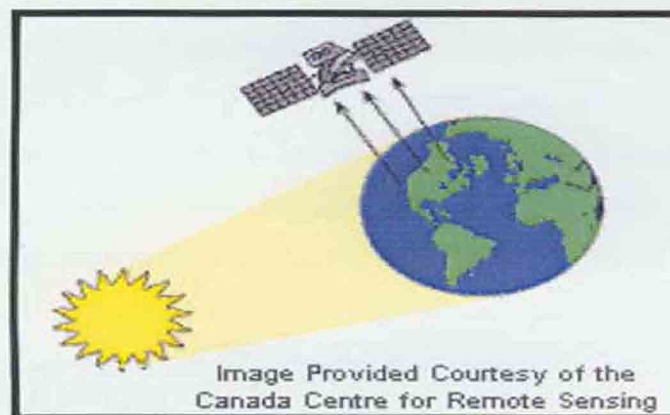


**Fig: 2.6** Example of a Passive Sensor



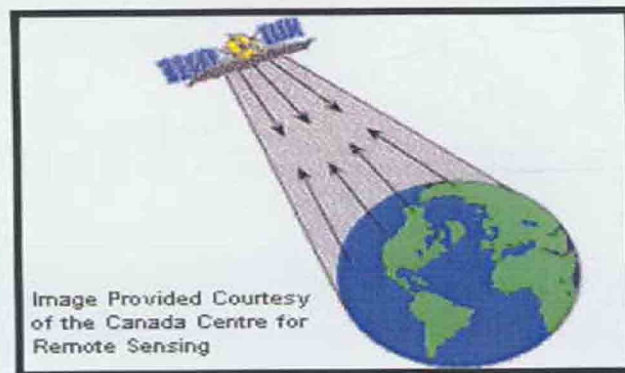


**Fig: 2.7** Example of an Active Sensor

**Active sensors** are different from passive sensors as shown in Figure 2.7. Unlike passive sensors, active sensors require the energy source to come from *within* the sensor. For example, a laser-beam remote sensing system is an active sensor that sends out a beam of light with a known wavelength and frequency. This beam of light hits the earth and is reflected back to the sensor, which records the time it took for the beam of light to return. Topographic LIDAR laser beach mapping data included on this CD-ROM are collected with an active sensor.

### **Atmospheric windows for remote sensing bands**

Atmosphere selectively transmits energy of certain wavelengths; those wavelengths that are relatively easily transmitted through the atmosphere are referred as atmospheric windows (Campbell, 1996. Introduction to Remote Sensing, Fourth Edition by James B. Campbell.)

The Earth's atmosphere is largely or partially transparent to a range of electromagnetic wavelength. All spectral regions are affected to some extent by absorption in the atmosphere but there are two nearly transparent ranges, the optical window and the radio window, and several narrow, partial infrared windows.

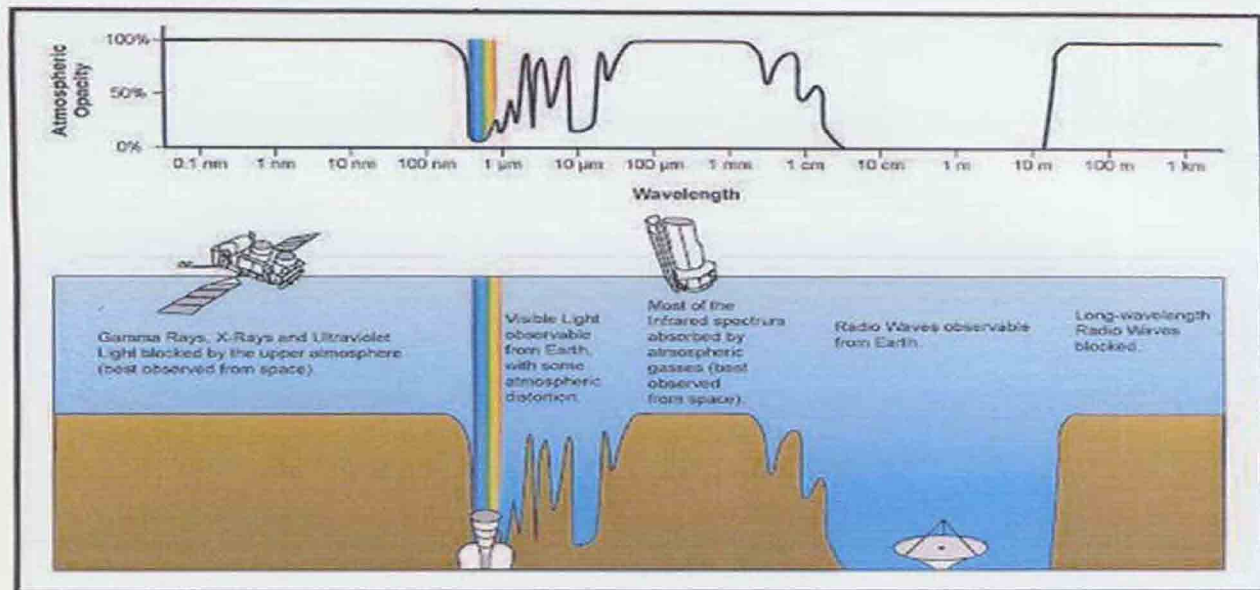


**Fig. 2.8** Atmospheric windows in the electromagnetic spectrum. (Note that the spectrum of colors from red to blue is shown in reverse.)  
Image credit: NASA

The optical window allows through visible light, from red, as far as the A band of molecular oxygen ( $O_2$ ) at 0.7600  $\mu$ , to violet and a little beyond, as far as at the ozone ( $O_3$ ) cut-off at 0.2950  $\mu$ . Shorter wavelengths are blocked by atoms and molecules of oxygen, nitrogen, and other gases, and by geocoronal hydrogen and helium.

The radio window spans a wavelength range from about one millimeter to about 30 meters. Lower wavelengths are reflected by the ionosphere, while shorter wavelengths suffer increasing amounts of molecular absorption.

Several narrow infrared windows exist at micrometer wavelengths, the photometric designations of these are J (1.25  $\mu$ ), H (1.6  $\mu$ ), K (2.2  $\mu$ ), L (3.6  $\mu$ ), M (5.0  $\mu$ ), N (10.2  $\mu$ ), and Q (21  $\mu$ ). There are also small but useable windows at 350 and 460  $\mu$ . Because water vapor is one of the main absorbers of infrared, observatories for studying infrared must be sited in particularly dry or mountainous regions where the effect of water vapor is reduced and/or the atmosphere is thinner.

**Table. 2.2** Major atmospheric windows available for remote sensing

Spectral region	Spectral Wavelength (micrometers)
Ultraviolet and visible	0.30 – 0.75
Near Infra-red	0.77 – 0.91
	1.00 – 1.12
	1.19 – 1.34
	1.55 – 1.75
	2.05 – 2.40
Middle Infra-red	3.50 – 4.16
	4.50 – 5.00
Thermal Infra-red	8.00 – 9.20
	10.20 – 12.40
	17.00 – 22.00
Microwave	2.06 – 2.22
	3.00 – 3.75
	7.50 – 11.50
	20.00 – and above

It can be seen from above Table 2.2 that all the wavelengths shorter than 0.3 micrometer are closed for remote sensing while major principal windows lie in visible, infra-red and microwave regions.

## **2.5 Remote Sensing for vegetation classification**

Vegetation is important because it provides a basic foundation for all living beings. Classifying vegetation, using remote sensing, is valuable because it can determine vegetation distribution and occurrence and how factors such as moisture, latitude, elevation above sea level, length of the growing season, solar radiation, temperature regimes, soil type and drainage conditions, topographic aspect and slope, prevailing winds, salt spray and air pollutants influence it.

Leaf properties that influence the leaf optical properties are the internal or external structure, composition, age, water status, mineral

stresses, and the health of the leaf. It is important to note that the reflectance of the optical properties of leaves are the same, regardless of the species as shown in figure 2.9. What may differ for each leaf, is the typical spectral features recorded for the three main optical spectral domains; leaf pigments, cell structure and water content.

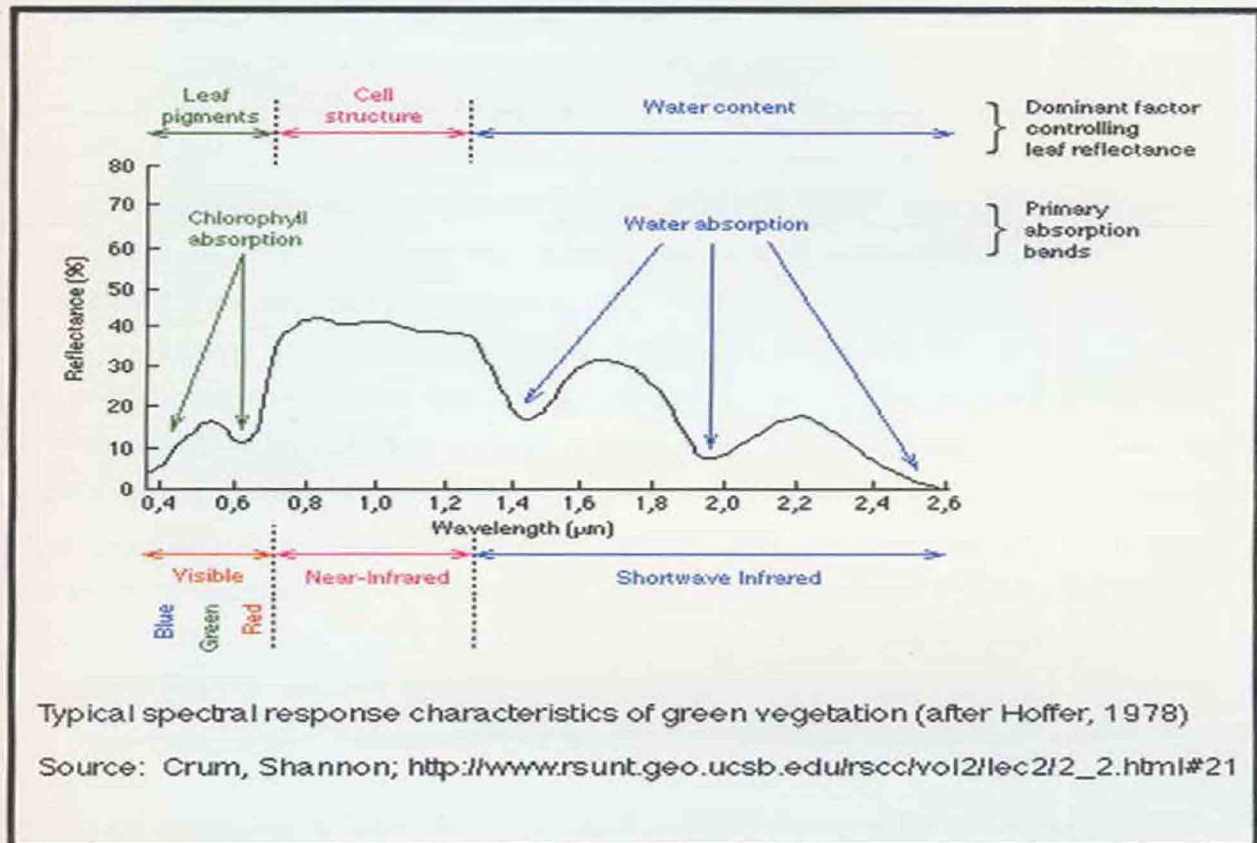


Fig. 2.9 Typical Spectral response characteristics of green vegetation

## **2.6 Resolution**

Resolution is a commonly used term in remote sensing. There are four types of resolution- spatial, temporal, spectral and radiometric.

**Spatial resolution** is the smallest unit of an image and is measured by a pixel (picture element). The spatial resolution is defined by the distance on the ground that corresponds to a single pixel. A spatial resolution of 10 meters means that an individual pixel represents an area on the ground of 10 meters by 10 meters. Thus any objects which are smaller than 10 meters will not be distinguishable in the image. A high spatial resolution (1-2 meters) has been strongly demanded for agricultural applications where within field variability is to be studied. Low spatial resolution (20-30 meters) has limited the use of satellite imagery and encouraged the development of a new generation of land observation satellites to be launched.

**Temporal resolution** is the frequency with which an image of a specific area or object can be acquired. To date, one of the problems associated with satellite imagery has been the temporal resolution. In farming systems where there is a constant change during a growing season, the time between satellite revisits has not been frequent enough for crop monitoring. Airborne systems have offered greater flexibility when scheduling flyovers, their limiting factor being local weather conditions.

**Spectral resolution** refers to the wavelength intervals to which the sensor can detect. Sensors which can discriminate fine spectral differences are said to have a high spectral resolution. For example, a sensor which can measure over a 0.05  $\mu\text{m}$  interval such as in many hyperspectral systems, has a fine spectral resolution. Detecting over a broad wavelength band of the electromagnetic spectrum such as in a 35 mm camera using color film, has a coarse spectral resolution as the film records the entire visible spectrum.



**Radiometric resolution** is the number of data file values associated with a pixel for each band of data detected. When describing a camera or sensor, this is referred to as the number of bits into which the recorded data can be divided. In a 12 bit panchromatic camera system for example, the pixel values may range from 0 (corresponding to black) where there was no electromagnetic radiation recorded to a maximum intensity or brightness value (corresponding to white) of 4096 (2<sup>12</sup>).

## **2.7 Image analysis and interpretation**

To gain the benefits from remotely sensed data, farmers and consultants must understand and be able to interpret the image. Knowledge of the commercial products (and their differences) that are available and selecting from among them the product which will offer the most value can be a challenge. The agricultural community needs knowledgeable interpreters to help improve the adoption of remote sensing. The success of image interpretation depends on the quality of the image and the experience of the interpreter.

There is a wide range of enhancement tools available which can help make an image more precisely interpretable for specific applications. Enhancement and classification tools are often used to highlight features. The techniques employed will depend on the type of remote sensed data as well as on the objectives of the end user. Techniques commonly used include:

- 1. Change detection** - studying vegetation changes by subtracting one image from another image acquired at an earlier date.
- 2. Classifications** - (both supervised or unsupervised) The pixels of an image are sorted into classes and each class is given a unique color. A supervised classification requires knowledge of the data as the analyst selects pixels that correspond to known features (such as differences in the land cover). An unsupervised classification is more computer automated and clusters pixels which have similar spectral characteristics.

**Table 2.3 Current and Future Indian Satellite Missions**

Satellite	Sensors	Band interval ( $\mu\text{m}$ )	Spatial resolution	Temporal resolution (days)	Agricultural usage
<b>Polar orbiting</b>					
CARTOSAT-2	Pancromatic camera (PAN)	0.45 to 0.85 $\mu\text{m}$	0.8 m	4 days	The data from the satellite will be used for detailed mapping and other cartographic applications at cadastral level, urban and rural infrastructure development and management, as well as applications in Land Information System (LIS) and Geographical Information System (GIS).
IRS-P5 (CARTOSAT - 1)	Charge Coupled Devices		2.5 m	5 days	Surveillance, disaster management etc.
IRS-P6 (RESOURCE SAT-1)	LISS-III (medium resolution multi-spectral sensor)	Band 2 (green 52-59 $\mu\text{m}$ ) Band 3 (red 0.62 - 0.68 $\mu\text{m}$ ) Band 4 (NIR 0.77-0.86 $\mu\text{m}$ ) Band 5 (SWIR 1.5- 1.7 $\mu\text{m}$ )	23.5 m	25 days	To provide continued remote sensing data services on an operational basis for integrated land and water resources management at micro level, with enhanced spectral and spatial coverage and stereo imaging.

							To further carry out studies in advanced areas of user applications like improved crop discrimination, crop yield, crop stress, pest/disease Surveillance, disaster management etc.
	LISS-IV (A high resolution multispectral sensor)	Band 2:0. (green 52-59 $\mu\text{m}$ ) Band 3 (red: 0.62 - 0.68 $\mu\text{m}$ ) Band 4 (NIR: 0.77 - 0.86 $\mu\text{m}$ ) Band 5 (SWIR)	5.8 m	5 days			
	AWiFS (An Advanced Wide Field Sensor)	Band 2 (green 52-59 $\mu\text{m}$ ) Band 3 (red 0.62 - 0.68 $\mu\text{m}$ ) Band 4 (NIR 0.77 - 0.86 $\mu\text{m}$ ) Band 5 (SWIR 1.5 - 1.7 $\mu\text{m}$ )	56 m	5 days revisit period			



Geostationary					
KALPANA-1/ METSAT	VHRR	Visible (VIS : 0.55-0.75µm), water vapour (WV : 5.7-7.1µm), Thermal infrared (IR : 10.5-12.5µm)	2km x 2km 8km x 8km 8km x 8km	At hourly interval	Meteorological and agro-meteorological applications
INSAT-3A	VHRR	Visible (VIS : 0.55-0.75µm), water vapour (WV : 5.7-7.1µm), Thermal infrared (IR : 10.5-12.5µm)	2km x 2km 8km x 8km 8km x 8km 1km x 1km 1km x 1km 1km x 1km	At three hourly interval	
	CCD	Red (0.62-0.68µm). Near infrared (0.77-0.86µm), Shortwave infrared (1.55-1.69µm)			

In future, the launch of INSAT-3D geostationary satellite with six channel 'Imager' with 4km split thermal channels and 19-channel 'Sounder', and RISAT-1 with active microwave payload, SAR (Synthetic Aperture Radar) would help in crop health monitoring.

## **2.8 Potential Agricultural Applications of Remote Sensing**

### **2.8.1 Crop inventory and yield prediction**

At the regional and national scale, the USDA's National Agricultural Statistics Service (NASS) and the Foreign Agricultural Service (FAS) have explored the use of remotely sensed images for crop identification, inventory of areas planted and estimation of potential harvest amounts (Wade *et al.*, 1994). For grain crops, images near the time of flowering (i.e. tasseling in corn) are optimal for yield forecasting. Upon reaching the reproductive stage, most grain crops have completed their vegetative growth; therefore, yield influencing developments occurring after flowering may not be visible in the canopy. For other plants such as soybeans, more accurate yield predictions may be obtained later in the growing season due to continued vegetative development of the plants that reveal influences on yield. Current methods of yield prediction are often based on vegetation indices such as the Normalized Difference Vegetation Index (NDVI). These indices combine image information from near infrared and visible red bands in ratios of various forms. At the scale of farm and field, remotely sensed images have been used to give relative estimates of yield variation within a field prior to harvest. These compare well with actual yield maps. In India, Crop Acreage and Production Estimation (CAPE) is operational to make regular inventories of major crops (rice, wheat, cotton, potato etc.) using IRS-LISS III and IRS-P6 AWiFS data. This gives single forecast within the crop season. In FASAL (Forecasting Agriculture output using Space Agrometeorology and Land based observations) programme, multiple crop forecasts within a crop season are addressed.

## **2.8.2 Useful agromet parameters retrievable with satellite based RS data**

Some useful parameters related to agrometeorology can be retrieved using optical, thermal infrared and microwave data from satellite platform.

### **A. Vegetation indices**

Using the distinct spectral signature of plants with low reflectance in the visible (0.4-0.7  $\mu\text{m}$ ) and very high reflectance in the near infrared region (0.7-1.2  $\mu\text{m}$ ) of the solar spectrum, the spectral contrast can be used for identifying the presence of green vegetation and evaluating some characteristics (e.g., cover and biomass) through various vegetation indices, such as the Normalized Difference Vegetation Index (NDVI).

The Normalized Difference Vegetation Index (NDVI) is a simple numerical indicator that can be used to analyze remote sensing measurements, typically but not necessarily from a space platform, and assess whether the target being observed contains live green vegetation or not.

$$NDVI = \frac{(NIR - RED)}{(NIR + RED)}$$

The reason NDVI is related to vegetation is that healthy vegetation reflects very well in the near infrared part of the spectrum. Green leaves have a reflectance of 20 percent or less in the 0.5 to 0.7 micron range (green to red) and about 60 percent in the 0.7 to 1.3 micron range (near infra-red). The visible channel gives some degree of atmospheric correction. The value is then normalized to the range  $-1 \leq NDVI \leq 1$  to partially account for differences in illumination and surface slope.

NDVI provides a crude estimate of vegetation health and a means of monitoring changes in vegetation over time. The possible range of

values is between -1 and 1, but the typical range is between about -0.1 (NIR less than VIS for a not very green area) to 0.6 (for a very green area).

**Simple Ratio:** It is a ratio of near infrared to red reflectance and is related to change in amount of green biomass, pigment content as well as its concentration and leaf water stress etc.

$$SR = NIR/RED$$

#### **SAVI (Soil-Adjusted Vegetation Index)**

Soil-Adjusted Vegetation Index L ranges from 0 for very high vegetation cover to 1 for very low vegetation cover, minimizes soil brightness- induced variations. L = 0.5 can reduce soil noise problems for a wide range of LAI.

$$SAVI = \frac{\rho_{NIR} - \rho_R}{\rho_{NIR} + \rho_R + L} * (1 + L)$$

#### **PVI (Perpendicular Vegetation Index)**

Perpendicular Vegetation Index, orthogonal to the soil line, attempts to eliminate differences in soil background and is most effective under conditions of low LAI and is applicable for arid and semi-arid regions.

$$PVI = \frac{\rho_{NIR} - a\rho_R - b}{\sqrt{a^2 + 1}}$$

#### **EVI (Enhanced Vegetation Index)**

The enhanced vegetation index (EVI) was developed to optimize the vegetation signal with improved sensitivity in high biomass regions and for improved vegetation monitoring through a de-coupling of the canopy background signal and a reduction in atmosphere influences. The equation takes the form,

$$EVI = G * \frac{P_{NIR} - P_{Red}}{P_{NIR} + C_1 * P_{Red} - C_2 * P_{Blue} + L}$$

where,

$P_{NIR}$  = NIR Reflectance

$P_{Red}$  = Red Reflectance

$P_{Blue}$  = Blue Reflectance

$C_1$  = Atmosphere Resistance Red Correction Coefficient

$C_2$  = Atmosphere Resistance Blue Correction Coefficient

$L$  = Canopy Background Brightness Correction Factor

$G$  = Gain Factor

The coefficients adopted in the EVI algorithm are,  $L=1$ ,  $C_1 = 6$ ,  $C_2 = 7.5$ , and  $G$  (gain factor) = 2.5.

### **NDWI (Normalised Difference Water Index)**

It is well known that the SWIR is absorbed by water irrespective of whether water exists as free water bodies or the water contained in plant cells. To assess water content in a normalised way, the NDWI (Normalised Difference Water Index) was introduced by Gao (1996). This index increases with vegetation water content or from dry soil to free water.

NDWI can be used to detect drought stress and is expressed as-

$$NDWI = NIR - SWIR / NIR + SWIR$$

### **B. Surface albedo**

The amount of solar radiation (0.4 - 4.0  $\mu m$ ) reflected by a surface is characterized by its hemispherical albedo, which is defined as the reflected radiative flux per unit incident flux. This is an important parameter for computing earth radiation budget and climate models. Pre-requisite for its computation is generation of broadband surface reflectances. The computation is basically double integration, over wavelength and angular geometry. The following algorithms of albedo retrieval are in use world over.

- (i) Narrow band-to-broad band conversion and / or conversion of broadband reflectances to shortwave band
- (ii) Minimum ground brightness in a time series
- (iii) Contrast ratio approach
- (iv) BRDF method

### **C. Land Surface Temperature (LST)**

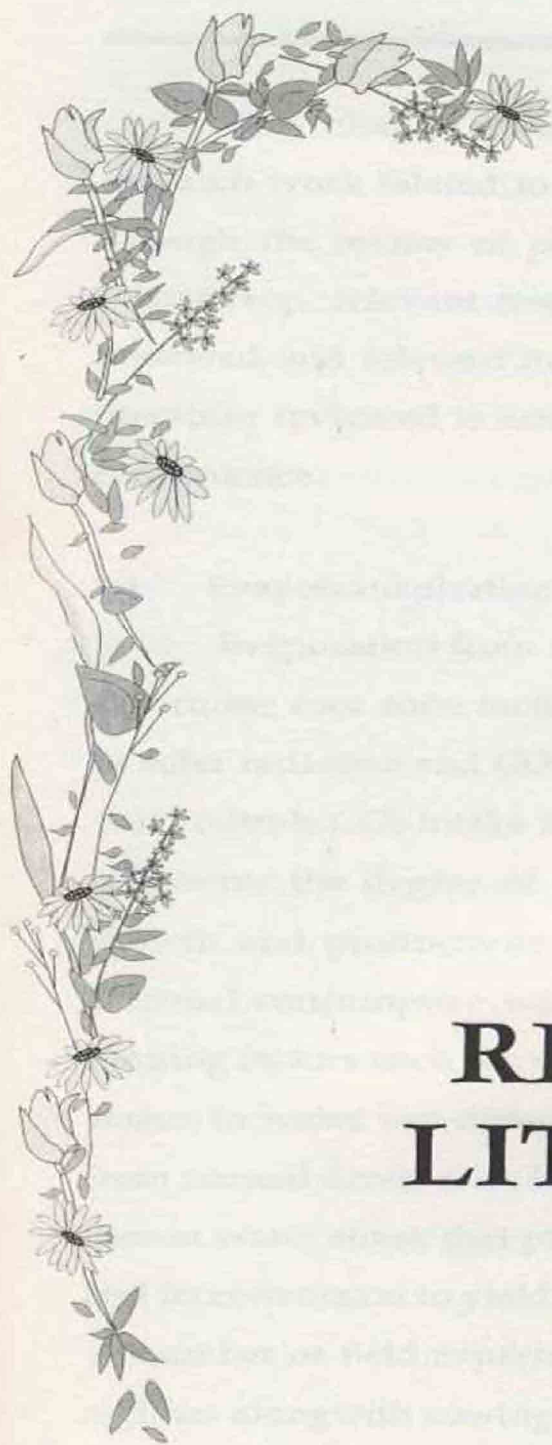
Surface temperature is an important quantity for crop modeling such as energy and water exchange between atmosphere and vegetation surface. Three major categories of LST retrieval algorithm have been developed (i) Mono window (ii) Split window and (iii) multiangle methods (Dash *et al*, 2002) based on sensor characteristics. Technique (i) produces least accuracy (3 – 4K) when single thermal channel as in INSAT 3A / Kalpana – 1 VHRR is available. Local or general split-window technique can be applied when two or more thermal channels are available as in case of NOAA AVHRR and MODIS TERRA/AQUA respectively. This technique is able to compensate for water vapour but requires prior estimation of surface emissivity. The error is of the order of 2-3K. The multi-angle method can work with advanced sensors such as ASTER and allows separation of component temperatures, such as foliage and soil.

### **D. Surface wetness / surface soil moisture**

Regional and national agricultural drought monitoring are highly dependent on spatial and temporal variability of large area soil moisture or wetness information. It is difficult to collect reliable information over a large area using conventional methods involving point measurements. Generally, thermal and microwave sensors are used for surface moisture estimation. Thermal IR techniques include (i) thermal inertia (van de Griend *et al.*, 1985), (ii) temperature-vegetation triangular space (Gillies *et al.*, 1997), (iii) Directional thermal radiometry and, (iv) morning rise in land surface temperature (Wetzel and Woodward, 1987). Microwave

radiations are capable of penetrating clouds and vegetation cover and hence microwave sensors offer great potential in soil moisture determination over cropped areas. The measurement of soil water content by means of microwave sensors relies on the large difference between the dielectric properties of dry soil and liquid water. Microwave RS techniques have been shown to provide soil moisture estimates in the upper layer of soils up to 10cm. Both active and passive microwave sensors are being used for moisture estimation. The major drawback with the passive sensors is their poor spatial resolution.

With the launch of the AQUA satellite in June 2002 and ADEOS II in December 2002, data from the Advanced Microwave Scanning Radiometer (AMSR) are becoming available at two equatorial overpass times per day. The C-band of the AMSR (6.9 GHz) has better sensitivity than the 19.4 GHz channels of the Special Sensor Microwave Imager (SSM/I) for retrieving soil moisture. In the past, soil moisture has been measured from space using SSM/I with the 19, 37, and 85 GHz channels. The sensitivity is higher at lower frequencies (L-band: 1.4 GHz and C-band: 6.9 GHz) and decreases as the frequency of observation increases due to increased contribution from the atmosphere and vegetation.



# REVIEW OF LITERATURE





### III. REVIEW OF LITERATURE

---

This chapter contains the available literature published on the research work related to the problem chosen as reviewed by the author. Though the review of pertinent literature has been mainly confined to wheat crop, relevant research work on some other crops has also been reviewed and relevant information is included wherever necessary. The literature reviewed is arranged under the following broad headings, for convenience.

#### 3.1 Evapotranspiration versus crop growth and yield

Evaporation from soil surface and transpiration from crop canopy determine root zone moisture availability for photosynthesis in presence of solar radiation and CO<sub>2</sub>. Water stress effects regulate stomatal opening that controls CO<sub>2</sub> intake and radiation use. Therefore, water use strongly influences the degree of radiation use and CO<sub>2</sub> intake by crops. Crop growth and productivity are ultimately influenced in a major way by seasonal consumptive water use i.e. cumulative ET in addition to other limiting factors such as : nutrients, pest and disease. Sensitivity of growth stages to water use differ from crop to crop. Stage specific ET anomaly from normal determines likelihood of occurrence of early, middle and late season water stress that produce differential effects on final crop biomass and its conversion to yield.

A number of field experiments were conducted with different irrigation regimes alongwith sowing dates to quantify water use or ET and biomass or yield relations in different crops including Wheat (*Triticum aestivum* L.). Yields in the inland Pacific Northwest were limited by inadequate water supply late in the growing season. Choosing a suitable planting date and genotype with the appropriate phenology that matches crop growth to the water supply will produce optimum grain yields. A study was conducted (Chen *et al.*, 2003) to investigate the effects of (i) planting

and (ii) wheat genotype differences on grain yield, evapotranspiration (ET), and water-use efficiency (WUE). A 3-yr experiment was conducted on a Walla Walla silt loam (coarse-silty, mixed, mesic Typic Haploxeroll) near Pendleton. Six winter and two spring wheat cultivars were planted in seven planting treatments (planting practices that include planting date, seeding rate, drill type, row space, and seeding depth). Planting treatments significantly affected ET after adjusting for vapor pressure deficit (ET/VPD). Winter and spring wheat planted in the spring had approximately 380 to 650 mm kPa<sup>-1</sup> less ET/VPD (approximately 110–160 mm ET) than that planted in the fall. However, WUE was not significantly affected by planting treatments and cultivars.

Kiziloglu *et al.*, (2006) conducted field experiments to study the effects of water deficits on potato (*Solanum tuberosum* L.) evapotranspiration, tuber yield and water-use efficiency. The experiments were carried out under cool season semiarid climatic conditions in Erzurum province located in the east of Turkey in spring seasons during 2003 and 2004. The experiment included six water deficits: 0% (well-irrigation), 20, 40, 60, 80 and 100% (non-irrigation). Results indicated that deficit irrigation influenced evapotranspiration, tuber yield and water-use efficiency. Potato evapotranspiration decreased as water deficit increased. Seasonal evapotranspiration was 445.2 mm in well-irrigated treatment and 195.2 mm non-irrigated treatment. Potato yield and water-use efficiency were also found to decrease as water deficit increased. Potato yield of well-irrigated treatment was 26.43 t ha<sup>-1</sup> while it was 8.28 t ha<sup>-1</sup> in non-irrigated treatment. A linear relationship was found between evapotranspiration and tuber yield. Water use efficiency was 59.56 kg/ha/mm for well-irrigated treatment and 42.13 kg/ha/mm for non-irrigated treatment. The seasonal yield response factor ( $k_y$ ) for potato was also found as 1.1

A crop water-stress sensitivity index was developed by Zhang *et al.* (1999) and also the establishment of the relationship between seasonal evapotranspiration (ET) and wheat yield, and crop water production functions for North China plain. By relating relative yield to relative ET deficit, they found that crop was more sensitive to water stress between stem elongation to heading and from heading to milking stages. Grain yield response to the amount of irrigation (IRR) was developed using a quadratic function and was used to analyze different irrigation scenarios.

The effect of water supply on seasonal absorption of photosynthetically active radiation and radiation-use efficiency (RUE) of aboveground biomass production was studied by Manderscheid and Weigel (2007) to understand the processes contributing to final yield. Wheat was grown under sufficient water supply or drought stress in lysimeters with a soil depth of 0.4 m (first year) or in the field with unrestricted root growth (second year). Drought stress was started after the first node stage by halving the water supply. Drought stress always decreased the green area index and accelerated canopy senescence, which in the second year resulted in a decrease of 23% in the seasonal radiation absorption. .

Fractional ground cover, fractional PAR interception ( $f$ ), canopy extinction coefficient ( $k$ ) and radiation-use efficiency (RUE) for wheat, pea and mustard were examined in a field experiment conducted over 5 years in a semi-arid environment in Australia by O'Connell *et al.*, (2004). Two crop sequences were compared: fallow-wheat-pea and mustard-wheat-pea. Significant periods of water stress occurred in some years. Complete ground cover was not achieved and  $f$  ranged to maxima of 0.77, 0.80 and 0.80 in wheat, pea and mustard, respectively. Estimates of  $k$  for wheat, pea and mustard were 0.82 ( $\pm 0.05$ ), 0.76 ( $\pm 0.03$ ) and 0.68 ( $\pm 0.12$ ), respectively. Estimated RUE (aboveground biomass) of 1.81 ( $\pm 0.05$ ), 1.52

( $\pm 0.05$ ) and  $1.92 (\pm 0.12) \text{ g MJ}^{-1}$  intercepted PAR for wheat, pea and mustard, respectively which was measured over the vegetative phase. Seasonal conditions had minimal impact on  $k$  and RUE. Radiation use efficiency was generally lower than the maxima reported in the literature. But they were similar to others reported in comparable environments and matched predicted unstressed RUE for  $C_3$  plants.

### **3.2 Evapotranspiration using surface energy balance**

Broadly two approaches are used for deriving evapotranspiration (ET) using water balance and energy balance method. Water balance ET is conventionally measured through Lysimeter generally on weekly basis, but not on daily and diurnal basis. Moreover, installation of lysimeter disturbs the naturality of agricultural site. Simulation of soil water balance also generates ET on daily basis (Bhattacharya and Sastry, 2000). Diurnal energy balance measurements can lead to compute ET on hourly, as well as on daily basis. It was proved by Wallace (1995) from analysis of multiple year datasets over different crops over multiple locations that energy balance ET is more representative than water balance ET due to the consideration of surface resistances from canopy and soil.

#### **3.2.1 Using *in situ* measurements**

##### **3.2.1.1 Field scale**

Studies were conducted to measure radiation and energy balance components diurnally using portable equipment at periodic interval over crop fields to derive energy balance components to obtain latent heat fluxes which are convertible to ET. These were correlated with crop phenological stages and growth behaviour. The energy balance components were measured above the surface of an irrigated wheat and maize field over three successive years using the Bowen ratio technique

by Shen-YanJun *et.al.* (2004). The experiments were carried out at Luancheng Experimental Station of Agro-ecosystem (LESA), Heibei, China, from December 1999 through to September 2001. The latent heat flux LE also showed apparent correspondence with the development of phenology, e.g. LAI. The diurnal course of the Bowen ratio in different seasons which can be categorized into three typical patterns: (1) a 'wheat pattern', characterized by a steep morning peak followed by a decrease with the daytime mean value of around 0.30; (2) a 'maize pattern', which is a relatively flat course with a daytime mean beta of around 0.20-0.25; and (3) a 'winter pattern', with a near-noon high peak with a daytime mean data of more than 10 times than those for wheat or maize. There were linear correlations between evaporative fraction (EF) and LAI for both wheat and maize before senescence. The correspondence of EF appeared more dependent on LAI for maize than for wheat. The EF did not appear correlated to soil water status, whereas the Bowen ratio was affected by extractable soil water content for wheat to some extent. No correlation for maize was found.

Surface energy fluxes were measured over irrigated groundnut during winter (dry) season using Bowen ratio ( $\beta$ ) micrometeorological method in a representative groundnut growing areas of eastern India, i.e. Dhenkanal, Orissa by Kar and Kumar (2007). The experiment was conducted to optimize irrigation scheduling in groundnut. Study revealed that net radiation ( $R_n$ ) varied from 393–437 to 555–612  $\text{Wm}^{-2}$  during two crop seasons (2004–2005 and 2005–2006). The soil heat flux ( $G$ ) was higher ( $37\text{--}68 \text{ W m}^{-2}$ ) during initial and senescence growth stages as compared to peak crop growth stages ( $1.3\text{--}17.9 \text{ W m}^{-2}$ ). The latent heat flux (LE) showed apparent correspondence with the growth which varied between 250 and 434  $\text{W m}^{-2}$  in different growth stages. The diurnal variation of Bowen ratio ( $\beta$ ) revealed that there was a peak in the morning (9.00–

10.00 a.m.) followed by a sharp fall with the mean values varying between 0.24 and 0.28.

### 3.2.1.2 Landscape scale

Generally, Bowen ratio, micrometeorological and eddy correlation towers are used for diurnal measurements of sensible and latent heat fluxes that represent fluxes over a fetch. Fetch represents horizontal uniformity of the landscape irrespective of height. Tower heights are determined from fetch ratio. For agricultural studies these ratios varied from 1: 50 to 1:100. So, when tower height is 10m, fetch should be 1000m if ratio is 1:100. It depends on the goal of experiment.

A couple of studies of tower based observations were organized through international programmes. The use of Bowen ratio or eddy covariance towers, with sufficient fetch (Anthoni *et al.* 2004), was demonstrated in different field campaigns for validating surface energy and water fluxes in FIFE (First International Satellite Land Surface Climatology Project Field Experiment)(Sellers *et al.* 1988, Hall *et al.* 1992), EFEDA (Echival Field Experiment in Desertification Threatened Area) (Bolle and Streckenbach 1993), Monsoon'90 (Kustas *et al.* 1994), Soil Moisture-Atmosphere Coupling Experiment (SMACEX02) (Su *et al.* 2005), Oklahama mesonet (Kustas *et al.*, 2006), SMOSREX (Rosnay, 2005).

In order to study energy and water cycles in the Huaihe River Basin, micrometeorological measurements were carried out in Shouxian County, Anhui Province, during HUBEX/IOP (May to August 1998 and June to July 1999). The employed techniques included Bowen Ratio-Energy Balance (BREB) and Eddy Covariance (EC) methods. The basic characteristics of energy balance components in the district were analyzed by Zhu *et al.*, 2003. Furthermore, the results were compared with those from other regions of China. The main results were as follows: (1) There was a consistency between the available energy ( $R_n - G$ ) and the sum

of sensible (H) and latent (E) when heat fluxes were measured by the EC method (H+E)<sub>ec</sub>, but E<sub>br</sub> was slightly larger (about 10%) than E<sub>ec</sub>; (2) Most of the net radiation (R<sub>n</sub>) was used to evaporate water from the surface. During HUBEX/IOP in 1998 and 1999, the mean daily amounts of R<sub>n</sub> were 13.89 MJ m<sup>-2</sup>d<sup>-1</sup> and 11.83 MJ m<sup>-2</sup>d<sup>-1</sup>, and the mean Bowen Ratios ( $\beta$ ) were 0.14 (over ruderal) and 0.06 (over paddy) respectively; (3) The diurnal variation characteristic of  $\beta$  was larger and unsteady at sunrise and sunset, and smaller and steady during the rest of the daytime. Local advection appeared in the afternoon over paddy areas in 1999; (4) In comparison with the results from other regions of China, the mean  $\beta$  was the lowest (0.06) over paddy areas in the Huaihe River Basin and the highest (0.57) during June–August 1998 in Inner Mongolia grassland. The Bowen Ratio  $\beta$  is mainly related to the soil humidity.

A land surface processes experiment was carried out during January 1997 to February 1998 in Gujarat region to validate surface flux outputs (Rajagopal, 2001) from global circulation model (GCM) at 1°X1°. Five 10m micrometeorological towers were located at Anand (AN), Sanand (SN), Derol (DE), Arnej (AR), Khandha (KH) with Anand as central location. The effects of bare land and cropped surfaces on radiation and energy fluxes were examined by Shekh *et.al* (2001) during intensive observational period of May, July, September and December during the Land Surface Processes Experiment (LASPEX) in 1997 in Gujarat, India. Cover crops included short grass, sunnhemp, groundnut and wheat with different canopy heights. Results revealed that net radiation varied with crop density. Reflectivity of short wave radiation was reduced in cropped fields. Sensible heat flux was greatest during May and December, and least during July and September. Latent heat fluxes were higher during the monsoon season.

### 3.2.1.3 Regional scale

The problems associated with the validation of satellite-derived estimates of the surface fluxes at regional scale ( $> 1\text{km}$  spatial scale) were addressed to and the possibility of using the Large Aperture Scintillometer (LAS) was investigated by Watts *et al* (2000). Area integrated continuous measurements of sensible heat flux and ET in combination with average Bowen ratio or net radiation over a spatial scale of 250m to 4.5km could be done using scintillometry with LAS. This is now a generally accepted device for routinely obtaining area-averaged sensible heat flux even on a scale of upto 10 km. This is independent of fetch requirement and is applicable for regional flux measurements over heterogeneous terrain also. These measurements are now being used for direct validation of sensible and ET estimates from moderate to coarser resolution satellite sensor (ERS2/ATSR2, VEGETATION, LANDSAT7, NASA-EOS) observations.

Data were collected over an extensive site of semi-arid grassland in northwest Mexico during the summer of 1997 as part of the semi-arid land-surface-atmosphere (SALSA) program Chehbouni *et al* (1998). These data were used to validate NOAA AVHRR sensible heat fluxes and ET, which is an optical instrument that consists of a transmitter and receiver. In practice, the LAS beam height often varies along the path due to a variety of reasons. Hartogensis *et al.* (2003) explained what effective height to use in such situations, while analyzing scintillometer data to derive sensible heat flux. Several aspects were covered: a slanted path over flat terrain, structured terrain, and varying path height due to the curvature of the earth's surface. To test the derived effective height formulation present LAS data taken in September and October 1996 at a rangeland site in Sonora, Mexico were used. In experiment 1, the LAS was set up over a slant path, ranging roughly between 10 and 45 m above the



surface over a 3200-m path. In experiment 2, a horizontal LAS path was used at approximately 30 m over a path length of 1100 m. The resulting sensible heat fluxes were compared with eddy-covariance data and show satisfactory results for both the full and one of the approximate formulations of the effective height.

An incoherent scintillometer with 0.31-m aperture was tested along a 9.8-km path over grassland. Scintillometer derived heat fluxes were compared with *in situ* eddy covariance measurements by Kohsiek *et al.* 2002. Albeit with considerable scatter, the fluxes compared well with each other during daytime. During nighttime credible fluxes were also obtained. The scintillometer functioned satisfactorily for 96% of the seven-week period.

Large Aperture Scintillometers, Bowen ratio and eddy covariance measurements were employed to study sensible heat flux over homogeneous bare soil surface from March 20<sup>th</sup> to April 20<sup>th</sup>, 2002, at XiaoTangshan area, Beijing by Shaomin *et al* (2003). The diurnal variation of sensible heat flux from LAS was analyzed to find out relation between sensible heat flux and weather conditions. Further, test comparisons of the scintillometer flux measurements with the measurements of Bowen ratio and eddy correlation methods had shown good agreement; the correlation coefficients were over 0.8.

To validate the accuracy of remote sensing flux model and to test the sensitivities of parameters, one Large Aperture Scintillometer (LAS), one Eddy covariance (EC) system and other supporting observations were used to estimate sensible heat flux of a typical natural surface by Zhu *et al* (2004). The remote sensing model was Surface Temperature - Resistance (STR) model. The results obtained from different spatial scales were inter-compared. Shows that (1) there are better changing trend of sensible heat fluxes obtained by LAS and EC and STR methods; (2) the

remote sensing assessed sensible heat flux was a good agreement with measurements by using LAS and EC,  $H_{STR}$  is rough 8% larger than  $H_{LAS}$ , (3) LAS is reliable to validate pixel sensible heat flux derived by remote sensing model.

A large-aperture scintillometer (LAS) was operated continuously during a period of more than one year over a heterogeneous land surface in Central Europe at the transition between marine and continental climates by Beyrich *et al* (2002). The LAS measurements of the refractive index structure parameter,  $C_N^2$ , were used to estimate the sensible heat flux. This was possible for about 60 to 80% of the time under daytime conditions during the summer, with lower values obtained for the cold season (October to March). Using data from a three-week long field experiment, the LAS-based heat flux was compared with a weighed average of local heat flux measurements over the main land use classes (forest, agriculture, water) in the area, resulting in reasonable agreement. LAS-based heat fluxes were then used for comparison with the heat flux values of a numerical weather prediction model. An over-prediction of the model heat flux was found in summer but the model values were lower than the LAS derived data during the cold season.

Schuttemeyer *et al* (2006) conducted a study to examine the seasonal cycle of the components of the surface energy balance in the Volta basin in West Africa as part of the GLOWA-Volta project. The regional climate is the basin characterized by a strong north-south gradient of mean annual rainfall and the occurrence of pronounced dry and wet seasons within one annual cycle, causing a strong seasonal variation in the natural vegetation cover. The observations were conducted with a combined system, consisting of a Large Aperture Scintillometer (LAS) for areally averaged sensible heat flux, radiometers and sensors for soil heat flux. For comparisons the eddy-covariance (EC)

method providing the fluxes of momentum, sensible and latent heat were utilized as well. The measurements of a seasonal cycle in 2002/2003 were gathered including the rapid wet-to-dry transition after the wet season at two locations in Ghana, one in the humid tropical southern region and one in the northern region. A direct comparison and the energy balance disclosure of two methods was investigated for daytime and nighttime separately. An attempt was made to understand and explain the differences between the results of the two methods and the closure of energy budget found for these. It was found that the two systems corresponded well during daytime. During nighttime the LAS seems to perform more realistically than the EC system. Considering the fact that a LAS system was much easier to use in the climate conditions of the Volta basin, it is concluded that the LAS approach was very suitable in this type of climate conditions.

A large aperture scintillometer (LAS) and radiowave scintillometer (RWS) were installed over a heterogeneous area Meijninger *et al.* (2004) to test the applicability of the scintillation method. The water vapour fluxes derived from combined LAS-RWS system, also known as two-wave length method, agreed fairly well with aggregated water vapour fluxes derived from in-situ eddy covariance measurements. The water vapour fluxes derived from a stand-alone LAS were also analyzed. It was found that a single LAS and an estimate of the area averaged available energy (using a simple parameterization scheme) could also provide also reasonable area-averaged water vapour fluxes.

### 3.2.2 Model simulation

Many parameterization schemes were developed to model land surface processes. These are called LSMs. These models are mostly embedded in regional or global climate models Such as: MM5, WRF for

regional, T80, T120 . These models were also used with biosphere component together called soil vegetation atmosphere transfer (SVAT) schemes . Off-line runs of SVATs simulate energy balance components.

Nagai (2003) described the validation and sensitivity analysis of an atmosphere-soil-vegetation model. The model consisted of one-dimensional multilayer sub models for the atmosphere, soil and vegetation and a radiation scheme for the transmission of solar and long wave radiation in the canopy. The model framework was validated by the comparison of ground measured surface heat fluxes between calculations and observations. The total LH on the cloudy day increased and the difference between the total LH on the clear and cloudy days became small in the new models. While by changing the stomatal resistance scheme from Deardorff to the Jarvis-type scheme, the underestimation of LH at morning decreased, but the overestimation of LH at midday remained.

A model was developed by Wang *et al.*, 2006 that coupled canopy photosynthesis and transpiration of winter wheat. The model combined a two-layer evapotranspiration model with a coupled photosynthesis-stomatal conductance model to study the diurnal variations of CO<sub>2</sub>, water and heat fluxes of winter wheat. Field experiments were conducted in Yucheng Comprehensive Experimental Station in the North China Plain to evaluate the model. Half-hourly data of weather variables and CO<sub>2</sub>, water and heat fluxes were obtained by the eddy covariance method in 2002–2003. An analysis of measured flux data showed that there was an evident midday depression of photosynthesis, caused by stomatal closure due to high vapor water deficit and canopy temperature though the soil was well irrigated. There was a close agreement between simulated and measured net radiation, CO<sub>2</sub> flux, sensible and latent heat fluxes, which proved the predictive power of the coupled photosynthesis and

transpiration model. The response of CO<sub>2</sub> flux, canopy conductance and latent heat flux to changes in climatic factors was discussed, which indicated that the model could be used to predict CO<sub>2</sub>, water and heat fluxes of wheat not only in the North China Plain, but also in other climatic regions in China

A four-layer hydrologic model, coupled to a vegetation growth model, had been used to investigate the differences between aerodynamic surface temperature and radiative surface temperature over sparsely vegetated surface (Chehbouni *et al.*, 1996). The rationale for the coupling of the two models was to assess the dependency of these differences on changing surface conditions (i.e., growing vegetation). A simulation was carried out for a 3-month period corresponding to a typical growth seasonal cycle of an herbaceous canopy in the Sahel region of West Africa (Goutorbe *et al.*, 1993). The results showed that the ratio of radiative-aerodynamic temperature difference to radiative-air temperature difference was constant for a given day. However, the seasonal trend of this ratio changed with respect to the leaf area index (LAI). A parameterization involving radiative surface temperature, air temperature, and LAI was then developed to estimate aerodynamic-air temperature gradient, and thus sensible heat flux. This parameterization was validated using data collected over herbaceous site during the Hapex-Sahel experiment. This approach was further advanced by using a radiative transfer model in conjunction with the above models to simulate the temporal behavior of surface reflectances in the visible and the near-infrared spectral bands. The results showed that sensible heat flux could be fairly accurately estimated by combining remotely sensed surface temperature, air temperature, and spectral vegetation index. The results of this study might represent a great opportunity of using remotely

sensed data to estimate spatiotemporal variabilities of surface fluxes in arid and semiarid regions as claimed by the author.

A two source (canopy + soil) SVAT model called Atmosphere Land Exchange (ALEX) was employed to simulate energy balance components and ET on hourly and daily basis by Anderson *et al.* (2000). Simulated ET over corn and soybean crops was found to have 24% mean absolute difference with respect to measurements.

The ISBA (Interactions between Soil, Biosphere, and Atmosphere) model is a SVAT scheme which is able to simulate the energy and water budget with soil and surface characteristics and climate forces (Noilhan and Mahfouf, 1996). Rivalland *et al.* 2005 used this SVAT model on a 5 × 5 km<sup>2</sup> agricultural regions in the South-East of France (Alpilles/ReSeDA) with the aim of monitoring surface energy and mass exchange at high spatial resolution (20m) and low spatial resolution (1km). In order to validate SVAT simulation results, the surface energy fluxes and soil water content evolution simulated by the model were compared with ground measurements in specific fields (Oliosio *et al.*, 2002). In the first step, this comparison showed that the standard parameterization of ISBA led to a large underestimation of evapotranspiration. In the second step, the assimilation of remote sensing data in the SVAT model at airborne acquisition dates made it possible to correct spatial soil water content characteristics.

The SVAT model DAISY was modified so as to be able to utilize remote sensing (RS) data in order to improve prediction of evapotranspiration and photosynthesis at plot scale. The link between RS data and the DAISY model was the development of the minimum, unstressed, canopy resistance during the growing season. Energy balance processes were simulated by applying resistance networks and a two-source model. Model data were validated against measurements

performed in a winter wheat plot by Peter *et al.* (2000). Crop dry matter content and leaf area index were modelled adequately. Simulated and observed energy fluxes were generally in good agreement when water supply in the root zone was not limiting. With decreasing soil moisture content during a longer drought period, model latent heat flux was lower than that observed, which called for both improved parameterizations of environmental controls for improved estimation of the canopy resistance parameter.

### **3.2.3 Using RS-based observations**

#### **3.2.3.1 From ground platform**

Attempts have been made in the past by a number of workers to use ground RS-based canopy thermal data for estimation of crop evapotranspiration using number of energy balance models including some physical constants. Chakraborty and Arora, (2003) carried out the study to deal with an integrated approach for estimation of crop evapotranspiration for rice and wheat by vegetation index-temperature trapezoid (VITT) approach using spectral indices from ground based spectroradiometer measurements and canopy thermal data. The results revealed that VITT approach was more suitable for estimation of crop evapotranspiration rate for higher value of spectral indices. The study also emphasized the failure of the model to estimate the evapotranspiration rate of the crop for lower values of the spectral indices.

Crop coefficient methodologies are widely used to estimate actual crop evapotranspiration ( $ET_c$ ) for determining irrigation scheduling. Generalized crop coefficient curves presented in the literature are limited

in providing estimates of  $ET_c$  for “optimum” crop condition within a field, which often need to be modified for local conditions and cultural practices, as well as adjusted for the variations from normal crop and weather conditions that might occur during a given growing season. Consequently, the uncertainties associated with generalized crop coefficients can result in  $ET_c$  estimates that are significantly different from actual  $ET_c$ , which could ultimately contribute to poor irrigation water management. Limited research also showed that VIs can be used to estimate basal crop coefficient ( $K_{cb}$ ) for several crops, including corn and cotton. Douglas *et al.*, (2005) developed a model for estimating  $K_{cb}$  values from observations of the normalized difference vegetation index (NDVI) for spring wheat. The  $K_{cb}$  data were derived from back-calculations of the FAO-56 dual crop coefficient procedures using field data obtained during two wheat experiments conducted during 1993–1994 and 1995–1996 in Maricopa, Arizona. The performance of the  $K_{cb}$  model for estimating  $ET_c$  was evaluated using data from a third wheat experiment in 1996–1997, also in Maricopa, Arizona. The  $K_{cb}$  was modelled as a function of a normalized quantity for NDVI, using a third-order polynomial regression relationship ( $r^2=0.90$ ,  $n=232$ ). The estimated seasonal  $ET_c$  for 1996–1997 season agreed to within –33 mm (–5%) to 18 mm (3%) of measured  $ET_c$ . However, the mean absolute percent difference between the estimated and measured daily  $ET_c$  varied from 9% to 10%, which was similar to the 10% variation for  $K_{cb}$  that was unexplained by NDVI. The preliminary evaluation suggested that ground based remotely-sensed NDVI observations could provide real-time  $K_{cb}$  estimates for determining the actual wheat  $ET_c$  during the growing season.

The sensible heat loss from a stand of winter wheat was calculated from Thermal infrared radiometric measurements of crop surface temperature, measurements of air temperature, and an atmospheric



resistance to momentum transfer; corresponding latent heat flux was obtained through the energy balance equation (Huband and Monteith 2004). These estimates of sensible and latent heat were compared with fluxes from the Bowen Ratio method. When radiative temperature was derived using a measured canopy emissivity of 0.98, calculations of sensible heat flux were systematically 50–100 W m<sup>-2</sup> less than corresponding flux values obtained by Bowen Ratio values. The two techniques agreed more closely when an apparent emissivity of 0.96 was used with an apparent reflectivity of 0.03. The mean difference between the estimates of latent heat flux was then  $-16 \pm 32$  W m<sup>-2</sup>. The surface temperature method showed less systematic error in comparison with the Bowen Ratio values than did estimates using the aerodynamic method. Relationships between vegetation indices (NDVI and SAVI) and crop coefficients (the ratio of measured to reference evapotranspiration) were derived with four different models (Shuttleworth, Penman, Priestley-Taylor and Makkink), using ground-based surface reflectance measured over the crop. Continuous measurements of surface fluxes and other meteorological variables were made following almost the entire vegetative cycle of the plant using a station equipped with standard meteorological instruments and an eddy-correlation system. Actual evapotranspiration was computed as the product of the estimated crop coefficients, derived from field radiometer measurements, and reference evapotranspiration. In comparison with ground data, RMSE values were on the order of 1 mm per day.

Measurements were made at New Delhi (India) on wheat (*Triticum aestivum* L.) and mungbean (*Vigna radiata* L.) crops grown during winter and summer seasons respectively, to evaluate the use of the equation of Bartholic, Namken and Wiegand (1970) for estimating daytime evapotranspiration from a single measured canopy temperature with

infrared thermometer (Gupta and Sastry, 1986). Measurements made on eleven days indicated that a single observation of canopy temperature taken at any time between noon and 14:00hrs. could be used to compute daytime evapotranspiration with an error (underestimate) of less than 27% as compared with values measured by the Bowen ratio method. The regression equation  $ET_0 = 0.618 + 0.96 ET_1$  had a coefficient of determination of 0.927. This could be used to relate daytime evapotranspiration using Bowen ratio method ( $ET_0$ ) to that estimated by the Bartholic-Namken-Wiegand equation ( $ET_1$ ) for wheat and mung bean crops grown under adequately watered conditions in the New Delhi region.

### **3.2.3.2 Satellite platform**

Satellite based energy balance schemes aimed at ET estimation on spatial domain at local (<100m), regional (100m-1km) and global (>1km) scales mostly used clear sky optical and thermal observations from different polar orbiting and geostationary sensors. Use of passive microwave data to derive ET in cloudy sky conditions was demonstrated by Kustas et al (1994). The work done with data from polar and geostationary satellite sensors is summarized below:

Methods for satellite based ET estimation generally use surface energy balance approaches. These can be broadly categorized into (a) single source (Bastiaanssen et al., 1998) and (b) two source (Norman et al., 1995) processes. Though accuracy of ET estimates from two-source approach is better than single source approach (French et al., 2005; Timmermans et al., 2007), the former requires more ancillary data support and coefficients through ground-based experimentation.

#### 3.2.3.2.1 Polar orbiting

The crop water stress index (CWSI), developed at the USDA-ARS U.S. Water Conservation Laboratory, Phoenix, Arizona, is a commonly used index for detection of plant stress based on the difference between foliage and air temperatures. Application of CWSI at local and regional scales has been hampered by the difficulty of measuring foliage temperature of partially vegetated fields. Most hand-held, airborne, and satellite-based infrared sensors measure a composite of both the soil and plant temperatures. The concept termed as vegetation index/temperature (VIT) trapezoid was an attempt to combine satellite based spectral vegetation indices with composite surface temperature measurements to allow application of the CWSI theory to partially-vegetated fields without knowledge of foliage temperature (Moran *et al.*, 1994). Based on this approach, a new index [water deficit index (WDI)] was introduced for evaluating evapotranspiration rates of both full-cover and partially vegetated sites. By definition, WDI is related to the ratio of actual and potential evapotranspiration; in practice, WDI can be computed using remotely sensed measurements of surface temperature and reflectance (red and near-infrared spectrum) with limited on-site meteorological data (net radiation, vapor pressure deficit, wind speed, and air temperature). Both the VIT trapezoid and WDI concepts were evaluated using 1) a simulation of a two-component (soil and vegetation) energy balance model and 2) existing data from an experiment in an alfalfa field in Phoenix, Arizona. Results from both studies showed that Landsat derived WDI provided accurate estimates of field evapotranspiration rates with  $RMSE \pm 29 Wm^{-2}$ .

Quantifying evapotranspiration (ET) from agricultural fields is important for field water management, water resources planning, and

water regulation. Traditionally, ET from agricultural fields has been estimated by multiplying the weather-based reference ET by crop coefficients ( $K_c$ ) determined according to the crop type and the crop growth stage. Recent development of satellite remote sensing ET models enabled to estimate ET and  $K_c$  for large population of fields. This study by Tasumi *et al* (2005) evaluated the distribution of  $K_c$  over space and time for a large number of individual fields by crop type using ET maps created by a satellite based energy balance (EB) model. Variation of  $K_c$  curves was found to be substantially larger than that for the normalized difference vegetation index because of the impacts of random wetting events on  $K_c$ , especially during initial and developmental growth stages. Two traditional  $K_c$  curves that were widely used in Idaho for crop management and water rights regulation were compared against satellite-derived  $K_c$  curves. Simple adjustment of the traditional  $K_c$  curves by shifting dates for emergence, effective full cover, and termination enabled traditional curves to fit better  $K_c$  curves as determined by the energy balance model.

Using remote-sensing data and ground-based data, Zhang *et al.*, (2006) constructed an integrated algorithm for estimating regional surface latent heat flux ( $LE$ ) and daily evapotranspiration ( $ET_d$ ). In the algorithm, they first used trapezoidal diagrams relating the surface temperature and fractional vegetation cover ( $f_c$ ) to calculate the surface temperature-vegetation cover index (TVCI), a land surface moisture index with a range from 0.0 to 1.0. A revised sine function was used to assess  $ET_d$  from  $LE$  estimated at satellite overpass time. The algorithm was applied to farmland in North China Plain using Landsat Thematic Mapper (TM) / Enhanced Thematic Mapper Plus (ETM+) data and synchronous surface-observed data as inputs. The estimated  $LE$  and  $ET_d$  were tested against measured data from a Bowen Ratio Energy Balance (BREB) system and a

large-scale weighing lysimeter, respectively. The algorithm estimated  $LE$  with a root mean square error (RMSE) of  $50.1 \text{ W m}^{-2}$  as compared to measurements with the BREB System, and  $ET_d$  with an RMSE of  $0.93 \text{ mm d}^{-1}$  as compared with the measurement by the lysimeter.

The surface fluxes obtained with the Surface Energy Balance Algorithm for Land (SEBAL), using remote sensing information and limited input data from the field were validated with data available from the large-scale field experiments EFEDA (Spain), HAPEX-Sahel (Niger) and HEIFE (China). In 85% of the cases where field scale surface flux ratios were compared with SEBAL-based surface flux ratios, the differences were within the range of instrumental inaccuracies (Bastiaanssen *et al.*, 1998). Without any calibration procedure, the root mean square error of the evaporative fraction  $\Lambda$  (latent heat flux/net available radiation) for footprints of a few hundred metres varied from  $\Lambda_{\text{RMSE}}=0.10$  to 0.20. Aggregation of several footprints to a length scale of a few kilometres reduced the overall error to 5%. Fluxes measured by aircraft during EFEDA were used to study the correctness of remotely sensed watershed fluxes (1 000 000 ha): The overall difference in evaporative fraction was negligible. For the Sahelian landscape in Niger, observed differences were larger (15%), which could be attributed to the rapid moisture depletion of the coarse textured soils between the moment of image acquisition (18 September 1992) and the moment of *in situ* flux analysis (17 September 1992). For HEIFE, the average difference in SEBAL estimated and ground verified surface fluxes was  $23 \text{ W m}^{-2}$ , which, considering that surface fluxes were not used for calibration, was encouraging. SEBAL estimates of evaporation from the subsealevel Qattara Depression in Egypt (2 000 000 ha) were consistent with the numerically predicted discharge from the groundwater system. In Egypt's Nile Delta, the evaporation from a distributed field scale water balance

model at a 700 000 ha irrigated agricultural region led to difference of 5% with daily evaporative fluxes obtained from SEBAL. It was concluded that, for all study areas in arid zones, the errors were averaged out if a larger number of pixels were considered. Part 1 of this paper deal with the formulation of SEBAL.

A decoupling technique was applied with Landsat-5 TM optical and thermal data by Boegh *et al.*, (2002) for a composite evaluation of atmospheric resistance, surface resistance and evapotranspiration rate ( $\lambda E$ ). The method used three equations to solve for three variables: the atmospheric resistance between the surface and the air ( $r_{ae}$ ); the surface resistance ( $r_s$ ); and the vapour pressure at the surface ( $e_s$ ). The novelty of this approach was the estimation of  $e_s$ , which was assessed using the decoupling coefficient ( $\Omega$ ). The input parameters were: surface temperature ( $T_s$ ), net radiation ( $R_n$ ), soil heat flux ( $G$ ), air temperature ( $T_a$ ), and air humidity ( $e_a$ ). A time series (100 days) of field data collected over wheat crop using eddy covariance towers were used to validate latent heat flux estimates. The control of  $r_s$  on  $\lambda E$  was expressed through the Surface Control Coefficient ( $SCC=1-\Omega$ ), which was compared with soil moisture data. The application of the technique in a remote sensing monitoring context was demonstrated for a Danish agricultural landscape containing crops at different stages of development. For the satellite-based estimation of  $\lambda E$  and  $SCC$ , the variables  $T_s$ ,  $R_n$ , and  $G$  were calculated on the basis of Landsat-5 TM. The method was directly applicable without any calibration when the soil surface was moist or when the vegetation cover was dense. Only for a dry bare soil surface, where the effective source area of water vapour was below the surface, the modification of a surface humidity parameter ( $h_{s,max}$ ) was required.

Accurate estimation of surface energy fluxes from space at high spatial resolution has the potential to improve prediction of the impact of

land-use changes on the local environment and to provide a means to assess local crop conditions. To achieve this goal, a combination of physically based surface flux models and high-quality remote-sensing data are needed (French *et al.*, 2005). Data from the ASTER sensor are particularly well-suited to the task, as it collects high spatial resolution (15–90 m) images in visible, near-infrared, and thermal infrared bands. Data in these bands yield surface temperature, vegetation cover density, and land-use types, all critical inputs to surface energy balance models for assessing local environmental conditions. Surface energy flux retrieval from ASTER was demonstrated using data collected over an experimental site in central Iowa, USA, in the framework of the Soil Moisture Atmosphere Coupling Experiment (SMACEX). This experiment took place during the summer of 2002 in a study of heterogeneous agricultural croplands. Two different flux estimation approaches, designed to account for the spatial variability, were considered: the Two-Source Energy Balance model (TSEB) and the Surface Energy Balance Algorithm or Land model (SEBAL). ASTER data were shown to have spatial and spectral resolution sufficient enough to derive surface variables required as inputs for physically based energy balance modeling. Comparison of flux model results against each other and against ground based measurements was promising, with flux values commonly agreeing within  $\pm 50 \text{ Wm}^{-2}$ . Both TSEB and SEBAL showed systematic agreement and responded to spatially varying surface temperatures and vegetation densities. Direct comparison against ground Eddy covariance data suggested that the TSEB approach was helpful over sparsely vegetated terrain.

Evapotranspiration (ET) cannot be measured directly from satellite observations but remote sensing can provide a reasonably good estimate of evaporative fraction (EF), defined as the ratio of ET and available radiant energy. Nishida *et al.*, 2003 developed an algorithm for estimating

evaporation fraction (EF), expressed as a ratio of actual evapotranspiration (ET) to the available energy (sum of ET and sensible heat flux), from satellite data. The algorithm was a simple two-source model of ET. They characterized a landscape as a mixture of bare soil and vegetation and thus they estimated EF as a mixture of EF of bare soil and EF of vegetation. In the estimation of EF of vegetation, they used complementary relationship of the actual and the potential ET for the formulation of EF. In that, they used the canopy conductance model for describing vegetation physiology. On the other hand, "VI-Ts" (vegetation index-surface temperature) diagram were used for estimation of EF of bare soil. They validated EF from this prototype algorithm using NOAA/AVHRR data with actual observations of EF at AmeriFlux stations (standard error  $\approx 0.17$  and  $R^2 \approx 0.71$ ). Global distribution of EF every 8 days were targeted to be operationally available using this algorithm and data of MODIS on EOS-PM (Aqua).

Evapotranspiration (ET) using the Integral NOAA-imagery processing Chain (iNOAA-Chain) was quantified by implementing visible and thermal satellite information on a regional scale by Verstraeten *et al.*, (2005). ET was calculated based on the energy balance closure principle. The combination of evaporative fraction (EF), soil heat flux and instantaneous net radiation, resulted in an instantaneous spatial distribution of ET values. Surface broadband albedo and land surface temperature (LST) served to determine EF. EF was derived using four methods based on NOAA/AVHRR satellite imagery. Instantaneous evapotranspiration, i.e. at time of satellite overpass, on European continental scale with emphasis on forest stands was estimated using iNOAA-Chain. Finally, the estimated net radiation ( $R_n$ ), soil heat fluxes ( $G_0$ ) and evaporative fraction and evapotranspiration at time of satellite overpass were validated against EUROFLUX site data for the growing



season of 1997 (March-October). The regression line for the pooled  $R_n$  (iNOAA-Chain versus EUROFLUX) had a slope, intercept, Pearson product moment correlation coefficient ( $R^2$ ) and relative root mean square error (RRMSE) of respectively 0.943, 17.120, 0.926 and 5.5%. They observed a slight underestimation of the iNOAA-Chain estimated EF. The regression line for pooled EF data for the best performing method (SPLIT-method) was found to have a slope of 0.935, an intercept of 0.041 and the  $R^2$  0.847. A pooled RRMSE EF value of 12.3% was found. Error propagation analysis revealed that the relative error on evapotranspiration at satellite overpass time was at least 27%.

It was feasible to estimate EF using a contextual interpretation of radiometric surface temperature ( $T_s$ ) and normalized vegetation index (NDVI) from multiple satellites. Recent studies have successfully estimated net radiation ( $R_n$ ) over large heterogeneous areas for clear sky days using only remote sensing observations. With distributed maps of EF and  $R_n$ , it is now possible to explore the feasibility and robustness of ET estimation from multiple satellites. Batra *et al.*, 2006 presented the results of an extensive inter-comparison of spatially distributed ET and related variables (NDVI,  $T_o$ , EF and  $R_n$ ) derived from MODIS and AVHRR sensors onboard EOS Terra, NOAA14 and NOAA16 satellites respectively. Their results showed that although, NDVI and  $T_s$  differed with the sensor response functions and overpass times, contextual space of NDVI- $T_o$  diagram gave comparable estimates of EF. The utility of different sensors is demonstrated by validating the estimated ET results to ground flux stations over the Southern Great Plains with a root mean square error of 53, 51 and 56.24  $Wm^{-2}$ , and a correlation of 0.84, 0.79 and 0.77 from MODIS, NOAA16 and NOAA14 sensors respectively.

Two models were evaluated for their ability to estimate land surface evaporation at 16-day intervals using MODIS remote sensing data

and surface meteorology as inputs by Cleugh *et al.*, 2007. The first was the aerodynamic resistance–surface energy balance model, and the second was the Penman–Monteith (P–M) equation, where the required surface conductance was estimated from remotely-sensed leaf area index. The models were tested using 3 years of evaporation and meteorological measurements from two contrasting Australian ecosystems, a cool temperate, evergreen *Eucalyptus* forest and a wet/dry, tropical savanna. The aerodynamic resistance–surface energy balance approach failed because small errors in the radiative surface temperature translated into large errors in sensible heat, and hence into estimates of evaporation. The P–M model adequately estimated the magnitude and seasonal variation in evaporation in both ecosystems (RMSE =  $27 \text{ W m}^{-2}$ ,  $R^2 = 0.74$ ), demonstrating the validity of the proposed surface conductance algorithm. This, and the ability to constrain evaporation estimates *via* the energy balance, demonstrated the superiority of the P–M equation over the surface temperature-based model. There was no degradation in the performance of the P–M model when gridded meteorological data at coarser spatial ( $0.05^\circ$ ) and temporal (daily) resolution were substituted for locally-measured inputs. The P–M approach was used to generate monthly evaporation climatology for Australia from 2001 to 2004 to demonstrate the potential of this approach for monitoring land surface evaporation and constructing monthly water budgets from 1-km to continental spatial scales.

A global satellite based evapotranspiration (ET) algorithm based on Penman–Monteith approach (RS-PM) (Cleugh *et al.*, 2007) was applied with MODIS TERRA data at  $0.05^\circ$  grid (Mu *et al.*, 2007). This algorithm considered both surface energy partitioning process and environmental constraints on ET. They calculated spatial ET with both revised RS-PM algorithm with interpolated ground based meteorological data and the

RS-PM algorithm using Global Modeling and Assimilation Office (GMAO v. 4.0.0) meteorological data and compared the resulting ET estimates with observations from 19 AmeriFlux eddy covariance flux towers. They used meteorological and remote sensing data to estimate global ET by (1) adding vapor pressure deficit and minimum air temperature constraints on stomatal conductance; (2) using leaf area index as a scalar for estimating canopy conductance; (3) replacing the Normalized Difference Vegetation Index with the Enhanced Vegetation Index thereby also changing the equation for calculation of the vegetation cover fraction ( $F_c$ ); and (4) adding a calculation of soil evaporation to the previously proposed RS-PM method. Results indicated that revised RS-PM algorithm substantially reduced the root mean square error (RMSE) of the 8-day latent heat flux (LE) averaged over 19 towers from  $64.6 \text{ W/m}^2$  (RS-PM algorithm) to  $27.3 \text{ W/m}^2$  (revised RS-PM) with tower meteorological data, and from  $71.9 \text{ W/m}^2$  to  $29.5 \text{ W/m}^2$  with GMAO meteorological data. The average LE bias of the tower-driven LE estimates to the LE observations changed from  $39.9 \text{ W/m}^2$  to  $-5.8 \text{ W/m}^2$  and from  $48.2 \text{ W/m}^2$  to  $-1.3 \text{ W/m}^2$  driven by GMAO data. The correlation coefficients increased slightly from 0.70 to 0.76 with the use of tower meteorological data. Revised RS-PM algorithm was applied to the globe to obtain the annual global ET (MODIS ET) for 2001. As expected, the spatial pattern of the MODIS ET agreed well with that of the MODIS global terrestrial gross and net primary production (MOD17 GPP/NPP), with the highest ET over tropical forests and the lowest ET values in dry areas with short growing seasons.

A complementary approach (Venturini *et al.*, 2007) was formulated and tested over South Great Plains (SGP), USA to derive clear sky evaporative fraction (EF) and evapotranspiration (ET) maps using MODIS TERRA optical-thermal band and 1000mb air temperature data without

auxiliary or site-specific relationships. This formulation was based on Granger's complementary relationship and Priestley–Taylor's equation. The proposed model eliminated the wind function and resistance parameters commonly applied to ET calculation by including a relative evaporation parameter (ET/E<sub>pot</sub>). Estimates of ET showed an overall RMSE and bias of 33.89 and – 10.96 Wm<sup>-2</sup>, respectively.

#### **3.2.3.2.2 Geostationary**

In the framework of European Energy and Water Balance Monitoring System (EWBMS), an operational system of actual evapotranspiration and biomass development on the basis of European geostationary satellite (METEOSAT) data was developed. Because of its operational characteristics, the method is such that it requires minimal input other than the METEOSAT data and can run fully automatic on a microcomputer. The methodology, including: calibration, atmospheric correction, radiation and energy balance mapping, and biomass simulation has been described by Rosema (1993). The method was applied during a complete growing season to a part of West Africa. Processing results in the form of METEOSAT-derived evapotranspiration (MDE) and METEOSAT-derived biomass (MDB) maps were generated. They were compared with NOAA-NDVI data and verified with rainfall and biomass “ground truth.” A “triangular regression analysis” was introduced to assess the stochastic errors in the satellite and ground data. It was finally concluded that METEOSAT could provide precise estimates of areal evapotranspiration and biomass at 0.05° grid. In terms of areal biomass, the stochastic errors in MDB and NDVI were both small compared to pixel sampling error in the biomass field data.

An operational Chinese Energy and Water Balance Monitoring System (CEWBMS) is in place through Sino-Dutch collaboration (Rosema *et al.*, 2004) using optical and thermal data from Chinese Geostationary

Satellite (FEN YUNG 2) and Geostationary Meteorological Satellite (GMS), Japan. This system is meant for drought monitoring, crop yield forecasting and desertification monitoring. Seasonal cumulative ET was found to be correlated well with district maize yield of China.

An operational two-source (soil + vegetation) model (Anderson *et al.*, 1997) was reported for evaluating surface energy fluxes at spatial scale using time rate of change in radiometric surface temperature ( $T_{RAD}$ ) during morning hours measured through GOES (Geostationary Operational Environmental Satellite), USA. This is known as Atmosphere Land Exchange Inversion (ALEXI) model which was adapted from two-source scheme, ALEX (Atmosphere Land Exchange) formulated by Norman *et al.* (1995) to simulate energy balance at point scale. The ALEX-ALEXI-disALEXI suite was framed and tested by Anderson *et al.* (2003) to downscale coarser resolution ( $0.05^\circ$ ) ALEXI energy flux outputs to field scale using Landsat thermal infrared radiometry. A climatological study of evapotranspiration and moisture stress across USA was conducted based on three years (2002-2004) daily GOES thermal data (Anderson *et al.*, 2007) both in clear and cloudy sky conditions. Evapotranspiration flux estimates yielded 20% errors at hourly timescales and 15% errors at daily timesteps. GOES stress, relative evapotranspiration (RET), were compared with Palmer drought stress index (PDSI). Spatial coherence between these two were observed but more spatial variability was evident in GOES RET as compared to PDSI derived from interpolated *in situ* rainfall measurements.

In India, energy and water balance monitoring project (Bhattacharya *et al.*, 2007) was carried out between 2002-2007 to derive evapotranspiration using surface energy balance approach and Indian geostationary sensor (KALPNA-1 / INSAT) optical and thermal data at  $0.08^\circ$  grid. Geostationary ET was compared with MODIS AQUA ET at

0.01° grid validated only over crop patches. RMS error was found to be 23Wm<sup>-2</sup>. The ET estimation using MODIS TERRA-AQUA data over semi-arid agroecosystems and its validation was not reported in this study.

### 3.3 RS-based yield prediction

#### 3.3.1 Spectral yield model

Remote sensing tools can provide information about vegetation in various wavebands (Moulin *et al.*, 1998). Remotely sensed observations in narrow optical bands can be related to various canopy state variables. To achieve these, canopy state variables can be retrieved using remotely sensed measurements through physical radiative transfer models or empirical relationships.

Ground radiometric measurements performed over winter wheat fields have shown that production was strongly correlated to cumulative amount of vegetation indices (Tucker *et al.*, 1981). Tucker *et al.* (1985) obtained similar results and proposed an empirical model for biomass using satellite data. According to Hatefield (1983), vegetation index values at heading could be related to potential yield provided no accident occurred at that stage.

Spectral yield models were developed using single or multi-date normalized difference vegetation index (NDVI) (Quarmby *et al.*, 1993) or vegetation condition index (VCI) (Hayes and Decker, 1996) with coarser resolution remote sensing data from satellite platform. These statistical models based on spectral indices could explain only up to 55% yield variability. A non-linear form relating vegetation indices (VI) to crop grain yields normalized for differences in acquisition dates was suggested. It was based on the assumption that deviations in VI near the peak VI followed a quadratic behaviour (Dadhwal and Sridhar, 1997). This form gave a higher  $R^2$  value than a simple VI-yield linear model on a

multi-year, multi-location dataset of IRS (Indian Remote Sensing Satellite-1A). LISS-I (Linear Imaging Self Scanner-I) derived near-infrared (NIR)/red radiance ratios and wheat grain yields in a study site in Madhya Pradesh (India). As the suggested model included time of peak as a variable, it allowed integration of results from other sources, such as, weather-based crop phenology model or high repetivity spectral data into the VI-yield relation.

Hamar *et al* (1996) established a linear regression model to estimate corn and wheat yield at regional scale based on vegetation spectral indices computed with Landsat MSS data. Such relationships were due to the fact that, the time profile of visible and near infrared signatures was limited with the evaluation of (i) canopy development (ii) capability to absorb photosynthetically active radiation and with phenological potential, all of which finally determined potential yield (Sellers, 1985, Asrar, 1984). However, these empirical relations between cumulative VIs and dry biomass only have a local value. To extend wider applicability of model, it is necessary to describe how photosynthetically active radiation is absorbed, converted into dry biomass and partitioned into harvested organs.

Large-area yield prediction early in the growing season is important in agricultural decision-making. This study derived maize (*Zea mays* L.) leaf area index (LAI) estimates from spectral data and used these estimates with a simple LAI-based yield model to forecast yield under irrigated conditions in large areas in Sinaloa, Mexico. Leaf area index was derived from satellite data with the use of an equation developed with LAI measurements from farmers' fields during the 2001–2002 autumn–winter growing season by Gonzalez *et al* (2005). These measurements were correlated with normalized difference vegetation index from 2002 Landsat ETM+ (enhanced thematic mapper) data. The relation was then

tested with 2003 Landsat data. A yield model was validated with maximum LAI and yield data measured in farmers' fields in northern and central Sinaloa during three consecutive autumn–winter growing seasons (1999–2000, 2000–2001, and 2001–2002). The yield model was further validated with 2002–2003 autumn–winter ground LAI (gLAI) and satellite-derived LAI (sLAI) data from 71 farmers' fields in northern and central Sinaloa. Grain yield was predicted with a mean error of  $-9.2\%$  with maximum gLAI and  $-11.2\%$  with sLAI. Results indicated that the yield model using LAI could forecast yield in large areas in Sinaloa in the middle of the growing season with a mean absolute error of  $-1.2 \text{ Mg ha}^{-1}$ . The use of sLAI in place of ground measurements increased the mean absolute error by  $0.3 \text{ Mg ha}^{-1}$ . Nevertheless, the use of sLAI would eliminate laborious LAI measurements for large-area yield prediction in Sinaloa. Gonzalez *et al.* (2002) developed and validated a method of monitoring and estimating corn (*Zea mays* L.) yield by means of satellite and ground-based data. In autumn–winter 1999 and spring–summer 2000, eight locations under irrigated and nonirrigated conditions in corn valleys of Mexico were localized by Global Positioning Systems (GPS) and were sampled every 15 day interval. Photosynthetic active radiation (PAR), leaf area index (LAI), crop development stage (DVS), planting dates, and grain yield data were gathered from the field. The normalized difference vegetation index (NDVI) was derived from NOAA-Advanced Very High Resolution Radiometer (AVHRR) images. A growth model was developed to integrate satellite and ground data. Net primary productivity (NPP) was estimated using PAR and NDVI. Dry weight increase ( $\text{kg ha}^{-1} \text{ d}^{-1}$ ) was determined considering NPP and the partitioning factor. Results indicated that the model accounted for 89% of the variability in yields under irrigated conditions and 76% under nonirrigated conditions.



Kancheva *et al.* (2007) proposed and investigated the performance of an approach for providing crop condition assessment and yield forecasts. In order that crop information intended to be obtained from remotely sensed data the approach comprised : (i) development of models between plant spectral reflectance and biophysical parameters for estimation of crop state variables from satellite radiometric data, (ii) development of yield forecasting models from single-date and time-series spectral data (iii) verification of remote sensing predictions through comparison with estimations from yield relationships with crop agronomical parameters. The algorithm was realized on winter wheat. *In-situ* high-resolution visible and near-infrared reflectance data were acquired throughout the growing season, along with detailed datasets of crop parameters. Spectral-biophysical models were developed relating crop variables and yield to different spectral predictors. The algorithm was tested and validated using airborne remote sensing data. A good correspondence was found between predicted and actual yield.

### 3.3.2 Agromet model

#### 3.3.2.1 Multiple regression

Recently, combination of multi-source satellite derived LST, NDVI and soil moisture at coarser resolution ( $\geq 8\text{km}$ ) were used to develop statistical yield models to predict Iowa state wheat and soybean yield (Prasad *et al.*, 2006). Minimization of least square loss function was carried out through iterative convergence using pre-defined empirical equation that provided acceptable lower residual values with predicted values very close to observed ones ( $R^2 = 0.78$ ) for Corn and Soybean crop ( $R^2 = 0.86$ ). Similar model could be developed for different crops at other locations.

The application of satellite-derived indices for assessment of crop growth conditions in semi-arid countries is well known. Dabrowska *et al.*, (2002) described the application of these indices outside semi-arid areas, in Poland, a country with a sufficient water supply. Two indices, Vegetation Condition Index (VCI) and Temperature Condition Index (TCI), were computed for Poland for each week for a period of 14 years. These indices were correlated with cereal yield anomalies for each of 49 regions of Poland. Two critical periods in crop development were found: early spring (14-16 weeks of the year) and early summer (22-25 weeks) when the state of crop development determines the magnitude of yield. The indices computed for these two periods were used in a yield prediction model. The results were compared with data provided by the Central Statistical Office. The average error of cereal yield estimates for 49 regions was lower than 4%. It did not apply to detect cropwise yield anomaly within cereals.

Remote sensing (RS) data acquired by satellite have wide scope for agricultural applications owing to their synoptic and repetitive coverage. Especially the spectral indices deduced from visible and near-infrared RS data have been extensively used for crop characterization, biomass estimation, crop condition monitoring, crop yield condition monitoring and crop yield monitoring and forecasting. Manjunath *et al.*, (2002) reported the development of operational spectrometeorological yield models of wheat crop using spectral index viz., normalized difference vegetation index (NDVI ), derived from NOAA-AVHRR data and monthly rainfall data. The AVHRR data spanning seven crop growing seasons, rainfall data from the rain gauge stations and crop yield data from crop cutting experiments (CCE) conducted by the state Directorate of Economics and Statistics (DES) were the basic input parameters. The statistical multiple linear regression yield models had been developed for

fifteen geographically large wheat growing districts of Rajasthan state in India. The spectrometeorological yield models were validated by comparing the predicted district-level yields with those estimated from the crop cutting experiments. The yield models based on NDVI (spectral), rainfall (meteorological) and both NDVI and rainfall (spectrometeorological) have been tried. The models had been developed for districts, groups of districts comprising agroclimatic zones, and groups of agroclimatic zones. The incorporation of monthly rainfall in the regression yield models in addition to NDVI improved the model performance significantly. Amongst the three categories of models attempted, the spectrometeorological yield models had the highest predictive capability as shown by the validation results. The district-level models showed highest correlation with yield and were followed by agroclimatic zonal and group-of-zones level models.

The application of crop simulation models to yield estimation on a regional scale is generally constrained by the lack of spatially distributed information on major environmental and agronomic factors affecting crop conditions. The use of remote sensing data can circumvent this problem by providing actual estimates of these conditions with various spatial and temporal resolutions. Moriondo *et al.*, (2007) presented the development and testing of a methodological framework which utilized NDVI data taken from satellite platforms and a simulation model (CROPSYST) to estimate wheat yield. This operation relied on two main steps, the first being the computation of above-ground wheat biomass obtained through the use of NDVI-derived FAPAR estimates. The second step consisted of the final repartition of the estimated biomass into crop yield, which was obtained through the use of an harvest index computed by integrating the CROPSYST development sub-model and NDVI data.

The proposed methodology was applied in two Italian provinces where wheat is widely grown (Grosseto and Foggia). In both cases, attention was first devoted to the production of multi-year NDVI data sets descriptive of wheat conditions. Next, the current methodology was applied to estimate wheat yield. The results obtained showed the high accuracy of the method in estimating wheat yield at the provincial level. Correlation coefficients equal to 0.77–0.73 were obtained between measured and simulated crop yields, with corresponding root mean square errors (RSME) of 0.47 and 0.44 Mg/ha for Grosseto and Foggia, respectively

### **3.3.2.2 Efficiency model**

Gross primary productivity (GPP) estimates based on radiation use efficiency (RUE), PAR & fAPAR at 1km spatial resolution from the Moderate Resolution Imaging Spectroradiometer (MODIS) were converted to wheat yields which were compared with observed yields for countries, climate districts and entire states for the 2001 and 2002 growing seasons in Montana and North Dakota by Reeves *et al* (2005). Analyses revealed that progressive levels of spatial aggregation generally improved relations between estimated and observed wheat yield. However, only state level yield estimates were sufficiently accurate ( $\leq 5\%$  deviation from observed yield). The statewide yield results were encouraging because they were derived without the use of retrospective empirical analyses, which constituted a new opportunity for timely wheat yield estimates for large regions. Additionally, this study identified six practical limits to estimating wheat yield using MODIS GPP.

A study was carried out to estimate regional wheat yield by remote sensing from the parametric Monteith's model, in an intensive agricultural region (Haryana state) in India by Patel *et al.* (2006) using

MODIS fAPAR products. Discrimination and area estimates of wheat crop were achieved by spectral classification of image from AWiFS (Advanced Wide Field Sensor) on-board the IRS-P6 satellite. Remotely sensed estimates of the fraction of absorbed photosynthetically active radiation (fAPAR) and daily temperature were used as input to a simple model based on RUE to estimate wheat yields at the pixel level. Major winter crops (wheat, mustard and sugarcane) were discriminated from single-date AWiFS image with an accuracy of more than 80%. The physical range of yield estimates from satellites using Monteith's model was within reported yields of wheat for both methods of fAPAR, in an intensive irrigated wheat-growing region. Comparison of satellite-based and official estimates indicated errors in regional yields within 10% for 70% cases. The validation with district level wheat yields revealed a root mean square error of 0.3 tha<sup>-1</sup>.

### **3.3.2.3 Relative evapotranspiration (RET)**

The relative evapotranspiration, RET (AET / PET), is a direct physical input as stress factor to crop water productivity functions and yield modelling (Doorenbos and Kassam, 1979). RET derived from Meteosat geostationary sensor could explain yield variability to the extent of 70 – 94 percent for maize in Africa and Europe (Robeling *et al.*, 2004) at national scale. In India, the RET based approach was adopted to characterize growing environment of rice (Sarkar *et al.*, 2007) and yield prediction (Sarkar *et al.*, 2006) using five years' time series composited NOAA AVHRR optical and thermal data at 8km.

### **3.3.3 RS forcing to crop simulation model**

Methods for the application of crop growth models, remote sensing and their integrative use for yield forecasting and prediction have

been presented by Bouman (1995). NOAA AVHRR satellite imagery has been traditionally used to monitor vegetation changes that are used indirectly to assess crop condition and yields. Additionally, the 1-km spatial resolution of NOAA AVHRR is not adequate for monitoring crops at the field level. Imagery from MODIS sensor onboard the NASA TERRA satellite offers an excellent opportunity for daily coverage at 250-m resolution, which is adequate to monitor field sizes that are larger than 25 ha. A field study was conducted in the predominantly corn and soybean area of Iowa to evaluate the applicability of the 8-day MODIS composite imagery in operational assessment of crop condition and yields (Doraiswamy *et al.*, 2004). Ground-based canopy reflectance and leaf area index (LAI) measurements were used to calibrate the models. The MODIS data was used in a radiative transfer model to estimate LAI through the season. LAI was integrated into a climate-based crop simulation model to scale from local simulation of crop development and responses to a regional scale. Simulations of corn and soybean yields at a  $1.6 \times 1.6 \text{ km}^2$  grid scale were comparable to county yields reported by the USDA–National Agricultural Statistics Service (NASS).

Remote sensing and crop models have proved to be useful to monitor vegetation and estimate above ground biomass (Rodriguez *et al.*, 2003). NDVI from VEGETATION, MODIS, and Landsat reflectance data were compared with field measurements. The phenology was inferred from evolution of NDVI and the main stages were identified. LAI obtained from reflectance was used with the STICS model to give estimates of grain yield which were within about 5% of those of field measurements.

The use of crop models on large areas for diagnosing crop growing conditions or predicting crop production is hampered by the lack of sufficient spatial information about model inputs. Launay and Guerif

(2005) proposed a way of spatializing the model that assimilated information obtained from remote sensing images made during the growing season. The method was applied to yield estimates from the SUCROS sugar beet model, run for about 50 fields within two sugar factory areas. The assimilation of four to six SPOT and aerial photography data values into the SUCROS model, coupled with the scattering by arbitrarily inclined leaves (SAIL) reflectance model, re-estimated crop establishment and root system settling parameters, to which the model was particularly sensitive. The field-by-field yield estimates were improved (i.e., with remote sensing data assimilation, the relative root mean square error decreased from 20% to about 10%). The key factors of the method were the number and timing of images that determine the number and the type of parameters that could be estimated. The main limitation of this method was the lack of robustness of the crop model in simulating LAI in serious drought conditions.

A demonstration of regional wheat yield assessment by WTGROWS in a spatial framework of 5' x 5' geographical grid over Haryana for crop season 1996-97 was made by Sehgal *et al.*, (2001). The inputs used were RS based wheat distribution map, RS-based LAI, daily weather and surfaces, soil properties map as well as crop management input database in a GIS environment. The issues related to framework design, generating various inputs in the required spatial format, and its implementation as a Crop Growth Monitoring System (CGMS) were discussed. Further the study explored the possibilities and issues in linking remote sensing inputs into the CGMS framework to improve its performance.

The above review has indicated that different satellite based energy balance estimates lead to computation of ET over agro-ecosystems at local, regional and global scales within reasonable error limits. These

ET estimates are possible to be made available on regular basis at regional to country scale. Time series ET products can be used to predict regional yield that needs less processing time and optimal combinations of input satellite and ground based data. Though a concerted effort has been made to apply different satellite based ET techniques over homogeneous agroecosystems in India, these techniques need to be well-tested over semi-arid and heterogeneous agroecosystems in India before they could be applied for yield prediction study.





# **MATERIALS AND METHODS**



## IV MATERIALS AND METHODS

---

A satellite based single source energy balance algorithm was used with MODIS TERRA, AQUA optical and thermal data to estimate different energy balance components and latent heat flux as a residual over wheat crop.

In the first phase of study, validation of energy balance estimates was carried out using *in situ* attended observations as well as area averaged unattended observations within a 5km x 5km wheat growing region of Kheda district in Gujarat. This validation experiment was carried out for two consecutive wheat seasons, 2005-06 and 2006-07.

In the second phase of the study, time series regional evapotranspiration (ET) was estimated between November to March at every eight-day for past three *rabi* seasons : 2002-03, 2003-04 and 2004-05, using MODIS time composited reflectances and land surface temperatures (LST). Regional wheat yield was predicted using time series ET and associated spatially derived variables using two different approaches over dominant wheat growing districts of Gujarat. Predicted yield was validated using reported district average yield using independent datasets.

Therefore, the study has two distinct work components:

- (a) Estimation of energy balance components using MODIS products and their validation
- (b) Regional wheat yield prediction over Gujarat and its validation

Different sections required to discuss materials used and methodology adopted to complete above work components have been arranged in following order:

- 4.1 Approach for estimating surface energy balance components and evapotranspiration

- 4.2 Regional yield prediction approaches
- 4.3 Satellite data used and their processing
- 4.4 Validation methodology
  - 4.4.1 Energy balance estimates
    - 4.4.1.1 Characteristics of validation region
    - 4.4.1.2 Climate
    - 4.4.1.3 Description of the Soil
    - 4.4.1.4 Cropping pattern
    - 4.4.1.5 Management practices
    - 4.4.1.6 *In situ* measurements and preparation of validation datasets
      - 4.4.1.6.1 Attended
      - 4.4.1.6.2 Unattended
- 4.5 Statistical analysis

#### **4.1 Approach for estimating surface energy balance components and evapotranspiration**

Actual evapotranspiration (AET) or ET can be estimated from latent heat fluxes ( $\lambda E$ ) and latent heat (L) of evaporation. Latent heat flux ( $\lambda E$ ) is generally computed as a residual of surface energy balance. A single (soil-vegetation complex as single unit) source surface energy balance can be written as

$$\lambda E = Rn - G - H - M$$

(1)

The energy component for metabolic activities (M) is very small and hence can be neglected. The equation 1 can be rewritten as

$$\lambda E = Rn - G - H$$

(2)

$Rn$  = net radiation,  $H$  = sensible heat flux,  $G$  = ground heat flux,  $Q$  = net available energy  $Q$ .

Assuming energy balance closure at any instance during a day, equation 2 can also be written as

$$\lambda E_{ms} = Q_{ms} \cdot \Lambda_{ms} = (Rn - G)_{ms} \cdot \Lambda_{ms} \quad (3)$$

Where  $\Lambda_{ms}$  = Instantaneous evaporative fraction

#### 4.1.1 Estimation of $\Lambda_{ms}$

In the present study,  $\Lambda_{ms}$  was estimated from LST- albedo two dimensional scatterogram using technique given by Roerink *et al.* (2000) and further used by Verstraeten *et al.* (2005) over European forest with NOAA AVHRR data and by Bhattacharya *et al.* (2007) over Indian agroecosystems using MODIS AQUA data. LST and albedo from MODIS TERRA and AQUA observations corresponding to overpass timings, 11: 00-11:30hrs and 13:00-13:30hrs Local Mean Time (LMT), respectively were used to derive  $\Lambda_{ms}$ . The conceptual diagram is shown in Figure 1.

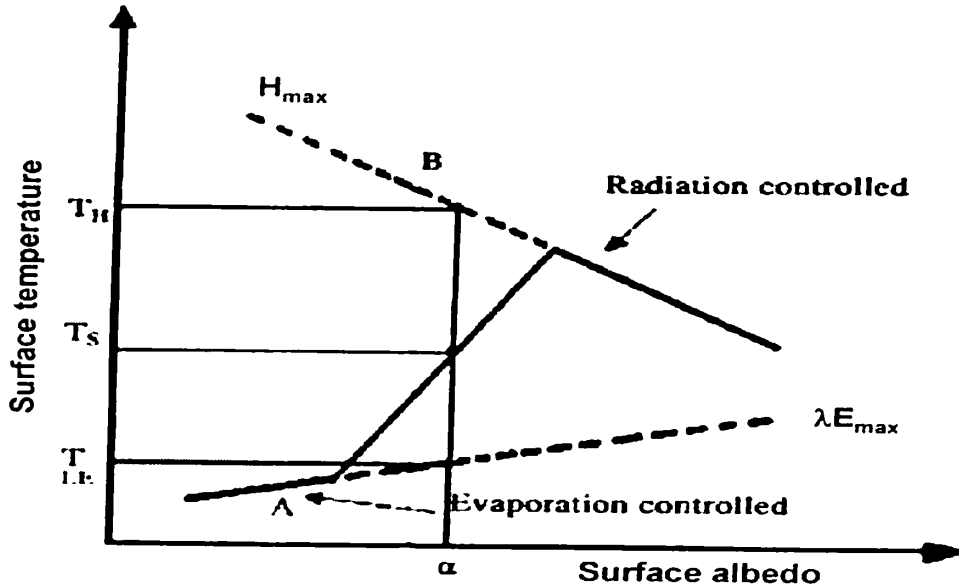


Figure 4.1 Conceptual diagram of two-dimensional scatter of land surface temperature (LST) and surface albedo

A simple method to obtain ' $\Lambda_{ms}$ ' is to use 2D scatter of surface albedo and land surface temperature (Su & Menenti, 1999; Su et al., 1999; Roerink et al., 2000) to find out dry and wet edges from LST – albedo empirical relations. LST is surface temperature that represents integrated effect from soil-vegetation cover complex (Bhattacharya & Dadhwal, 2003). It maintains equilibrium between energy supply (radiation balance) and energy used (energy balance). Surface albedo determines the amount of outgoing shortwave radiation.

Surface wetness affects both surface reflectance and land surface temperature. If soil is wet, its reflectance decreases than when it is dry. It can be decreased 2-3 times than when it is dry which affects surface available energy. Soil moisture controls LST. It is higher with increasing dryness. But the relation between the two changes continuously throughout the day. The combination of relation between surface soil moisture content, reflectance and LST showed a correlation between LST and reflectance of the 3<sup>rd</sup> order polynomial type (Bastiaanssen, 1995; Bastiaanssen et al., 1998a)

$$\Lambda_{mon} = \frac{\lambda E}{H + \lambda E} \approx \frac{Ts_H - Ts}{Ts_H - Ts_{wz}} \quad (4)$$

$Ts_H$  = LST on dry edge computed as linear function of surface albedo

$Ts_{wz}$  = LST on wet edge computed as linear function of surface albedo

$Ts$  = Pixel LST

#### 4.1.2 Estimation of $Q_{ms}$

Instantaneous net available energy ( $Q_{ms}$ ) =  $Rn_{ms} - G_{ms}$  (5)

$G_{ms}$  = instantaneous ground heat flux

Clear sky instantaneous net radiation ( $Rn_{ms}$ ) was computed from surface radiation budget.

$$Rn_{ms} = Rns_{ms} - Rnl_{ms} \quad (6)$$

$Rns_{ms}$  = instantaneous net shortwave radiation ( $Wm^{-2}$ )

$$= Rs_{ms} (1 - \alpha) \quad (7)$$

$\alpha$  = surface albedo which was computed by converting seven narrow-band optical reflectances using coefficients given by Liang (2002)

$Rs_{ms}$  = instantaneous insolation ( $Wm^{-2}$ ) computed using WMO clear sky model

$$Rs_{ms} = a.I_0.\varepsilon.(SIN\gamma)^b \quad (8)$$

The coefficients, 'a' and 'b' were worked out to be 0.75 and 1.28 over Indian sub-continent by Bhattacharya *et al* (2007)

$I_0$  = solar constant =  $1367 Wm^{-2}$

$\varepsilon$  = sun-earth distance correction factor

$Rnl_{ms}$  = instantaneous net longwave radiation ( $Wm^{-2}$ )

= downwelling longwave - outgoing longwave

$$= \varepsilon_s \varepsilon_a \sigma T_a^4 - \varepsilon_s \sigma T_s^4$$

$T_s$  = land surface temperature ( $^{\circ} K$ ). Here MODIS land surface temperature (LST) products from TERRA and AQUA were used.

$\sigma$  = Stephan-Boltzmann constant ( $5.67 \times 10^{-8} Wm^{-2}s^{-1}K^{-4}$ )

$\varepsilon_s$  = surface emissivity was estimated from NDVI based method given by Van de Griend and Owe (1993)

$\varepsilon_a$  = air emissivity estimated from air temperature using empirical model given by Campbell and Norman (1998).

Air temperature ( $T_a$ ) at satellite overpass was estimated from NDVI-LST 2D triangular scatter by extracting LST at maximum NDVI within a spatial domain of  $20 \times 20$  pixels.

Instantaneous ground heat flux ( $G_{ms}$ ) was estimated as:

$$= Rn_{ins} \left[ \frac{(Ts - 273.15)}{\alpha} \right] \left[ (0.0032\alpha + 0.0062\alpha^2)(1 + 0.978NDVI^4) \right]$$

Bastiaanssen *et al.* (1998) (9)

#### 4.1.3 Estimation of daytime net available energy ( $Q_d$ ) and latent heat flux ( $\lambda E_d$ )

$$\lambda E_d = \Lambda_d \cdot Q_d \quad (10)$$

$$Q_d = \int_1^2 Q(t) \quad (11)$$

Where,  $\lambda E_d$  = daytime average latent heat fluxe ( $Wm^{-2}$ )

$Q_d$  = daytime average net available energy ( $Wm^{-2}$ )

$\Lambda_d$  = daytime average evaporative fraction

On clear sky days, diurnal  $Rn$  and  $Q$  follow typical sinusoidal variation between sunrise ( $t = t1 = t_{rise}$ ) to sunset ( $t = t2 = t_{set}$ ) like insolation (Zhang & Lemeur, 1995; Bisht et al, 2005). But diurnal variation of sensible ( $H$ ) and latent heat ( $\lambda E$ ) fluxes may not show sinusoidal variation since they depend on highly dynamic behaviour of stability conditions of overlying atmosphere. Instantaneous evaporative fraction during daytime hours was assumed constant throughout the day in many satellite based ET algorithms (Baastiaanssen et al., 1998; Farah et al., 2004).

So,  $\Lambda_{ins} \approx \Lambda_d$

$$Rn_d(Wm^{-2}) = \left( \frac{2Rn_{noon}}{\pi SIN \left[ \left( \left( \frac{t_{set} - t_{rise}}{t_{set} - t_{rise}} \right) \right) \pi \right]} \right) \quad (12)$$

-

$$Q_d (Wm^{-2}) = \left( \frac{2Q_{ins}}{\pi SIN \left[ \left( \left( \frac{t_{sat} - t_{rise}}{t_{set} - t_{rise}} \right) \right) \pi \right]} \right) \quad (13)$$

where,

$t_{sat}$  = Time of satellite overpass

$t_{rise}$  = LMT (hrs) at sunrise

$t_{set}$  = LMT (hrs) at sunset

But evapotranspiration occurs only during daylight hours because of positive net energy input during daytime. But net surface available energy becomes negative during night, which gets balanced with sensible heat flux towards surface. Therefore, daily evapotranspiration (ET) can be computed from daytime average latent heat fluxes.

$$ET (mmd^{-1}) = \frac{daylength \times \lambda E_d}{24 \times 28.588} \quad (14)$$

$$daylength(hrs) = t_{set} - t_{rise}$$

## 4.2 Regional yield prediction approaches

Two approaches were attempted based on

(i) Water use efficiency (WUE) and (ii) Radiation use efficiency (RUE)

### (i) Water use efficiency (WUE) based approach

The water use efficiency is defined as ratio of final yield of crop and total accumulated AET during crop growth cycle. In the present study districtwise water use efficiency was derived from historical district average yield and seasonal accumulated AET (derived from MODIS data) on the basis of crop phenological calendar for major wheat growing districts of Gujarat. Wheat mask was generated for all major wheat growing districts of



Gujarat using MODIS AQUA 250 meter eight day composite, so only wheat pixels could be extracted for AET accumulation. The eight day AET composite was derived from MODIS-AQUA at 1km. The derived districtwise WUE was used to predict districtwise crop yield at the end of crop season.

$$Yield = WUE \sum_{i=1}^n ET_i \quad (15)$$

In order to predict crop yield well in advance and before physiological maturity, accumulation period needed to be varied districtwise. It was reduced octad by octad from physiological maturity in each step and then WUE was computed for each step using historical grain yield and accumulated AET. These methods were repeated till 50% of length of growing period was reached. Moreover, crop stagewise WUE was also computed and further used to predict final yield.

**(ii) Radiation use efficiency (RUE) based approach**

*The net amount of biomass (net primary production, NPP) accumulated during a time period by green vegetation is product of the absorbed photosynthetically active radiation and its efficiency to convert it into biomass. The crop yield can be derived by product of total net amount of biomass (NPP) accumulated during whole crop growth and harvest index (HI).*

$$YIELD = \sum_i NPP_i \times HI \quad (16)$$

In the present study, NPP was estimated on spatial (x) (1km) and temporal (t) (8 day) domain by using LAI derived fAPAR and maximum radiation use efficiency (RUE) of crop. The maximum RUE was constrained by using temperature scalars and water scalar following CASA (Carinege Ames Stanford Approach) approach (Field *et al.*, 1995). The output of clear

sky model was found have RMSE of 7 % of observed mean while tested over 12 stations in India (Mallick, 2007).

$$NPP = S(x, t) \cdot fAPAR(x, t) \cdot RUE_{max} T_1(x, t) T_2(x, t) W(x, t) \quad (17)$$

here  $S(x, t)$  is solar isolation,  $fAPAR(x, t)$  is fraction of photosynthetically active radiation absorbed by crop,  $RUE_{max}$  is maximum radiation use efficiency,  $T_1(x, t)$  and  $T_2(x, t)$  are temperature scalars and  $W(x, t)$  is water scalar.

APAR was calculated at each time step as the product of PAR and fAPAR. PAR was calculated as 45 % of the daily total solar surface irradiance. Temperature scalars in this approach were used to capture two aspects of physiological regulation of the plant growth by temperature. One of the scalars,  $T_1(x, t)$ , sets limits on acclimation, reflecting the evidence that inherent biochemical constraints on photosynthesis act to reduce NPP at both very low and high temperatures.

$$T_1(x, t) = 0.8 + 0.02 * T_{opt}(x) - 0.0005 * [T_{opt}(x)]^2$$

(18)

The second  $T_2(x, t)$  scalar expressed the hypothesis that, at every site, growth acclimated to the temperature during the month of greatest NDVI and NPP was suppressed by temperature warmer or cooler than that during the month of maximum NDVI.

$$T_2(x, t) = \frac{1}{\{1 + \exp[0.2(T_{opt}(x) - 10 - T(x, t))]\}} * \frac{1}{\{1 + \exp[0.3(-T_{opt}(x) - 10 + T(x, t))]\}}$$

(19)

where,  $T$  is the mean temperature and  $T_{opt}$  the optimum temperature during the month of maximum NDVI.

In this present study water scalar was calculated as evaporative fraction which is

$$W = \Lambda / ns \quad (20)$$

$T_1$  and  $T_2$  scalars were derived by calibrating MODIS AQUA day-night land surface temperature (LST) mean with ground based daily observed mean air temperature of different agromet surface observatory over Gujarat.

The accumulated time for NPP during crop growth cycle depends on the phenological calendar of a particular district. The accumulation of NPP starts with the emergence and it continues up to physiological maturity. Districtwise wheat calendars were obtained from India Meteorological Department (<http://imdagrimet.org/cwc.htm>).

#### **4.3 Satellite data used and their processing**

The optical and thermal observations from MODIS at TERRA (11:00-11:30hrs LMT overpasses) and AQUA (13:00-13:30hrs LMT overpasses) (<http://modis.gsfc.nasa.gov>) platform were basic satellite data sources for this study. A set of operational land related georegistered spatial products that were getting generated on daily and eight day composite basis from both the sensors were used. The process of achieving composite basis was done as maximum value composite (MVC) in each pixel out of consecutive eight days. These were available on tile by tile basis. The dimensions of each tile are usually fixed for different spatial resolutions. Tiled products on seven band surface reflectances and land surface temperatures (LST) corresponding to H24V06 tile having coverage over Gujarat and adjacent regions were used. Surface reflectances are atmospherically corrected at-sensor reflectances (Vermote *et al.*, 2002) in optical bands (band 1 to 7: 0.648  $\mu\text{m}$ , 0.858  $\mu\text{m}$ , 0.470  $\mu\text{m}$ , 0.555  $\mu\text{m}$ , 1.240  $\mu\text{m}$ , 1.640  $\mu\text{m}$ , and 2.130  $\mu\text{m}$  respectively) ranging from red to short-wave infrared (SWIR). Generalized split window and day-night algorithm (Wang *et al.*, 1983 ) were used to generate LST. Basic dimension of reflectance products available at 463.3125 m resolution was 2400 x 2400 and it was 1200 x 1200 at 926.625 m resolution for LST. These were generated as integerised sinusoidal (ISIN) grid

projection. Reflectances were resampled upto 926.625 m before further processing. Daily reflectance and LST products from TERRA and AQUA corresponding to clear days of *in situ* observations were used to compute energy balance components. These clear sky dates are given in Table 4.1.

**Table 4.1** Clear sky dates of daily MODIS reflectance and LST products used for estimating energy balance components

(0.648, 0.858, 0.470, 0.555, 1.64, 2.13)

rabi seasons	Dates of daily MODIS reflectance and LST products	
	TERRA	AQUA
2005-06	15 days ( January 26 , 28, 30) ( February 2, 4, 7, 9, 11, 18, 23, 26) ( March 1)	12 days ( January 14, 16, 26, 28, 30) ( February 2, 4, 7, 9, 11, 23, 26) (March 1, 3, 12 )
2006-07	16 days (December 13, 16, 20, 23, 30) (January 10, 12, 16, 18, 21, 26) (February 2, 6, 10, 13, 17, 20, 26) (March 2, 7)	16 days (December 13, 16, 20, 23, 30) (January 10, 12, 16, 18, 21, 26) (February 2, 6, 10, 13, 17, 20, 26) (March 2, 7)

Time series of eight-day composit reflectances and LST during wheat growing period between November to middle of March in past years 2002-03, 2003-04 and 2004-05 were scheduled for using them for yield prediction purposes. A total of 96 eight-day composites for each of reflectances and LST were scheduled for use. The choice of sensors depended on accuracy of estimates of energy balance components and ET from TERRA and AQUA. Pixel wise data on reflectances and LST were obtained as integer digital numbers (DN) in hierarchial data format (HDF). Scale factors and offsets available with HDF files were used to convert DN values into real quantities. Pixelwise solar zenith angles were also provided with reflectance products. These were used for insolation ( $R_s$ ) estimation. Seven narrow band

reflectances were converted to surface albedo ( $\alpha$ ). Reflectances in red and near-infrared (NIR) corresponding to band 1 and band 2 were used to compute normalized difference vegetation index (NDVI) and surface emissivity ( $\epsilon_s$ ) from it. Air temperature ( $T_a$ ) at time of satellite overpass was taken as minimum LST corresponding to maximum NDVI from LST-NDVI scatterogram. It was further used to compute pixelwise air emissivity ( $\epsilon_a$ ). All these radiation budget parameters alongwith LST were further converted to surface radiation balance i.e. instantaneous net radiation and ground heat fluxes using equations 5 to 8. LST- albedo scatterogram produced instantaneous evaporative fraction ( $\Lambda_{ms}$ ). Daytime net radiation, net available energy, latent heat fluxes and ET were computed using equations 9 to 13. Same processing steps were adopted both for TERRA and AQUA. Flow chart of data processing is shown in Figure 4.2.

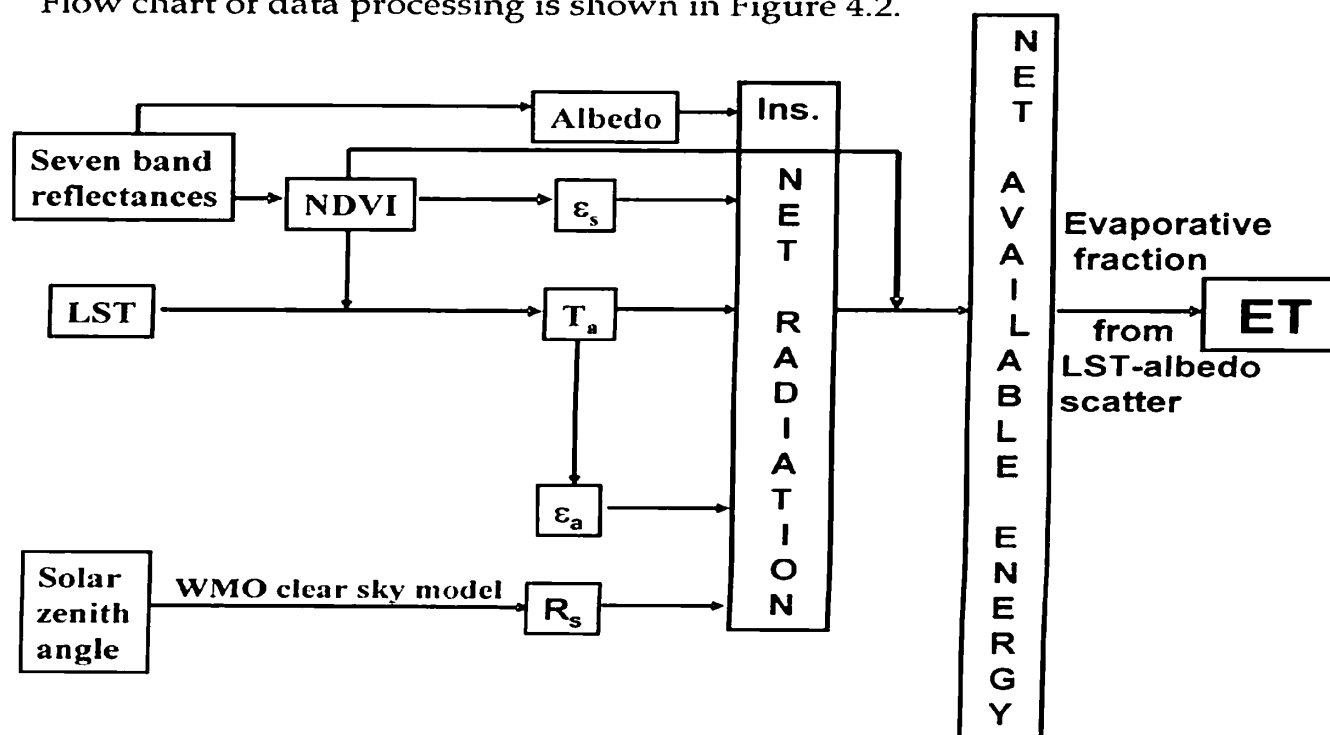
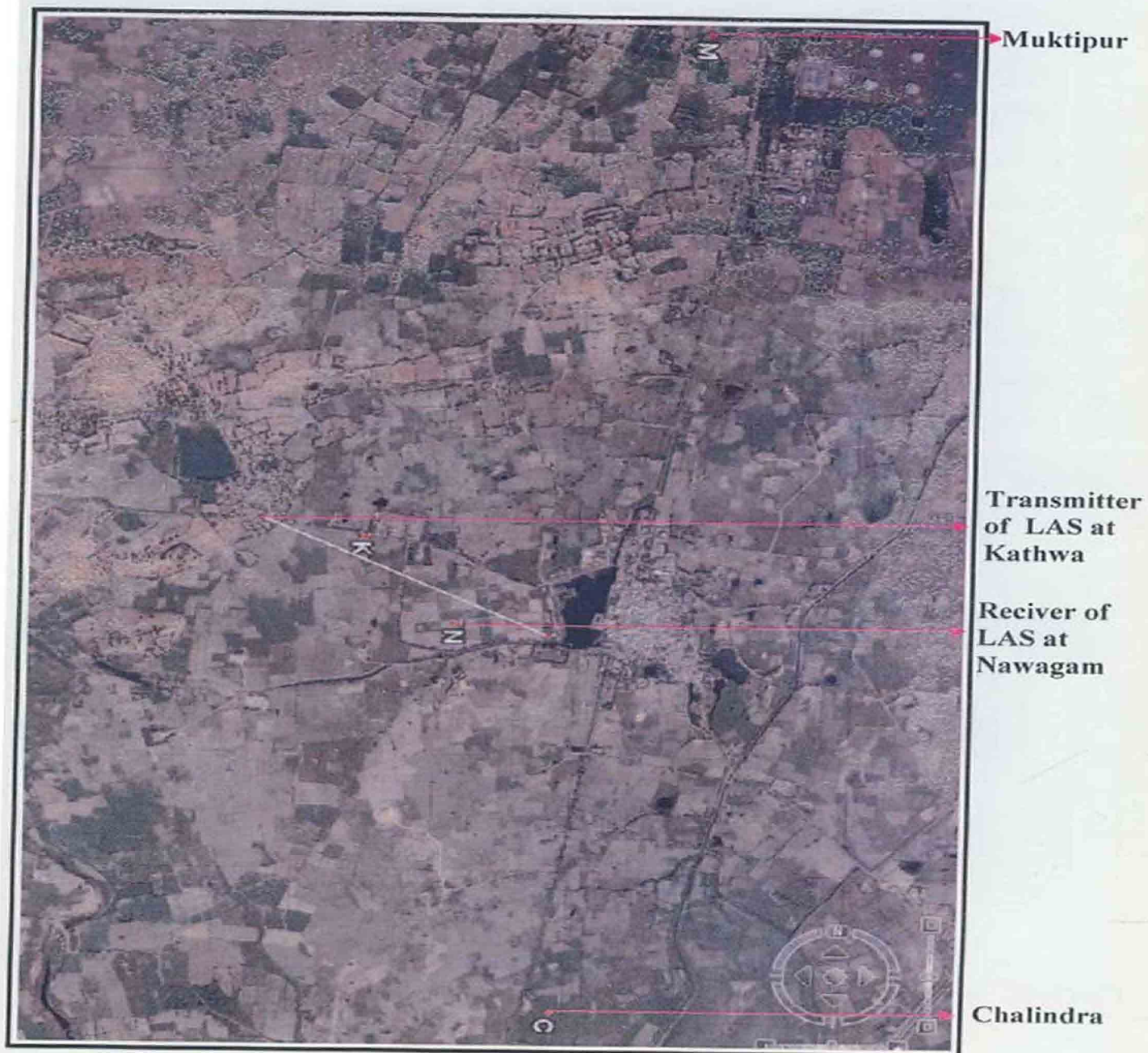


Fig. 4.2 Data processing flow using MODIS TERRA and AQUA product for Energy Balance

#### **4.4 Validation methodology**

##### **4.4.1.1 Characteristics of validation region**

A 5 km X 5 km agricultural grid comprising 3 villages Chalindra ( $22^{\circ} 46' 41.165$  N  $72^{\circ} 34' 28.412$  E), Muktipur ( $22^{\circ} 49' 32.754$  N  $72^{\circ} 34' 41.770$  E) and Nawagam ( $22^{\circ} 46' 45.639$  N  $72^{\circ} 34' 31.118$  E) in Kheda district of Gujarat state was selected for *in situ* measurements and validation of satellite based energy balance estimates. Measurements were recorded from at least 1 km X 1 km continuously growing wheat patch from each of these villages during 2005-06 *rabi* season in Chalindra and 2006-07 Muktipur *rabi* season in Nawagam in the vicinity of rice research station of Anand Agricultural University. The locations of 1 km X 1 km crop patches are shown in fig. 3.



**Fig. 4.3 Location of Study Region**



#### 4.4.1.2 Climate

The location of validation region falls under middle Gujarat Agro-climatic Zone-III. Its climate has been classified as semi-arid tropical. The region is located on the bank of Sabarmati river. The average annual rainfall of Nawagam is 870 mm and is received through Southwest monsoon wind currents during the 3<sup>rd</sup> week of June to the 2<sup>nd</sup> week of September. The winter is medium cool and dry. Summer is quite dry and hot. The month of January is the coolest month of winter with mean monthly minimum temperature varying from 9.4 °C to 29.6 °C. On the other hand, May is the hottest month in which the maximum temperature varies from 21.0° C to 43.3 °C.

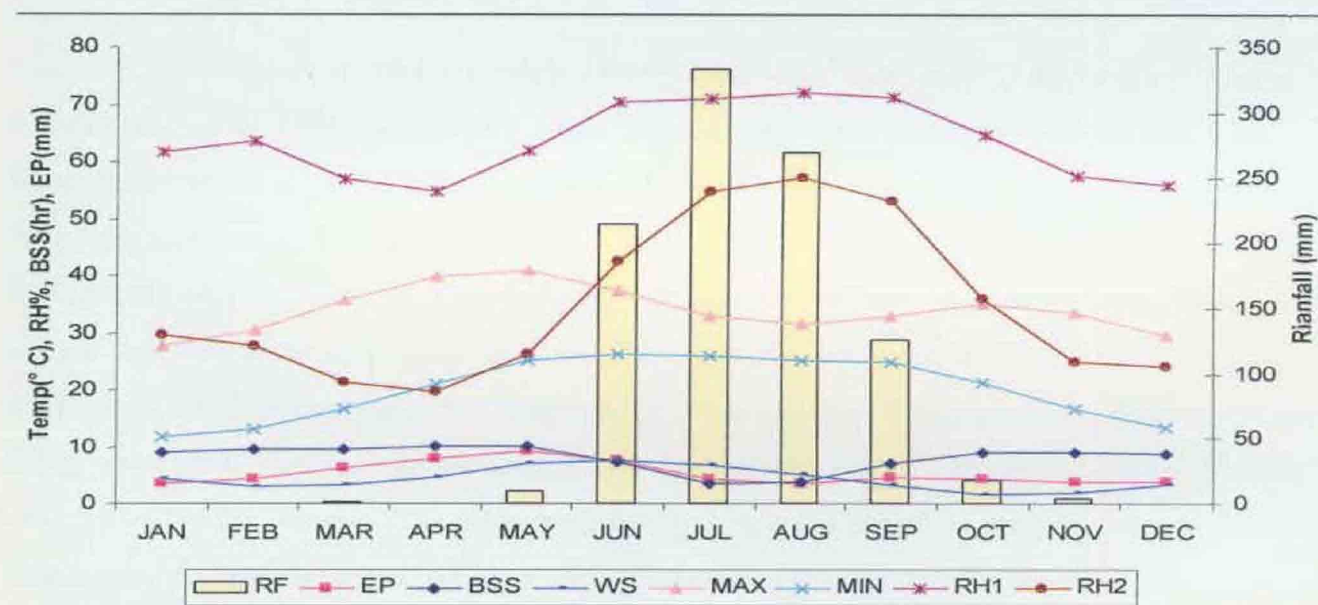


Fig. 4.4 Average weather parameters at Nawagam from 1997-2006.

Mean monthly average of weather variables were computed from previous 10 years (1997-2006) weather record at Nawagam station. The monthly weather parameters are shown in Fig. 4. The maximum temperature (MAX) ranged between 27.6 °C to 40.6 °C while minimum temperature (MIN) ranged between 11.9 °C to 26.3 °C. The monthly total pan evaporation



(PE) increased from January upto May. It decreased between June to December. The range of evaporation was 3.6 to 9.4 mmd<sup>-1</sup>. The Bright Sunshine Hours (BSS) varied between 3 to 10 hrs. Wind speed ranged between 1.6 km hr<sup>-1</sup> to 7.6 km hr<sup>-1</sup>. The maximum rainfall (RF) occurred in the month of July followed by August, June and September months. The Maximum morning and afternoon relative humidity (RH) period was from June to October, and the range was 55 % to 72 % and 20 % to 57 % in morning and afternoon, respectively.

The monthly range, mean, standard deviation (SD) and coefficient of variation (CV) of different weather variables were computed for the wheat growing period between November to March from previous 10 years data at Nawagam station. The trends of weather parameters have been as shown in Table 4.2. Ranges of TMAX and TMIN were the highest in February, but CV was highest in December (5%) for TMIN and in February (11%) for TMAX. Ranges of RH<sub>1</sub> and RH<sub>2</sub> were highest in January and February, respectively. The highest and lowest CV were 57%, 38.4% in November, December for RH<sub>1</sub> and 71.6%, 40% in December, January for RH<sub>2</sub>, respectively. Range of wind speed was the highest in December. Variability was substantially higher in December (41.9%), February (50.5%) and March (60.2) than that for other months. BSS range was highest in March. Its CV varied between 2-7%. Scanty rainfall occurred in November and March from western disturbances. Range of monthly total of pan evaporation (PE) was the highest in March, but CV was highest in December (14.2%).

**Table 4.2.** Climatic variability of weather parameters during wheat growing period at Nawagam for the period 1997-2006

Month	PE (mmd <sup>-1</sup> )	BSS (hrs)	RF mmd <sup>-1</sup>	WS kmhr <sup>-1</sup>	TMAX (°C)	TMIN (°C)	RH1 (%)	RH2 (%)
<b>NOV</b>								
Range	98.3-114.5	8.4-9.6	0-35.6	1-2.9	32.7-34.6	15.2-18.3	62-79	26.8-40
Mean	117.7	9	4.0	2.1	33.6	16.8	56.3	24.3
SD	16.5	0	11.9	0.6	0.6	1.1	32.3	14.3
CV	14	4	300.0	27.7	1.8	6.6	57.3	59.0
<b>DEC</b>								
Range	81.5-126.5	7.8-9.4	0-0	1-5.5	27-30.9	11.9-15.2	62-76	26.5-32.6
Mean	104.8	9	0.0	3.4	29.6	13.2	54.0	20.4
SD	14.9	1	0.0	1.4	1.5	1.1	30.9	14.6
CV	14.2	7	0.0	41.9	5.0	8.3	57.3	71.6
<b>JAN</b>								
Range	106.4-134.2	8.3-9.4	0-0	2.2-6	25.8-28.7	11.1-13.1	57-77	24.5-38.7
Mean	119.5	9	0.0	4.4	27.5	11.9	60.7	29.2
SD	8.4	0	0.0	1.2	0.8	0.7	23.9	11.7
CV	7.0	4	0.0	26.4	2.7	5.6	39.4	40.0
<b>FEB</b>								
Range	124.2-168.6	9.2-9.7	0-3.2	0.4-4.6	28.9-32.8	11.9-15.4	61-77	22.3-41.8
Mean	145.1	9	0.4	3.1	30.3	13.2	63.2	28.2
SD	14.2	0	1.1	1.6	1.3	1.5	24.2	12.0
CV	9.8	2	300.0	50.5	4.2	11.2	38.4	42.6
<b>MARCH</b>								
Range	205.2-256.9	8.7-10.2	0-2	1-5.3	33.5-36.2	15-17.6	54-74	16-32
Mean	235.9	10	0.2	3.6	35.5	16.6	56.7	21.1
SD	19.4	0	0.7	2.2	1.3	0.7	22.1	9.0
CV	8.2	5	300.0	60.2	3.7	4.5	39.0	42.9

#### 4.4.1.3 Description of the soil

The soil of the validation region and its surroundings is medium black deep to very deep, poorly drained and salt affected. Texture of the soil is loamy sand with water holding capacity as 18% and bulk density as 1.35 g cm<sup>-3</sup>. Soil pH is neutral to alkaline (7.2-7.9) with low organic matter (0.55-0.62) and nitrogen (0.46 – 0.53 kg ha<sup>-1</sup>) with medium available phosphorus (88 – 92 kg ha<sup>-1</sup>) and maximum available potassium (688 – 889 kg ha<sup>-1</sup>). The soil properties are summarized in Table 4.3.

**Table 4.3. Soil physical and physicochemical properties**

Soil Properties			
Physical		Physicochemical	
Texture	Loamy sand	CEC c mol (p <sup>+</sup> ) kg <sup>-1</sup>	11.6
FC (Vol. %)	18.0 %	PH	7.2 – 7.9
PWP (Vol. %)	5.0 %	Organic Carbon (%)	0.55-0.62
Bulk density (g cm <sup>-3</sup> )	1.35	Available N <sub>2</sub>	0.46 – 0.53 kg ha <sup>-1</sup>
		Available P <sub>2</sub> O <sub>5</sub>	88 – 92 kg ha <sup>-1</sup>
		Available K <sub>2</sub> O	688 – 889 kg ha <sup>-1</sup>

#### 4.4.1.4 Cropping pattern

The validation was carried out on wheat (*Triticum aestivum* L.) crop. The dominant cultivar was GW-496 which is widely grown in Gujarat. This cultivar is a cross between HD 2278 and CPAN 1861. This was released by Wheat Research Station, GAU, Junagadh and has been recommended for general cultivation since 1990. It is a semi-early (105-115 days), semi-erect variety with good tillering capacity and is fairly resistant to rust and smut. Rice - wheat cropping sequence is the most prevalent in the area. Good irrigation facility ensures conducive conditions for *rabi* crop, mostly wheat.

#### **4.4.1.5 Management practices**

The land of the experimental field was prepared by removing the stubbles of the rice crop and was subsequently ploughed with tractor drawn mould board plough. Breaking the clods by means of a cultivator followed this operation. Planking was done thereafter. After carrying out the land preparation field was ready for sowing. After application of the basal dose of fertilizers in the field, wheat seeds were subsequently broadcast manually in lines at a depth of 5 cm. Line to line spacing was 22.5 cm. The crop was uniformly fertilized with 120:60:40 kg NPK per ha. Half the dose of nitrogen and the entire quantity of phosphorus ( $P_2O_5$ ) and potash ( $K_2O$ ) were applied as basal dose before sowing seed. The rest half of the dose of nitrogen was applied immediately after attaining crown root initiation. Irrigation was given as per normal practices. A known quantity of 60 mm of water was applied to the experimental field. The sources of irrigation were tube well and canal. As precautionary measures Chloropyriphos @4.5 ml plot<sup>-1</sup> was applied with irrigation for control of termite during the crop growth periods in both the years. Interculturing by hand weeding was carried out after CRI stage during both the years.

#### **4.4.1.6 *In situ* measurements and preparation of validation datasets**

##### **4.4.1.6.1 Attended**

Ground based measurements were carried out using portable instruments during both the *rabi* seasons 2005-06 and 2006-07 of wheat crops. Different measured parameters, instruments and frequency of measurements are summarized in Table 4.4. The measured parameters have been grouped into A. Radiation and energy balance, B. Soil related parameters and C. Biometric.

**Table 4.4** Observational details

Ground measured parameters	Instruments	Location	Frequency
A. Radiation and energy balance		Chalindra and Muktipur in	7-14 days interval
(i) Insolation / PAR	Pyranometer (Kipp and Zonen, Holland)	three replication for each village during 2005-06	
(ii) Albedo			
(iii) Net radiation (Rn)	Net radiometer (Kipp and Zonen, Holland)	Nawagam in two replications during 2006-07	
(iv) Bowen ratio (β)	Multi-level portable weather station (MAWS) / Large Aperture Scintilometer (LAS)		
(v) Ground heat fluxes (G)	Thermal conductivity sensor (Kipp and Zonen, Holland)		
B. Soil related parameters			
(i) Soil moisture	Gravimetric method	At 10cm, 20cm depths	14 days interval
C. Biometric			
(i) LAI, FAPAR, Biomass	Canopy analyzer (Delta-T Devices ltd., UK)	All locations	14 days interval
(ii) Yield			At harvesting

The net radiation, insolation, albedo and thermal conductivity were measured at hourly interval during 2005-06 at Chalindra and Muktipur while for 2006-07 these were measured at half hourly interval at Nawagm. The observations were recorded at 7 to 14 day interval during wheat growing period. Soil moisture was measured using gravimetric method at 14 days interval. The biometric measurements on LAI, FAPAR and biomass were also carried out at 14 day interval.

#### **A. Radiation and energy balance**

##### **A.1 Insolation**

Incident solar radiation received at the ground is the driving input to energy balance, productivity and crop simulation models. It was measured using SPLITE pyranometer (Plate 1). The instrument used a photodiode detector, which created a voltage output that was proportional to incoming solar radiation. Its sensitivity was proportional to the cosine of the angle of incidence of the incoming radiation, allowing accurate and consistent measurements. The spectral range was 0.4 - 1.1 $\mu$ m, sensitivity was 100  $\mu$ V/W/m<sup>2</sup> and response time was less than 1 s.

##### **A.2 Net radiation**

NR LITE was used for measurements of net radiation which is the balance between incoming and outgoing radiation in short wave and long wave bands respectively. The detector was Teflon coated weather resistant black conical absorber as shown in plate 2. It was based on thermopile sensor. The voltage was proportional to the net radiation. It could be directly connected to a voltmeter or a data logger with an mV input. The spectral range was 0.2 to 100 $\mu$ m, with sensitivity 10  $\mu$ V/W/m<sup>2</sup> and range 2000 to +2000 W/m<sup>2</sup> having a response time of 20 s.

### **A.3 Thermal property analyzer**

For measurement of ground heat flux, KD2 Thermal Property Analyzer was used (plate 3). The instrument consisted of a needle known as sensor alongwith hand held display monitor that showed the output of thermal conductivity, soil temperature and thermal diffusivity. The observations were taken at three different depths viz. 0.2m, 0.4m and 0.6m for calculation of ground heat flux through soil layers.

### **A. 4. Bowen ratio**

This is the ratio of energy available for sensible heating to energy available for latent heating . The Bowen ratio technique required measurements of air temperature and water vapor pressure at two vertical points (separated by a distance of about 1 m) above the canopy (typically at 0.5 and 1.5 m above canopy for wheat crop). Portable Automatic weather recording instrument was placed inside the wheat field for continuous measurements of the temperature, wind speed and humidity at different heights over validation region.

#### **A.4.1 Pocket weather meter**

For measurement of air temperature, relative humidity, current wind speed the Kestrel 4000 pocket wind meter was used as shown in plate 4. It was easy to read because having backlit display. The temperature range was 29.0 to 70.0 °C with accuracy of 1.0 °C. The relative humidity sensor had range of 5.0 to 95.0 % non-condensing with accuracy of 3.0 %RH. The wind speed sensor had the range of 0.4 to 40.0 ms<sup>-1</sup> and accuracy of 3% of full scale reading.

#### **A.4.2 Multi-level automatic weather station (MAWS)**

The wind speed, temperature and relative humidity were measured in wheat crop at five heights (0.25, 0.5, 0.75, 1.0, 1.25m above ground) using

portable MAWS installed in Chalindra as shown in plate 6 and plate 5 for automatic weather station at Nawagm. Subsequently Bowen ratios were computed from the ratio of temperature and vapour pressure gradients obtained through multi-height measurements.



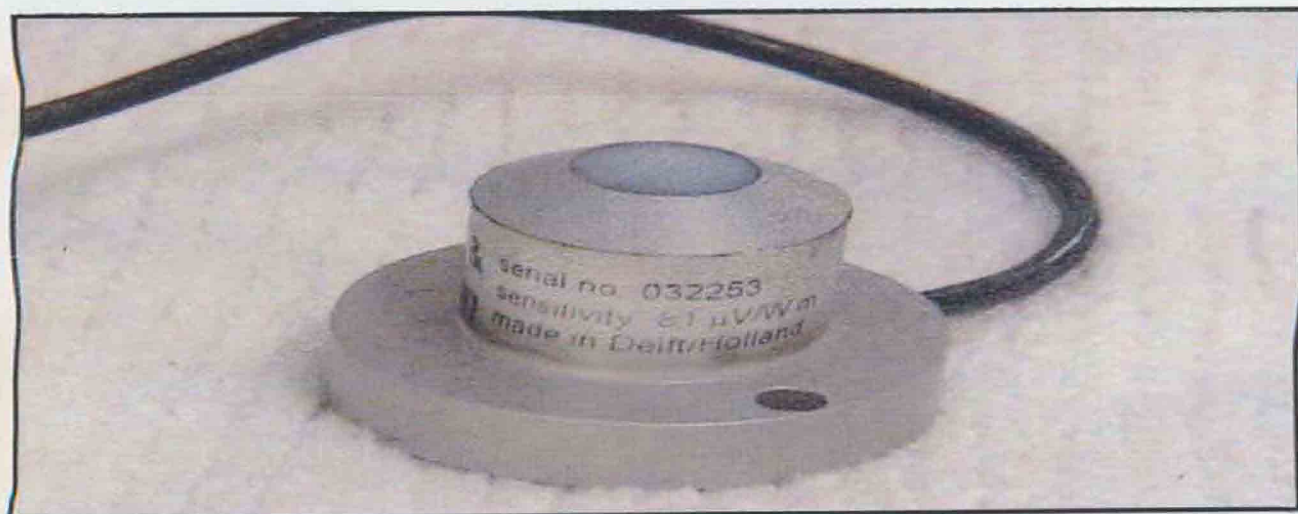


Plate 1: (a) Pyranometer (b) Net Radiometer (c) Thermal Property Analyzer



**Plate 3:** Multi-level automatic weather station at Chalindra in Wheat Field

## **B. Soil related parameters**

Soil moisture content at 10cm and 20cm soil depths was determined using gravimetric method before and after each irrigation. Soil samples were collected in Keen's boxes. These were covered with the lid and taped immediately. Soil samples were weighed before and after oven drying at 105 °C for 24 hrs, until a constant weight was recorded. Conversion of soil moisture into volumetric content was done using equation 21.

$$\theta_g = [(W_w - W_d) / (W_d - W_c)] \times 100 \quad (21)$$

$$\theta_v = \theta_g \times \text{Bulk density}$$

where,

$\theta_g$  = gravimetric water content (g of water g<sup>-1</sup> of soil)

$\theta_v$  = volumetric water content (m<sup>3</sup>m<sup>-3</sup>)

$W_w$  = Weight of moist soil and container (g)

$W_d$  = Weight of oven dry soil and container (g)

$W_c$  = weight of container (g)

## **C. Biometric parameters**

### **C.1 Total dry matter**

Five plants were uprooted randomly from one meter square area in the field to record total dry matter. Leaves, stem, root and spikes were separated and initially dried in shade. They were then dried in oven at 65°C for 72 hours till a constant weight was reached.

### **C.2 Phenological observations**

Based on the observations on individual plants on days of *in situ* measurements, occurrence of different phenological events viz., emergence, crown root initiation, tillering, boot, ear emergence, anthesis, milking, dough stage and physiological maturity were identified (Zadoks *et al.*, 1974). When



50% of the plants on a plot reached the particular event, that particular day was reckoned as the day of the onset of that event.

### **C.3 Leaf area index (LAI)**

The Leaf Area Index (LAI) is the ratio of total upper leaf surface of a crop divided by the surface area of the land on which the crop grows. LAI influences radiation interception, transpiration and photosynthesis. LAI was measured directly by Sun Scan Canopy Analysis System (Plate 6) at 14 day interval. This time period comprised noon hour (1200-1300 h) of the day. The Sun Scan Canopy Analysis System compute and displayed LAI with an accuracy of  $\pm 0.1$  over the range of LAI less than 10 and solar zenith angle less than  $60^\circ$ . Thus, noon hour measurement exhibited more accuracy (Sun Scan System, 1996).



S

**Plate 4: Sun Scan Canopy Analysis System**

#### **C.4 Grain and straw yield**

In each of the farmer's plot 1m x 1 m area was selected for crop cutting in replicates to find out the average yield which was subsequently converted on the weight of the grains into per hectare basis. After nipping the kernels, the straw was subjected to sun drying for over a period of a week till constant weight was obtained. The same weight was then converted on a hectare basis.

##### **4.4.1.6.2 Unattended**

##### *Large Aperture Scintillometer (LAS) measurements*

The Large Aperture Scintillometer (LAS) provides continuous area integrated sensible heat flux measurement throughout the day at desired time interval. The LAS worked on the principle that as an electromagnetic (EM) beam of radiation propagates through the atmosphere it is distorted by a number of processes. These processes removed energy from the beam and led to attenuation of the signal. The most serious mechanism that influenced the propagation of EM radiation were small fluctuations of refractive index of air (n). Its fluctuations led to intensity fluctuations, which were known as scintillations. The fluctuations in the refractive index are usually caused by fluctuations in the density of air, which are in turn caused by temperature (T) and humidity (Q) fluctuations.

The LAS having ability to measure the 'amount' of scintillations, which could be expressed as the structure parameter of the refractive index of air ( $C_n^2$ ).

Once the structure parameter of the temperature was known, the sensible heat flux (H) could be derived from the relation

$$\frac{C_n^2}{T^2} (Z_{LAS} - d)^{5/3} = f \left[ \frac{Z_{LAS} - d}{L_{MO}} \right] \quad (22)$$

Here  $Z_{LAS}$  is the height of the LAS above the surface,  $d$  is the zero plane-displacement height and  $T_*$  is the temperature while  $(C_T^2)$  represents the structure parameters of temperature

$T_*$  is the temperature scale defined as

$$T_* = \frac{-H}{\rho C_p u_*} \quad (23)$$

and  $L_{MO}$  is the Obukhov length.

For most day time (unstable) conditions and when the LAS is installed relatively high ( $Z_{LAS} > 10m$ ) the contribution of the friction velocity is relatively small. For these conditions the free convection method could be applied.

$$H = \rho C_p 0.48 (Z_s - d) \left( \frac{g}{T} \right)^{1/2} (C_T^2) \quad (24)$$

The Bowen ratio is defined as the ratio between the sensible ( $H$ ) and latent heat flux ( $LE$ ).

$$LE = \frac{H}{\beta} \quad (25)$$

In the above relation (24)  $\rho$  is the density of air ( $\sim 1.2 \text{ kg m}^{-3}$ ),  $C_p$  is the specific heat of air ( $\sim 1005 \text{ J kg}^{-1} \text{ K}^{-1}$ ), ' $g$ ' is gravitational acceleration ( $\sim 9.81 \text{ m s}^{-2}$ ).

The selected area, i.e. the area from which the turbulence in the scintillometer path, extends from the scintillometer base line up-wind for a certain distance. This depends on the height of the scintillometer and the stability of the atmosphere. This disturbance aspect has been taken into account that for different wind directions in which the source area falls within the, more or less homogenous area of interest. The signal becomes saturated if the scattering goes above a certain limit, as linear theory on which scintillometer equations are based, no longer holds true.

LAS system (model LAS 150, Kipp & Zonen B.V. Netherland) was installed in for the first time for agricultural studies in India. The LAS site at Navagam (Main Rice Research Station under Anand Agricultural University) is under the semiarid zone and follows the rice-wheat cropping system.

The LAS (Figure 5) receiver was mounted on the roof of the Research Centre building at a height of 10 m (along with tripod) from the ground so that there could be no decrease in scintillation. In dry condition higher installation height is required to prevent loss of scintillation as compared to installation under wet condition. The transmitter was installed on a roof of a farmer's house in adjacent Kathwada village, with a diagonal distance of 1.5 km from rice research farm to avoid signal saturation. In the path length, between receiver and transmitter, there was no concrete construction and the whole area was homogenous agricultural land with rice-wheat cropping system. The attached data logger recorded weather parameter (temperature, pressure, wind speed and relative humidity) and the structure parameter of the refractive index at 10 minute interval which acted as an input file for deriving heat fluxes from the WINLAS software. These further required surface roughness, zero plane displacement and path length for computation of sensible heat fluxes (H).

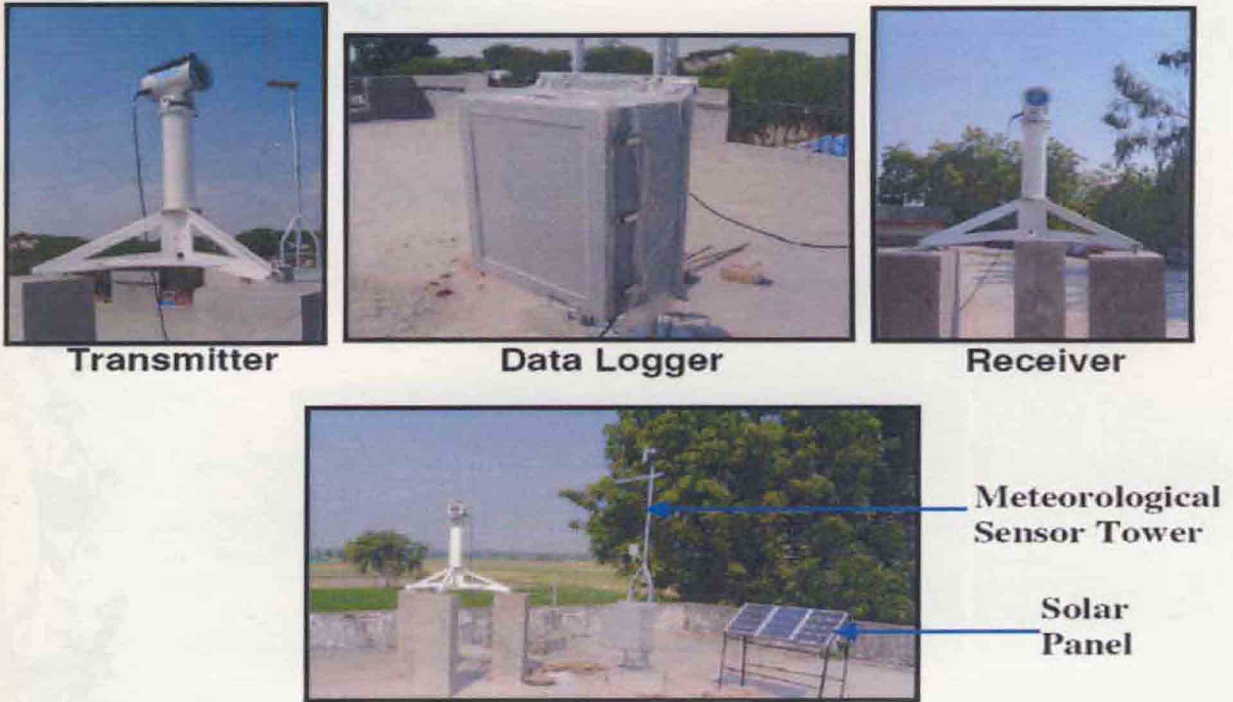


Figure 4.5. Large Aperture Scintillometer and its components

#### 4.5 Statistical analysis

Error statistics of satellite based estimates were computed using mean absolute error (MAE) and root mean square error (RMSE) by comparing them with measurements. They were calculated according to Willmott (1982) as follows and were based on the terms ( $P_i - O_i$ ):

$$MAE = \sum_{i=1}^n [P_i - O_i] / n \quad (23)$$

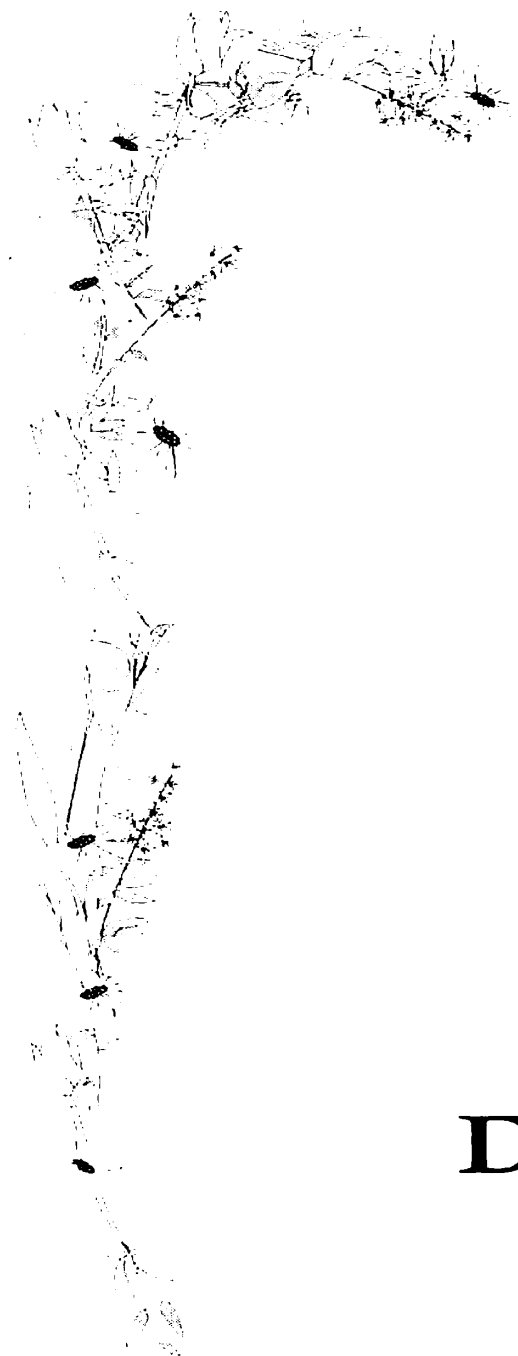
and

$$RMSE = \left[ \sum_{i=1}^n (P_i - O_i)^2 / n \right]^{1/2} \quad (24)$$

where,

$P_i$  = i-th estimate,  $O_i$  = i-th observations or measurements,  $n$  = no. of datasets





# **RESULTS AND DISCUSSION**



## V. RESULTS AND DISCUSSION

---

The present investigation was carried out during the *rabi* seasons of the years 2005-06 and 2006-07 with the prime objective of estimating the surface energy budget components and its use for wheat yield prediction using satellite data over semi-arid agro-ecosystem. The satellite based estimations or predictions were compared with *in situ* measurements or reported estimates. The results are presented and discussed under titled paragraphs in pursuance of the objectives set forth for the study. Sections are followed as:

- 5.1 Characterization of energy budget over semi-arid wheat
- 5.2 Validation of satellite based estimates net radiation and latent heat fluxes
- 5.3 Spatio-temporal variability
- 5.4 Wheat mask generation
- 5.5 Multi-temporal analysis of energy budget estimates in wheat
- 5.6 Evapotranspiration and consumptive water use (CWU) of wheat
- 5.7 District level wheat yield prediction
- 5.8 Comparison of regional wheat yield distribution from two approaches

### 5.1 Characterization of energy budget over semi-arid wheat

Radiation components are markedly influenced by local atmospheric conditions, plant density and geometry, surface wetness conditions. It plays an important role not only in plant growth and development process such as photosynthesis but also determines the climate near ground through the feedback mechanism. The net radiation,

which is the balance of net shortwave and net longwave radiation, is the fundamental source of energy responsible for exchange processes *between surface (soil + canopy) and atmosphere. In the present section*, the temporal variation of measured (insolation, net radiation, evaporative fraction) and satellite (albedo, NDVI and LST) based radiation parameters during wheat growth period in 2005-06 and 2006-07 over the study region is presented below.

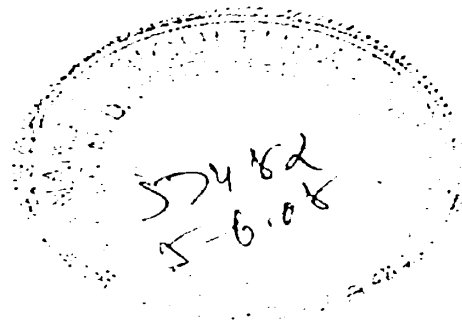
### **5.1.1 Temporal evolution of different radiation parameters**

#### **5.1.1.1 Using *in situ* measurements**

The measured clear sky instantaneous insolation at MODIS TERRA and AQUA overpasses are shown in Figure 5.1 (a) and 5.1 (b) for 2005-06 and 2006-07, respectively. In both the wheat growing seasons, insolation at TERRA overpass did not show substantial day-to-day fluctuations but a slow increase between 400 – 600 Wm<sup>-2</sup>. As expected, insolation at noontime AQUA overpass was substantially higher with a gradual increasing trend between 650 – 950 Wm<sup>-2</sup>. The overall clear sky atmospheric transmissivity varied between 0.7-0.8. Two important atmospheric variables, ozone content, columnar water vapour and aerosol are generally responsible for perturbations in clear sky insolation. Among them, aerosol loading is the major component, which is generally low at rural background or over agricultural patches (Gadhavi and Jayaraman, 2004). The small range of transmissivity could be due to low impact of aerosol due to relatively low reduction in visibility in rural settings.

The ratios of measured net radiation at different hours from morning to evening and average daytime net radiation were computed for both the seasons (Table 5.1) at vegetative, flowering, grain filling and physiological maturity stages of wheat crop. At all the stages, a diurnal trend was observed with peak at noon hours between 12:00-13:00 hrs having increasing trend in the morning hours (8:00-11:00 hrs) and gradual decline towards afternoon hours (14:00-16:00 hrs.). But the average of

hourly ratios were found to be marginally increased from 0.9-1.1 in 2005-06 and rigidly increased from 1.27-1.87 in 2006-07 from vegetative to physiological maturity. Though diurnal trend could be attributed to daily solar cycle but the ratios differ largely between two seasons. The interseasonal differences could be attributed to variability in prevailing soil and canopy conditions and their location specific diurnal interactions with atmosphere. Soil moisture is a key variable affecting the surface energy balance in terrestrial ecosystems (Chapin *et al.*, 2000; Clein *et al.*, 2000; McGuire *et al.*, 2000). Variations in soil moisture influence the partitioning of the net into latent, sensible and ground heat flux (Hinzman and Kane 1992; McFadden *et al.*, 1998).



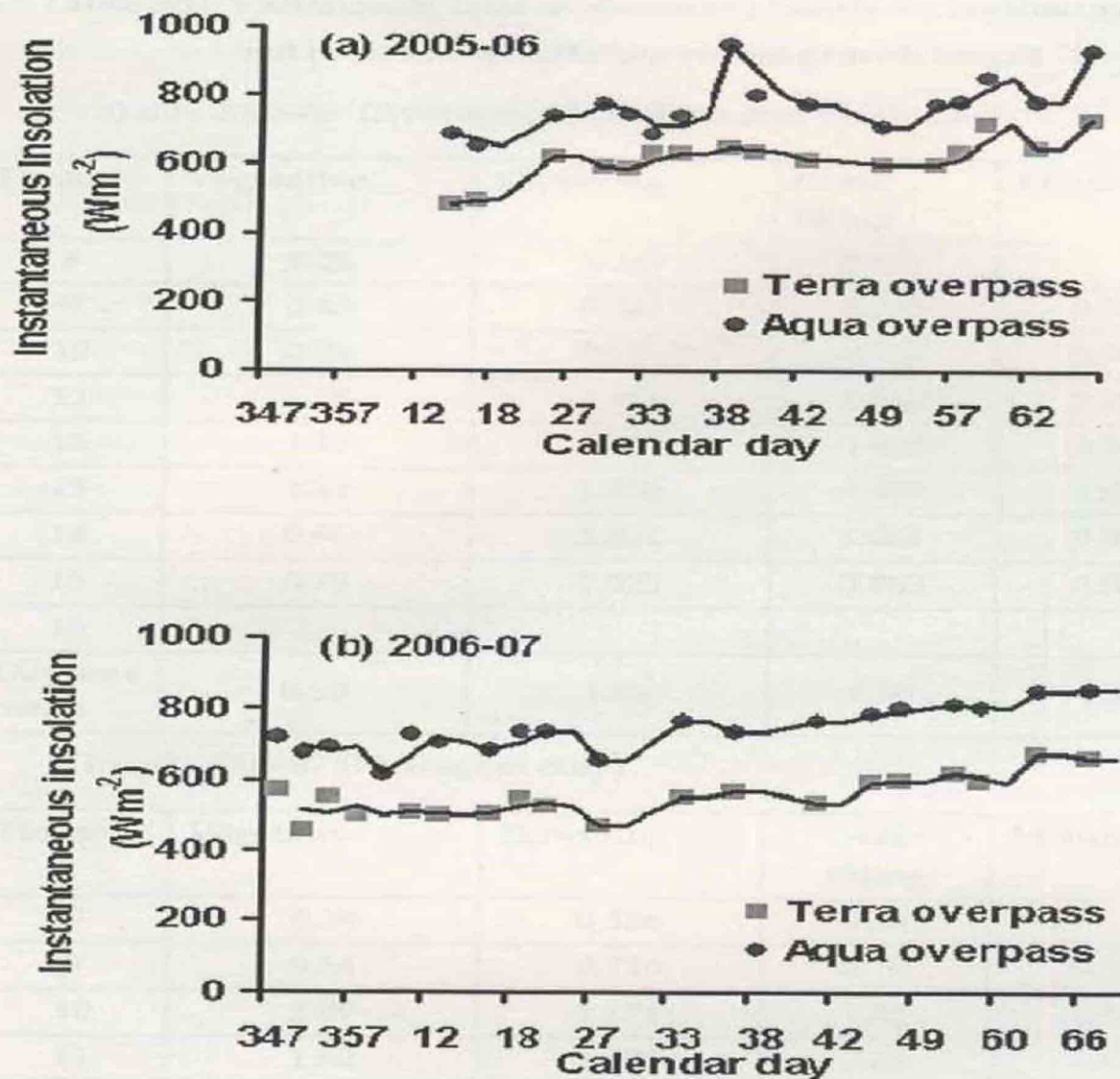


Fig. 5.1 Temporal variation of measured instantaneous insolation at MODIS TERRA ( 11.00 hrs) and MODIS AQUA (13.30 hrs) overpass timings for *rabi* (a) 2005-06 and (b) 2006-07 over study site

**Table 5.1: Variation of ratio of measured hourly to daytime average net radiation at different wheat growth stages**

a) *rabi* 2005-06 (Average of Muktipur and Chalindra)

Hours	Vegetative	Flowering	Grain filling	Maturity
8	0.24	0.257	0.362	
9	0.45	0.547	0.537	0.539
10	0.83	0.954	0.947	0.993
11	1.16	1.328	1.266	1.224
12	1.39	1.631	1.448	1.570
13	1.41	1.550	1.489	1.550
14	0.96	1.201	1.061	0.996
15	0.79	1.022	0.863	0.809
16				
<b>Daytime mean</b>	<b>0.90</b>	<b>1.06</b>	<b>1.00</b>	<b>1.10</b>

b) *rabi* 2006-07 (Nawagam only)

Hours	Vegetative	Flowering	Grain filling	Maturity
8	0.38	0.356	0.56	
9	0.54	0.716	0.79	0.91
10	1.09	1.174	1.45	1.40
11	1.62	1.803	2.10	2.02
12	1.95	2.114	2.45	2.54
13	1.93	2.170	2.47	2.53
14	1.76	2.011	2.33	2.35
15	1.34	1.606	1.87	1.91
16	0.80	1.019	1.28	1.30
<b>Daytime mean</b>	<b>1.27</b>	<b>1.44</b>	<b>1.70</b>	<b>1.87</b>

Evaporative fraction at different hours was computed as a ratio of latent heat fluxes ( $\lambda E$ ) and net available energy ( $R_n - G$ ) from the

measurements. Latent heat fluxes were computed from measured net available energy ( $Q$ ) and Bowen ratio ( $\beta$ ) at each hour on IOP day. Ratios of hourly evaporative fraction to the daytime average for both the seasons are presented in Table 5.2 (a) and (b). It remained below 1.0 at most of the hours except few when it crossed 1.0. Hour to hour differences were quite evident ranging from 0.49-0.95, 0.54-1.25 in vegetative, 0.62-1.0, 0.61-0.78 in flowering, 0.57-1.0, 0.55-0.80 in grain filling and 0.17-0.56, 0.27-0.75 in physiological maturity in both the seasons, respectively. A constant evaporative fraction is assumed in many modeling studies to extrapolate instantaneous ET to daily scale. A detailed analysis of diurnal behavior of evaporative fraction in heterogeneous semi-arid agricultural landscapes was reported by Gentine *et al.*, 2007. Its diurnal modeling schemes were also introduced by Chehbouni *et al.*, 2007. Present study region was located in semi-arid climate having low agricultural density. Similar findings were also made by Mallick *et al.*, 2007 regarding lack of self-conservativeness in evaporative fraction over semi-arid agro ecosystems in India. In both the seasons, the overall average of ratio of evaporative fraction decreases towards maturity (0.39-0.55) from relatively higher value (0.69-0.77) at vegetative stages. The variation of hourly ratio of evaporative fraction showed that the ratios at noon 13:00 hrs are very close to the overall mean of hourly ratios for all growth stages except one or two cases in both the seasons. Therefore, a noon time evaporative fraction could better represents the daytime average as compared to evaporative fraction at other timings of the day.

**Table 5.2: Variation of ratio of measured hourly evaporative fraction ( $\lambda E/R_n-G$ ) at different wheat growth stages**

a) *rabi* 2005-06

Hours	Vegetative	Flowering	Grain filling	Maturity
8	0.49	1.000	1.000	
9	0.71	0.871	0.782	0.508
10	0.83	0.660	0.578	0.510
11	0.89	0.622	0.571	0.277
12	0.86	0.677	0.585	0.595
13	0.95	0.748	0.667	0.590
15	0.73	0.739	0.753	0.667
15.3	0.77	0.772	0.598	0.753
<b>Daytime mean</b>	0.779	0.761	0.692	0.557

b) *rabi* 2006-07

Hours	Vegetative	Flowering	Grain filling	Maturity
8	0.547	0.681	0.734	
9	0.561	0.645	0.592	0.175
10	0.570	0.631	0.599	0.234
11	0.647	0.610	0.550	0.511
12	0.626	0.758	0.582	0.564
13	0.664	0.724	0.593	0.428
14	0.650	0.646	0.737	0.618
15	1.254	0.782	0.807	0.251
16	0.756	0.774	0.620	
<b>Daytime mean</b>	0.697	0.695	0.646	0.397



#### 5.1.1.2 Using satellite based observations

The MODIS TERRA and AQUA albedo, NDVI, and LST averaged from  $2 \times 2$  pixels over study region were extracted for *in situ* measurement days during wheat growth period for both *rabi* 2005-06 and 2006-07. The temporal variation of MODIS based albedo from TERRA and AQUA during wheat growth period are plotted in Figure 5.2 (a) and (b) for *rabi* 2005-06 and 2006-07. Both TERRA and AQUA albedo over wheat showed similar seasonal fluctuations between 0.20 – 0.32 in 2005-06 and 0.15-0.35 in 2006-07. Though clear sky surface albedo at specific location is time-invariant for a day if surface wetness remains unchanged, little differences were still found in 2005-06 between TERRA and AQUA albedo. The differences became quite large in 2006-07 with systematic lower estimates in AQUA albedo on all days. Albedo was computed from MODIS seven band surface reflectances, which were generated through atmospheric corrections of top-of-atmospheric (TOA) reflectances. Errors in atmospheric inputs at TERRA and AQUA overpasses might propagate errors in surface reflectances and so linearly for albedo also. Like albedo, NDVI is also generated from reflectances but little differences in TERRA and AQUA NDVI were evident as compared to albedo differences. NDVI is a ratio based on two surface reflectances only. But albedo is the sum of weighted reflectances over seven bands. This difference of treating surface reflectances could lead to less differences in NDVI as compared to albedo. NDVI was found to vary between 0.2 – 0.65 over wheat crop (Figure 5.3 (c) and (d)). As compared to surface albedo, more seasonal fluctuations in MODIS TERRA and AQUA LST were found in both the seasons within 25-38°C in 2005-06 (Figure 5.4 e) and 23-35°C in 2006-07 (Figure 5.4 f).

A seasonal growth behavior in NDVI appeared from its temporal profile, over wheat. Earlier workers (Groten, 1993, Doraiswamy and Cook, 1995) have utilized the NDVI growth profile parameters to

classify vegetation, multiple crops, phenological events and predict wheat yield (Lloyd, 1990; White *et al.*, 1997). Though albedo did not show any seasonality but it decreases as the growth advances. Albedo generally decreases from low to high vegetation cover (Frank, 1984; Wang and Davidson, 2007). LST is mainly driven by surface soil wetness, cover types and its fraction. Therefore, it did not have any seasonality but showed considerable season fluctuations.

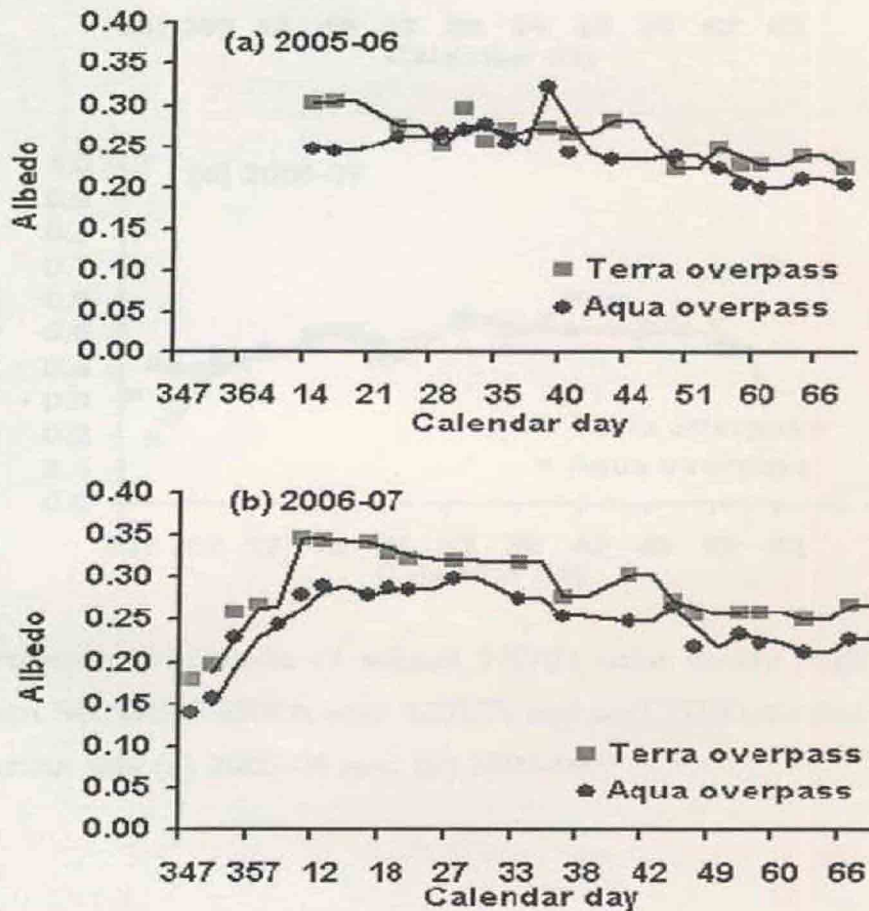


Fig. 5.2 Temporal variation of wheat albedo over study region derived from MODIS TERRA and AQUA surface reflectances during *rabi* (a) 2005-06 and (b) 2006-07

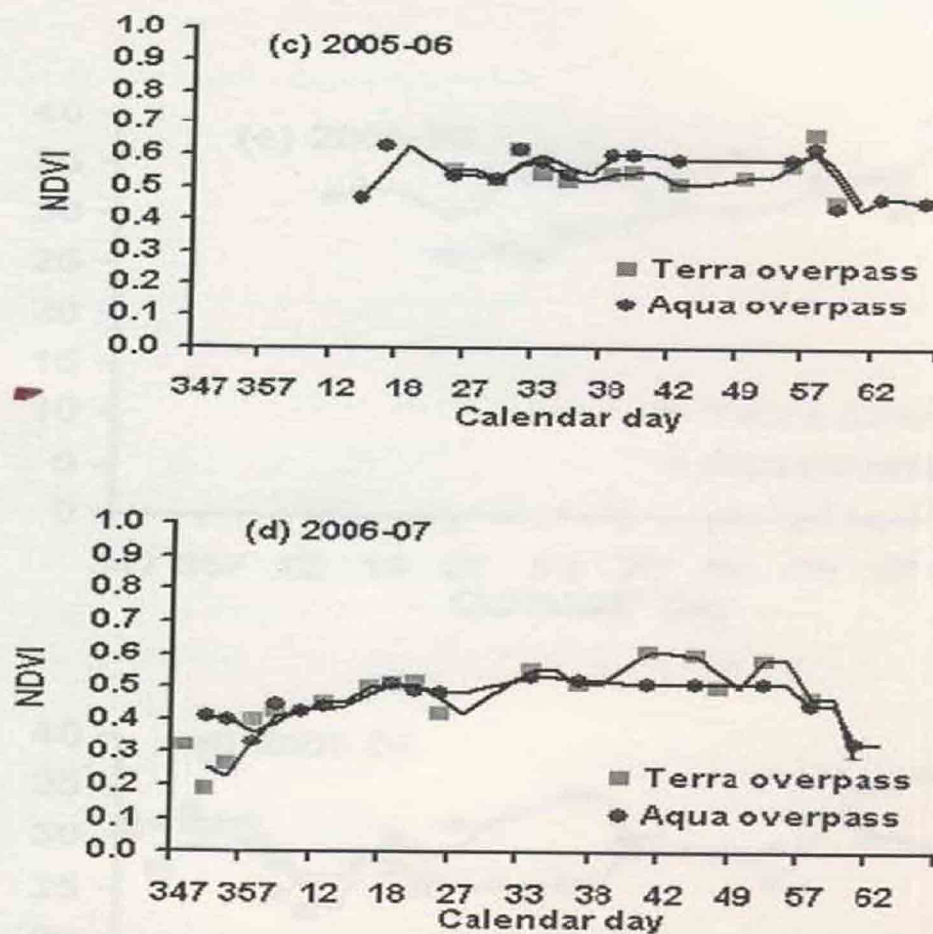


Fig. 5.3 Temporal variation of wheat NDVI over study region derived from MODIS TERRA and AQUA red and NIR surface reflectance during *rabi* (a) 2005-06 and (b) 2006-07

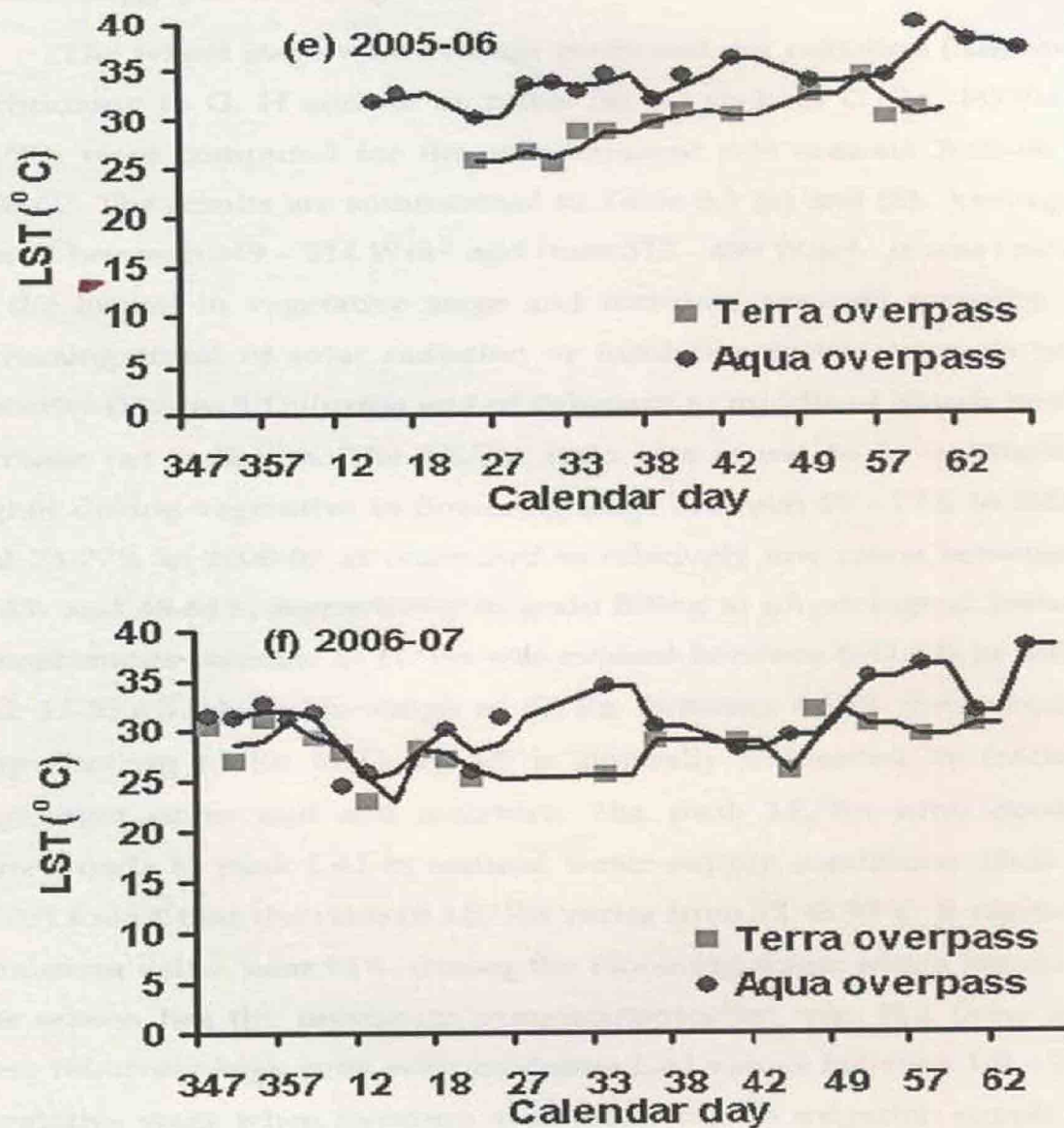


Fig. 5.4 Temporal variation of wheat LST over study region derived from MODIS TERRA and AQUA during *rabi* (a) 2005-06 and (b) 2006-07

### 5.1.2 Energy partitioning behavior

The wheat stage wise average measured net radiation ( $R_n$ ) and its partitioning to  $G$ ,  $H$  and  $\lambda E$  as ratios (in %) such as  $G/R_n$ ,  $H/R_n$  and  $\lambda E/R_n$  were computed for the measurement *rabi* seasons 2005-06 and 2006-07. The results are summarized in Table 5.3 (a) and (b). Average  $R_n$  varied between 349 – 514  $Wm^{-2}$  and from 312 – 439  $Wm^{-2}$ . It was found to be the lowest in vegetative stage and increases towards maturity. The increasing trend of solar radiation or insolation inputs towards wheat maturity (Figure 5.1) during end of February to middle of March tends to increase net radiation. The  $\lambda E/R_n$  ratio was found to be substantially higher during vegetative to flowering stage between 63 – 77% in 2005-06 and 74-77% in 2006-07 as compared to relatively low ratios between 52-59.6% and 48-64%, respectively in grain filling to physiological maturity. A continuous increase in  $H/R_n$  was evident between 6-41.4% in 2005-06 and 17-55.6%. A stable range of  $G/R_n$  between 4-10% was obtained. Apportioning of  $R_n$  to  $G$ ,  $H$ ,  $\lambda E$  is generally influenced by fractional vegetation cover and soil moisture. The peak  $\lambda E/R_n$  ratio normally corresponds to peak LAI in assured water supply conditions. Shen *et al* (2002) found that the ratio of  $\lambda E/R_n$  varies from 71 to 93%. It reaches its maximum value, near 93%, during the blooming stage, which means that this season has the maximum evapotranspiration rate. But these ratios were relatively high even with moderate LAI values between 1.9 – 2.8 at vegetative stage when moisture availability due to irrigation supply was very high. Though mean LAI was almost close to peak LAI during grain filling (2.6-3.5), the  $\lambda E/R_n$  were relatively less. The prevailing heat stress as evidenced through monotonously increasing fraction of sensible heat fluxes could impose thermal stress in wheat over this semi-arid agro ecosystem. This reduces transpiration rate and  $\lambda E/R_n$  ratio toward grain filling in wheat. This again was increased towards maturity causing fall in

$\lambda E/R_n$  ratio. Cooler thermal environment in wheat is pre-requisite for better transpiration rate, photosynthesis and translocation of food to form yield attributes. Any heat stress throughout its growth stages leads to premature yellowing and low productivity (Singh *et al*, 2003). This is one of the major reasons into shorter wheat duration and low yield in Gujarat as compared to Punjab, U.P., M.P., Bihar and Rajasthan, respectively.

**Table 5.3: Stage wise net radiation partitioning over semi-arid wheat using Bowen ratio energy balance (BREB) measurements**

a) *rabi* 2005-06

Phenological stages	Mean net radiation (Wm <sup>-2</sup> )	Mean G / Rn (%)	Mean H / Rn (%)	Mean LE / Rn (%)	Mean LAI
Vegetative	349	7.37	6.07	77	2.8
Flowering	419	10	26.5	63.5	3.8
Grain filling	421	5.58	34.8	59.6	3.5
Maturity	514	6.62	41.4	52	2.5

b) *rabi* 2006-07

Phenological stages	Mean net radiation (Wm <sup>-2</sup> )	Mean G / Rn (%)	Mean H / Rn (%)	Mean LE / Rn (%)	Mean LAI
Vegetative	312	9.6	17	74	1.9
Flowering	397	6	29	77	2.8
Grain filling	439	3.6	39	64	2.6
Maturity	437	4	55.6	48	2.5

## 5.2 Validation of satellite based estimates of energy budget components

Estimates of two energy budget components, net radiation ( $R_n$ ) and latent heat flux ( $\lambda E$ ) were compared with *in situ*  $R_n$  and  $\lambda E$  measurements. Average of  $2 \times 2$  pixels both the components at measurement sites were extracted for comparison.

### 5.2.1 Net radiation

The estimates of instantaneous and day time  $R_n$  using MODIS TERRA and AQUA LST, NDVI, albedo were compared with *in situ* measurements. Error statistics comprising of bias, MAE, RMSE are presented in Table 5.4 (a) for instantaneous and Table 5.4 (b) for daytime estimates. These varied between 12 -14  $Wm^{-2}$ , 31- 35  $Wm^{-2}$ , 38-48  $Wm^{-2}$ , respectively at TERRA overpass. The overall correlation coefficient ( $r$ ) was found to be 0.86 with datasets pooled over both the seasons for TERRA overpasses producing RMSE of the order of 42  $Wm^{-2}$ . At AQUA overpasses, the bias, MAE, RMSE varied from 8-19  $Wm^{-2}$ , 49-86  $Wm^{-2}$  and 45-92  $Wm^{-2}$ , respectively with overall  $r = 0.88$ . The RMSE over pooled datasets was 71  $Wm^{-2}$ . The RMSE over pooled estimates at TERRA and AQUA overpasses were found to be 58  $Wm^{-2}$  with  $r = 0.93$  (Figure 5.5 a).

The daytime  $R_n$  estimates from TERRA showed 16-22  $Wm^{-2}$  bias, 41-71  $Wm^{-2}$  MAE and 50-76  $Wm^{-2}$  RMSE with ' $r$ ' varying between 0.47 - 0.67. The RMSE for pooled estimates with two year TERRA datasets was 67  $Wm^{-2}$ . The bias, MAE and RMSE for daytime  $R_n$  estimates from AQUA were found to be 10-15  $Wm^{-2}$ , 31-44  $Wm^{-2}$  and 35-49  $Wm^{-2}$ , respectively with ' $r$ ' varying between 0.85 - 0.92. The RMSE over AQUA pooled estimates was 40  $Wm^{-2}$  (12% of mean). Though the error of instantaneous net radiation at TERRA overpasses were less than those at AQUA overpasses, but the errors from daytime estimates were less in AQUA than those from TERRA. The 1:1 validation plot of AQUA estimated daytime  $R_n$  and measured  $R_n$  is shown in Figure 5.5. The

daytime estimates were generated from single clear sky instantaneous estimates from either TERRA and AQUA using sinusoidal integration. It was found by earlier workers that daytime net radiation estimates from single morning (10.30 to 11.00 AM) and afternoon (14.00 to 15.00 hrs) estimates showed overestimation (Bisht *et al.*, 2005) and underestimation (Nishida *et al.*, 2003). Only, noon time estimates (at 12.00 to 13.00 hrs) can lead to better representation of daytime net radiation. The resulting error from AQUA daytime estimates is little higher than obtained over homogenous agro-ecosystems (Mallick *et al.*, 2007) in India. Though it is higher than the to errors over sparse and heterogeneous agro-ecosystems in LASPEX region with NOAA AVHRR data, the overall RMSE is lower than globally reported error in daytime net radiation estimates (Gupta *et al.*, 2001) obtained by several workers with NOAA AVHRR (Hurtado and Sobrino, 2001) and MODIS TERRA (Bisht *et al.*, 2005) optical and thermal data.

**Table 5.4** Validation of MODIS based net radiation estimates

a) Instantaneous estimates

MODIS overpasses	Bias	MAE	RMSE	Correlation coefficient ( r )
At TERRA				
2005-06	12	31	38	0.86
2006-07	14	35	48	0.86
Pooled	13	33	42	0.86
At AQUA				
2005-06	8	49	45	0.87
2006-07	19	86	92	0.92
Pooled	14	62	71	0.88
TERRA +AQUA	14	47	58	0.93

b) Daytime estimates

MODIS overpasses	Bias	MAE	RMSE	Correlation coefficient ( r )
At TERRA				
2005-06	22	71	76	0.67
2006-07	16	41	50	0.47
Pooled	20	59	67	0.44
At AQUA				
2005-06	10	31	35	0.85
2006-07	15	44	49	0.92
Pooled	12	36	40	0.88



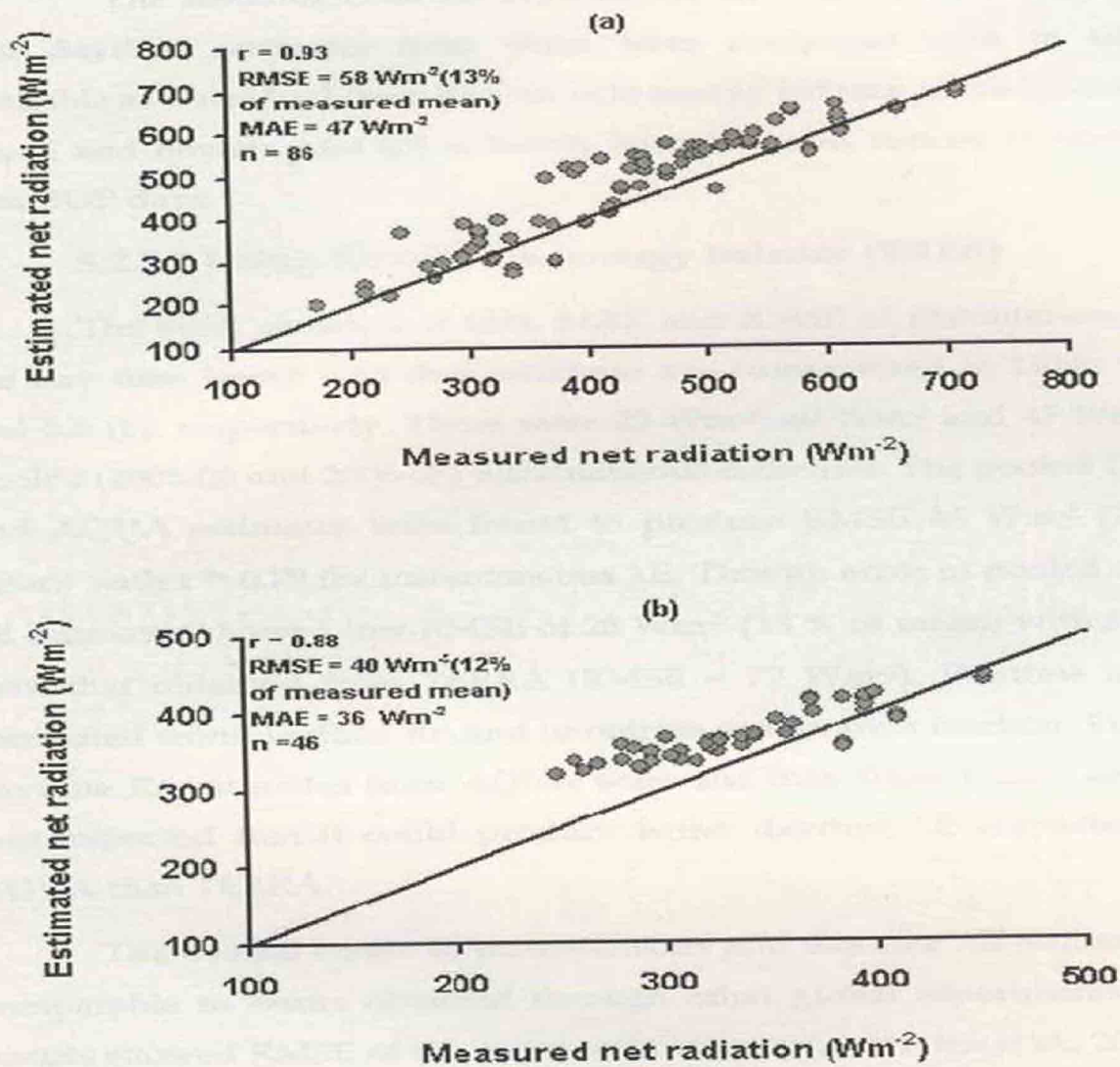


Fig. 5.5 Validation plot of estimated and measured (a) instantaneous (TERRA+AQUA) and (b) daytime net radiation (AQUA only)

### 5.2.2 Latent heat fluxes

The instantaneous  $\lambda E$  estimates from TERRA and AQUA data and daytime estimates from them were compared with *in situ*  $\lambda E$  available as a residual from Bowen ratio energy balance measurements on  $R_n$ ,  $G$  and Bowen ratio ( $\beta$ ) at hourly basis between sunrise to sunset on clear IOP days.

#### 5.2.2.1 Using Bowen ratio energy balance (BREB)

■ The error statistics of bias, MAE and RMSE of instantaneous and the day time latent heat flux estimates are summarized in Table 5.5 (a) and 5.5 (b), respectively. These were 22  $Wm^{-2}$ , 40  $Wm^{-2}$  and 47  $Wm^{-2}$  for pooled (2005-06 and 2006-07) instantaneous estimates. The pooled TERRA and AQUA estimates were found to produce RMSE 46  $Wm^{-2}$  (22% of mean) with  $r = 0.79$  for instantaneous  $\lambda E$ . Though error in pooled AQUA  $\lambda E$  estimates showed low RMSE of 28  $Wm^{-2}$  (13 % of mean) with  $r = 0.76$  than that obtained from TERRA (RMSE = 77  $Wm^{-2}$ ). Daytime  $\lambda E$  was computed from daytime  $R_n$  and noontime evaporative fraction. Errors of daytime  $R_n$  estimates from AQUA were less than those from TERRA. It was expected that it could produce better daytime  $\lambda E$  estimates from AQUA than TERRA.

The overall errors in instantaneous and daytime  $\lambda E$  estimates are comparable to errors obtained through other global experiments. Their results showed RMSE of the order of 34  $Wm^{-2}$  (Verstraeten *et al.*, 2005) for instantaneous and of the order of 27  $Wm^{-2}$  (Cleugh *et al.*, 2007) 34  $Wm^{-2}$  (Venturiani *et al.*, 2008) 53  $Wm^{-2}$  (Batra *et al.*, 2006) for daytime using single source energy balance estimates.

**Table 5.5 Error statistics of MODIS based latent heat flux estimates ( $\lambda E$ )****a) Instantaneous**

MODIS overpasses	Bias	MAE	RMSE	Correlation coefficient (r)
At TERRA				
2005-06	19	31	38	0.92
2006-07	25	47	58	0.49
Pooled	22	36	46	0.78
At AQUA				
2005-06	15	42	49	0.74
2006-07	13	35	42	0.81
Pooled	14	40	47	0.75
TERRA + AQUA				
2005-06	18	37	49	0.91
2006-07	13	35	42	0.65
Pooled	16	36	46	0.79

**b) Daytime**

MODIS overpasses	Bias	MAE	RMSE	Correlation coefficient (r)
At TERRA				
2005-06	38	68	83	0.50
2006-07	29	59	64	0.65
Pooled	35	65	77	0.51
At AQUA				
2005-06	13	24	29	0.73
2006-07	12	21	26	0.82
Pooled	13	23	28	0.76

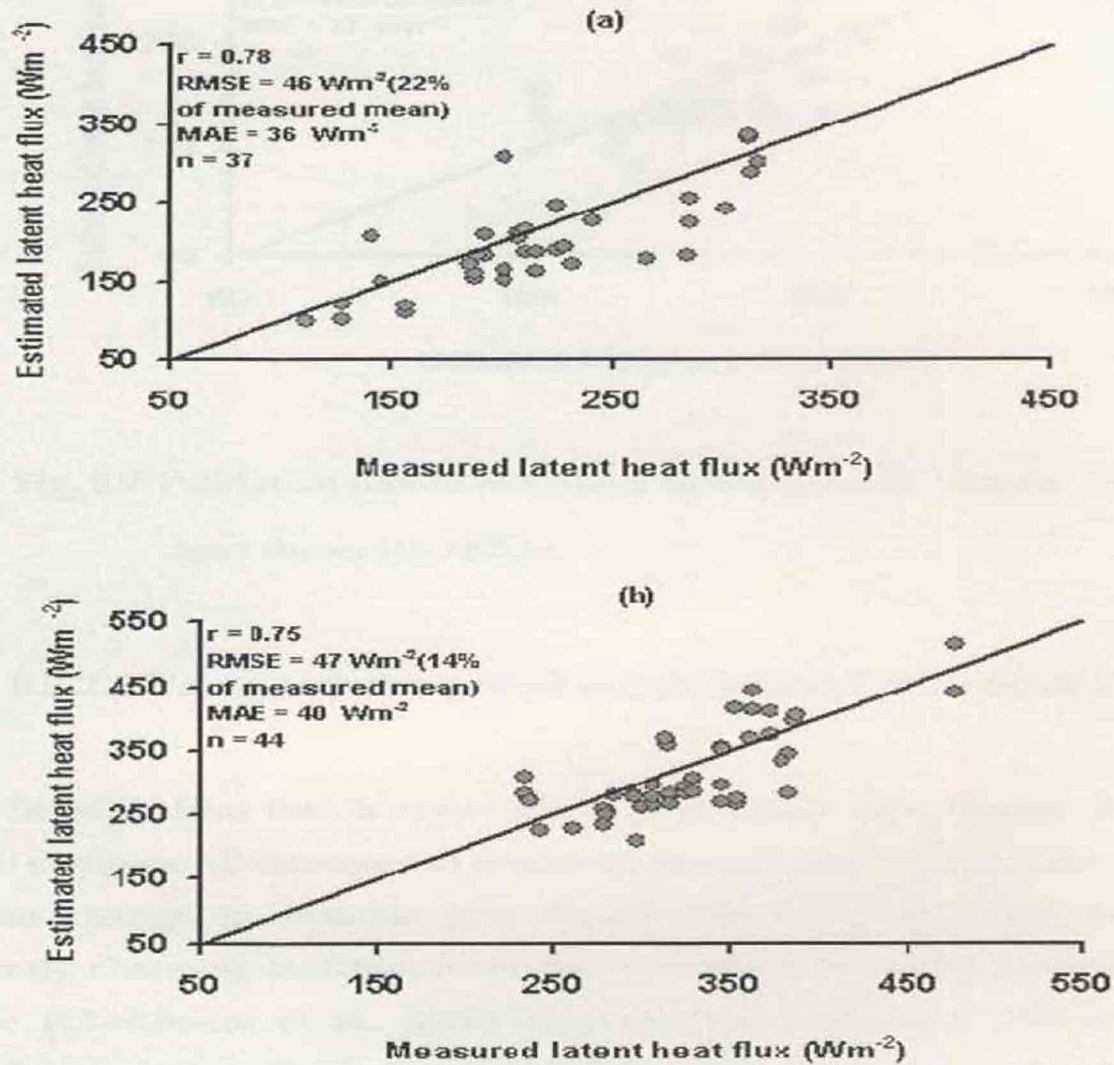


Fig. 5.6 Validation plot of estimated and measured instantaneous latent heat fluxes for (a) TERRA and (b) AQUA



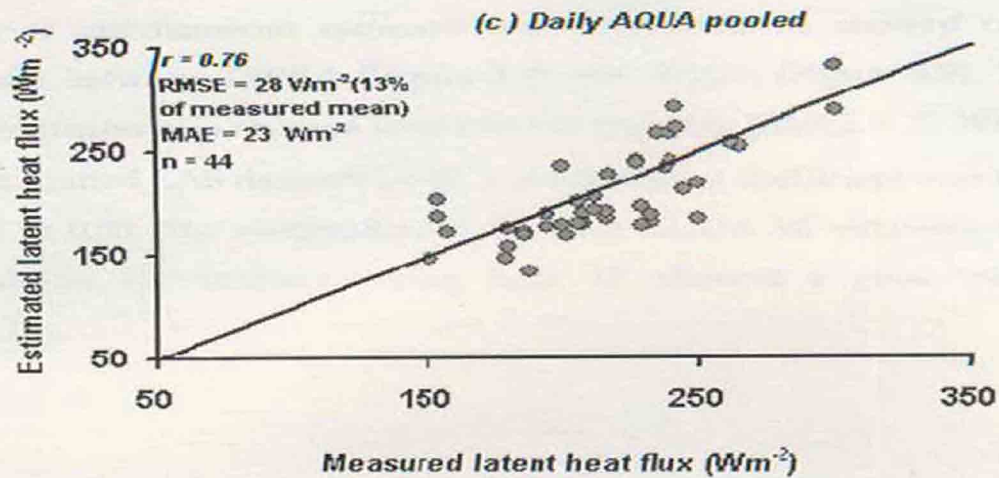


Fig. 5.7 Validation plot of estimated and measured daytime latent heat fluxes for AQUA

#### 5.2.2.2 Using area integrated sensible heat fluxes from LAS

Sensible heat flux is very critical in properly representing Bowen ratio to compare  $\lambda E$  estimates at moderate spatial scale ( $\sim 1\text{km}$ ). Moreover, frequent change in sensible heat fluxes over 1 sq. km area due to frequently changing stability, instability conditions specially in semi-arid climate (Chehbouni *et al.*, 2000) may not be sufficiently represented through one or two Bowen ratio samples within the study area at each hour. Rather area averaged sensible heat flux measurements over MODIS 1 sq. km pixel along with measurements on  $R_n$  and  $G$  can represent better *in situ*  $\lambda E$  while validating its satellite based estimates.

As a follow up to that, instantaneous and daytime  $\lambda E$  estimates were compared with limited  $\lambda E$  generated through area averaged 'H' from large aperture scintillometer (LAS). The percent error was drastically reduced to 9% of mean having absolute RMSE  $29 \text{ Wm}^{-2}$  with

increase in  $r$  ( $= 0.97$ ) for TERRA and AQUA (Figure 5.8). The seasonal variation of instantaneous estimates and measurements showed close resemblance between TERRA (Figure 5.9) and AQUA (Figure 5.9). The daytime estimates also showed increment in accuracy ( $RMSE = 27 \text{ Wm}^{-2}$ ) even with limited LAS datasets ( $n=8$ ) and correlation coefficient was also increased to 0.85. The comparison of daytime AQUA  $\lambda E$  estimates and area averaged  $\lambda E$  computed using LAS 'H' showed a good match (Figure 5.10).

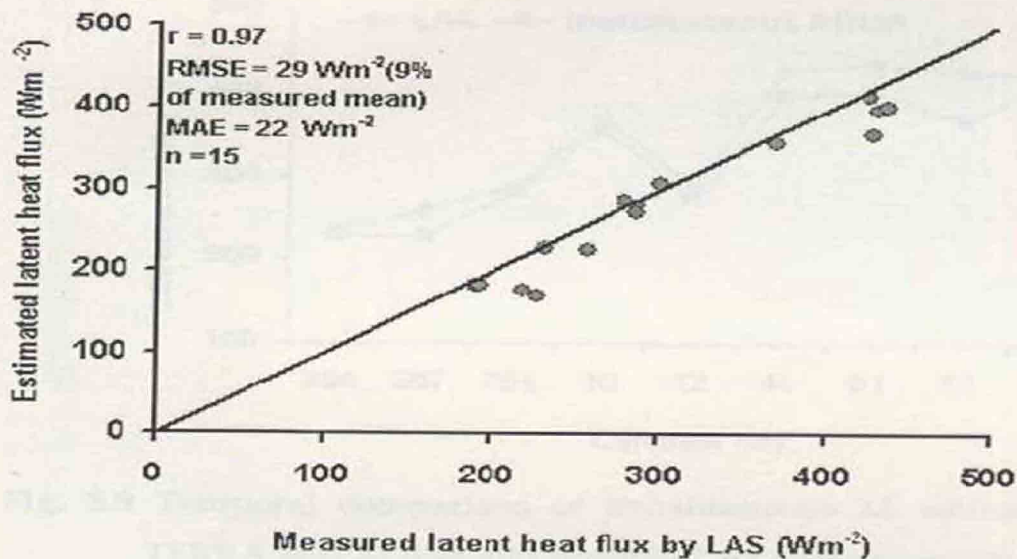


Fig. 5.8 Validation of TERRA and AQUA ' $\lambda E$ ' estimation with *in situ* measurements when area averaged LAS 'H' was used

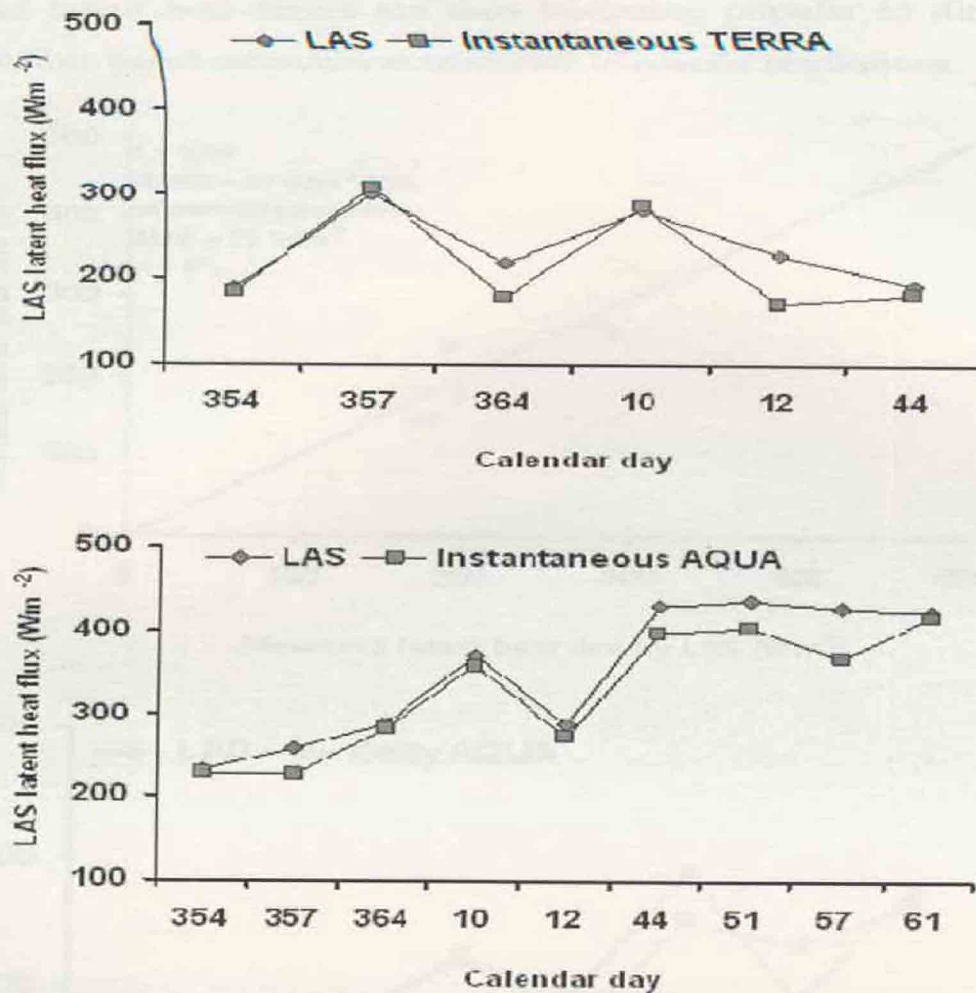


Fig. 5.9 Temporal comparison of instantaneous  $\lambda E$  estimates from TERRA and AQUA and through LAS measurements

The results indicated that satellite based  $\lambda E$  estimates at moderate resolution could have shown less error when area averaged heat flux measurements are used for  $\lambda E$  validation. The LAS has some advantages over BREB and eddy correlation (EC) flux measurements. The measurement from latter two represent fluxes from a landscape needing a certain fetch. These fluxes cannot be extendable beyond the 'fetch'. But LAS does not require any 'fetch'. It measures area averaged fluxes at 250m to 10. km (Watts *et al.*, 2000) both over homogenous and heterogeneous terrains. The LAS area averaged measurements in



sensible and latent heat fluxes are thus becoming popular to directly validate satellite based estimates at moderate to coarser resolutions.

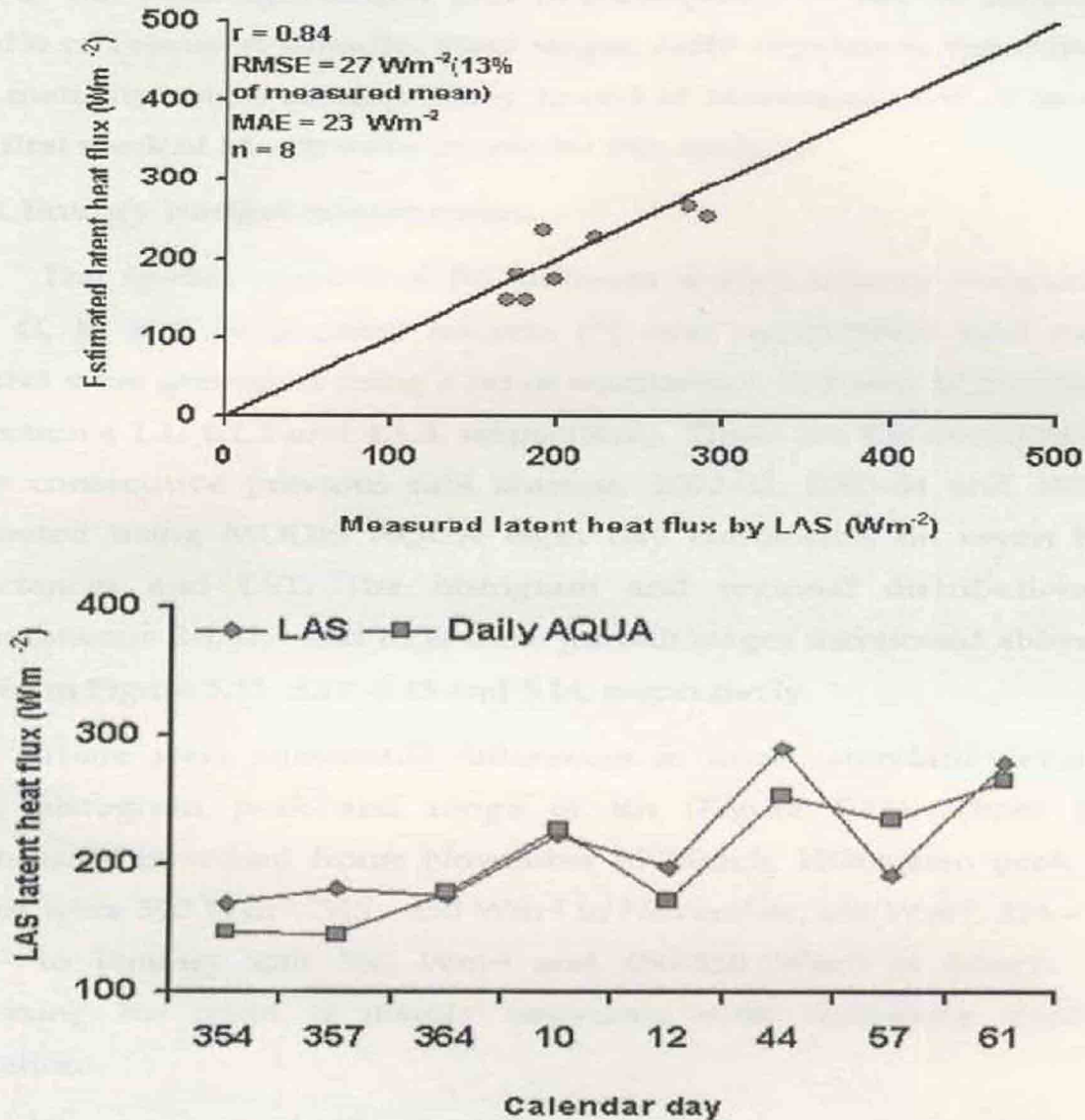


Fig. 5.10 Validation plot of estimated and measured daytime latent heat flux with AQUA and LAS

### 5.3 Spatio-temporal variability

In Gujarat, a short *rabi* season, spread over end of November to middle of March, exists. Agricultural growth occurs during this period



mostly in irrigated conditions. Besides wheat, tobacco, cumin and mustard are major crops, which have differences in the length of growing period. But peak agricultural growth corresponds to end of January to middle of February. Broadly, three stages, early vegetative, reproductive and maturity stages corresponding to end of November, end of January and first week of March were chosen for this analysis.

### **5.3.1 Energy budget components**

The spatial outputs of the different energy balance components ( $R_n$ ,  $G$ ,  $IE$  and evaporative fraction ( $\lambda$ ) over agricultural land use in Gujarat were generated using a set of equations 4, 7, 9 and 10 mentioned in section 4.1.1, 4.1.2 and 4.1.3, respectively. These are the averages over three consecutive previous rabi seasons, 2002-03, 2003-04 and 2004-05 generated using MODIS AQUA eight day composites on seven band reflectances and LST. The histogram and regional distributions of instantaneous  $R_n$ ,  $G$ , and  $IE$  at three growth stages mentioned above are shown in Figure 5.11, 5.12, 5.13 and 5.14, respectively.

There were substantial differences in mean, standard deviation (SD), histogram peak and range of  $R_n$  (Figure 5.11). These have consistently increased from November to March. Histogram peak and ranges were  $390 \text{ Wm}^{-2}$ ,  $345 - 450 \text{ Wm}^{-2}$  in November,  $440 \text{ Wm}^{-2}$ ,  $354 - 481 \text{ Wm}^{-2}$  in January and  $550 \text{ Wm}^{-2}$  and  $450-650 \text{ Wm}^{-2}$  in March. The increasing  $R_n$  trend is mainly associated with increasing trend in insolation.

The means and SD of  $G$  (Figure 5.12) did not show substantial differences between November and January. These varied between  $70-75 \text{ Wm}^{-2}$  and  $6-9 \text{ Wm}^{-2}$  respectively. But the ranges were different. It was high in January ( $40-90 \text{ Wm}^{-2}$ ) as compared to November ( $50-84 \text{ Wm}^{-2}$ ). A substantial increase in mean ( $123 \text{ Wm}^{-2}$ ) and SD ( $10 \text{ Wm}^{-2}$ ) was prominent in March. This could be due to increase in  $R_n$  input to  $G$  computation (equation 9). A high spatial variability in fractional vegetation cover is

expected in March due to differently maturing crops within agricultural land use. This must have yielded to higher SD.

There are certain pockets such as area adjacent to Sabarmati river basin in Kheda district where  $\lambda$  was consistently high ( $> 0.5$ ) due to cultivation of rabi crops with assured irrigation facility. The distribution clearly indicated that  $\lambda$  had hardly crossed 0.5 in majority of the agricultural grids ( $0.01^\circ$ ) throughout rabi season in this semi-arid climate. Though mean and SD of  $\lambda$  (Figure 5.13) did not show any substantial differences among November, January and March. But shape of histogram largely differed. Eighty percent of pixels corresponds to a range, 0.1 – 0.5 in November as compared to 90 % of pixels in January and 97 % in March. Histogram peak (0.35) was in January corresponding to peak agricultural growth as compared to 0.3 in November having early vegetative and 0.25 in March corresponding to physiological maturity.

The mean LE (Figure 5.14) was found to be the highest ( $140 \text{ Wm}^{-2}$ ) in March corresponding to peak growth as compared to other two stages in November ( $111 \text{ Wm}^{-2}$ ) and January ( $129 \text{ Wm}^{-2}$ ). The higher variability in vegetation fraction due to differentially maturing crops in March could have produced highest SD ( $59 \text{ Wm}^{-2}$ ) in March as compared to  $48 \text{ Wm}^{-2}$  in January and  $52 \text{ Wm}^{-2}$  in November. There were wide differences in histogram shape, range and distribution within it. Ninety percent of agricultural grids showed LE in the range of 20-220  $\text{Wm}^{-2}$  in November as compared to 85 % in January and 75 % in March. A consistent higher  $\lambda$  and  $\lambda\text{E}$  zone appeared over Kheda district, which is known to be the most agriculturally productive district in Gujarat.

The above outputs with histograms could capture significant regional spatio – temporal variability in energy balance components during rabi growth period over Gujarat.

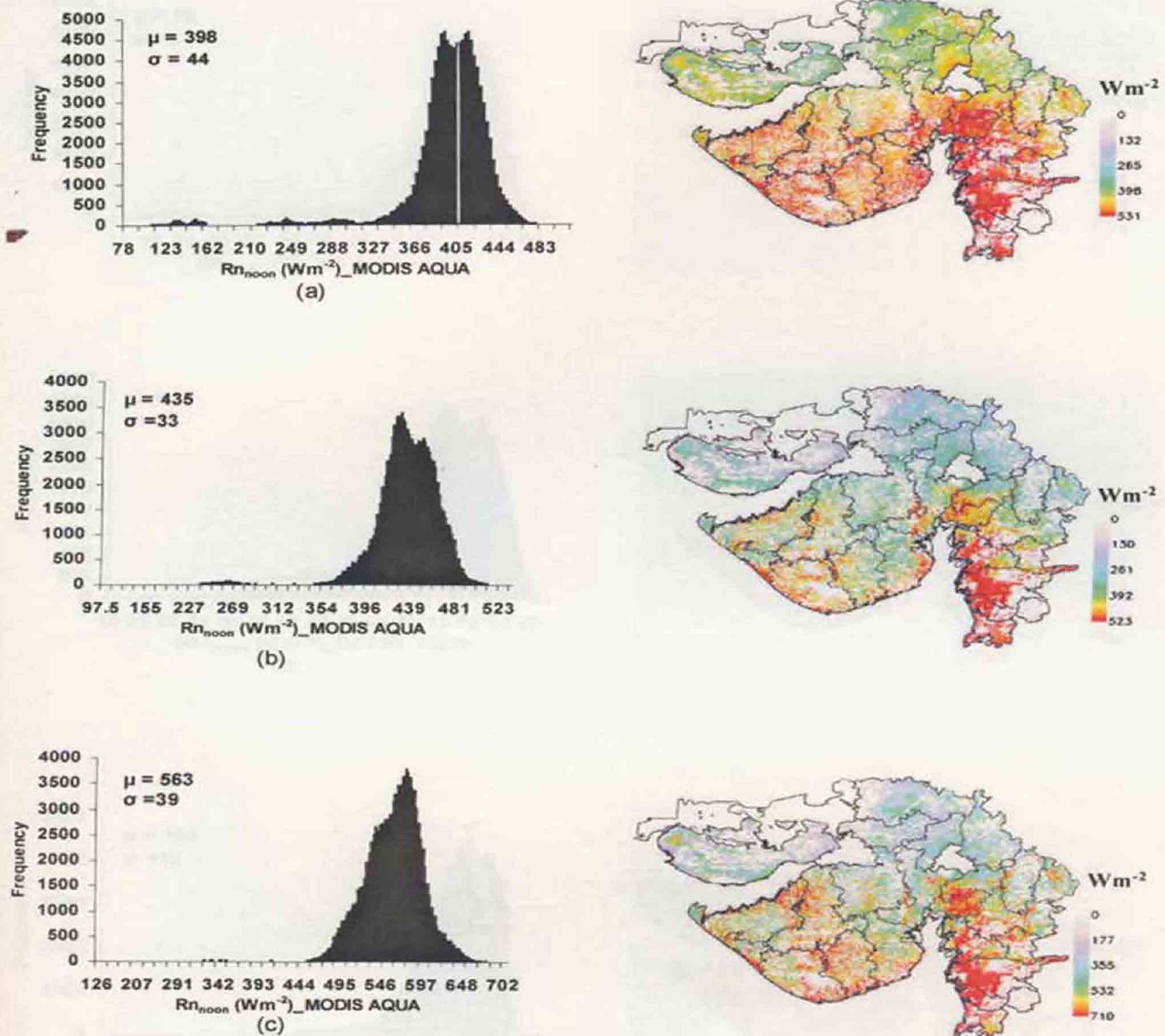


Fig.5.11 Histogram analysis of spatial distribution of net radiation (Rn) over agricultural land use in *rabi* at (a) end of November (b) middle of January (c) in 1<sup>st</sup> week of March

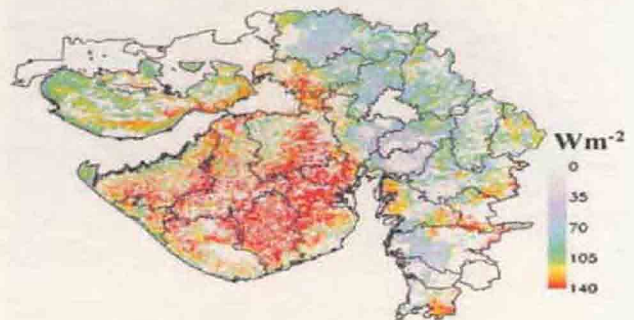
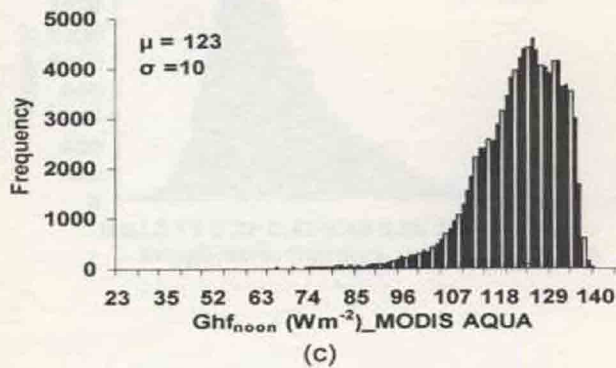
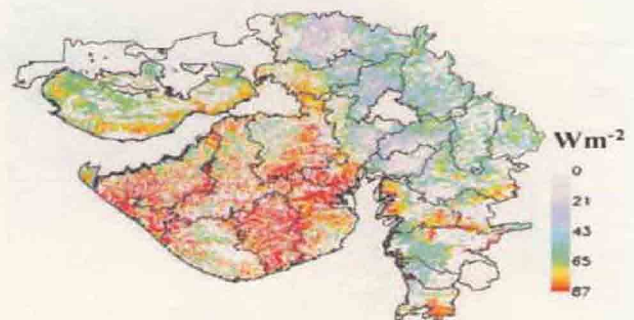
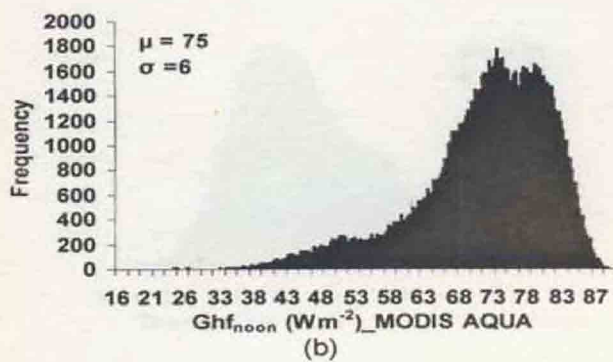
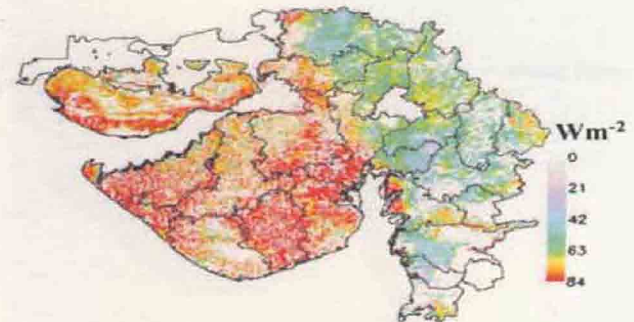
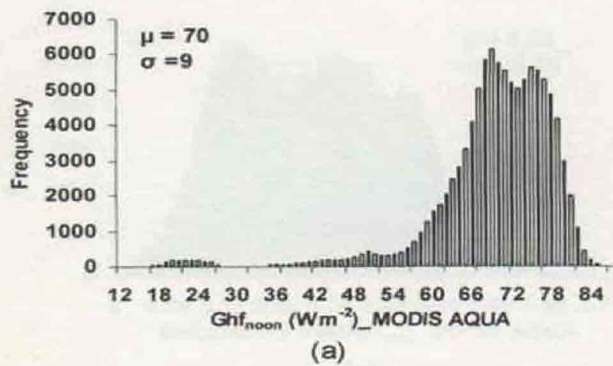


Fig. 5.12 Histogram analysis of spatial distribution of ground heat flux (G) over agricultural land use in *rabi* at the (a) end of November (b) end of January (c) in 1<sup>st</sup> week of March



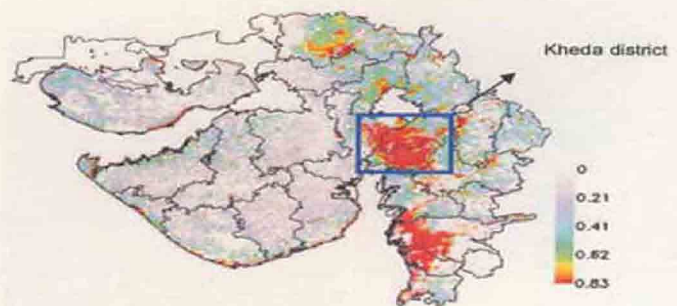
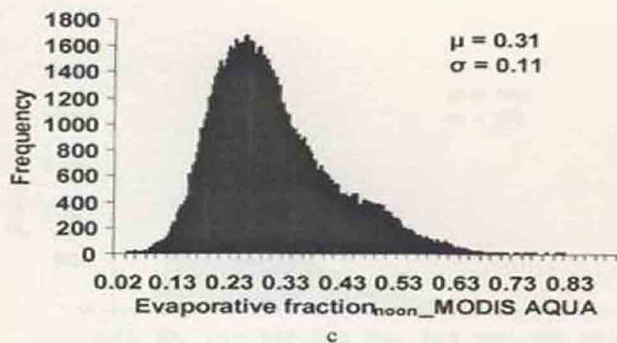
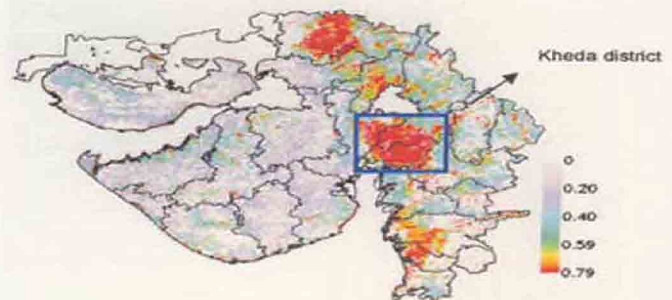
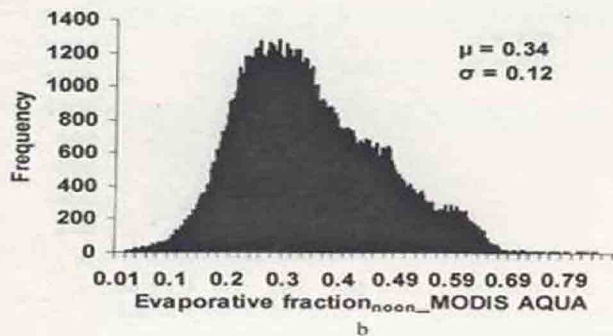
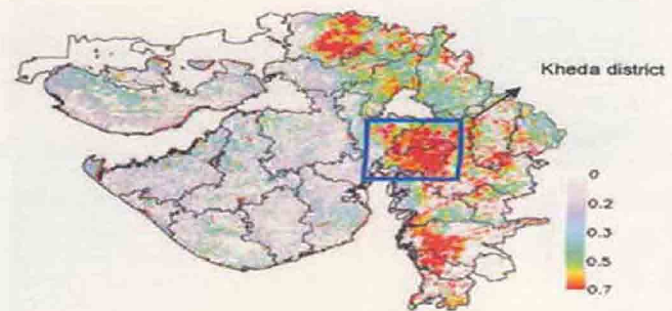
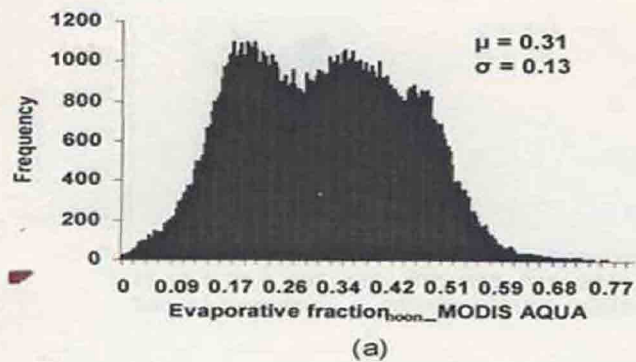


Fig. 5.13 Histogram analysis of spatial distribution of evaporative fraction  $\Lambda$  over agricultural land use in *rabi* at the (a) end of November (b) end of January (c) in 1<sup>st</sup> week of March

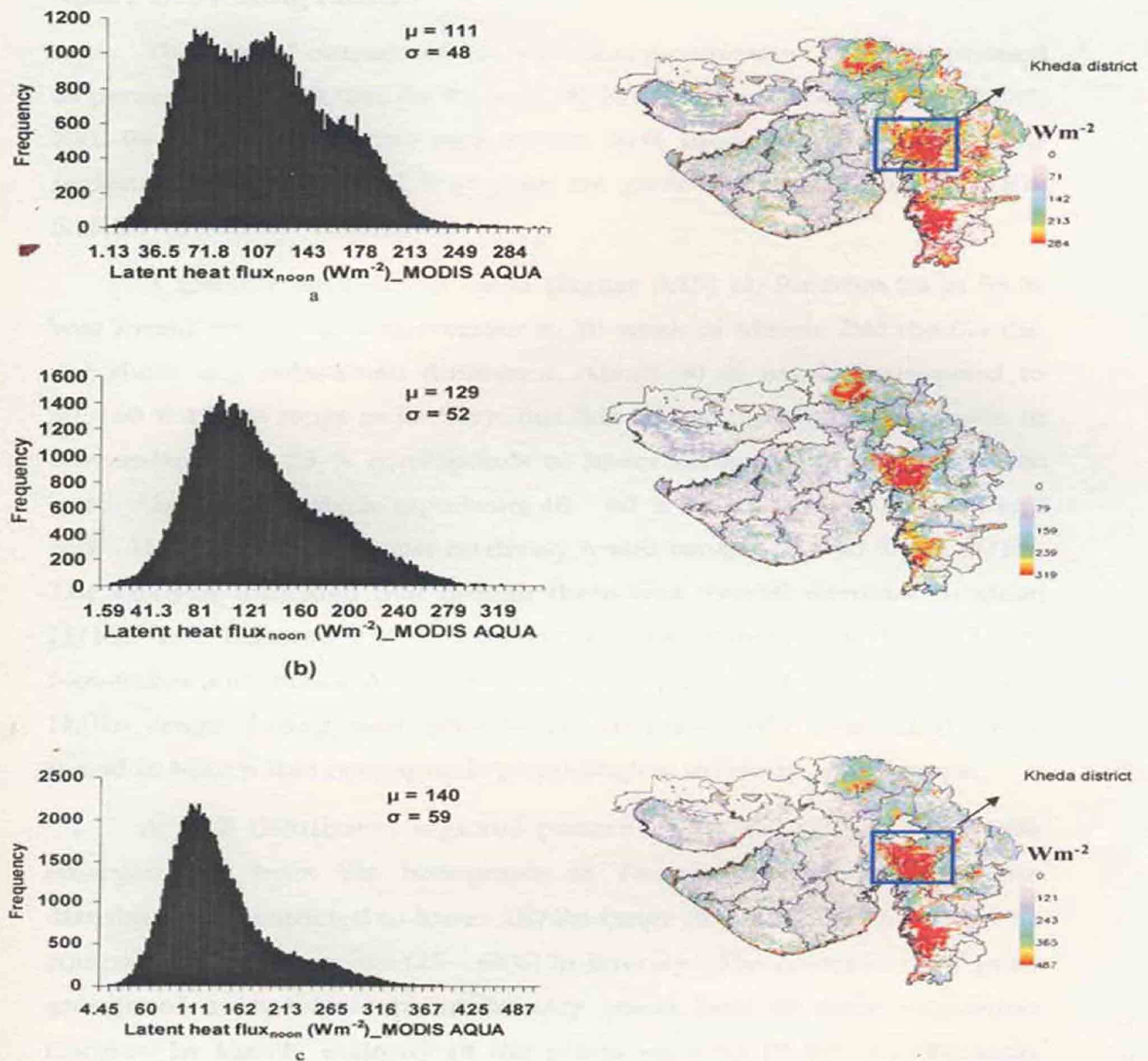


Fig. 5.14 Histogram analysis of spatial distribution of latent heat flux ( $\lambda E$ ) over agricultural land use in *rabi* at the (a) end of November (b) middle of January (c) in 1<sup>st</sup> week of March

### 5.3.2 Partitioning ratios

The spatial outputs of net radiation partitioning ratios (expressed as percent of Rn), H/Rn, G/Rn and  $\lambda E/Rn$ , averaged across *rabi* 2002-03, 2003-04 and 2004-05 over agricultural land uses were generated. The regional distributions and histogram are given in Figure 5.15 for H/Rn, 5.16 for G/Rn, 5.17 for  $\lambda E/Rn$ .

A gradual decrease in mean (Figure 5.15) H/Rn from 55 to 53 % was found from end of November to 1<sup>st</sup> week of March. But the SD did not show any substantial difference. About 90 % pixels correspond to 40 – 60 % H/Rn range in January. But this range envisages 75 % pixels, in November. Rest 25 % corresponds to lower range (28 – 40%) of H/Rn ratio. About 90 % pixels represents 40 – 60 % H/Rn range in March and rest 15 % pixels represents relatively lower range (27 – 40 %) in H/Rn. The analysis indicated that though there was overall decrease in mean H/Rn, but regional H/Rn distribution was towards higher side in November and included more proportion of pixels in the relatively lower H/Rn range during peak growth. A November like peak H/Rn was found in March that corresponds physiological maturity of *rabi* crops.

A well distributed regional pattern in  $\lambda E/Rn$  (Figure 5.17) was emerged out from the histograms in November and January. The distribution is restricted to lower  $\lambda E/Rn$  range (8 – 50 %) in November as compared to higher range (15 – 60%) in January. The coincidence of peak growth of most *rabi* crops in January could lead to more vegetation fraction. In March, majority of the pixels showed 10-35%  $\lambda E/Rn$  ratio corresponding to physiological maturity.

The regional distribution of energy partitioning ratios showed logical variation in accordance with phenological development during *rabi* growing period over Gujarat.

Quite a good regional distribution in G/Rn (Figure 5.16) was also found in January restricted to the range of 7 -20 %. But majority of the grids showed higher G/Rn ratio in the range of 15-20% in November and 19-25% in March that corresponds to relatively low fractional vegetation cover. Several studies attempted to model G/Rn ratio using NDVI (Moran *et al.*, 1989) or other vegetation indices such as SAVI (Boegh *et al.*, 2002) or fractional vegetation cover (Verstraeten *et al.*, 2005) through linear relationship. Though regional mean in G/Rn did not show any significant difference over the growing period, but pattern of distribution was very much influenced by phenological development that led to change in canopy fraction.



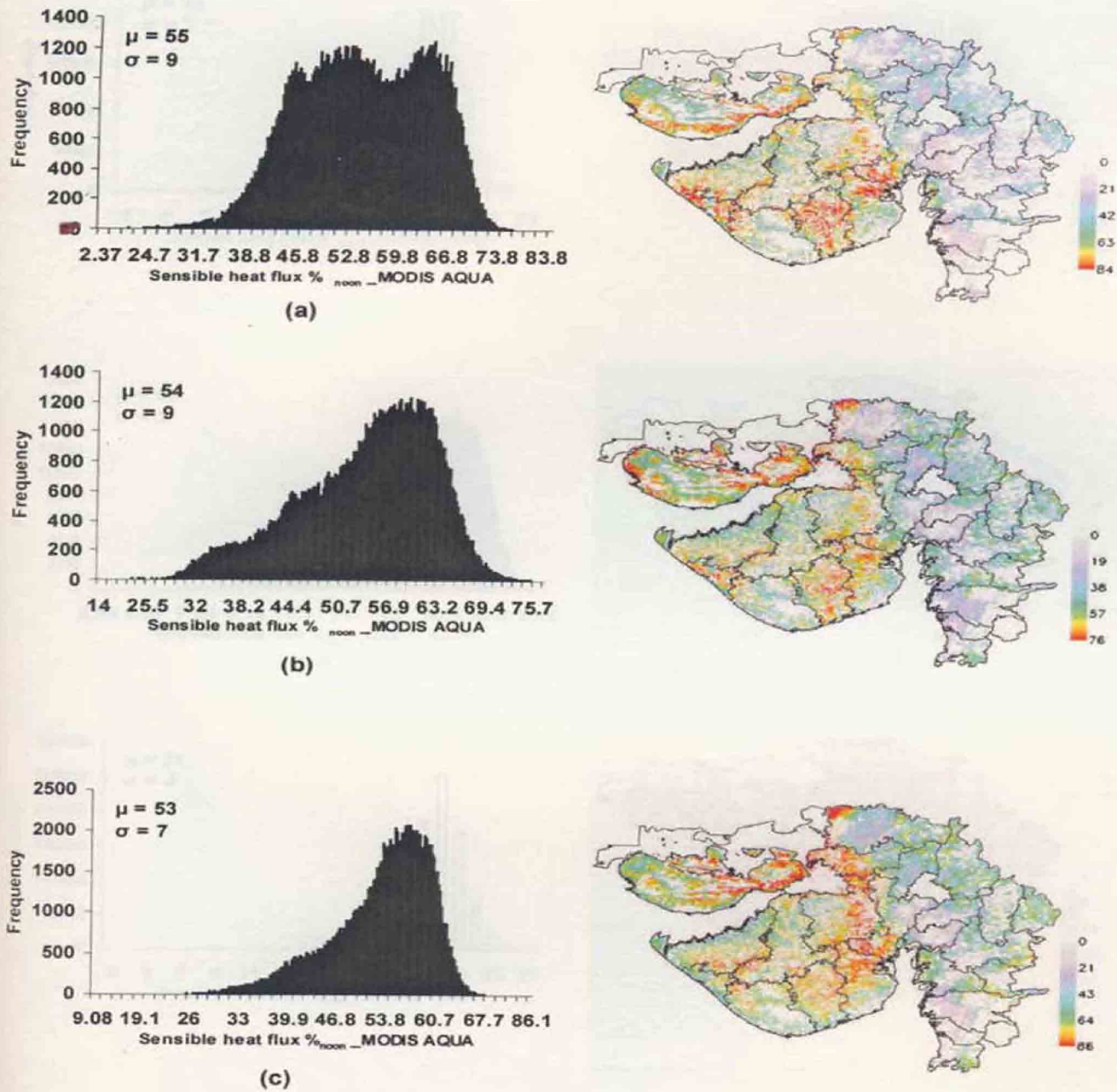


Fig. 5.15 Histogram analysis of spatial distribution of H/Rn ratio over agricultural land use in *rabi* at the (a) end of November (b) end of January (c) in 1<sup>st</sup> week of March

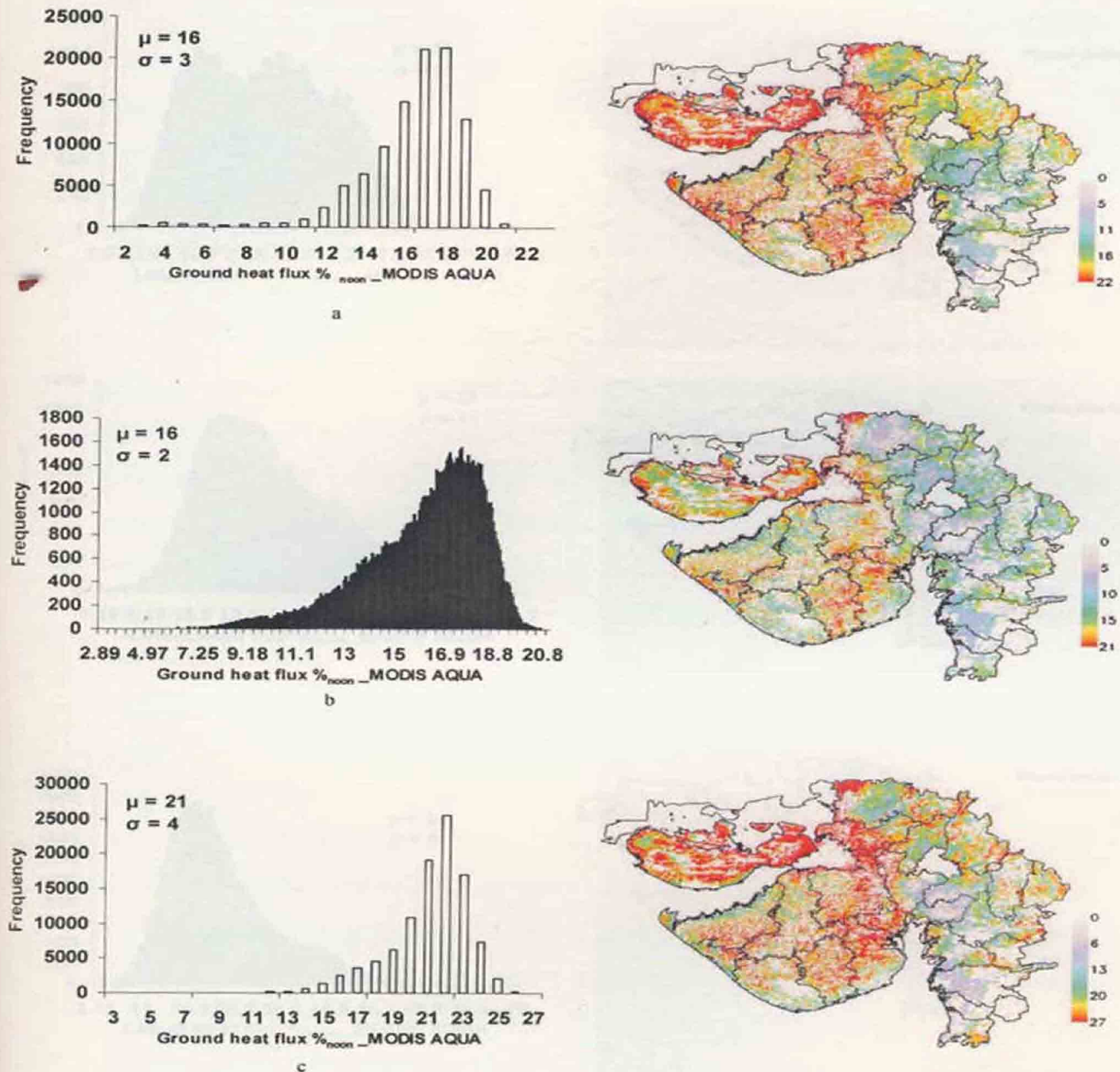


Fig. 5.16 Histogram analysis of spatial distribution of G/Rn ratio over agricultural land use in *rabi* at the (a) end of November (b) end of January (c) in 1<sup>st</sup> week of March

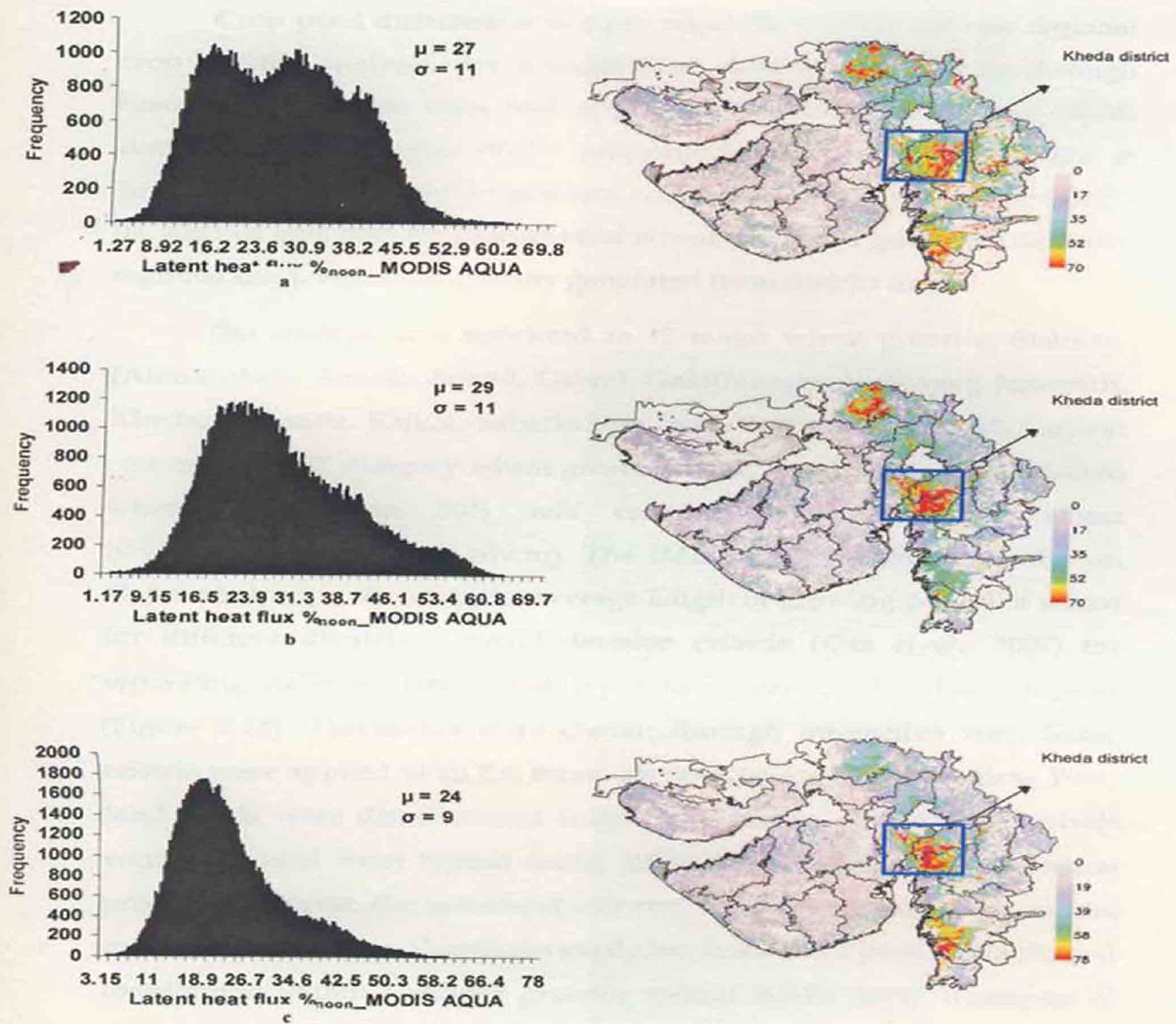


Fig. 5.17 Histogram analysis of spatial distribution of  $\lambda E/R_n$  ratio over agricultural land use in *rabi* at the (a) end of November (b) end of January (c) in 1<sup>st</sup> week of March



#### 5.4 Regional wheat mask generation

Crop pixel distribution is a pre-requisite to carry out any regional crop specific analysis. An unsupervised classification scheme through hierarchical decision rules was applied to MODIS AQUA 250m NDVI data. Stacks of eight-day NDVI composite for the period 1 November to 16 March were prepared to generate wheat mask of Gujarat for *rabi* 2002-03, 2003-04 and 2004-05. District level wheat mask was generated first and regional mask was subsequently generated from district mask.

The analysis was restricted to 12 major wheat growing districts. (Ahmedabad, Amreli, Anand, Dahod, Gandhinagar, Jamnagar, Junagarh, Kheda, Mehsana, Rajkot, Sabarkantha, and Vadodara). Though Gujarat comes under 'B' category wheat growing state, the districts were selected where more than 50% *rabi* cropped area is under wheat ([www.agriculture.gujarat.gov.in](http://www.agriculture.gujarat.gov.in)). The IMD published crop calendar on Gujarat helped in deciding the average length of growing period of wheat for different districts. General decision criteria (Das *et al.*, 2007) for separating different land cover types are given in the flow diagram (Figure 5.18). Thresholds were chosen through interactive way. Same criteria were applied to all the three *rabi* seasons for all the districts. First, land pixels were discriminated from water bodies. *Rabi* cropped pixels were separated from typical forest NDVI profile and other vegetation profile. In Gujarat, the associated *rabi* crops along with wheat are cumin, mustard and tobacco. Cumin generally has low NDVI peak, bell - shaped distribution within a shorter growing period (65-70 days). Examples of characteristic NDVI profiles of wheat, mustard, tobacco, forest and cumin are shown in Figure 5.19 a, b, c, d and e, respectively. Based on the unique crop profile characteristics wheat pixels were discriminated. Regional 250m wheat mask was resampled to MODIS AQUA energy balance and ET output grid (0.01°).

Similar hierarchical decision rules and profile characteristics were also used by Das *et al.* (2007) for rice mask generation over Punjab using SPOT VGT 1 km ten-day composites and wheat over Rajasthan using NOAA AVHRR multi-date data (Potdar and Majunath, 1999). It is difficult to accurately discriminate crops using moderate to coarser spatial resolution satellite data. However, the high temporal data allow to characterize full resolution of crop grown cycle. Moreover, WiFS multi-date data with 188 m spatial resolution and 5-day revisit were used till recently to discriminate wheat (Rajak *et al.*, 2002).

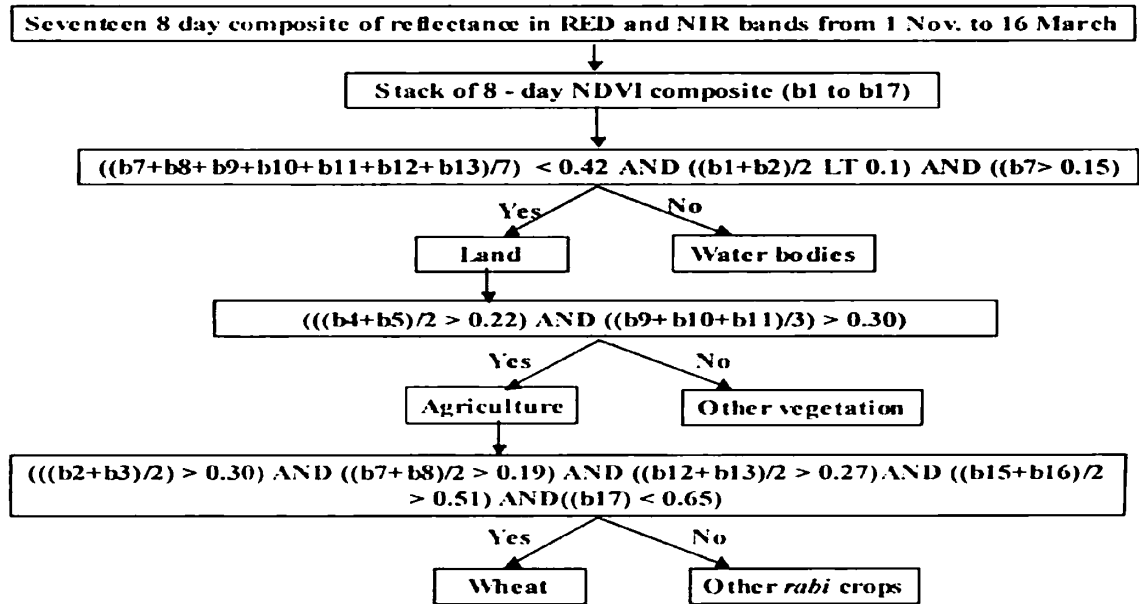
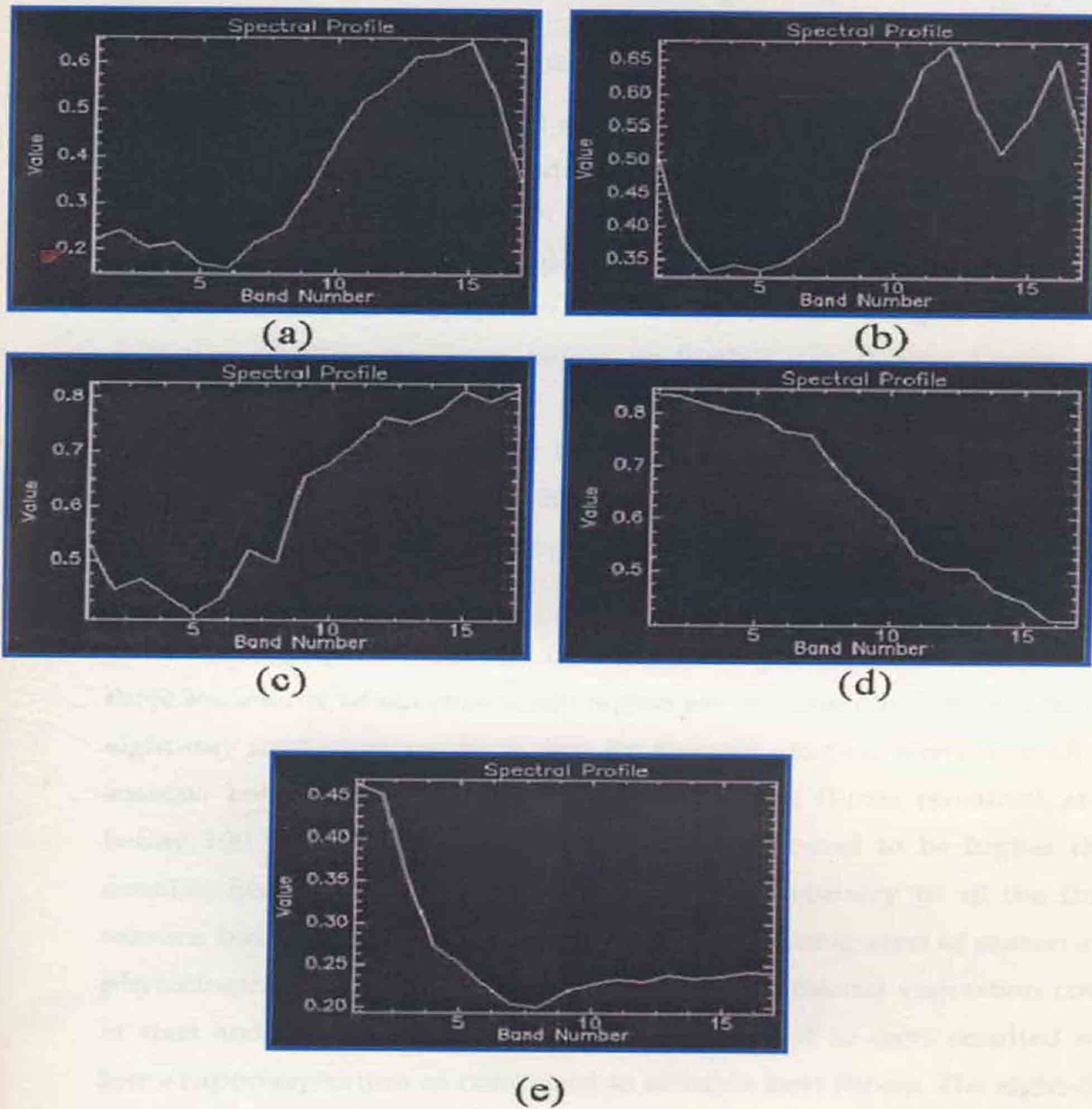


Fig.5.18 Criteria used in hierarchical decision tree to generate district wheat mask in Gujarat

**b: eight-day NDVI composite between**

b1: 305 to 312 Calendar days	b9: 3 to 10
b2: 313 to 320	b10: 11 to 18
b3: 321 to 328	b11: 19 to 26
b4: 329 to 336	b12: 27 to 34
b5: 337 to 344	b13: 35 to 42
b6: 345 to 352	b14: 43 to 50
b7: 353 to 360	b15: 51 to 58
b8: 360 to 2	b16: 59 to 66
	b17: 67 to 75



**Fig. 5.19** Characteristic NDVI profiles from MODIS AQUA 250 m for (a) wheat (b) mustard (c) tobacco (d) forest and (e) cumin

## **5.5 Multi-temporal analysis of energy budget estimates in wheat**

### **5.5.1 Energy budget components**

The resampled regional wheat masks were utilized to accumulate evapotranspiration (ET) to produce regional consumptive water use for 2002-03, 2003-04 and 2004-05. A consistency check is very much necessary in relation to wheat phenological development through multi-temporal analysis of MODIS AQUA derived energy balance component and net radiation partitioning ratios before its further use. Regional outputs of energy budget components and net radiation partitioning ratios, generated at 0.01° grid using MODIS AQUA data were retained over wheat grids only for 2002-03, 2003-04 and 2004-05. These were extracted over wheat grid corresponding to *in situ* measurement sites at every eight-day interval.

The temporal variation of energy budget components for all the three seasons of wheat over study region are presented in Figure 5.20. The eight-day instantaneous noon time  $R_n$  showed gradual increase in all the seasons between 400 – 600  $Wm^{-2}$ . Ground heat fluxes remained at or below 100  $Wm^{-2}$ . The latent heat fluxes were found to be higher than sensible heat flux between January to end of February in all the three seasons but remained below sensible heat flux during start of season and physiological maturity. The dryness and low fractional vegetation cover at start and end of wheat growing period seemed to have resulted into low evapotranspiration as compared to sensible heat fluxes. The eight-day noontime  $\lambda E$  and  $H$  were found to vary between 80 – 300  $Wm^{-2}$  and 180 – 280  $Wm^{-2}$ , respectively. The temporal variation of  $G$ ,  $H$ ,  $\lambda E$  were consistent with wheat development.

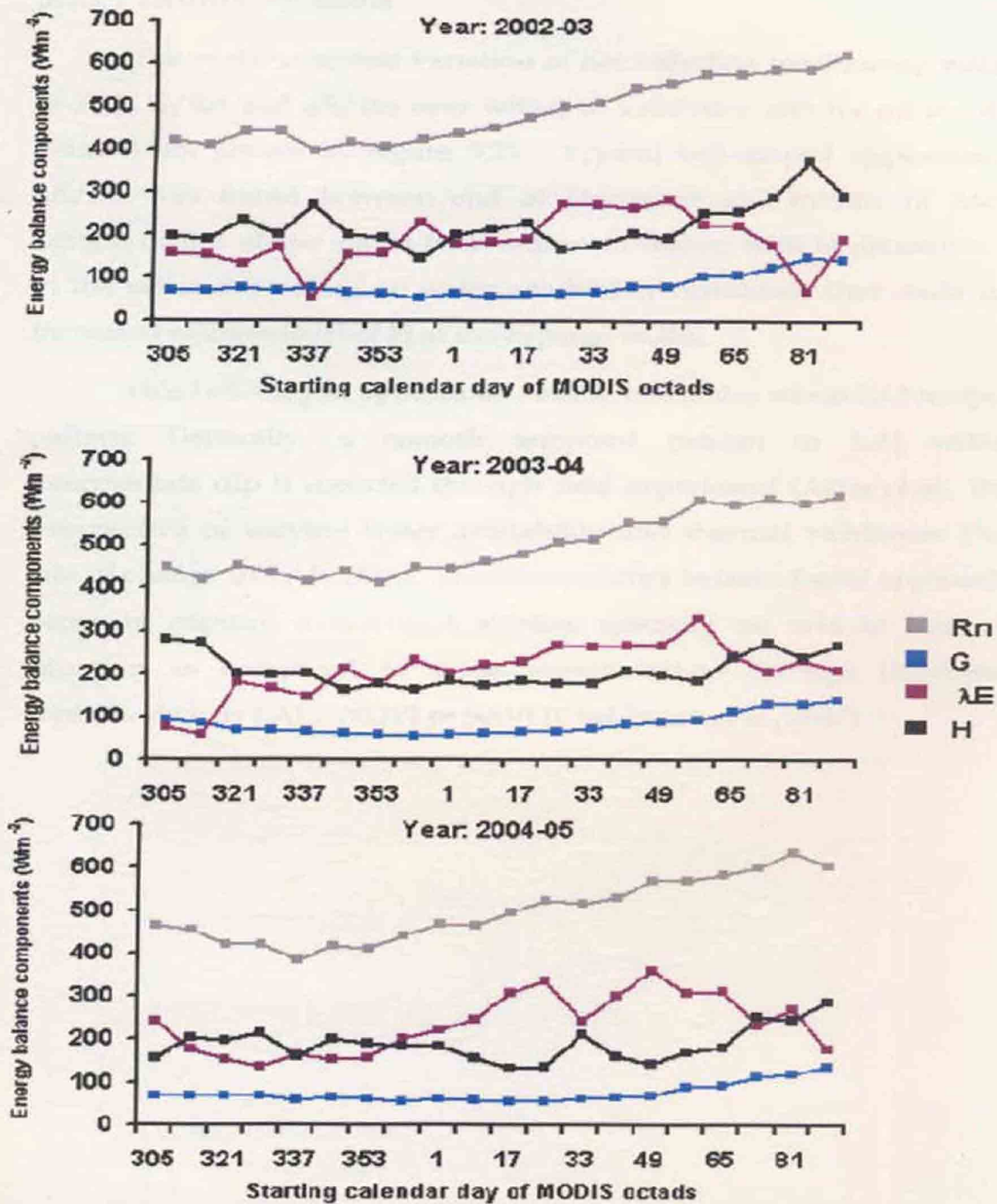


Fig.5.20 Temporal evolution of noon time estimates of energy budget components in wheat over validation site during 2002-03, 2003-04 and 2004-05 from eight-day MODIS AQUA products



### 5.5.2 Partitioning ratios

The multi-temporal variation of net radiation partitioning ratio (% of  $R_n$ ),  $G/R_n$  and  $\lambda E/R_n$  over wheat in validation site for all the three seasons are shown in Figure 5.21. Typical bell-shaped appearance in  $\lambda E/R_n$  was found between end of December and middle of March.

- Length of this shape varies from season to season with intermediate dip in the ratios depending on water availability conditions that could have increased relative level of  $H$  at the expense of  $R_n$ .

This bell-shaped appearance closely resembles wheat LAI temporal pattern. Generally, a smooth temporal pattern in LAI without intermediate dip is reported through field experiment (Asrar *et al.*, 1984) irrespective of varying water availability and thermal validation. Only, rate of change in LAI differs. Therefore, energy balance based approach is better to capture intermittent stresses specially on arid to semi-arid situation as compared to stress representation through biophysical controls such as LAI / NDVI or SAVI (Chehbouni *et al.*, 2007).

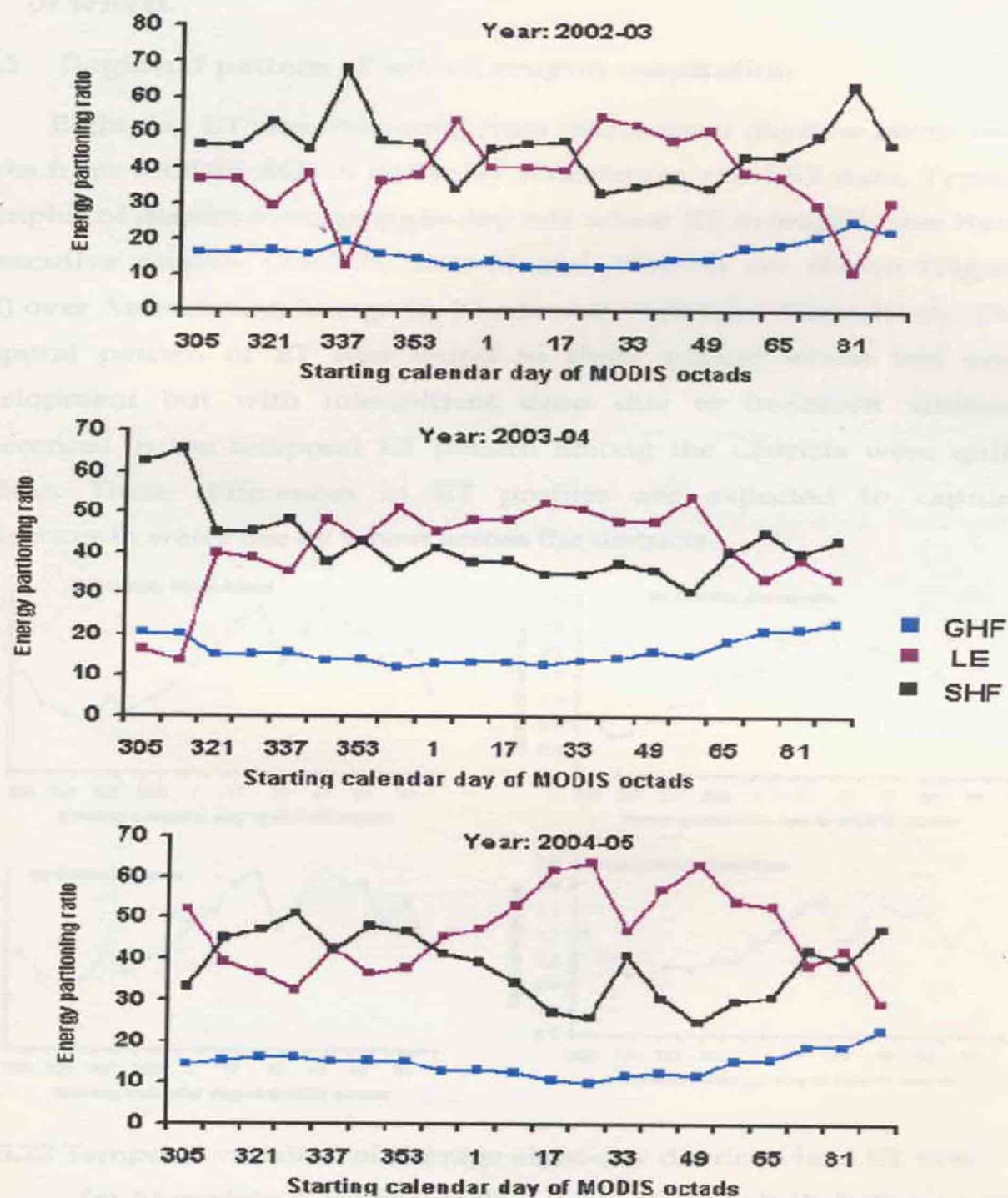


Fig.5.21 Multi-temporal analysis of energy partitioning ratios in wheat over validation site from eight-day MODIS AQUA products during 2002-03, 2003-04 and 2004-05

## 5.6 Evapotranspiration (ET) and consumptive water use (CWU) of wheat

### 5.6.1 Regional pattern of wheat evapotranspiration

Eight day ET was computed from estimates of daytime latent heat fluxes from MODIS AQUA eight-day reflectances and LST data. Typical examples of district average eight-day *rabi* wheat ET averaged over three consecutive seasons (2002-03, 2003-04 and 2004-05) are shown (Figure 5.22) over Ahmedabad, Junagadh, Kheda and Vadodara, respectively. The temporal pattern of ET was found to show typical wheat leaf area development but with intermittent drop due to in-season stresses. Differences in the temporal ET pattern among the districts were quite evident. These differences in ET profiles are expected to capture differences in water use by wheat across the districts.

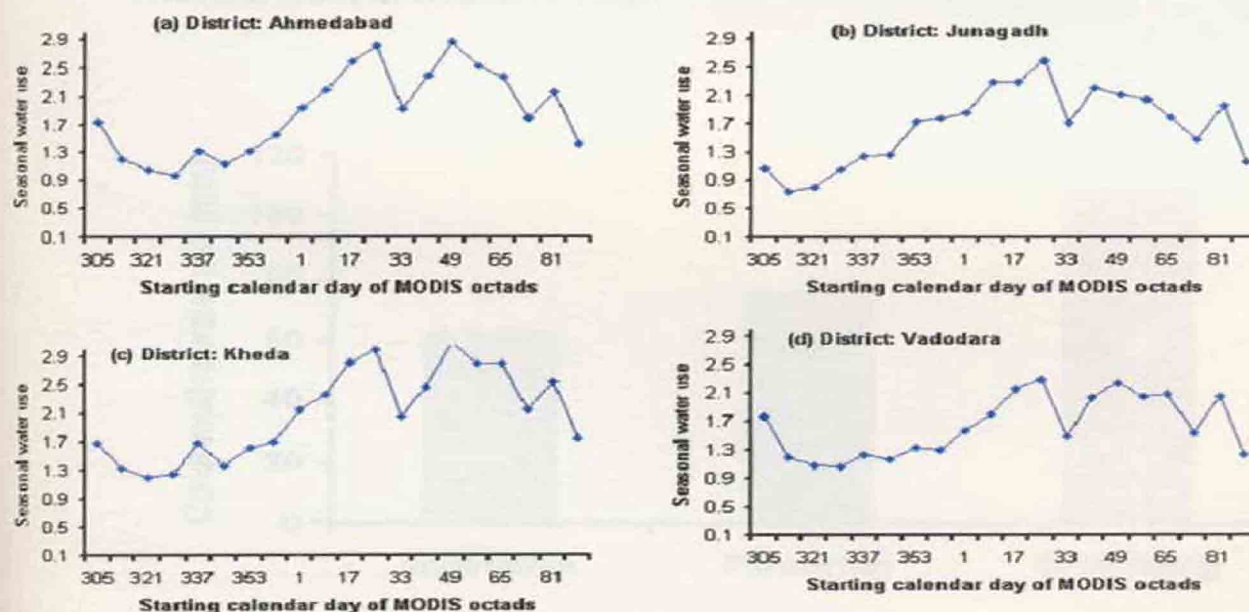


Fig. 5.22 Temporal variation of average eight-day district wheat ET over (a) Ahmedabad, (b) Junagadh, (c) Kheda and (d) Vadodara

### 5.6.2 Regional pattern of wheat consumptive water use

District wise consumptive water use (CWU) was computed by summing up eight-day ET for the wheat grid over entire growth period followed by averaging CWU over wheat grids for three major critical growth stages, vegetative, flowering and grain filling. These were carried out for all individual *rabi* seasons 2002-03, 2003-04 and 2004-05. Regional mean CWU was computed from district means over all the three seasons in Figure 5.23. There was gradual increase in mean CWU from vegetative (60 mm) to grain filling (100 mm) stages. Anonymous (2004) reported that the consumptive water use rate was increased progressively with the advance of crop growth from 0.83 mm day<sup>-1</sup> during the early stages of growth (within a first 40 days) to peak rate of 3.25 mm day<sup>-1</sup> during flowering under 70% available soil water and decreased subsequently with the onset of senescent stage.

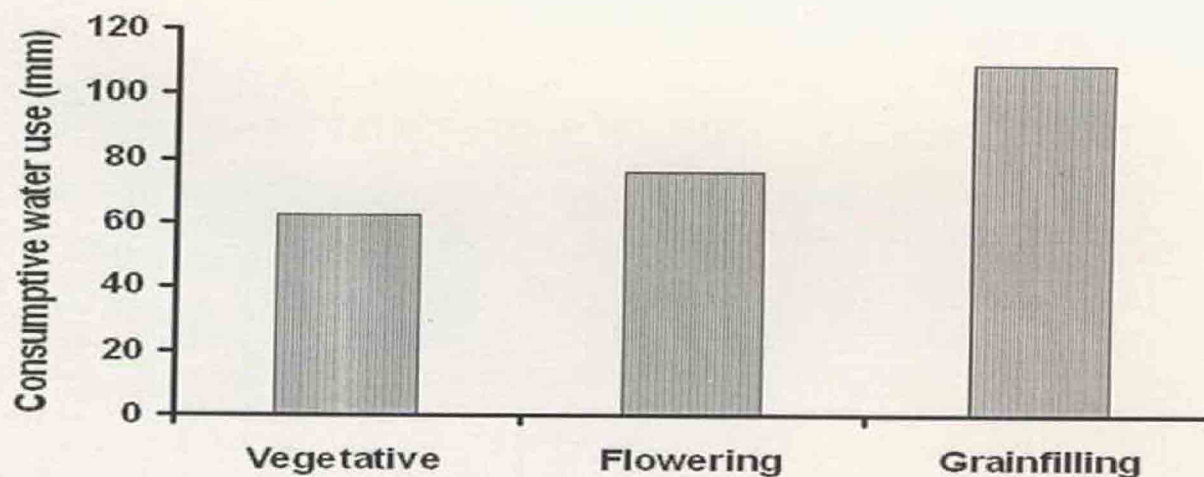


Fig. 5.23 Mean regional wheat consumptive water use (CWU) at different phenophases in Gujarat

Anonymous (2004) made similar observations on the consumptive use rate and found the same as 0.8 mm at early stages and 4.0 mm day<sup>-1</sup> during peak growing period. Majumadar and Mandal (1984) also noted that lysimetric average daily consumptive use was lowest (1.65 mm day<sup>-1</sup>) during the first 20 days of crop growth and that increased gradually reaching the peak of 5.17 mm day<sup>-1</sup> during 87 to 98 days after sowing. Water use during physiological maturity is not critical for wheat growth and productivity and are, therefore not shown here.

There were substantial positive or negative deviations in CWU from regional mean at critical growth stages of wheat. These are presented in Figure 5.24 for all the three wheat growth seasons 2002-03, 2003-04 and 2004-05. This indicated that the inter seasonal differences at critical growth stages may have differential effects on photosynthesis and its translational process to yield from season to season (Reynolds *et al.*, 2000).



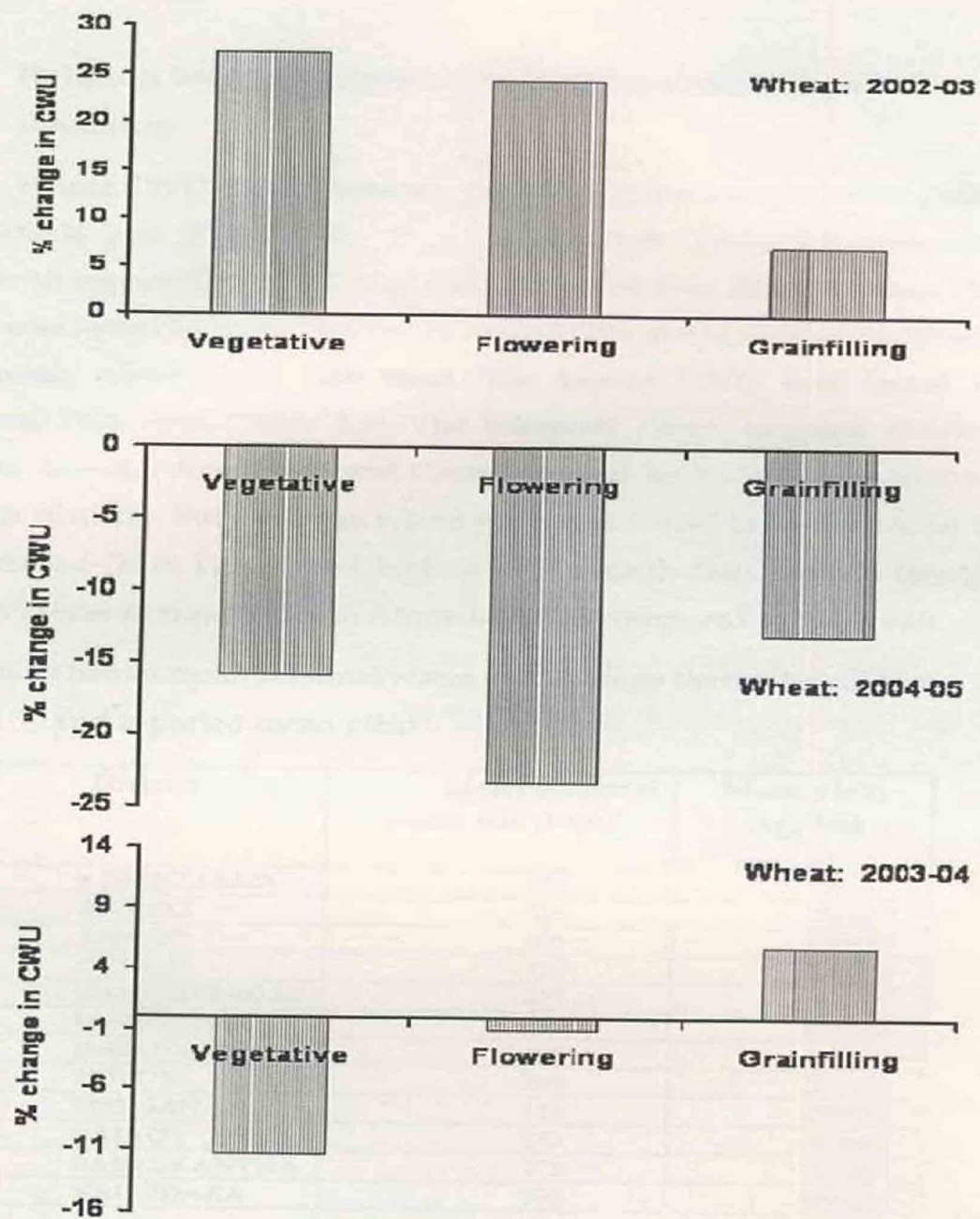


Fig. 5.24 Percent change from mean in regional wheat consumptive water use (CWU) at critical phenophases in Gujarat

### 5.6.3 Relation between deviation in CWU and district yield deviation

Wheat CWU were averaged over three consequent seasons (2002-03, 2003-04 and 2004-05) for 12 wheat districts. These are presented alongwith reported district wheat yield averaged over three seasons. The CWU was found to be the highest in Anand (291 mm) followed by Kheda (269 mm), Ahmedabad (238 mm). The lowest CWU was found in Mehsana (114 mm) (Table 5.6). The relatively better irrigated districts such as Anand, Ahmedabad and Kheda showed high CWU as compared to other districts. But the mean wheat yield was found to be the lowest in Ahmedabad (1516 kg/ha) and highest in Junagadh (3450 kg/ha) though the CWU was 45 mm higher in Ahmedabad as compared to Junagadh.

**Table 5.6** District mean seasonal water use, average thermal condition and reported mean yield

District	Mean seasonal water use (mm)	Mean yield (kg/ha)
AHMEDABAD	238	1516.00
AMRELI	126	2965.67
ANAND	291	1899.67
DAHOD	179	1902.00
GANDHINAGAR	232	2888.67
JAMNAGAR	176	3075.33
JUNAGARH	193	3450.33
KHEDA	269	2521.33
MEHSANA	114	2587.33
RAJKOT	173	3420.67
SABARKANTHA	175	2162.00
VADODARA	208	2264.33

The general thermal environment in Junagadh is relatively cooler because of the presence of the relatively hilly terrain. Thermal environment in wheat plays a major role in wheat in addition to water use specially for conversion of photosynthates to yield attribute

(Reynolds *et al.*, 2000) during grainfilling stage. Even with plenty of soil moisture, an anomaly in air temperature during middle to latter part could lead to low wheat yield (Midmore *et al.*, 1982; Rawson, 1986). This is more important in semi-arid climatic situation like Gujarat where length of winter is very short. Therefore, a straightforward predictive relation between district mean CWU and mean yield will not hold good. Rather, district CWU deviations and yield deviations from mean may produce better predictive relations.

In order to investigate the impact of deviation in CWU on yield deviation, percent deviation of district mean wheat CWU from three seasons (2002-03, 2003-04 and 2004-05) were plotted against deviation in reported district wheat yield from three seasons district mean. District CWU means were derived in two ways

- (i) By simple averaging over wheat grids and
- (ii) Area weighted through different CWU classes over wheat grids. The deviation from simple averaging produced (Figure 5.25 (a)) better correlation ( $r = 0.74$ ) than with area weighting ( $r = 0.66$ ). The plot of CWU deviation from area weighted mean and deviations in reported yield is shown in Figure 5.25 (b). This relation indicated the potential of satellite based water use for predicting district average yield or its deviations. But this requires more number of satellite data to be processed and analysis of yield for 5-7 years to have a good model. Another way to utilize CWU is its calibration through districtwise water use efficiency (WUE) and use it for yield prediction. Intra-regional differences in thermal environment will be also embedded in the districtwise calibration factors.



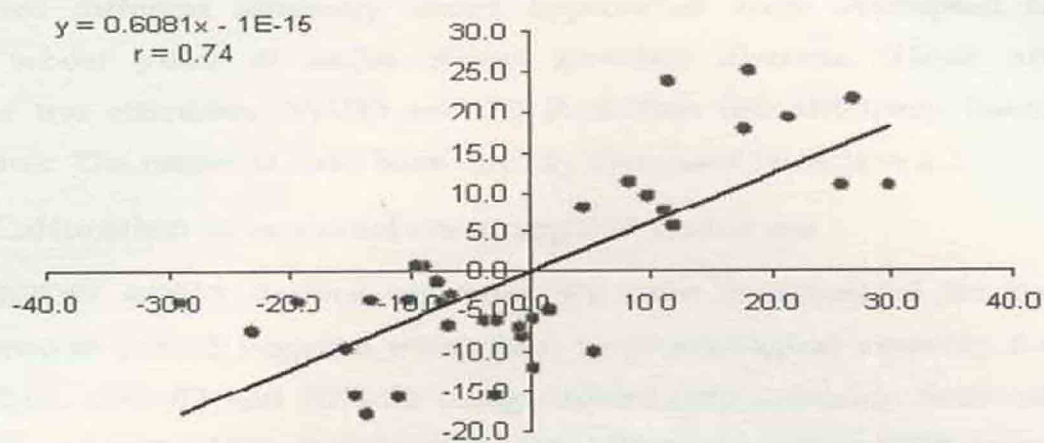


Fig. 5.25 (a) Plot of district percent deviation in consumptive water use (CWU) from simple average and percent yield deviation

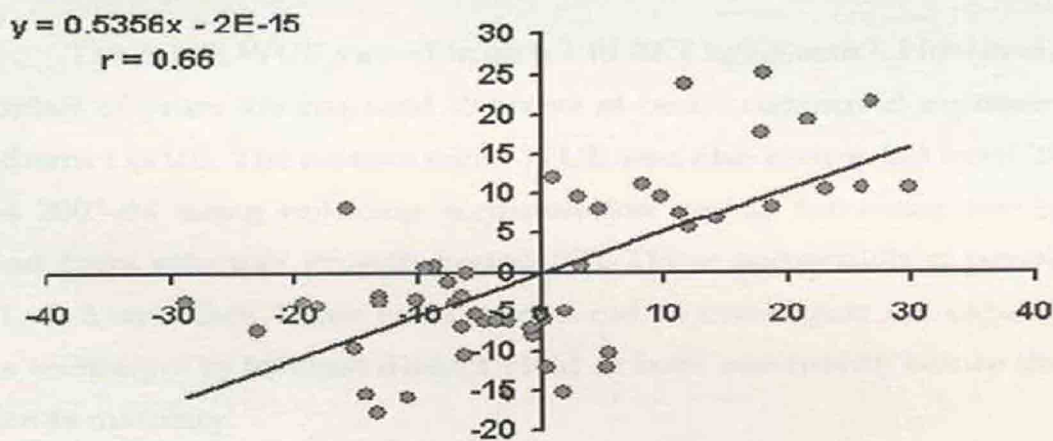


Fig. 5.25 (b) Plot of district percent deviation in consumptive water use (CWU) from area weighted mean and percent yield deviation

## 5.7 District level wheat yield prediction

Two different efficiency based approaches were attempted to predict wheat yield of major wheat growing districts. These are (i) Water use efficiency (WUE) and (ii) Radiation use efficiency based approaches. The methods have been already discussed in section 4.2.

### 5.7.1 Calibration of seasonal consumptive water use

MODIS AQUA derived eight-day ET were accumulated for the wheat growth period between emergence to physiological maturity for *rabi* 2002-03, 2003-04 and 2004-05 using district crop calendar. Seasonal CWU was computed for all the *rabi* seasons. District average CWU were computed from wheat grids. The district average water use efficiency (WUE) of wheat for the effective growth period were computed from the middle year 2003-04. The district WUE acts as calibration factor between CWU and reported yield.

The mean WUE varied from 6.1 to 23.2 kgha-mm<sup>-1</sup>. However, more number of years are required to arrive at better computed representation of district WUE. The district mean WUE was also computed from 2002-03 and 2003-04 using reducing accumulation period for water use by one octad from effective growth period (G). These accumulation periods are G-1, G-2, and G-3. These were carried out to investigate the capability of this technique to forecast district yield at least one month before the crop attends maturity.

District mean WUE were also computed from three critical wheat growth stages, vegetative, flowering and grain filling using the ratio of reported yield and stage specific water use in 2003-04. WUE were generally higher in vegetative and flowering stages as compared to grain filling. It varied between 19.95 – 74.56 kgha-mm<sup>-1</sup>, 16.46-84.37 kgha-mm<sup>-1</sup> and 8.05-39.17 kgha-mm<sup>-1</sup>, in vegetative, flowering and grain filling, respectively (Table 5.7). Atmospheric thermal regime in Gujarat is generally higher than intensive wheat growing regions such as Punjab,

Haryana and Rajasthan specially during the conversion of photosynthates. This could possibly lead to less realization of yield from consumptive water use. The present wheat classification based on 250 m MODIS data and the accuracy of classification improves with finer resolution of sensors between 15-60 m as applied to ASTER, LANDSAT TM and LISS III and AWiFS. The possibility of misclassification would likely to increase such Moderate resolution sensors. Standard sowing data was assumed for computation of water use for all the years in different districts based on IMD crop calendar. There fore year to year variation of sowing date avoid propagate errors in CWU computation. These are the two major possible causes of getting higher WUE certain districts.

**Table 5.7: Stage wise WUE over different districts**

District	WUE ( kg/ha-mm )		
	Vegetative	Flowering	Grain filling
AHMEDABAD	18.95	16.46	8.05
AMRELI	79.93	50.36	39.17
ANAND	23.80	19.45	24.13
DAHOD	42.36	45.75	18.03
GANDHINAGAR	40.96	37.37	17.38
JAMNAGAR	64.97	38.99	28.46
JUNAGARH	74.56	51.80	36.93
KHEDA	25.00	34.70	13.49
MEHSANA	75.98	84.37	38.30
RAJKOT	62.76	42.89	38.38
SABARKANTHA	37.74	39.88	16.26
VADODARA	42.02	40.23	23.11

### 5.7.2 Validation of WUE based yield prediction

The district mean WUE and AQUA based seasonal water use for preceding (2002-03) and succeeding (2004-05) years were used to predict district wheat yield. The correlation between reported and predicted yield was 0.87 (Figure 5.26) with RMSE 441 kg/ha<sup>-1</sup> (18% of mean). The

accuracy of this method is better than NDVI or any other VI based empirical yield prediction models. The VI based methods explain only up to 50-60 % yield variability (Hayes and Decker, 1996; Quarmby *et al.*, 1993). Though Potdar and Manjunath (1990), Manjunath *et al.*, 2002 have found better multiple regression ( $r = 0.9$ ) between 20-day NOAA

AVHRR district mean wheat NDVI and reported yield in Rajasthan. But the model was not verified to predict wheat yield from independent datasets. Bhattacharya *et al.*, 2007 found that errors from single source, AET/ET estimates increase as the surface heterogeneity increases. Therefore, accuracy of yield prediction from single source ET estimates diminishes from homogenous wheat growth conditions (e.g. Punjab) to heterogeneous conditions (e.g. Rajasthan, M. P.). A two source formulation (Anderson *et al.*, 2000) from satellite data captures both homogenous and heterogeneous conditions because it considers separate couplings of soil and canopy with atmosphere. The comparison of two-source and single source ET estimates showed better ET estimates from two source scheme (Timmermans *et al.*, 2007). The use of two source ET formulation and generation of district WUE from multiple years may predict regional wheat yield better than the present accuracy in semi-arid heterogeneous conditions in Gujarat.

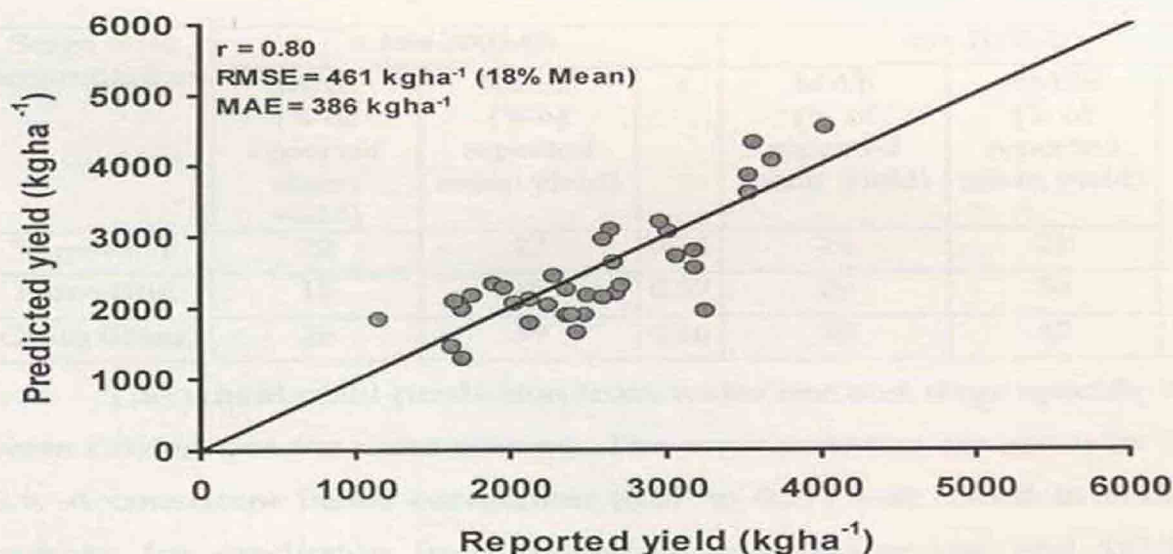


Fig. 5.26 Validation of WUE based predicted district yield and reported yield

**Table 5.8** Error statistics of WUE based district yield prediction using different accumulation period for seasonal water use

Accumulation period	<i>rabi</i> 2002-03			<i>rabi</i> 2004-05		
	MAE (% of reported mean yield)	RMSE (% of reported mean yield)	r	MAE (% of reported mean yield)	RMSE (% of reported mean yield)	r
G	12	14	0.63	17	21	0.81
G-1	12	14	0.61	16	21	0.80
G-2	14	17	0.46	15	19	0.80
G-3	19	23	0.25	13	18	0.73

Little lower correlation and relatively higher percent RMSE were obtained for predicted wheat yield with reducing accumulation periods (G-1, G-2 and G-3). The correlation varied from 0.25 to 0.80 and RMSE were found to vary between 14 - 21 % of reported mean.

**Table 5.9** Error statistics of district wheat yield prediction from WUE based approach using stage wise water use

Stage wise accumulation	<i>rabi</i> 2002-03			<i>rabi</i> 2004-05		
	MAE (% of reported mean yield)	RMSE (% of reported mean yield)	r	MAE (% of reported mean yield)	RMSE (% of reported mean yield)	r
Vegetative	22	27	0.16	14	21	0.75
Flowering	15	18	0.57	29	34	0.77
Grain filling	28	39	0.66	28	42	0.31

The wheat yield prediction from water use and stage specific WUE were carried out for same seasons. The error statistics are given in Table 5.9. A consistent better correlation (0.57 to 0.77) was found in both the seasons for prediction from flowering stage water use and WUE as compared to other two critical stages. The RMSE ranged between 18-34% of observed mean for prediction from this stage.

### **5.7.3 Generation of basic inputs for estimating net primary productivity (NPP)**

A radiation use efficiency (RUE) based net primary production (NPP) model (CASA) was used to compute total above ground biomass at 0.01° grid over wheat crop. This biomass was subsequently converted to wheat yield. Model details are given in section 4.2. The eight-day NPP was determined from daily clear sky insolation, fAPAR, maximum RUE ( $RUE_{max}$ ) constrained by water and temperature scalars. These were accumulated over wheat growth period for 2002-03 and 2004-05 over wheat grids of 0.01°. Evaporative fraction determined through LST-albedo 2D scatter was used as water scalar. The MODIS AQUA data derived inputs used in the model are LAI, daily mean air temperature, noon time LST and albedo. The average daily transmissivity available through IMD pyranometer measurements were used to compare daily clear sky insolation input to the model.

#### **5.7.3.1 LAI / fAPAR estimation**

A common exponential model,  $LAI = 0.0568 \text{ EXP } (6.0183 * NDVI)$ , was formed between measured LAI and MODIS AQUA 250m NDVI with a number of ( $n = 20$ ,  $r = 0.85$ ) measurements over dominant wheat growing states in India. This model was extrapolated to wheat growing pixels over study region in Kheda district. This produced a RMSE of 0.9 (25% of measured mean) with  $r = 0.75$ .

The temporal variation of measured and estimated LAI over measurement site over Chalindra and Muktipur was quite matching (Figure 5.29) during wheat 2005-06. LAI was found to vary between 1.2 – 5 and 2.5 – 5 at Chalindra and Muktipur, respectively. Empirical model showed relatively higher error in LAI estimation using moderate resolution MODIS AQUA 250m NDVI as compared to estimation accuracy with RMSE of 0.689 using finer resolution (Chaurasia *et al.*, 2006) data from IRS LISS III (23.5 m) and AWIFS (50m) at field scale (Chaurasia



*et al.*, 2007). The recent studies showed the ability of canopy reflectance inversion scheme to reduce errors in LAI estimation using moderate resolution MODIS TERRA reflectances (Houborg *et al.*, 2007) and finer resolution SPOT VGT reflectances (Houborg and Boegh, 2007) data in an association of different crops over a large agricultural patch.

Extinction coefficient ( $k_c$ ) at different growth stages of wheat were computed from *in situ* measurements on PAR, fAPAR and LAI over wheat during 2005-06. This varied between 0.65 to 0.75. Using stage specific  $K_c$  and estimated LAI, regional fAPAR was generated. This was used as input to CASA model for productivity estimation.

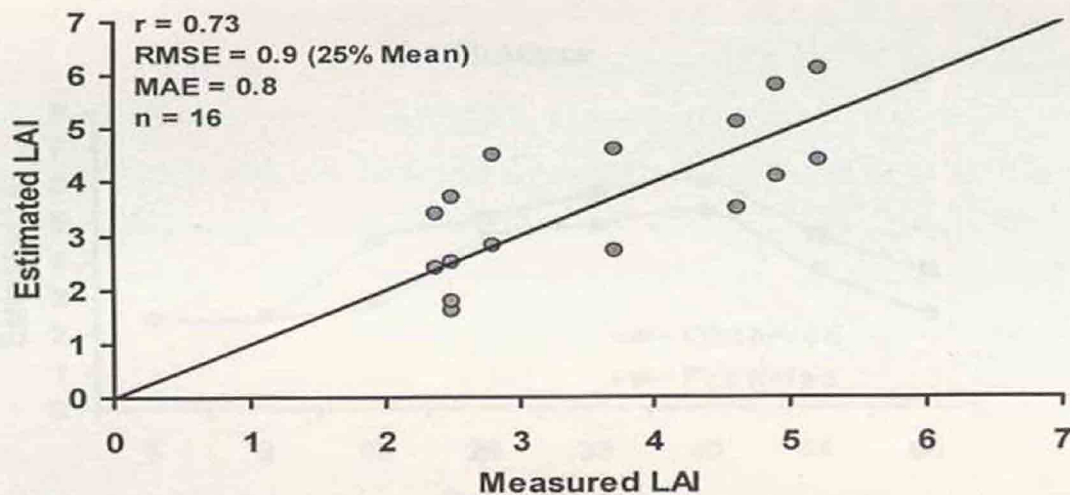


Fig. 5.27 Validation plot of estimated LAI from MODIS AQUA 250m NDVI

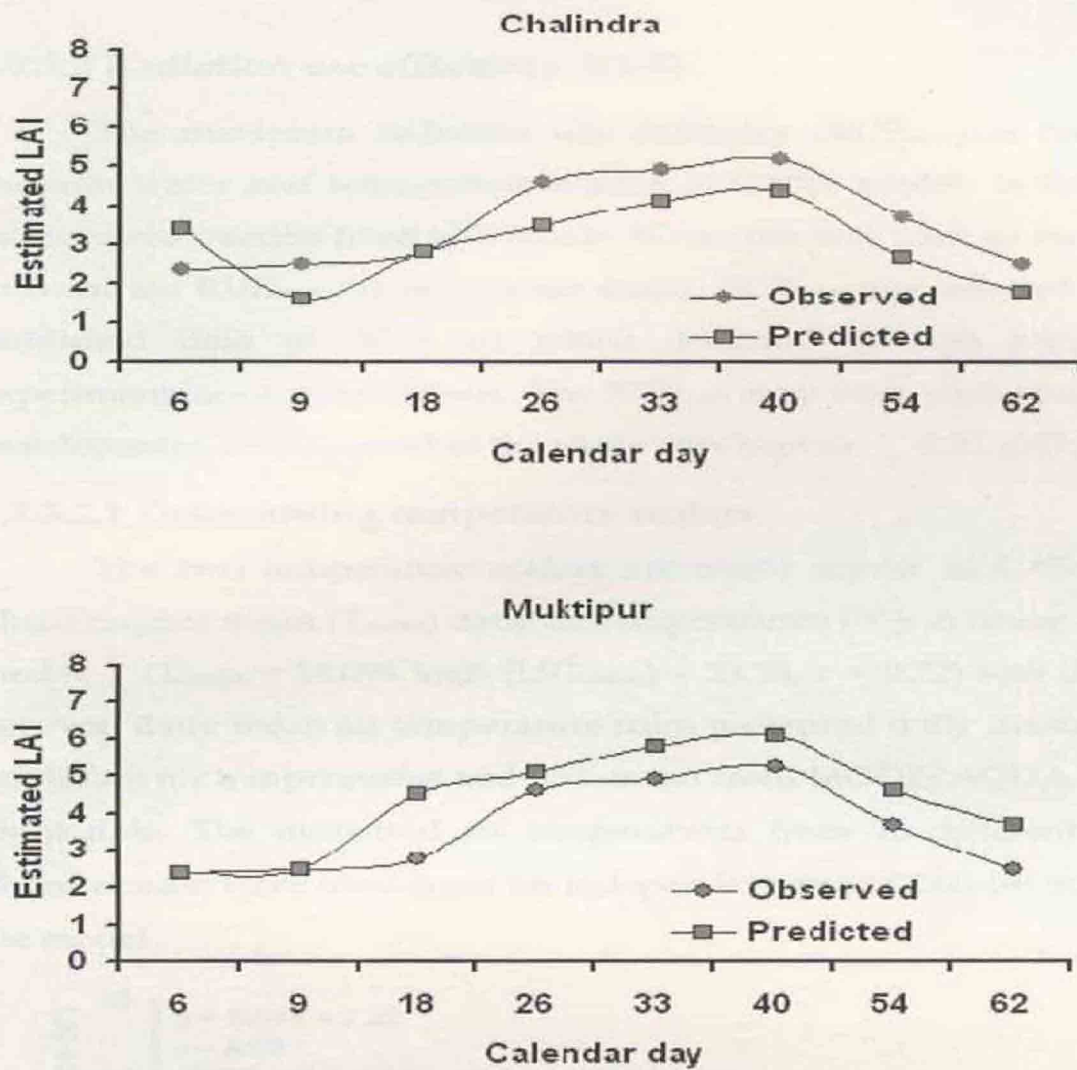


Fig. 5.28 Temporal variation of measured and estimated LAI at Chalindra and Muktipur



### 5.7.3.2 Radiation use efficiency (RUE)

The maximum radiation use efficiency ( $RUE_{max}$ ) is constrained through water and temperature scalars in CASA model. In this model, evaporative fraction from LST-albedo 2D scatter was used as water scalar to constrain  $RUE_{max}$ . In the present study,  $RUE_{max}$  was selected from the published data on RUE on wheat obtained through several field experimentations over Gujarat. The  $RUE_{max}$  may vary with phenological development.  $RUE_{max}$  used in the study was kept at  $2.02 \text{ gMJ}^{-1}$ .

#### 5.7.3.2.1 Determining temperature scalars

The two temperature scalars are major inputs to CASA model. These require mean ( $T_{mean}$ ) daily air temperatures ( $^{\circ}\text{C}$ ). A linear empirical model ( $T_{mean} = 14.098 \log E (LST_{mean}) - 23.54$ ,  $r = 0.99$ ) was developed between daily mean air temperature from measured daily maximum and minimum air temperatures and LST mean from MODIS AQUA from day night data. The measured air temperatures from 13 different agromet observatories were used from an independent year (2003-04) to develop the model.

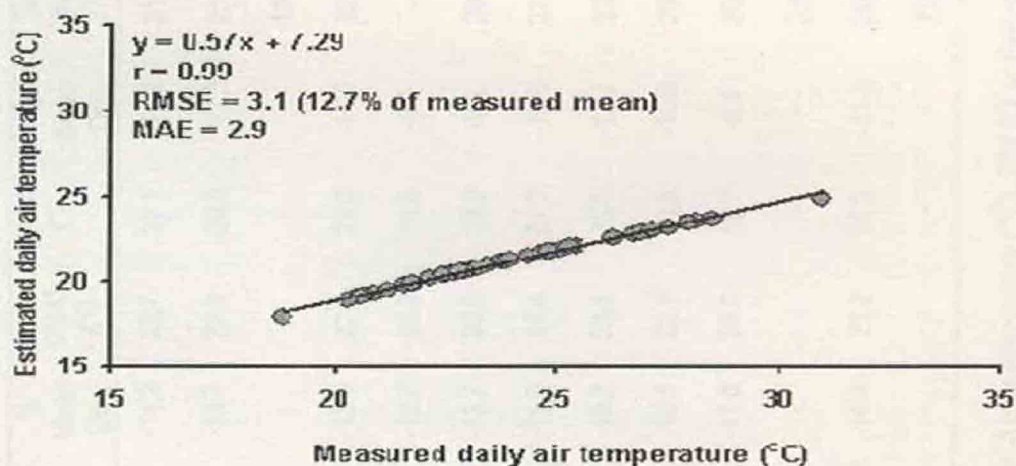


Fig. 5.29 Pooled validation of mean air temperature

Table: 5.10 Observed and estimated air temperature over different locations in Gujarat

Stations	Nov. OMAT (°C)	EMAT (°C)	% Mean Dev.	Dec. OMAT (°C)	EMAT (°C)	% Mean Dev.	Jan. OMAT (°C)	EMAT (°C)	% Mean Dev.	Feb. OMAT (°C)	EMAT (°C)	% Mean Dev.	March to OMAT (°C)	EMAT (°C)	% Mean Dev.
Dhandhuka	25.4	21.8	-14.2	22.7	20.1	-11.3	21.2	19.2	-9.2	-	-	-	28.5	23.4	-17.8
Godhra	24.9	21.5	-13.7	22.9	20.3	-11.3	21.6	19.5	-9.7	23.9	20.9	-12.4	28.0	23.2	-17.2
Jamnagar	-	-	-	-	-	-	18.8	17.6	-	21.7	19.6	-	25.3	21.8	-
Vadodara	25.1	21.6	-13.9	22.5	20.0	-11.0	22.8	20.2	-11.0	24.7	21.4	-13.3	27.5	22.9	-16.6
Khedrahma	24.0	20.9	-12.7	20.9	19.0	-9.0	-	-	-	-	-	-	-	-	-
Ladol	24.7	21.3	-13.7	20.9	19.0	-9.2	20.6	18.9	-8.6	22.7	20.2	-10.9	28.2	23.3	-17.4
Mangral	26.8	22.5	-15.9	24.4	21.2	-13.0	22.9	20.3	-11.2	24.0	21.0	-12.5	26.7	22.5	-15.7
Navsari	26.3	22.3	-15.2	23.5	20.6	-12.3	22.7	20.2	-10.9	24.4	21.2	-12.9	26.9	22.6	-15.9
Nawagam	24.8	21.4	-13.8	22.1	19.8	-10.6	20.6	18.8	-8.6	22.8	20.3	-11.1	27.2	22.8	-16.2
Radhanpur	23.1	20.4	-11.6	20.5	18.7	-8.8	20.3	18.6	-8.2	22.5	20.1	-10.7	-	-	-
surat	-	-	-	-	-	-	23.8	20.9	-	25.4	21.8	-	28.0	23.2	-
Tanchha	25.5	21.8	-14.4	23.2	20.5	-11.8	22.5	20.1	-10.8	24.8	21.5	-13.5	28.5	23.4	-17.8
Khandha	-	-	-	-	-	-	21.8	19.6	-9.9	27.1	22.7	-16.2	31.0	24.6	-20.5

OMAT = Observed mean Air temperature (°C), EMAT = Estimated mean Air temperature (°C), Blank boxes (-) = Measure temperature data are not available

The validation plot (Figure 5.29) of model estimates and measurements showed RMSE 3.1°C (12.7% of mean) in the estimated daily mean air temperatures. These errors are little higher than those (1.5 – 2.5°C) air temperatures estimated using satellite data on diurnal and daily scales (Stisen *et al.*, 2007).

The monthly mean air temperature was estimated for 2004-05 for a period of *rabi* season from November to March using LST MODIS AQUA over different stations of Gujarat (table 5.10). The percent mean deviation was in the range of -11.6 to -15.9, - 8.8 to -13.0, - 8.2 to - 11.2, -10.7 to -16.2 and -15.7 to -20.5 for November, December, January, February and March, respectively. The estimated air temperature was underestimated than the observed mean air temperature for all the months, but they maintain the same trend for all the months. The minimum percent mean deviation was occurred in the month of January and maximum was in the month of March.

#### 5.7.3.2.2 Evaporative fraction

The water scalar used to constrain  $RUE_{max}$  is through regional output of evaporative fraction ( $\Lambda$ ). A consistency check of regional wheat  $\Lambda$  from eight-day data was made by plotting 2D scatters with wheat NDVI averaged over 2002-03 and 2004-05 at vegetative, flowering, grain filling and maturity (Figure 5.30). The scatters varied from triangular shape to linearity between vegetative, flowering and grain filling stages. Towards maturity, this again tends to become triangular. Similar triangular relations were also reported by (Wang *et al.*, 2006) and Mallick *et al.*, 2007 between estimated  $\Lambda$  and NDVI as well as measured  $\Lambda$  and NDVI from data pooled over heterogeneous land cover types and fraction.

Evaporative fraction is mainly composed of two components, canopy and soil. Canopy component represents transpiration fraction.

Soil component represents soil evaporation fraction. Transpiration fraction is linearly related to leaf area development or vegetation indices (e.g. NDVI, SAVI).

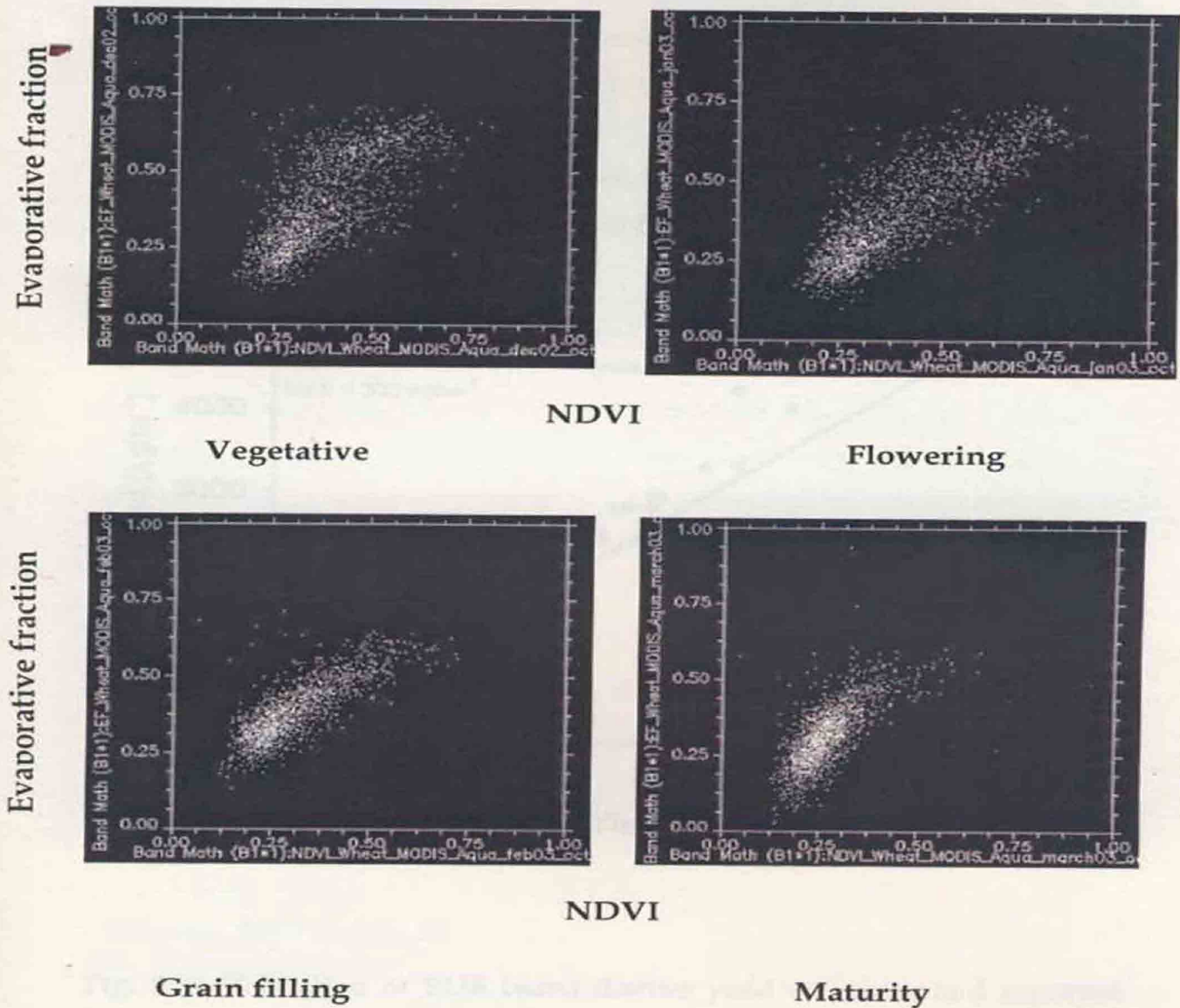


Fig. 5.30 Two-dimensional scatter of TERRA-AQUA evaporative fraction and NDVI at vegetative, flowering, grain filling and maturity

#### 5.7.4 Validation of RUE based yield prediction

Net primary productivity (NPP) of wheat was estimated using CASA model for 2002-03 and 2004-05. The actual wheat yield was obtained from NPP and average wheat harvest index (0.35) in the region. The district average CASA estimated wheat, yield were found to produce RMSE of the order of  $428 \text{ kg ha}^{-1}$  (17.7 % of reported mean) with correlation coefficient ( $r$ ) with 0.90 for data pooled over 2002-03 and 2004-05. The 1:1 validation plot is shown in Figure 5.31.

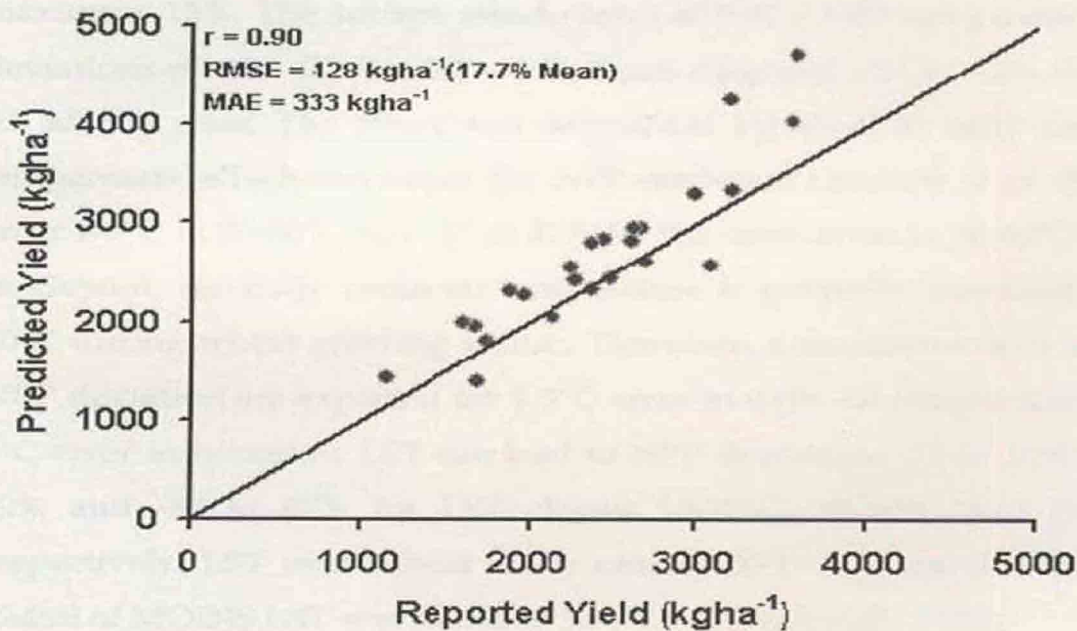


Fig. 5.31 Validation of RUE based district yield estimates and reported yield

#### 5.7.4.1 Sensitivity analysis of CASA model

CASA (Carinege Ames Stanford Approach) model NPP was put to sensitivity test to error associated using satellite based inputs such as LAI, albedo, daily mean air temperature and LST. The results of sensitivity analysis are summarized in Table 5.11. The NPP deviations are directly related to LAI and albedo errors but the impact of errors in daily air temperature and LST are just opposite. A 10-20% error in LAI for all classes can cause deviations in NPP to the order of 8-16%. Present LAI astimation produced about 25% error that can lead to NPP error of maximum 15%. The surface albedo error of 0.01 – 0.03 can produce NPP deviations of  $\pm 1 - 7\%$  for 0.1 – 0.2 albedo class and  $\pm 57$  to  $-15\%$  for 0.2 – 0.3 albedo class. The effect was substantial for error in daily mean air temperature which can cause tha NPP deviation between  $-6$  to  $-23\%$  for error  $1-3^{\circ}\text{C}$  in  $20-30^{\circ}\text{C}$  and  $-47$  to  $57\%$  for the same error in  $30-40^{\circ}\text{C}$  range. In Gujarat, the daily mean air temperature is generally restricted to  $20-30^{\circ}\text{C}$  during wheat growing season. Therefore, a maximum of  $-6$  to  $-23\%$  NPP deviation are expected for  $1-3^{\circ}\text{C}$  error in daily air temperature. A  $1-3^{\circ}\text{C}$  error in noontime LST can lead to NPP deviations  $-12$  to  $12\%$ ,  $-22$  to  $22\%$  and  $-87$  to  $87\%$  for LST classes  $10-20^{\circ}\text{C}$ ,  $20-30^{\circ}\text{C}$  and  $30-40^{\circ}\text{C}$ , respectively. LST over wheat rarely crosses  $30^{\circ}\text{C}$  in Gujarat. Moreover, RMSE of MODIS LST was found to be  $\pm 1.5^{\circ}\text{C}$  (Wan *et al.*, 2004).

Given the errors in satellite based inputs to CASA model, the estimated error in wheat NPP could be between 10-12% that could have propagated same level of error to predict yield. Rest 4-5% error in yield prediction through CASA model could be attributed to uncertainty associated with misclassification of wheat using 250m MODIS data.



**Table: 5.11** Sensitivity analysis CASA model NPP to different satellite derivable input parameters

Variable	Class	Errors	% Deviation in Net Primary Productivity (NPP)
LAI	1-2	$\pm 10 - 20 \%$	$\pm 8.5 - 16$
	2-3	$\pm 10 - 20 \%$	$\pm 7 - 15$
	3 - 4	$\pm 10 - 20 \%$	$\pm 6 - 13$
Albedo	0.1-0.2	$\pm 0.01- 0.03$	$\pm 1 - 7$
	0.2-0.3	$\pm 0.01- 0.03$	56 to -15
Noon time LST	10-20 ° C	$\pm 1 - 3$	- 12 to 12
	20-30 ° C	$\pm 1 - 3$	- 22 to 22
	30-40 ° C	$\pm 1 - 3$	- 87 to 87
Air Temperature	10-20 ° C	$\pm 1 - 3$	$\pm 8$ to 23
	20-30 ° C	$\pm 1 - 3$	- 1 to - 2.3
	30-40 ° C	$\pm 1 - 3$	- 47 to 57

#### 5.7.4.2 District wise Yield prediction

The district wise wheat yield predicted using two approaches showed variations with reported yield in both the approaches (Table 5.12). The percent deviation in yield by WUE and RUE approach was ranged between -24.95 to 23.15 and 2.91 to 33.25, respectively. The maximum percent deviation was found in WUE approach at Mehsana (- 33.25) but with minimum deviation by RUE approach 9.79 % for same district. The minimum percent deviation in yield prediction was occurred at Dahod, Gandhinagar, Rajkot for WUE approach while by RUE approach Ahmedabad, Jamnagar, and Mehsana districts. The RUE approach overestimated the wheat yield but in WUE expect Amreli, Jamnagar, Mehsana, sabarkantha and Vadodara rest of districts found to be overestimated.

**Table 5.12** District wise yield (2004-05) prediction using two approaches

District	Reported yield (kg ha <sup>-1</sup> )	WUE yield (kg ha <sup>-1</sup> )	% deviation	RUE yield (kg ha <sup>-1</sup> )	% deviation
AHMEDABAD	1754	2160	23.15	1805	2.91
AMRELI	3188	2550	-20.01	4248	33.25
ANAND	1885	2310	22.55	2321	23.13
DAHOD	1984	2090	5.34	2284	15.12
GANDHINAGAR	2977	3180	6.82	3288	10.45
JAMNAGAR	3196	2770	-13.33	3322	3.94
JUNAGARH	3579	4310	20.42	4727	32.08
KHEDA	2610	2950	13.03	2953	13.14
MEHSANA	2665	2000	-24.95	2926	9.79
RAJKOT	3547	3610	1.78	4021	13.36
SABARKANTHA	2370	2250	-5.06	2797	18.02
VADODARA	2250	2010	-10.67	2564	13.96

### 5.8 Comparison of regional wheat yield distribution from both approaches

Two yield prediction / estimation approaches were used in the present study. The RUE based NPP approach (CASA) showed little better accuracy in district wheat yield (17.7 % of reported mean) than WUE based approach (18 % of reported yield). Moreover, the latter requires historical data to calibrate seasonal water consumptive use. But the former requires no pre-calibration. Errors are associated with input parameters such as LST, albedo, air temperature and LAI. The improvement in the satellite derived input parameters may lead to better NPP estimation as well as yield. The distributions of wheat yield from both the approaches over selected districts in Gujarat for a common year (2004-05) are shown in Figure 5.32. Spatial pattern of yield are quite similar. There were also similarity in low (0 – 2000 kg ha<sup>-1</sup>), medium

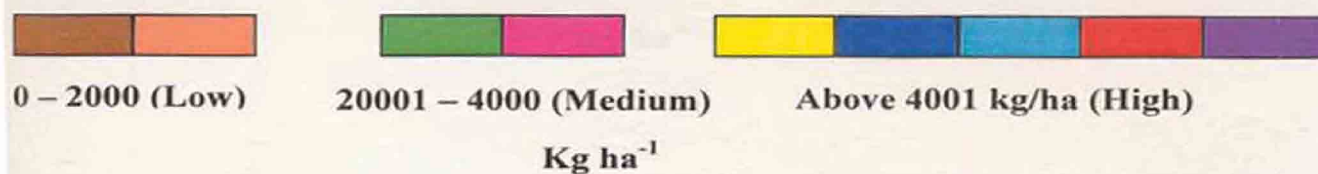
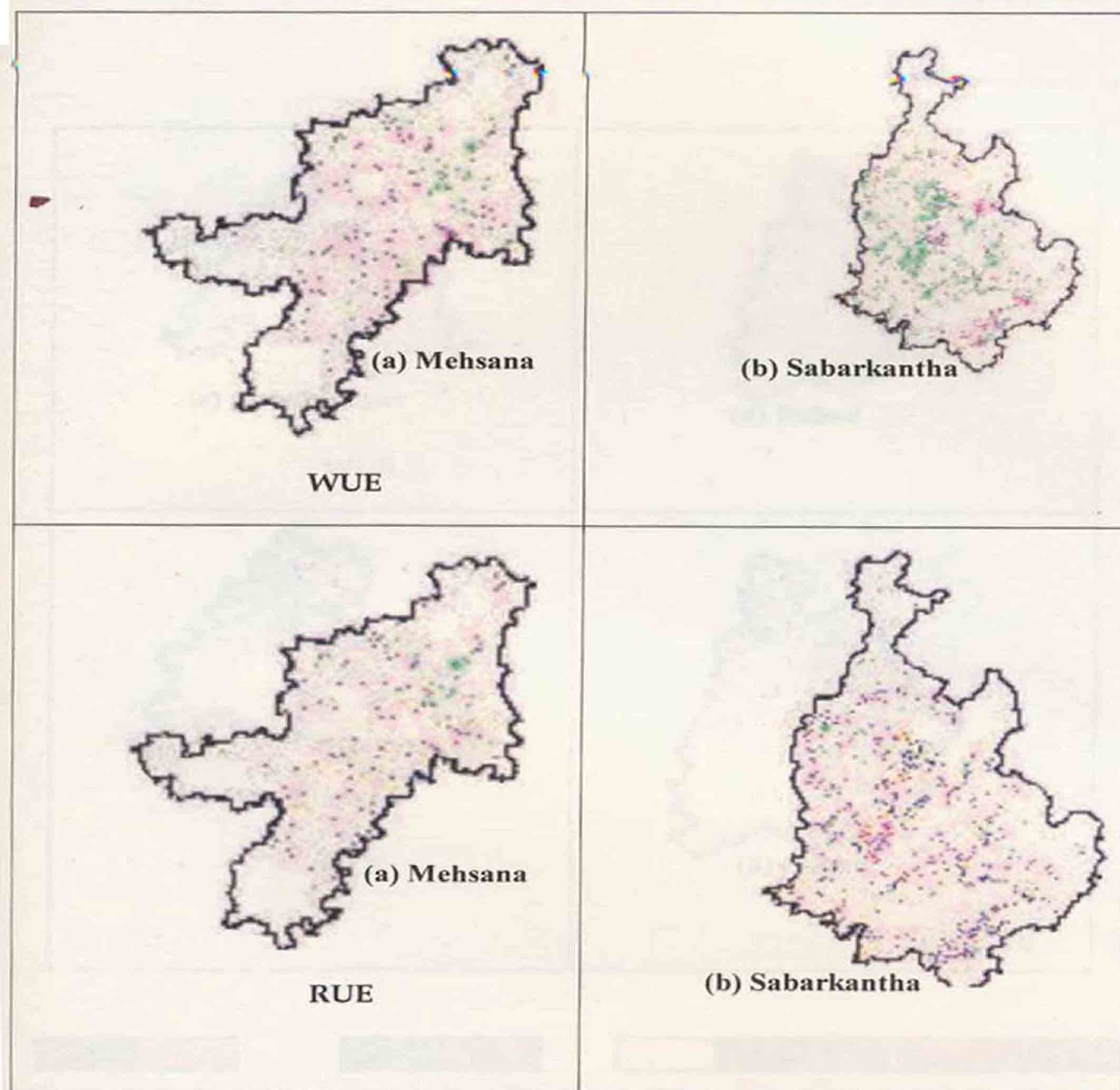


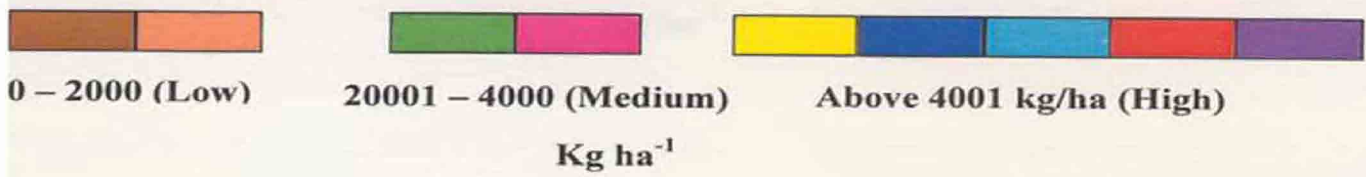
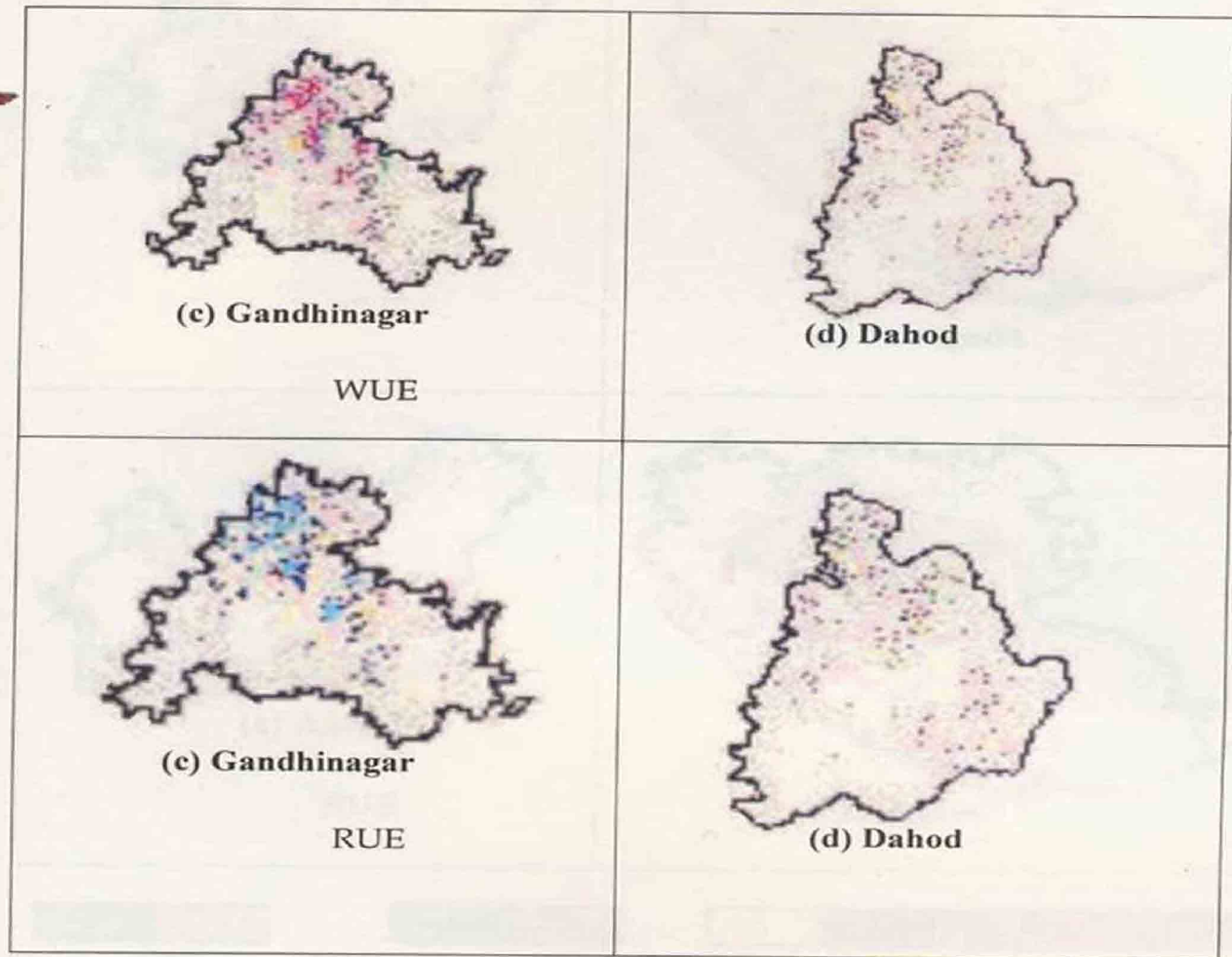
(2001 – 4000 kg ha<sup>-1</sup>) and high (> 4000 kg ha<sup>-1</sup>) yield regions from both the approaches.

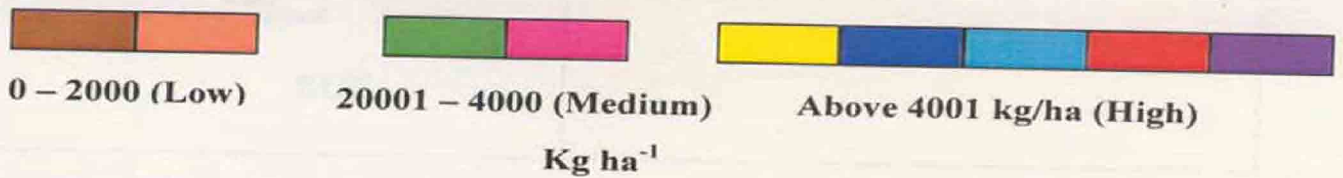
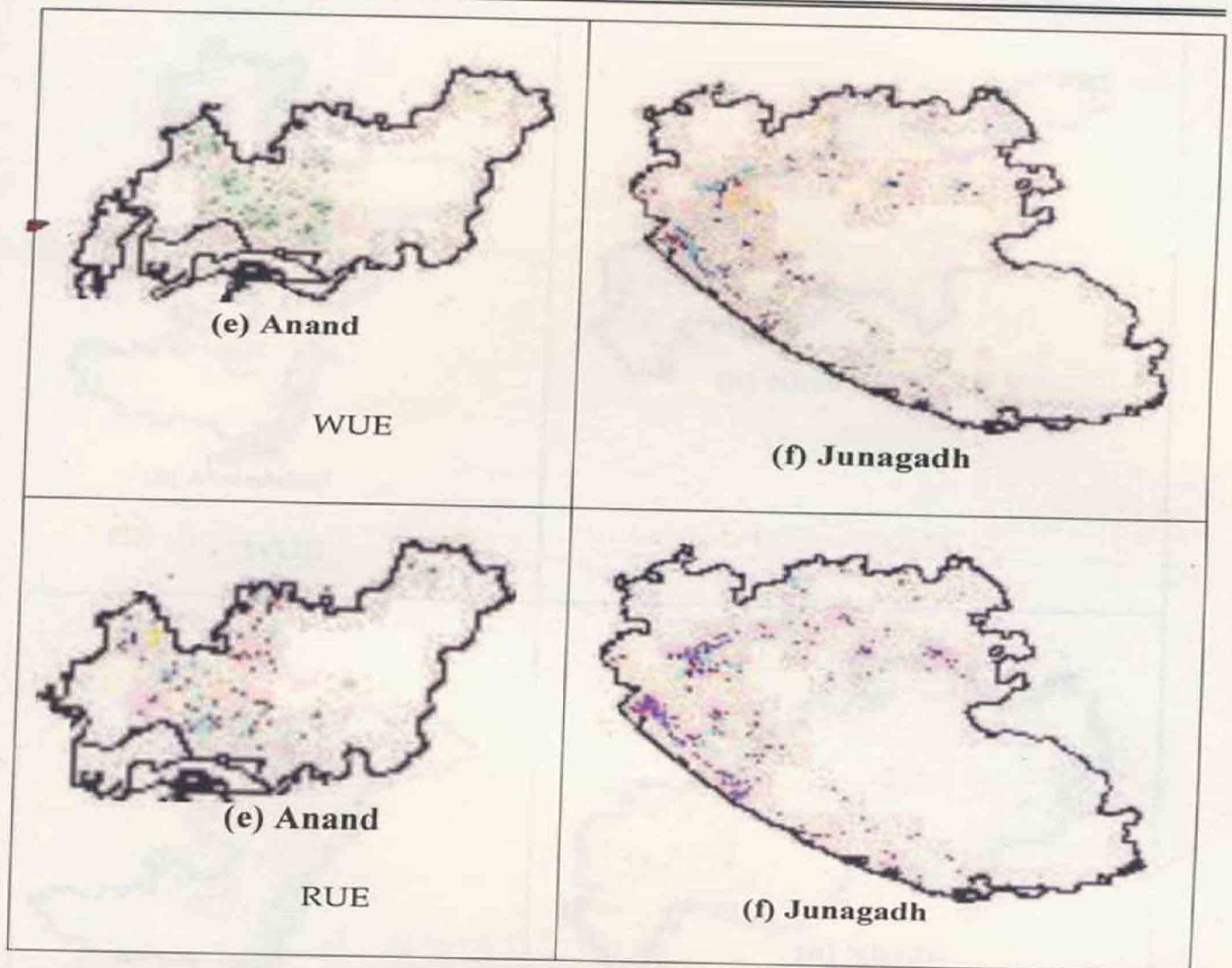
The present yield prediction approaches showed relatively better district yield estimates with accuracies more than conventional spectral yield models using single multi-date NDVI (Quarmy *et al.*, 1993) or vegetation condition index (VCI) (Hayes and Decker, 1996) with coarser resolution RS data. These statistical models could explain only upto 55% yield variability. Recently combination of land surface temperature (LST), NDVI and soil moisture from coarser resolution data ( $\geq 8$  km) were used to develop statistical models to predict IOWA state wheat and soyabean yield (Prasad *et al.*, 2006). These yielded to little higher prediction accuracy than VI based models.

Accuracies from present model are comparable to accuracies of district yield obtained through LAI forcing to WTGROWS crop simulation model to simulate district wheat yield of Haryana state (Sehgal *et al.*, 2002). Real time yield forecast assessment for wheat (Nain *et al.*, 2003), district- level forecast for Nainital (Nain *et al.*, 2000) and state level wheat yield for Uttar Pradesh (Nain *et al.*, 2002) have been demonstrated using multi-crop simulation framework available in DSSAT (Nain *et al.*, 2003). The full season is required to simulate crop yield. Moreover, its spatial implementation requires lot of soil, weather variables as well as cultivar specific genetic coefficient to be generated on spatial scale or zone wise.

Present approaches estimate surface as well as process variables to predict yield without any dependence on ancillary ground based inputs. Therefore these are easy to implement for real time yield assessment. The NPP based approach is more robust specially for wheat season because it incorporates effect of both water and temperature scalars. But the WUE based approach considers only water stress.









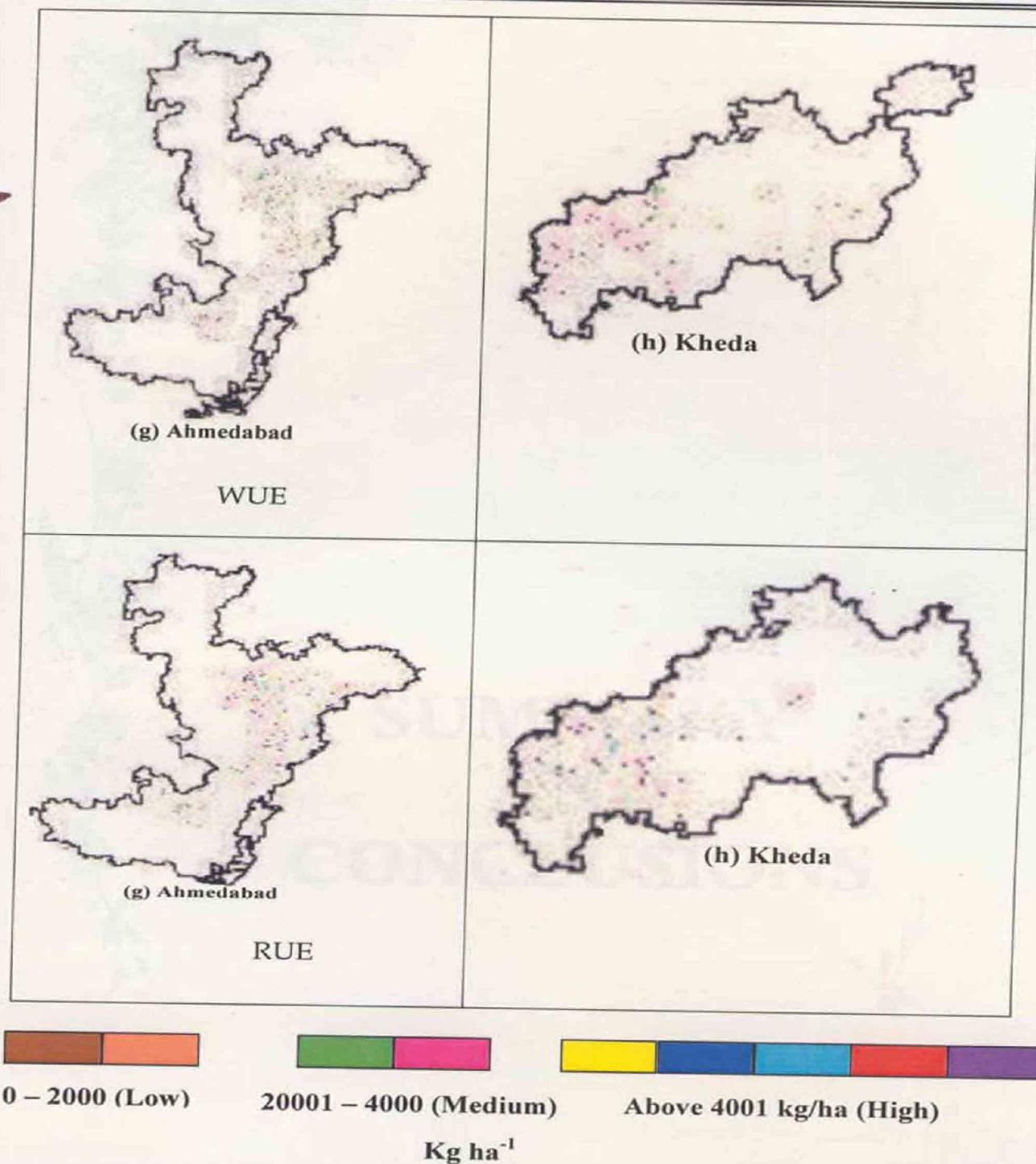


Fig. 5.32 Comparison of regional distribution of wheat yield for 2004-05 from (a) WUE based (b) RUE based approach



# **SUMMARY AND CONCLUSIONS**



## VI. SUMMARY AND CONCLUSION

---

Wheat is important staple food, widely grown in Gujarat having an area of 0.47 million hectares, with average production of 2435 kg ha<sup>-1</sup>. Timely prediction of wheat yield help grower, planners and government to maintain continuous flows of grain out of several factors governing yield of the crop water supply and weather condition are major one. The soil moisture status is indicator of evaporation from earth surface evaporation is physical factor governed by incident energy and the transfer processes. The present day methods available to predict yield and radiant energy is time consuming and costly. The use of remote sensing data in estimation of evapotranspiration and energy balance component are of immense useful, because it can give for the larger area. The present study focus on energy balance budget estimation in wheat crop over semi-arid agro-ecosystem using optical and thermal data from satellite platform during the year 2005-06 and 2006-07 with objectives of

1. To evaluate key energy balance components, estimated using polar orbiting satellite optical and thermal data.
2. Ground validation of satellite based energy budget estimates
3. Intercomparison of two remote sensing based wheat yield prediction approaches for dominant wheat districts of Gujarat and their validation.

A satellite based single source energy balance algorithm was used with MODIS TERRA, AQUA optical and thermal data to estimate different energy balance components and latent heat flux as a residual over wheat crop.

In the first phase of study, validation of energy balance estimates was carried out using *in situ* attended observations as well as area averaged unattended observations within a 5km x 5km wheat growing

region of Kheda district in Gujarat. This validation experiment was carried out for two consecutive wheat seasons, 2005-06 and 2006-07.

In the second phase of the study, time series regional evapotranspiration (ET) was estimated between November to March at every eight-day for past three rabi seasons : 2002-03, 2003-04 and 2004-05, using MODIS time composited reflectances and land surface temperatures (LST). Regional wheat yield was predicted using time series ET and associated spatially derived variables using two different approaches over dominant wheat growing districts of Gujarat. Predicted yield was validated using reported district average yield using independent datasets.

The measured clear sky instantaneous insolation at MODIS TERRA and AQUA shows substantial day-to-day fluctuations from 400-600  $\text{Wm}^{-2}$ . The atmospheric transmissivity varied between 0.7-0.8. The variation of ratio of measured hourly to day time average net radiation at different wheat growing stages were from 0.9 – 1.1 in 2005 – 06 and 1.27 – 1.87 in 2006 – 07 from vegetative to physiological maturity. The seasonal variation is attributed to variability in prevailing soil and canopy conditions. The evaporative fraction at different hours computed as a ratio of latent heat flux (LE) and net available computed from measured net available energy ( $R_n - G$ ). Latent heat flux were computed from measured net available energy and Bowen ratio. The ratio of hourly evaporative fraction to daytime average for both the seasons remain below 1.0 at most of the hour. However it varies from stage of crop. The temporal variation of MODIS based albedo from TERRA and AQUA during wheat growing period varied from 0.20 – 0.32 in 2005-06 and 0.15 – 0.35 in 2006-07. The NDVI was found to vary between 0.2 – 0.65 over wheat crop.

Average  $R_n$  varied between 349 – 514  $\text{Wm}^{-2}$  in 2005-06 and from 312 – 439  $\text{Wm}^{-2}$  in 2006-07. It was found lowest in vegetative stage and increased towards maturity. The  $\lambda E/R_n$  ratio was found to be



substantially higher during vegetative to flowering stage between 63 – 77% in 2005-06 and 74-77% in 2006-07 as compared to relatively low ratios between 52-59.6% and 48-64%, respectively in grain filling to physiological maturity.

The estimates of two energy budget components, net radiation ( $R_n$ ) and latent heat flux ( $\lambda E$ ) were compared with *in situ* measurements at Muktipur, Chalindra and Nawagam. The daytime  $R_n$  estimates from TERRA showed 16-22  $Wm^{-2}$  bias, 41-71  $Wm^{-2}$  MAE and 50-76  $Wm^{-2}$  RMSE with 'r' varying between 0.47 – 0.67. The RMSE for pooled estimates with two year TERRA datasets was 67  $Wm^{-2}$ . The bias, MAE and RMSE for daytime  $R_n$  estimates from AQUA were found to be 8-15  $Wm^{-2}$ , 31-44  $Wm^{-2}$  and 28-49  $Wm^{-2}$ , respectively with 'r' varying between 0.85 - 0.92. The RMSE over AQUA pooled estimates was 40  $Wm^{-2}$ . The error of instantaneous net radiation at TERRA overpasses were less than those at AQUA.

The instantaneous  $\lambda E$  estimates from TERRA and AQUA data and daytime estimates from them were compared with *in situ*  $\lambda E$  available as a residual from Bowen ratio energy balance measurements. The results indicated that error in pooled AQUA estimates are low 13 % with  $r = 0.76$ .

Sensible heat flux from large aperture scintillometer (LAS) reduced RMSE to 9% with increased correlation coefficient of 0.97 for TERRA and AQUA indicating that moderate satellite base  $\lambda E$  estimates at moderate resolution could have less error when area averaged heat flux measurements are used for  $\lambda E$  validation.

The histograms were developed for energy balance component ( $R_n$ ,  $G$ ,  $A$  and  $\lambda E$ ) for Gujarat using three consecutive *rabi* seasons, 2002-03, 2003-04 and 2004-05 generated using MODIS AQUA eight day composites on seven band reflectances and LST. These were substantial differences in mean, standard deviation (SD), histogram peak and range of  $R_n$  during different phenological stages of crop. These have

consistently increased from November ( $390 - 450 \text{ Wm}^{-2}$ ) to ( $450-650 \text{ Wm}^{-2}$ ) March.

A gradual decrease in mean  $H/R_n$  from 50 to 44 % was found from end of November to 1<sup>st</sup> week of March. A well distributed regional pattern in  $\lambda E/R_n$  was emerged out from the histograms in November and January. The distribution is restricted to lower  $\lambda E/R_n$  range (8 – 50 %) in November as compared to higher range (15 – 60%) in January. In March, majority of the pixels showed 10-35%  $\lambda E/R_n$  ratio corresponding to physiological maturity. The regional distribution of energy partitioning ratios showed logical variation in accordance with phenological development during *rabi* growing period over Gujarat. Similar pattern was also found for  $G/R_n$ . The pattern of distribution January (7 -20 %) to March (19-25%).

The hierarchical decision rules was applied to MODIS AQUA 250m NDVI data by considering eight-day composite NDVI for the period 1 November to 16 March for the year 2002-03 to 2004-5 to generate wheat mask of Gujarat. District mask was generated first and regional mask was subsequently generated from district mask. The wheat growing districts were only selected. The general criteria for separating different land cover types adopted as per Das *et al* (2007).

The regional wheat masks were utilized to accumulate evapotranspiration (ET) to produce regional consumptive water use for 2002-03, 2003-04 and 2004-05. The regional outputs of energy budget components and net radiation partitioning ratios, generated at  $0.01^\circ$  grid using MODIS AQUA data. These were extracted over wheat grid corresponding to *in situ* measurement sites for every eight-day. The eight-day noontime  $\lambda E$  and  $H$  were found to vary between  $80 - 300 \text{ Wm}^{-2}$  and  $180 - 280 \text{ Wm}^{-2}$ , respectively.

The eight day daily ET was computed from estimates of daytime latent heat fluxes from MODIS AQUA eight-day, for entire growing period. There were gradual increases in consumptive water use (CWU)

from vegetative (60 mm) to grain filling (100 mm) stages. The total consumptive use of water varied from district to district. It ranges from 114 mm in Mehsana to 291 mm in Anand. The districts having high consumptive water use do not have higher wheat yield. The districts have longer period low thermal regime had a high yield.

The district level yield was predicted by using seasonal consumptive water use efficiency. The MODIS AQUA derived eight day ET were accumulated for the wheat growth period between emergence to physiological maturity for *rabi* 2002-03, 2003-04 and 2004-05 using district crop calendar. The mean WUE varied from 6.1 to 23.2 kg ha<sup>-1</sup> mm<sup>-1</sup>. The WUE varied between 19.95 – 74.56 kg ha<sup>-1</sup> mm<sup>-1</sup>, 16.46-84.37 kg ha<sup>-1</sup> mm<sup>-1</sup> and 8.05-39.17 kg ha<sup>-1</sup> mm<sup>-1</sup>, in vegetative, flowering and grain filling, stages respectively.

The correlation between reported and predicted yield was 0.87 with RMSE 441 kg ha<sup>-1</sup> (18% of mean). The accuracy of this method is better than NDVI or any other VI based empirical yield prediction models.

A radiation use efficiency (RUE) based net primary production (NPP) model (CASA) was used to compute total above ground biomass at 0.01° grid over wheat crop and converted to wheat yield. The eight-day NPP was determined from daily clear sky insolation for all three years. The LAI and fAPAR were estimated using exponential model. This model was extrapolated to wheat growing pixels over study region. This produced a RMSE of 0.9 (25% of measured mean) with  $r = 0.75$ .

The measured and estimated LAI at Chalindra and Muktipur was matching and found to vary between 1.2 – 5. the regional wheat LAI output for major growth stages over wheat growing district indicated that large differences in LAI distribution was found. This was used as input for CASA model for productivity estimation. The temperature is a input in CASA. The empirical model between daily mean air temperatures measured in observatories and LST from MODIS AQUA was developed.

It is of the form ( $T_{\text{mean}} = 14.098 \log E (LST_{\text{mean}}) - 23.54$ ,  $r = 0.72$ ). The measured and estimated temperature showed RMSE of  $3.1^{\circ}\text{C}$  (12.7% of mean) in the estimated mean air temperatures.

The Net primary productivity (NPP) of wheat was estimated using CASA. The actual wheat yield was obtained from NPP and average wheat harvest index 0.35. The district average CASA estimated wheat, yield were found to produce RMSE of the order of  $428 \text{ kg ha}^{-1}$  (17.7 % of reported mean) with correlation coefficient ( $r$ ) with 0.90 for data pooled over 2002-03 and 2004-05.

The specific conclusions emerged out from the findings of the study are mentioned below.

- An approach for estimating regional scale clear sky evapotranspiration from single source surface energy balance using MODIS TERRA (morning overpass) and AQUA (noon overpass) reflectances and the LST was implemented over a semi-arid agro ecosystem in Gujarat. This requires no ground based data support.
- Validation of two major energy balance components, net radiation ( $R_n$ ) and latent heat flux ( $\lambda E$ ) over Chalindra, Muktipur and Nawagam showed that AQUA based estimates produced better accuracy than TERRA estimates on daily scale when compared to portable Bowen ratio energy balance measurements. The daytime estimates of  $R_n$  and  $\lambda E$  from AQUA produced RMSE of  $40 \text{ W m}^{-2}$  (12 % of measured mean) and  $28 \text{ W m}^{-2}$  (13 % of measured mean). The errors are comparable with the errors obtained through other global experiments.
- Accuracy of MODIS based  $\lambda E$  estimates was improved (9 % of measured mean) when compared with *in situ* measurements with limited area averaged sensible heat fluxes from Large

Aperture Scantillometer (LAS). The correlation coefficient between estimates and measurements was also improved ( $r = 0.97$ ).

- Regional distribution of energy balance components and  $R_n$  partitioning ratios over agricultural land use in Gujarat for three *rabi* (2002-03, 2003-04 and 2004-05) years were analyzed. This showed a logical spatio-temporal variation along with overall phenological development in *rabi* seasons.
- Generation of regional mask was attempted using multi-temporal eight-day MODIS AQUA 250m NDVI data using hierarchical decision tree rules by considering characteristic profiles of different crops. Twelve districts were only selected for this purpose based on the wheat area proportion of *rabi* net sown area.
- District wise average consumptive water use (CWU) were computed from MODIS AQUA 1km eight-day data. Deviations in district wheat consumptive water use (CWU) from mean were found to have good correlation ( $r = 0.74$ ) with reported district yield deviations. However, a larger number of years need to be considered to arrive at good predictive yield deviation model.
- Two wheat yield prediction approaches based on WUE and RUE were tested at regional scale. The former requires pre calibration but the latter does not require any calibration.
- RUE approach through CASA model was found to produce better yield prediction accuracy (RMSE 17.7 % of reported mean) as compared to the RMSE (18 % of reported mean) from WUE approach. Moreover, the correlation coefficient between

predicted and reported district yield was also found to be higher ( $r = 0.90$ ) in RUE based approach than the other one ( $r = 0.80$ ).

- CASA model uses both water and temperature scalars to derive biomass in terms of primary productivity. On the other hand WUE approach uses only water scalars. These differences are primarily responsible for making RUE approach superior than the other one.
- Regional variability of wheat yield for low, medium and high yield classes were capture from both the approaches. Majority of the wheat ( $0.01^\circ$ ) grids showed quite similar spatial pattern in these three major yield levels.
- Sensitivity analysis of basic input to CASA NPP showed the estimated error in wheat NPP could be between 10-12%. This could have propagated same level of error to predict yield. Rest 4-5% error in yield prediction through CASA model could be attributed to uncertainty associated with misclassification of wheat using 250m MODIS data.
- A satellite based single source surface energy balance and evapotranspiration scheme has been successfully implemented and validated for the first time over semi-arid wheat growing conditions in India and Gujarat in particular.
- This is the first time in India, that area integrated heat flux measuring equipment (LAS) was operational. It was proved that accuracy of satellite based estimates improve with the use of area averaged data from such measurements.
- The satellite based processing scheme does not require any ground data support.

- Efficiency based models can provide wheat yield prediction accuracies comparable with RS forced process models but the former is more robust, easy to handle for operational implementation.
- Among the different inputs to the productivity model accuracy of improvement in LAI retrieval through canopy reflectance inversion model is need of the hour rather than using VI based crop location specific regression models.

#### **SUGGESTIONS FOR FUTURE WORK**

- ❖ Fine tuning of evapotranspiration needs to be attempted using two-source energy balance formulation where soil evaporation and canopy transpiration can be estimated separately.
- ❖ ET in cloudy sky cases need to be addressed in future using cloudy sky net radiation and ET fraction through previous clear sky soil moisture availability.
- ❖ The hourly estimation of evapotranspiration from Geostationary satellite through energy balance approach should be attempted.



# CITATIONS





## REFERENCES

---

- Andersen, J.; Sandholt, I.; Jensen, K. H.; Refsgaard, J. C. and Gupta, H. (2002). Perspectives in using a remotely sensed dryness index in distributed hydrological models at the river-basin scale. *Hydrological Processes*, 16: 2973–2987.
- Anderson, M. C.; Norman, J. M.; Meyers, T. P. and Diak, G. R. (2000). An analytical model for estimating canopy transpiration and carbon assimilation fluxes based on canopy light-use efficiency. *Agricultural and Forest meteorology*. **101**: 265 – 289.
- Anderson, M.C.; Norman, J.M.; Diak, G.R.; Kustas, W.P. and Mecikalski, J.R. (1997). A two-source time-integrated model for estimating surface fluxes using thermal infrared remote sensing. *Remote Sensing of Environment*, **60**: 195-216.
- Anonymous (2000). Agricultural statistics at a glance 2000. Agricultural Statistics Division, Directorate of Economics & Statistics, Department of Agriculture & Cooperation, Ministry of Agriculture, Govt. of India, 2000, pp 19-21.
- Anonymous (2004). Agricultural statistics at a glance, p: 42-46.
- Anonymous (2004). Irrigation water management, Printice Hall of India, Pvt. Ltd. New Delhi. p 413-415
- Anthoni, P.M.; Freibauer, A.; Kolle, O. and Schulze, E. (2004). Winter wheat carbon exchange in Thuringia, Germany. *Agricultural and Forest Meteorology*, **121**: 55-67.
- Asrar, G.; Fuchs, M.; Kanemasu, E. T. and Hatfield, J. L. (1984). Estimating absorbed photosynthetic radiation and leaf area index from spectral reflectance in wheat. *Agronomy Journal*, **76**:300-306.

- 
- Bartholic J.P., Namken, L.R. and Wiegand, C.L. (1970) Combination equation used to calculate evaporation and potential evaporation. *USDA-ARS-Bull* 41-170: 14 pp.
- Bastiaanssen, W.G. M.; Menenti, M.; Feddes, R.A. and Holtslag, A.A.M. (1998). A remote sensing surface energy balance algorithm for land (SEBAL). Formulation 1. *Journal of Hydrology*, 212-213:198-212.
- Bastiaanssen, W.G.M.; Pelgrum, H.; Wang, J.; Ma, Y.; Moreno, J. F.; Roerink, G. J. and Wal, T. van der (1998). A remote sensing surface energy balance algorithm for land (SEBAL). Part 2: Validation. *Journal of Hydrology*, 212-213: 213-229.
- Batra, Namrata, Islam, Shafiqul, Venturini, Virginia, Bisht, Gautam and Jiang, Le. (2006). Estimation and comparison of evapotranspiration from MODIS and AVHRR sensors for clear sky days over the Southern Great Plains. *Remote Sensing of Environment*, 103, (1): 1-15.
- Beyrich, F.; De Bruin, H.A.R.; Meijninger, W.M.L.; Schipper J.W.; Lohse H. (2002). Results from One-Year Continuous Operation of a Large Aperture Scintillometer over a Heterogeneous Land Surface. *Boundary-Layer Meteorology*, 105, (1): 85-97.
- Bhattacharya, B. K. and Sastry, P. S. N. (2000). Comparative evaluation of three-crop growth models for the simulation of soil water balance in oilseed *Brassica*. *Agricultural Water Management*, 42, (1): 29-46.
- Bhattacharya, B.K.; Mallick, K.; Patel, N.K.; Padmanabhan, N.; Mahammad, S.; Ramakrishnan, R. and Parihar, J.S. (2007). A study on land surface radiation budget parameters using KALPANA-1 VHRR and INSAT 3A CCD data for agrometeorological applications. *Scientific Report*, EOAM/SAC/GEBMS/SN/07/2007.

## References

---

- Bisht, G.; Venturini, V.; Islam, S. and Jiang, L. (2005). Estimation of net radiation using MODIS (Moderate Resolution Imaging Spectroradiometer) data for clear sky days. *Remote Sensing of Environment*, 97: 52-67.
- Boegh, E.; Soegaard, H. and Thomsen, A. (2002). Evaluating evapotranspiration rates and surface conditions using Landsat TM to estimate atmospheric resistance and surface resistance. *Remote Sensing of Environment*, 79(2-3): 329-343.
- Bolle, H.J., and Streckenbach, B. (eds.) (1993). Flux estimates from remote sensing. The Echival Field Experiment in a Desertification Threatened Area (EFEDA), *final report*, 406-424, Berlin, August.
- Bouman, B.A.M. (1995). Crop modelling and remote sensing for yield production. *Netherlands Journal of Agricultural Science*, 43: 143-161.
- Camillo, P. J. (1991). Using one or two-layer models for evaporation estimation with remotely sensed data, in *Land Surface Evaporation: Measurements and Parameterization*, ed. T. J. Schmugge and J. C. Andre, New York: Springer-Verlag.
- Chakraborty, H. and Arora, R. P. (2003). Estimation of evapotranspiration of wheat crop in a rice-wheat cropping system by VITT approach using spectral indices and infrared thermometry. *Annals of Agricultural Research*, 24(1): 45-48.
- Chapin, F. S. III, A. D. McGuire, J. Randerson, R. Pielke Sr., D. Baldocchi, S. E. Hobbie, N. Roulet, W. Eugster, E. Kasischke, E. B. Rastetter, S. A. Zimov and S. W. Running (2000). Arctic and boreal ecosystems of western North America as components of the climate system *Global Change Biology* 6 (1): 211-223.

## References

---

- Chaurasia, S.; Bhattacharya, B. K.; Dadhwal, V. K. and Parihar, J. S. (2006). Field-scale Leaf Area Index estimation using IRS-1D LISS-III data. *Internatinal J. of Rem. Sens.* **27**(4): 637-644.
- Chaurasia, S.; Mallick, K.; Bhattacharya, B. K.; Vyas, S. P.; Sridhar, V. N.; Patel, N. K. and Parihar, J. S. (2007). Regional leaf area index map using Resourcesat-1 AWiFS data. Scientific Report, EOAM/SAC/CMD/2006. Space Application Center, Ahmedabad.
- Chehbouni, A.; Hoedjes, C. B.; Rodriquez, J. C.; Watts, C. J.; Garatuza J.; Jacob F. and Kerr Y. H. (2007). Using remotely sensed data to estimate aera-avargaed daily surface fluxes over semi-arid mixed agricultural land. *Agricultural and forest meteorology*, xxx (2007) xxx-xxx (Article in press).
- Chehbouni, A.; Seen, D. Lo.; Njoku, E. G. and Monteny, B. M. (1996). Examination of the difference between radiative and aerodynamic surface temperatures over sparsely vegetated surfaces. *Remote Sensing of Environment*, **58**(2):177-186.
- Chehbouni, A.; Watts, C.; Kerr, Y.H.; Dedieu, G.; Rodriguez, J.-C.; Santiago, F.; Cayrol, P.; Boulet, G. and Goodrich, D. (2000). Methods to aggregate turbulent fluxes over heterogeneous surfaces: application to SALSA data set in Mexico. *Agric. For. Meteorol.* **105**: 133-144.
- Chen, Chengci, Payne, William A.; Smiley, Richard W. and Stoltz, Michael A. (2003). Yield and Water-Use Efficiency of Eight Wheat Cultivars Planted on Seven Dates in Northeastern Oregon. *Agronomy Journal*, **95**: 836-843.
- Cleugh Helen A.; Leuning Ray; Mu Qiaozhen and Running Steven W. (2007). Regional evaporation estimates from flux tower and

- MODIS satellite data. *Remote Sensing of Environment*, 106(3): 285-304.
- Clein J., B. Kwiatkowski, A. D. McGuire, J. E. Hobbie, E. B. Rastetter, J. M. Melillo, and D. W. Kicklighter (2000). Modeling carbon responses of tundra ecosystems to historical and projected climate: A comparison of a plot- and a global-scale ecosystem model to identify process based uncertainties. *Global Change Biol.*, 6: 127-140.
- Dabrowska-Zielinska, K.; Kogan, F.; Ciolkosz, A.; Gruszczynska, M. and Kowalik, W. (2002). Modelling of crop growth conditions and crop yield in Poland using AVHRR-based indices. *International Journal of Remote Sensing*, 23:1109 – 1123.
- Dadhwal, V. K. and Sridhar, V. N. (1997). A non-linear regression form for vegetation index-crop yield relation incorporating acquisition date normalization. *International Journal of Remote Sensing*. 18(6) : 1403-1408
- Dash, P., Gottsche, F. M., Olesen, F. S., & Fischer, H. (2002). Land surface temperature and emissivity estimation from passive sensor data: Theory and practice – current trends. *International Journal of Remote Sensing*, 23, 2563–2594.
- Doorenbos, J. and Kassam, A.H. (1979). Yield response to water. *Irrigation and Drainage Paper no 33*, FAO, Rome.
- Doraiswamy, P. C., & Cook, P. W. (1995). Spring wheat yield assessment using NOAA AVHRR data. *Canadian Journal of Remote Sensing*, 21: 43- 51.
- Doraiswamy, P.C., Hatfield J., Jackson T.J., Akhmedov B., Prueger J. and Stern, A. (2004). Crop condition and yield simulations using

- Landsat and MODIS. *Remote Sensing of Environment*, **92** (2004) 548-559.
- Douglas J.; Hunsaker, Paul J.; Pinter Jr. and Bruce A. Kimball. (2005). Wheat basal crop coefficients determined by normalized difference vegetation index. *Irrigation Science*, **24** (1): 1-14.
- French, A.N.; Jacob, F.; Anderson, M.C.; Kustas, W.P.; Timmermans, W.; Gieske, A.; Su, Z.; Su, H.; McCabe, M. F.; Li, F.; Prueger, J. and Brunsell, N. (2005). Surface energy fluxes with the Advanced Spaceborne Thermal Emission and Reflection radiometer (ASTER) at the Iowa 2002 SMACEX site (USA). *Remote Sensing of Environment*, **99** (1-2): 55-65.
- Field, C.B.; Randerson, J.T. and Malmstrom, C.M. (1995). Global net primary production: combining ecology and remote sensing. *Remote Sensing of Environment*, **51**: 74-88.
- Gadgil, S., Abrol, Y.P. and Rao, P.R.S. (1999). On growth and fluctuation of Indian food grain production. *Current Science*, **76**(4): 548-556.
- Gadhavi H. and Jayaraman A. (2004). Aerosol characteristics and aerosol radiative forcing over Maitri, Antarctica. *Current Science*, **86**: 296-304.
- Gao, B.C., 1996, "NDWI - A normalized difference water index for remote sensing of vegetation liquid water from space". *Remote Sensing of Environment*, Vol. 58: 257-266.
- Gentine, P., Entekhabi, D., Chehbouni, A., Boulet, G., & Duchemin, B. (2007). Analysis of evaporative fraction diurnal behaviour. *Agricultural and Forest Meteorology*, **143**: 13-29.

- Gilles, R. R.; Carlson, T. N.; Cui, J.; Kustas, W. P. and Humes, K. P. (1997). Verification of the triangle method for obtaining surface soil water content and energy fluxes from remote measurements of Normalized Difference Vegetation Index (NDVI) and surface radiant temperature. *Int. J. Remote Sens.*, 18, 3145–3166.
- Gonzalez, Alma Delia Baez; Kiniry, James R.; Maas, Stephan J.; Tiscareno, Mario L.; Jaime Macias C.; Jose L. Mendoza; Clarence W. Richardson; Jaime Salinas G. and Manjarrez, Juan R. (2005). Large-Area Maize Yield Forecasting Using Leaf Area Index Based Yield Model. *Agron. Journal*, 97:418–425.
- Gouranga Kar and Ashwani Kumar, (2007). Surface energy fluxes and crop water stress index in groundnut under irrigated ecosystem. *Agricultural and Forest Meteorology*, 146 (1-2):94-106.
- Groten, S. M. E. (1993). NDVI-crop monitoring and early yield assessment of Brukina Faso. *International Journal of Remote Sensing*, 14, 1495– 1515.
- Gupta, P. L. and Sastry, P. S. N. (1986). Estimating evapotranspiration from midday canopy temperature. *Irrigation Science*, 7 (4): 237-243.
- Gupta, R. K.; Prasad, T. S. and Vijaya, D. (2001). Estimation of and validation of roughness length, surface temperature and sensible heat flux computed from remote sensing (WiFS and NOAA/AVHRR) data. *J. of Agrometeorology*, 3 (1 & 2): 189-215.
- Hall, F. G.; Huemmrich, K. F.; Goetz, S. J.; Sellers, P. J. and Nickerson, J. E. (1992). Satellite remote sensing of surface energy balance: Success, failures and unresolved issues in FIFE. *Journal of Geophysical Research*, 97, 19,061–19, 089.
- Hamar, D., Ferencz, C., Lichtenberg, J., Tarcsai, G., and Frencz-A' rkos, I., (1996). Yield estimation for corn and wheat in the Hungarian Great

- Plain using Landsat MSS data. *International Journal of Remote Sensing*, 17, 1689–1699.
- Hartogensis, O. K. C.; Watts, J.; Rodriguez, J.C. and De Bruin, H. A. R. (2003). Derivation of an Effective Height for Scintillometers: La Poza Experiment in Northwest Mexico. *Journal of Hydrometeorology*, 4 (5): 915-928.
- Hatfield, J.L.; Wanjura, D.F.; and Barker, G.L. (1985). Canopy temperature response to water stress under partial canopy. *Transactions of ASAE*, 28 : 1607-1611.
- Hayes, M.J. and Decker, W.L. (1996). Using NOAA AVHRR data to estimate maize production in the United States Corn Belt. *Int. J. Remote Sens.* 17: 3189–3200.
- Hinzman, L. and D. L. Kane (1992). Potential response of an arctic watershed during a period of global warming. *J. Geophys. Res.* 97: 2811–2820.
- Houborg Rasmus and Boegh Eva. (2007) Mapping leaf chlorophyll and leaf area index using inverse and forward canopy reflectance modeling and SPOT reflectance data. *Remote Sensing of Environment*, (press)
- Houborg, R.; Soegaard, H., and Boegh, E. (2007). Combining vegetation index and model inversion methods for the extraction of key vegetation biophysical parameters using Terra and Aqua MODIS reflectance data. *Remote Sensing of Environment*, 106: 39–58.
- Huband, N. D. S. and Monteith J. L. (2004). Radiative surface temperature and energy balance of a wheat canopy. *Boundary Layer Meteorology*. 36 (1-2): 107-116.
- Hurtado, E., and Sobrino, J. A. (2001). Daily net radiation estimated from air temperature and NOAA-AVHRR data: A case study for the



- Iberian Peninsula. *International Journal of Remote Sensing*, 22(8): 1521–1533.
- Kancheva, R.; Borisova, D. and Georgiev, G. (2007). Spectral Predictors of Crop Development and Yield. *Recent Advances in Space Technologies, 2007. RAST '07. 3rd International Conference*, 247 – 251.
- Kiziloglu, Fatih M.; Sahin, Ustun; Tunc, Talip and Diler, Serap. (2006). The Effect of Deficit Irrigation on Potato Evapotranspiration and Tuber Yield under Cool Season and Semiarid Climatic Conditions. *Journal of Agronomy*, 5 (2): 284-288.
- Kohsiek, W.; Meijninger, M. L.; Moene, A. F.; Heusinkveld, G.; Hartogensis, O. K.; Hillen W. C. A. M. and De Bruin, H. A. R. (2002). An Extra Large Aperture Scintillometer For Long Range Applications. *Boundary-Layer Meteorology*, 105 (1): 119-127.
- Kustas, W.P., Moran, M.S., Humes, K.S., Stannard, D.I., Pinter, P.J., Hipps, L.E., Swiatek, E. and Goodrich, D.C. (1994). Surface energy balance estimates at local and regional scales using optical remote sensing from an aircraft platform and atmospheric data collected over semiarid rangelands. *Water Resources Research*, 30(5), 1241-1260.
- Kustas, William P. (1990). Estimates of Evapotranspiration with a One- and Two-Layer Model of Heat Transfer over Partial Canopy Cover. *Journal of Applied Meteorology*, 29 (8): 704-715.
- Kustas W. P., Norman J.M., Anderson M.C. and French A.N. 2003: Estimating sub-pixel surface temperature and energy fluxes from the vegetation index-radiometric temperature relationship. *Remote Sens. Environ.*, 85, 429- 440.

- Kustas, William P.; Anderson, Martha C.; French, Andrew N. and Vickers, Dean, (2006). Using a remote sensing field experiment to investigate flux-footprint relations and flux sampling distributions for tower and aircraft-based observations. *Advances in Water Resources*, **29**: 355–368.
- Launay Marie and Guerif Martine, (2005). Assimilating remote sensing data into a crop model to improve predictive performance for spatial applications. *Agriculture, Ecosystems & Environment*, **111**(1-4): 321-339.
- Lloyd, D. (1990). A phenological classification of terrestrial vegetation cover using shortwave vegetation index imagery. *International Journal of Remote Sensing*, **11** : 2269–2279.
- Mallick, K., Bhattacharya, B.K., Chourasia, S., Dutta, S., Nigam, R., Mukherjee, J., Banerjee, S., Kar, G., Rao, V.U.M., Gadgil, A.S., & Parihar, J.S. (2007). Evapotranspiration using MODIS data and limited ground observations over selected agroecosystems in India. *International Journal of Remote Sensing*, **28** (10), 2091-2110.
- Mallick, K. (2007). Characterizing moisture availability and AET using space based remote sensing techniques. A Ph.D. thesis submitted to University of Pune.
- Manderscheid, R. and Weigel, H. J. (2007). Drought stress effects on wheat are mitigated by atmospheric CO<sub>2</sub> enrichment. *Agronomy for Sustainable Development* **27**: 79-87.
- Manjunath, K. R.; Potdar, M. B. and Purohit, N. L. (2002). Large area operational wheat yield model development and validation based on spectral and meteorological data, *International J. Remote sensing*. **23** : 3023-3038.

- Manjunath, K. R.; Potdar, M. B. and Purohit, N. L. (2002). Large area operational wheat yield model development and validation based on spectral and meteorological data. *International Journal of Remote Sensing*, **23**, (15, 22): 3023-3038.
- Mannstein, H. (1987). Surface energy budget, surface temperature and thermal inertia, in *Remote Sensing Applications in Meteorology and Climatology*, ed. R. A. Vaughan and D. Reidel, NATO ASI Ser. C: Math. Phys. Sci. Vol. 201, pp. 391- 410, Dordrecht, Netherlands: A Reidel Publishing Co.
- McFadden, J. P., F. S. Chapin III, and D. Y. Hollinger, (1998). Subgrid-scale variability in the surface energy balance of arctic tundra. *J. Geophys. Res.*, **103** : 28947-28961.
- Mcguire, A. D., J. S. Klein, J. M. Melillo, D. W. Kicklighter, R. A. Meier, C. J. Vorosmarty and M. C. Serreze (2000). Modelling carbon responses of tundra ecosystems to historical and projected climate: sensitivity of pan-Arctic carbon storage to temporal and spatial variation in climate. *Global Change Biology*, **6** (1): 141-159.
- Meijninger, W. M. L.; Green, A. E.; Hartogensis, O. K.; Kohsiek, W.; Hoedjes, J. C. B.; Zuurbie, R. M. and De Bruin, H. A. R. (2004). Determination of Area-Averaged Water Vapour Fluxes with Large Aperture and Radio Wave Scintillometers over a Heterogeneous Surface Flevoland Field Experiment. *Boundary-Layer Meteorology*, **105** (1): 63-83.
- Midmore, D. J.; Cartwright, P. M. and Fischer, R. A. (1982). Wheat in tropical environments. I. Phasic development and spike size. *Field crops Res.*, **5**: 185-200.

## References

---

- Moran, M. S.; Kustas, W. P.; Vidal, A.; Stannard, D. I.; Blanford, J. H. and Nichols, W. D. (1994). Use of ground-based remotely sensed data for surface energy balance evaluation of a semiarid rangeland. *Water Resources Research*, **30**, (5): 1339-1350.
- Moriondo, M.; Maselli, F. and Bindi, M. (2007). A simple model of regional wheat yield based on NDVI data. *European Journal of Agronomy*, **26**, (3): 266-274.
- Mu, Q.; Heinsch, F. A.; Zhao, M. and Running, S.W. (2007). Development of a global evapotranspiration algorithm based on MODIS and global meteorology data. *Remote Sensing of Environment*, **111** (4): 519-536.
- Nagai, Haruyasu (2003). Validation and Sensitivity Analysis of a New Atmosphere Soil Model. Part II: Impact on In-Canopy latent Heat Flux over Winter Wheat Field Determined by Detailed Calculation of Canopy Radiation Transmission and Stomatal Resistance. *Journal of Applied Meteorology*, **42**: 434-451.
- Nain, A. S.; Dadhwal, V. K. and Singh, T. P. (2000). Use of CERES-wheat model for predicting wheat yields of Nainital District (U.P.), *Indian J. of Agrometeorology*, **2**:113-122.
- Nain, A. S.; Dadhwal, V. K. and Singh, T. P. (2003). Analysis of spatial and temporal wheat yield variability in Punjab and Haryana and identification of coherent yield zones, *Indian J. of Agrometeorology*, **2**: 113-122.
- Nain, A. S.; Dadhwal, V. K.; Sehgal, V. K.; Vyas, S. P. and Parihar, J. S. (2002). Wheat yield development in Uttar Pradesh using simulation models. *Scientific Report*, RSAM/SAC/FASAL-TD/SN/15/2002.

- Nishida Kenlo; Ramakrishna R.; Nemani, Steven; Running, W. and Joseph M. Glassy (2003). An operational remote sensing algorithm of land surface 30 evaporation. *J. Geophys. Res.*, **108**(0): XXXX.
- Nishida, K.; Nemani, R. R.; Running, S. W. and Glassy, J. M. (2003). Remote sensing of land surface evaporation (i) theoretical basis for an operational algorithm. *J. Geophys. Res.* **108**.
- Noilhan, J. and Mahfouf, J.F. (1996). The ISBA land surface parameterization scheme. *Global Planetary Change*, **13**: 145-159.
- Norman, J.M.; Kustas, W.P. and Humes, K.S. (1995). Source approach for estimating soil and vegetation energy fluxes from observations of directional radiometric surface temperature. *Agricultural and Forest Meteorology*, **77**: 263-293.
- O'Connell, M. G.; O'Leary, G. J.; Whitfield, D. M. and Connor, D. J. (2004). Interception of photosynthetically active radiation and radiation-use efficiency of wheat, field pea and mustard in a semi-arid environment. *Field Crops Research*, **85** (2-3): 111-124.
- Olioso, A.; Braud, I.; Chanzy, A.; Courault, D.; Demarty, J.; Kergoat, L.; Lewan, E.; Ottele, C.; Prevot, L.; Zhao, W. G.; Calvet, J. C.; Cayrol, P.; Jongschaap, R.; Moulin, S.; Noilhan, J. and Wigneron, J. P. (2002). SVAT modeling over the Alpilles-ReSeDA experiment: comparing SVAT models over wheat fields. *Agronomie*, **22**(6): 651-668.
- Patel, N. R.; Mohammed, A. J. and Rakesh, D. (2006). Modeling of Wheat Yield Using multi-temporal Terra/MODIS Satellite Data. *Geocarto International*, **21** (1) : 43-50.
- Peter van der Keur Søren Hansen, Kirsten Schelde and Anton Thomsen, (2000). Modification of DAISY SVAT model for potential use of

- remotely sensed data,. *Agricultural and Forest Meteorology*, **106** (3): 215-231.
- Potadar, M. B. and Manjunath, K. R. (1990). Wheat growth profile: satellite monitoring and crop yield modeling. *International J. of Remt. Sens.*
- Prasad, A.K.; Chai, L.; Singh, R.P. and Kafatos, M. (2006). Crop yield estimation model for Iowa using remote sensing and surface parameters. *International Journal of Applied Earth Observation and Geoinformation*, **8**: 26–33.
- Quarmby, N.A.; Milnes, M.; Hindle, T.L. and Silicos, N. (1993). The use of multitemporal NDVI measurements from AVHRR data for crop yield estimation and prediction. *Int. J. Remote Sens.* **14**: 199–210.
- Rajagopal, E.N. (2001). Validation of land surface parameters in NCMRWF model with LASPEX dataset. *Journal of Applied Meteorology*, **3** (1&2):217-226.
- Rajak, D.R., Oza, M.P., Bhagia, N., Dadhwal, V.K. (2002). Relating Wheat Spectral Profile Paratmeters to Yield and Phenology. *Internat. Arch. Photogramm. Remote Sens. & Spatial Inf. Sci.*, **34** (7): 363-367.
- Rawson, H. N. (1986). High temperature-tolerant wheat: a description of variation and a search for some limitations to productivity. *Field Crops Res.*, **14**: 197-212.
- Reeves, M. C.; Zhao, M. and Running, S. W. (2005). Usefulness and limits of MODIS GPP for estimating wheat yield. *International Journal of Remote Sensing*, **26** (7) :1403–1421.
- Reynolds, M. P.; Delgado, M. I.; Rodriguez, M. G. and Saavedra, A. L. (2000). Photosynthesis of wheat in warm, irrigated environment I: Genetic diversity and crop productivity. *Field Crops Research*, **66**: 37-50.

## References

---

- Rivalland, V.; Demarty, J.; Oliso, A.; Weiss, M.; Rossello, P.; Jacob, F.; Inoue, Y. and Baret, F. (2005). Evapotranspiration Monitoring Using Remote Sensing Measurements Assimilated in a SVAT Model. *Geophysical Research Abstracts*, (7) : 423-428.
- Rodriguez, J.C.; Duchemin, B.; Watts, C.J.; Hadria, R.; Garatuza, J.; Chehbouni, A.; Boulet, G.; Armenta, M.; Er-Raki, S. (2003). Wheat yields estimation using remote sensing and crop modeling in Yaqui Valley in Mexico. *Geoscience and Remote Sensing Symposium*, 4: 2221 – 2223.
- Roebling, R. A.; Putten, Van, E.; Genovese, G. and Rosema, A. (2004). Application of Meteosat derived meteorological information for crop yield predictions in Europe. *International Journal of Remote Sensing*, 25 (23): 5389-5401.
- Roerink, G. J., Su, Z., and Menenti, M. (2000). S-SEBI: A simple remote sensing algorithm to estimate the surface energy balance. *Physics and Chemistry of the Earth*, 25, 147-157.
- Rosema A. (1993). Using METEOSAT for operational evapotranspiration and biomass monitoring in the Sahel region. *Remote Sensing of Environment*, 46 (1): 27-44.
- Rosema, A., Verhees, L.; Putten, E.; Gielen, H.; Lack, T. and Wood, J. (2004). European energy and water balance monitoring system. *The European Community Fourth Framework Programme for Research, Technological Development and Demonstration in The Field of Environment and Climate*, Scientific Report.
- Running, S.W. (1991). Computer simulation of regional evapotranspiration by integrating landscape biophysical attributes with satellite data, in

- 
- Land Surface Evaporation: Measurements and Parameterization*, ed. T. J. Schmugge and J. C. André, New York: Springer-Verlag.
- Running, S.W.C., Justice, V.; Salomonson, D.; Hall, J.; Barker, Y.; Kaufman, A.; Strahler, A.; Huete, J. P.; Muller, V.; Vanderbilt, Z. Wan and Teillet, P. (1994). Terrestrial remote sensing science and algorithms planned for EOS/MODIS, *Int. J. Remote Sens.*, **15**(17): 3587-3620.
- Sarkar, C.; Bhattacharya, B.K.; Gadgil, A.; Mallick, K.; Bairagi, G.D.; Patel, N.K. and Parihar J.S. (2006). Growing environment characterization of rice and yield prediction using time composited NOAA AVHRR optical and thermal data. In: *International Society of Photogrammetry and Remote Sensing Symposium* held between December 23-26, 2006 at Goa, India, Commission VI, WG VI/4, No. ICWG-24-030
- Sarkar, C.; Bhattacharya, B.K.; Gadgil, A.; Mallick, K.; Patel, N.K. and Parihar, J.S. (2007). Estimation of relative evapotranspiration from NOAA PAL to derive grow characteristics in India. *International Journal of Remote Sensing* (in press).
- Schmugge, T. J. and Becker, F. (1991). Remote sensing observations for the monitoring of land-surface fluxes and water budgets, in *Land Surface Evaporation: Measurements and Parameterization*, ed. T. J. Schmugge and J. C. André, New York: Springer-Verlag.
- Schuttemeyer, D.; Moene, A. F.; Holtslag, A. A. M.; Bruin, H. A. R. de. and Giesen, N. van de. (2006). Surface Fluxes and Characteristics of Drying Semi-Arid Terrain in West Africa. *Boundary-Layer Meteorology*, **118** (3): 583-612.
- Sehgal, V. K.; Rajak, D. R. and Dadhwal, V. K. (2001). Issue in linking remote sensing inputs in a crop growth monitoring system: results of a



## References

---

- case study. In 'Proc. of the ISRS National Symposium', 11-13 December, 2001, Ahmedabad, India.
- Sehgal, V. K.; Rajak, D. R.; Chaudhari, K. N. and Dadhwal, V. K. (2002). improved Regional Yield Prediction by Crop Growth Monitoring System using Remote Sensing Derived Crop Phenology. *Proc. Of international Archives of the photogrammetry, Remote sensing and Spatial Information Sciences, Commission VII Symposium on "Resource & Environmental monitoring", held at Hyderabad, India, IAPRS & GIS, vol. 34, Part 7, 329- 334, Dec. 3-6, 2002.*
- Sellers, P. J. (1985). Canopy reflectance, photosynthesis and transpiration. *International Journal of Remote Sensing*, **6**, 1335 – 1372.
- Sellers, P.J.; Hall, F.G.; Asrar, G.; Strebel, D.E.; and Murphy, R.E. (1988). The first ISLSCP field experiment (FIFE). *Bulletin of American Meteorological Society*, **69**: 22-27.
- Shaomin Liu; Miaofen Huang; Lijuan Han and Qijiang Zhu (2003). A study of surface sensible heat fluxes with Large Aperture Scintillometers. *Geoscience and Remote Sensing Symposium*, **5**: 3338 – 3340.
- Shekh, A. M., Kumar, M.; Pandey, V. and Gajjar, R.B. (2001). Radiation and energy budget components over cropped surface and bare soil during LASPEX-97. *Journal of Agrometeorology*, **3** (1/2): 57-65.
- Shen Yanjun, Zhang Yongqiang, Kondoh Akihiko, Tang Changyuan, Chen Jianyao, Xiao Jieying, Sakura Yasuo, Liu Changming, Li Weiqiang and Sun Hongyong (2004). Seasonal variation of energy partitioning in an irrigated lands. *Hydrological Processes* **18**: 2223-2234.

## References

---

- Singh, A.; Singh, R.; Rao, V.U.M. and Panuu, R. K. (2003). Effect of shade on phenological development, thermal and radiation use efficiency of wheat genotypes. *J. of Agromet*, 5:37-42.
- Stisen, S., Sandholt, I., Nørgaard, A., Fensholt, R., & Eklundh, L. (2007). Estimation of diurnal air temperature using MSG SEVIRI data in West Africa. *Remote Sensing of Environment*, 110: 262–274.
- Su, H.; McCabe, M. F.; Wood, E. F.; Su, Z. and Prueger, J. H. (2005). Modeling Evapotranspiration during SMACEX: Comparing Two Approaches for Local- and Regional-Scale Prediction. *Journal of Hydrometeorology*, 6 (6): 910–922.
- Tasumi, Masahiro; Allen, Richard G.; Trezza, Ricardo and Wright, James L. (2005). Satellite-Based Energy Balance to Assess Within-Population Variance of Crop Coefficient Curves. *Journal of Irrigation and Drainage Engineering*, 131 (1): 94-109.
- Timmermans, W. J.; Kustas, W. P.; Aderson M. C. and French A. N. (2007). An intercomparison of the Surface Energy Balance Algorithm for Land (SEBAL) and Two-Source Energy Balance (TSEB) modeling schemes. *Remote sensing of environment*, 108: 369-384.
- Tucker, C. J., Gatlinn, A. and Schneider, S. R. (1984). Monitoring vegetation in the Nile delta with NOAA-6 and NOAA-7 AVHRR photoprogramm. *Eng. Remote Sens.* 50: 53-60.
- Tucker, C. J., Justice, C. O. and Prince, S. D. (1986). Monitoring the grass land of the Sahel 1984-1985. *International J. Remote Sens.* 7: 1571-1581.
- Venturini, Virginia; Islam Shafiquel and Rodriguez, Leticia (2007) (**Corrected proof**). Estimation of evaporative fraction and evapotranspiration from MODIS products using a complementary based model. *Remote Sensing of Environment*, doi:10.1016/j.rse.2007.04.014.

## References

---

- Vermote, E.F., Elsaleous, N.Z. and Justice, C.O. (2002). Atmospheric correction of the MODIS data in the visible to middle infrared: first results. *Remote Sensing of Environment* (MODIS Land Special Issue), 83, 97-111.
- Verstraeten, W. W.; Veroustraete, F. and Feyen, J. (2005). Estimating evapotranspiration of European forests from NOAA-imagery at satellite overpass time: towards an operational processing chain for integrated optical and thermal sensor data products. *Remote-Sensing-of-Environment*, 96(2): 256-276.
- Van de Griend, A.A, Camillo, P.J. and Gurney, R.J. (1985) Discrimination of Soil Physical Parameters, Thermal Inertia and Soil Moisture from Diurnal Surface Temperature Fluctuations. *Water Resources Research*, 21, 997-1009.
- Wade, G., R. Mueller, P. Cook, and P. Doraiswamy, 1994. AVHRR map products for crop condition assessment: a geographic information systems approach, *Photogrammetric Engineering & Remote Sensing*. 60(9): 1145-1150
- Wallace, J. S. (1995). Calculating evaporation: resistance to factors, *Agriculture and Forest Meteorology*, 73 (3-4): 353-366.
- Wan, Z., Y. Zhang, Q. Zhang, and Z.-L. Li. (2004). Quality assessment and validation of the MODIS land surface temperature. *Int. J. Remote Sens.*, 25: 261-274.
- Wang, S., and Davidson, A. (2007). Impact of climatic variations on surface albedo of temperate grassland. *Agricultural and Forest Meteorology*, 142: 133-142.

## References

---

- Wang, Kaicun; Li, Zhanqing and Cribb, M. (2006). Estimation of evaporative fraction from a combination of day and night land surface temperatures and NDVI: A new method to determine the Priestley–Taylor parameter. *Remote Sensing of Environment*, **102**(3-4): 293-305.
- Watts, C. J.; Chehbouni, A.; Rodriguez, J. C.; Kerr, Y. H.; Hartogensis, O. and de Bruin, H. A. R. (2000). Comparison of sensible heat flux estimates using AVHRR with scintillometer measurements over semi-arid grassland in northwest Mexico. *Agricultural and Forest Meteorology*, **105**(1-3): 81-89.
- Wetzel, P. J. and Woodward, R. H. (1987). Soil Moisture Estimation Using GOES-VISSR Infrared Data: A Case Study with a Simple Statistical Method. *Journal of Applied Meteorology*, **26**(1):107-117.
- White, M. A.; Thornton, P. E. and Running, S. W. (1997). A continental phenology model for monitoring vegetation responses to interannual climatic variability. *Global Biogeochemical Cycles*, **11**: 217– 234.
- Yanjun Shen, Akihiko Kondoh, Changyuan Tang, Yongqiang Zhang, Jianyao Chen, Weiqiang Li, Yasuo Sakura, Changming Liu, Tadashi Tanaka and Jun Shimada (2002). Measurement and analysis of evapotranspiration and surface conductance of a wheat canopy. *Hydrol. Process.* **16**: 2173–2187.
- Zadoks, J. C.; Chang, T. T. and Konzak, C. F. (1974). A decimal code for growth stages of cereals, *Weed Res.* **14**: 415- 421.
- Zhang, H.; Wang, X.; You, M. and Liu C. (1999). Water-yield relations and water-use efficiency of winter wheat in the North China Plain. *Irrigation Science*, **19**(1): 37-45.

## *References*

---

- Zhang, L. Lemeur, R. and Goutorbe, J. P. (1995). A one-layer resistance model for estimating regional evapotranspiration using remote sensing data, in *Agricul. and Forest Meteorol.*, 77:241-261.
- Zhang, Y.; Liu, C.; Lei, Y.; Tang, Y.; Yu, Q.; Shen, Y. and Sun, H. (2006). An integrated algorithm for estimating regional latent heat flux and daily evapotranspiration. *International Journal of Remote Sensing*, 27(1): 129 – 152.
- Zhu Zhilin, Sun Xiaomin and Zhang Renhua, (2003). Statistical analysis and comparative study of energy balance components estimated using micrometeorological techniques during HUBEX/IOP 1998/99, *Advances in Atmospheric Sciences*, 20 (2): 285-291.
- Zhu, Zhilin; Sun, Xiaomin; Xu, Jinping; Wang, Weimin and Zhang, Renhua (2004). Using Large Aperture Scintillometer to validate pixel heat flux based on remote sensing models. *Geoscience and Remote Sensing Symposium*, 3: 1984-1987.

## DECLARATION

This is to declare that the whole of the research work reported here in the thesis towards the partial fulfillment of the requirement for the degree of **Doctor of Philosophy in Agricultural Meteorology** by the undersigned is the result of investigations done by him under the direct guidance and supervision of Dr. A. M. Shekh, Principal and Dean (B. A. College of Agriculture) and no part of work has been submitted for any other degree so far.

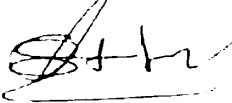
Kailas.

Place : ANAND

(DAKHORE KAILAS KAMAJI)

Date : 24<sup>th</sup> DEC., 2007

COUNTER SIGNED BY



(A. M. SHEKH)

Principal and Dean

B. A. College of Agriculture  
Anand Agricultural University  
ANAND - 388 110.